The impact of wind and mechanical stress on growth and development of *Brachypodium distachyon* stems

Agnieszka Gladala-Kostarz

A thesis submitted to Aberystwyth University for the degree of

Doctor of Philosophy in Biological Sciences

IBERS
Athrofa y Gwyddorau Biolegol, Amgylcheddol a Gwledig
Institute of Biological, Environmental and Rural Sciences

National Plant PHENOMICS Centre

18.09.2019

THESIS WORD COUNT

55326

DECLARATION

This work has not previously been accepted in substance for any degree and is not being concurrently submitted in candidature for any degree.

Signed (Candidate)

Date 18.09.2019

STATEMENT 1

This thesis is the result of my investigations, except where otherwise stated. Other sources are acknowledged by footnotes giving explicit references. A bibliography is appended.

Signed (Candidate)

Date 18.09.2019

STATEMENT 2

I hereby give consent for my thesis, if accepted, to be available for photocopying and inter-library loan, and for the title and summary to be made available to outside organisations.

Signed (Candidate)

Date 18.09.2019

"As many more individuals of each species are born than can possibly survive; and as, consequently, there is a frequently recurring struggle for existence, it follows that any being, if it vary however slightly in any manner profitable to itself, under the complex and sometimes varying conditions of life, will have a better chance of surviving, and thus be naturally selected. From the strong principle of inheritance, any selected variety will tend to propagate its new and modified form."

- Charles Darwin,

On the Origin of Species, 1859

Introduction, page 5.

ACKNOWLEDGEMENTS

I would like to begin by expressing my deepest gratitude to my supervisors. To Dr Maurice Bosch for his patience, guidance, experience, knowledge and advice but also for huge empathy, support and understanding he offered during the last few years. Without his contribution, most of what has been achieved would not exist. To Prof. John Doonan for his guidance, help, valuable advice and confidence in my research. I am very privileged to have worked with them and extremely grateful to have been given the opportunity to work on this project.

I also need to say thank you to Prof. Luis Mur for his help, advice and enthusiasm with metabolite analysis and Prof. Paul Knox for invaluable guidance with immuno and pectin experiments. Additionally, I would like to thank Alan Cookson for his assistance with SEM and to Dr Barbara Hauck and Dr David Walker for their help with cell wall composition analysis. I am also greatly indebted to Dr Candia Nibau, Dr Rakesh Bhatia, Emma Timms-Taravella, Dr Samantha Gill and Dr Fiona Cork for their help, assistance and technical advice from various biological sciences disciplines. A special acknowledgement I would like to address to Tom Thomas in the botany gardens for lovely morning chats during my glasshouse work, which brought the sun to even rainy weather. To everybody else who has helped me achieve my goals, I wish to express my deepest gratitude and ensure that any positive gesture will not be forgotten.

This PhD would have been much harder without the help and support of my best friends. I am forever grateful to Joanna Wilinska for being always there, for her dedication, loyalty and for having a glass of wine when needed ☺. I owe thanks to an extraordinary person in my life Martyna Andres-Brandyk I could say for everything, support, help, faith in me, dedication but especially for the most precious thing that can be given, for her time, it is priceless. I am honoured to have such wonderful people in my life.

I do not know how to begin with saying thank you to the people who mean the world to me, my family, especially my mum Anna and dad Zbigniew, for their support, giving me the liberty to choose what I desired the most. I salute them both for the selfless love, care, pain and sacrifice they did to shape my life and for helping me to become

the person I am now. I owe thanks to my brother for having that treasured feeling that I can always count on him no matter what. Also, I would like to express my thanks to my grandparents for their unconditional love and for enormous contribution in raising me in the most beautiful way I can imagine. Exceptional thanks to my grandma Jadzia for her support, faith in me and for valuable prayers. Special thanks go to my mother in law for her love and support. I would never be able to pay back the love and affection showed upon by all of you.

Finally, I would like to dedicate this work to my soul mate, best friend and my dearest husband, Piotr. You believed in me in the way, which reached directly to my mind and heart. Thank you for encouraging me in all of my pursuits and inspiring me to follow my dreams. Thank you for your unfailing love, patience and for being so understanding to all of my strange life rules and for putting up with me through the toughest moments of my PhD. Love you forever.

SUMMARY

The wind is an important abiotic stress from an agronomic and economic point of view. While the response of plants to various abiotic stresses is intensively studied, there is relatively little research on wind stress (WS) and mechanical stress (MS) in plants, especially in the grasses. This study aims to provide information on how wind stress and mechanical stress affect the growth and development of the model grass *Brachypodium distachyon*.

In particular, the study focussed on the consequences of WS and MS on cell wall composition and architectural features of the stems, as well as phenotypic, molecular and metabolic responses. The study includes a comparison of two genotypes of *Brachypodium*, Bd21 and ABR6.

Phenotypic observation demonstrated a reduction in main stem length and delayed flowering, reduction in seed yield and aboveground biomass for the two genotypes. More detailed analysis, including histology, anatomy, and composition analysis of stem cell walls, showed differences in response to WS and MS and between both genotypes Bd21 and ABR6. Investigation showed alterations in cell wall thickness of particular stem tissues as well as the organisation of stem tissues. Immunolocalisation using a range of monoclonal antibodies against non-cellulosic cell wall glycans, revealed differences in the labelling pattern obtained with pectin-related antibodies between treatments and genotypes. Mechanical stimulation enhanced pectin methylesterase activity and an increase in lignin content localised mostly in the cortex and interfascicular tissue. Differences in cell wall monosaccharide content were also observed. Sugar release after enzymatic hydrolysis was significantly reduced after both stress treatments. Furthermore, three-point-bending tests showed differences in the mechanical properties of stems exposed to WS/MS compared with control. In an attempt to provide functional information on the responses to WS and MS molecular and metabolomic analysis were performed. Molecular analysis revealed alterations in cell wall-related, LOX, and PME genes expression in response to WS and MS in both genotypes. Metabolic analysis unravelled pathways involved in response to mechanical stimulation.

The study showed that wind and mechanical stress induce significant architectural changes across multiple scales, from the whole plant to organ, tissue, cellular and molecular level highlighting the complex nature of how plants respond to mechanical stimulation.

Keywords: • *Brachypodium distachyon* • cell wall • wind stress • mechanical stress • mechanical stimulation • immuno-localisation • RT-PCR • metabolite profiling

TABLE OF CONTENTS

TABLE OF TABLES

TABLE OF FIGURES

ABBREVIATIONS

A_{280}	Absorbance measured at 280 nm
ABSL	Acetyl Bromide Soluble Lignin
AC	Specific Absorption Coefficient
AGPs	Arabinogalactan Proteins
ANOVA	Analysis of Variance
Ara	Arabinose
BS	Bundle Sheath
BSA	Bovine Serum Albumin
C	Control
^oC	Celsius degrees
cDNA	Complementary DNA
CFW	Calcofluor White
cm	Centimeter
C_{Mns}	Supernatant Concentration
Cp	Crossing point
CWM	Cell Wall Material
DMSO	Dimethyl sulfoxide
DNA	Deoxyribonucleic Acid
DNase	Deoxyribonuclease
dNTP	Deoxynucleotide Triphosphate
EDTA	Ethylenediaminetetraacetic Acid
ELISA	Enzyme-Linked Immunosorbent Assay
ESI	Electrospray Ionisation
EtOH	Ethanol
F	Force
FA	Ferulic Acid
FIE-HRMS	Flow Injection Electrospray High-Resolution Mass Spectrometry
Fuc	Fucose

Fw	Forward
g	Gram
Gal	Galactose
GAX	Glucuronoarabinoxylan
Glc	Glucose
GPa	Giga Pascal
HCA	Hydroxycinnamic Acid
HCl	Hydrochloric Acid
HG	Homogalacturonan
HPAEC-PAD	High-Performance Anion-Exchange Chromatography coupled to Pulsed Amperometric Detection
HPLC	High Performance Liquid Chromatography
H_2SO_4	Sulfuric Acid
IN	Internode
KEGG	Kyoto Encyclopedia of Genes and Genomes library
KOH	Potassium hydroxide
Lc	Lacuna
LOX	Lipoxygenase
Man	Mannose
MEADE	Methacrylate Embedding & Acetone De-Embedding resin
mg	Milligram
$MgSO_4$	Magnesium sulphate
min	Minute
mL	Milliliter
MLG	Mixed-Linkage (1→3, 1→4)-β-Glucan
mM	Millimolar
MP	Milk Protein
MPa	Mega Pascal
mRNA	Messenger RNA
MS	Mechanical Stress

MSEA	Metabolite Set Enrichment Analysis
NaCl	Sodium chloride
NaOH	Sodium hydroxide
Na_2HPO_4	Disodium phosphate
nkat	nanokatal
NREL	National Renewable Energy Laboratory
P	Phloem
PAD	Pulsed Amperometric Detector
PBS	Phosphate Buffered Saline
p-CA	p-Coumaric Acid
PCA	Principal Component Analysis
PCR	Polymerase chain reaction
PEM	Buffer consists of PIPES, EGTA, and $MgSO_4$
PIPES	piperazine-N,N'-bis(2-ethanesulfonic acid)
PL	Path Length
PLS-DA	Partial Least Squares Discriminant Analysis
PME	Pectin Methylesterase
PMEI	Pectin Methylesterase Inhibitor
Py	Parenchyma cells
RG-I	Rhamnogalacturonan I
RG-II	Rhamnogalacturonan II
Rha	Rhamnose
RIL	Recombinant Inbred Line
R_{in}	Inner radius
RNA	Ribonucleic Acid
R_{out}	Outer radius
rpm	Revolutions per minute
RT-PCR	Real-Time Polymerase Chain Reaction
Rv	Reverse

s	Second
SD	Standard Deviation
SE	Standard Error
SEM	Scanning Electron Microscope
SF	Sclerenchyma Fibres
SYBR	Synergy Brands, Inc
TCH	Touch (inducible genes)
VB	Vascular Bundles
V_R	Reaction Volume
UV	Ultraviolet
v/v	Volume per volume
XP	Xylem Parenchyma Cells
XT	Xylem Tracheids
XV	Xylem Vessels
Xyl	Xylose
WS	Wind Stress
W_S	Sample Weight
w/v	Weight per volume
3PBT	Three-Point Bending Test
µg	Microgram
µl	Microliter
µM	Micromolar
δ	Deflection

CHAPTER 1

CHAPTER 1 : GENERAL INTRODUCTION

1.1. INTRODUCTION

The Earths' climate and the environment is constantly changing. Weather events such as droughts, heat, flooding, and storms, become more frequent and occur in places where not observed before. These events affect everyone and everything, including plants, which are unable to relocate if environmental conditions threaten their survival. Throughout the evolutionary process, plants had to evolve many adaptations, which help them to survive in various and changing conditions (Chehab *et al.*, 2009).

Plant response to abiotic stresses such as drought, flooding, cold, salt, heavy metals, light and air pollutants are extensively studied (Le Gall *et al.*, 2015), while data regarding plant response to mechanical stimulation is very limited leaving several important questions to address. How do plants adapt to windy environments, what is changing in their phenotypic traits, mechanical properties, composition, and architecture of cell wall, and what genes are responsible for particular responses?

Wind stress has a significant influence on phenotypic traits in plants such as architecture and morphology. The plant organ most affected by wind exposure is the stem, which gives the plant stability and provides a lever to hold the plant upright (Tripathi *et al.*, 2003). After wind exposure, stems usually become smaller, stiffer and wider (Onoda & Anten, 2011; Hamant, 2013), which completely change their mechanical properties. These changes in the stem are often accompanied by a reduction in leaf size, resulting in a decrease in total above-ground biomass (Kern *et al.*, 2005).

Plant cell walls are like to significantly contribute to the visible changes on the whole-plant level. Grass cell walls can be thought of as a highly organised composite, comprised of cellulose embedded in a range of matrix polysaccharides belonging to the group of hemicelluloses and pectins, structural proteins and phenolic compounds. Plants cell walls protect plants from biotic and abiotic stresses such as wind. In order to adapt to particular environmental conditions, cell walls can change their biochemistry, reorganise components and hence, architecture (Sarkar *et al.*, 2009). Moreover, they are responsible for the mechanical properties of the plant, such as strength and

extensibility (Ochoa-Villarreal *et al.*, 2012). Unfortunately, the relationship between cell wall components and stem strength is still not clear (Wang *et al.*, 2012).

Society benefits greatly from grasses. They comprise one of the primary sources of food for people and also for feeding animals (Vogel *et al.*, 2006). Additionally, grasses, including those classified as bioenergy plants, are a great biomass source for the production of renewable energy (Bevan *et al.*, 2010). In recent years, winds and storms have become more frequent and intense, affecting plants directly. Strong winds are responsible for lodging, which is defined by the displacement of stems or roots from their vertical and proper placement (Le Gall *et al.*, 2015). From an ecological, economic and agricultural point of view, this situation is alarming, especially with regard to cereal crops. It leads to a considerable reduction in yield, quality and harvesting efficiency (Kong *et al.*, 2013). The most significant consequence is a deterioration in the quality of the grain (Winzeler *et al.*, 1999). Cereal crops, including wheat, barley, triticale, and rice, represent the most important species in the grasses (Poaceae) for civilisation. The consequences of wind on cereal crops are therefore relevant to the issue of food security, one of the most important issues in this century mostly because of a constantly growing population in the world combined with projected climate changes.

Sometimes it is challenging to study a particular issue in every single species. That is the main reason why researchers are looking for model plants. Because of the close relation to cereals and extensive research infrastructure, *Brachypodium distachyon* has become a model species in genetic, cytogenetic and, perhaps most importantly, in abiotic stress studies for grasses (Catalan *et al.*, 2012).

Thus, this thesis seeks to develop further understanding of the response of *Brachypodium distachyon* stems to wind and mechanical stress, identifying phenotypic, anatomical, compositional, molecular and metabolic alterations caused by such stresses. Identified traits connected with plant response upon mechanical stimulation will improve our capacity to evaluate and predict the performance of *Brachypodium distachyon* in response to extreme environments. This knowledge is essential, especially considering *Brachypodium* as a model plant for the grasses family.

1.2. ABIOTIC STRESSES

Plants experience constantly changing environmental conditions throughout their life. In some environments, changes are extreme and can occur periodically or permanently, which pressure plants to evolve some ability to perceive, respond, and adapt to their environment, and the associated stresses that environment generates (Priest *et al.*, 2014; Asensi-Fabado *et al.*, 2017). Stress is defined by the altered physiological condition initiated by factors that tend to alter equilibrium. Environmental stresses elicit a wide variety of plant responses, ranging from altered gene expression and cellular metabolism to changes in growth rate and plant productivity (Shao *et al.*, 2008). They are considered as the major cause of plant damage and reduced crop yield (Gupta, 2014). Stresses can be divided into two major categories biotic and abiotic. Biotic stresses are caused by infectious living organisms such as bacteria, viruses, fungi, or nematodes, but also by pests and weeds (Le Gall *et al.*, 2015). Abiotic stresses includes extreme levels of light (high and low), radiation (UV-B and UV-A), temperature [high and low (chilling, freezing)], water (drought, flooding, and submergence), chemical factors (heavy metals and pH), salinity due to excessive Na+, deficiency or excess of essential nutrients, gaseous pollutants (ozone, sulphur dioxide), and other less frequently occurring stressors (Pereira, 2016). While the above stresses are intensively studied, there is relatively little research on plants response to abiotic stress caused by-mechanical stimulation.

1.2.1. THIGMOMORPHOGENESIS

Plants cannot relocate if environmental condition threatens their survival, so throughout the evolution, they had to evolve many response mechanisms to environmental stresses such as mechanical stimulation (Chehab *et al.*, 2009). Mechanical stimulation includes many factors including touching, rubbing by animals and plants, visitation of flowers by pollinators, vibrations, rain, trampling by people but also wind (Jaffe & Forbes, 1993). Plants respond to mechanical stimulation by modifying their growth, development and composition. This phenomenon is being recognised at least since Theophrastus (Jaffe & Forbes, 1993), and it is called thigmomorphogenesis

(thigma is the Greek word for touch) (Chehab *et al.*, 2009). The first use of this term has been attributed to Mark Jaffe to describe mechanically-induced responses in plants (Jaffe, 1973). The response of plants to mechanical stimulation may differ significantly depending on species, but also within species between different populations (Jaffe & Telewski, 1984; Bossdorf & Pigliucci, 2009) which may be explained by different plant architectures (Speck & Rowe, 2003).

Wind is perhaps the most common factor of mechanical stimulation throughout a plants' life. Wind can have substantial economic impacts on forests, urban trees and, perhaps most important, on crops. Extreme winds can lead to lodging in cereal crops and have become an important issue from the agronomical and economic point of view (Reynolds, 2008). Lodging is defined as the displacement of stems or roots from their vertical and proper placement (Le Gall *et al.*, 2015). Losses in crop yield in the UK caused by lodging can reach 25% in some years, and the financial loses per year has been estimated at £105 million for wheat alone (Baker *et al.*, 2014). Wind complexity makes it challenging to study; nevertheless, it is important to get a deeper insight into how plants react to such a factor.

Although the response of plants to mechanical stimulation has been studied, this aspect remains poorly understood. Nevertheless, for now, it is known that the most dramatic changes are connected with phenotypic, anatomical, histological and molecular features.

1.2.1.1. PHENOTYPIC RESPONSES

Morphological changes are not rapid and usually, occur slowly over time. However, the responses can be substantial (Braam, 2005; Chehab *et al.*, 2009). Plants exposed to mechanical stimulation display different growth compared with controls. The most visible effect of mechanical stimulation generated by brushing, flexing, vibrations, touching and wind is a reduction in size (Onoda & Anten, 2011), which was observed in many species including *Arabidopsis thaliana* (Chehab *et al.*, 2009), papaya seedlings (Clemente, 2001), *Liquidambar styraciflua*, maize (Neel & Harris, 1971) and also in *Arundo donax* (Speck, 2003).

Reduction in size may be caused by many factors observed to change after mechanical stimulation. A decrease in aboveground biomass is a frequently noted response to mechanical stimulation (Retuerto & Woodward, 1992; Goodman & Ennos, 1996; Henry & Thomas, 2002; Anten *et al.*, 2005, 2009; Kern *et al.*, 2005; Murren & Pigliucci, 2005; Bossdorf & Pigliucci, 2009; Zhao *et al.*, 2018). Moreover, mechanical stimulation significantly affects leaf morphology and anatomy. Leaves exposed to mechanical stimulation usually are shorter, narrower and became thicker (Grace & Russell, 1977; Niklas, 1996; Cleugh *et al.*, 1998; Pruyn *et al.*, 2000; Kern *et al.*, 2005; McArthur *et al.*, 2010). There are also suggestions that petioles undergo changes after mechanical stimulation, resulting in shorter and more flexible petioles (Liu *et al.*, 2007). Moreover, it was observed that mechanical stimulation affects photosynthesis. However, results are extremely variable. Generally, photosynthesis increases for plants exposed to low winds compared to plants growing in calm conditions (Smith & Ennos, 2003). Nevertheless, stronger winds may reduce photosynthesis. Furthermore, responses may be complex, for example, wind-exposure of *Cecropia schreberiana* has been reported to lead to a decrease of photosynthetic rate and respiration on an area basis, but not on a leaf-mass basis (Cordero, 1999).

Mechanical stimulation also affects the development and growth of roots and shoots. Plants seem to allocate more biomass into roots than shoots (Crook & Ennos, 1994; Goodman & Ennos, 1996; Clemente, 2001; Marler, 2011), which indicates that larger root systems increase the anchorage strength of plants thus preventing plants from being uprooted under mechanical stress (Goodman & Ennos, 1996). The increase in root growth and alterations in mechanical properties after mechanical stimulation was observed in sunflower and maize (Goodman & Ennos, 1996), wheat (Crook & Ennos, 1994) and papaya (Marler, 2011).

Alterations in stem diameter are one of the most frequently observed features after mechanical stimulation. Nevertheless, no clear pattern of response was found across plants. A number of studies showed an increase in stem diameter (Biro *et al.*, 1980; Hunt & Jaffe, 1980; Pruyn *et al.*, 2000; Anten *et al.*, 2005; Zhao *et al.*, 2018), but also decrease in stem diameter (Henry & Thomas, 2002; Smith & Ennos, 2003; Paul-Victor &

Rowe, 2011). There are also reports that stem diameter is not affected by mechanical stimulation (Goodman & Ennos, 1996; Bossdorf & Pigliucci, 2009). Moreover, it is suggested that even within species, the response in stem diameter to wind stress can vary (Murren & Pigliucci, 2005). All changes in stem diameter may be connected with anatomical changes in internal tissues such as the cortex and vascular bundles (Jaffe, 1973, 1980; Biro *et al.*, 1980; Kern *et al.*, 2005).

It has also been demonstrated that exposure to mechanical stimulation significantly affects reproduction in plants. Mechanical stimulation considerably delayed the onset of flowering in tobacco (Anten *et al.*, 2005), *Capsella bursa-pastoris* (Niklas, 1998), white mustard (Retuerto & Woodward, 1992), *Brassica napus* (Cipollini, 1999) and *Arabidopsis thaliana* (Bossdorf and Pigliucci, 2009; Johnson et al., 1998). Moreover, other processes involved in reproductive success were altered, such as delay in anthesis (Mitchell *et al.*, 1975; Akers & Mitchell, 1983), reduction in number of flower buds (Jaffe, 1973), reduction in seed number, seed weight and thus total yield (Niklas, 1998; Bossdorf & Pigliucci, 2009; Zhang *et al.*, 2013b).

It was reported that wind-induced mechanical stimulation on bean resulted inincreased resistance to pests, and increased resistance to at least one arthropod herbivore and one leaf pathogen. The author suggested that exposure of plants to natural environmental stresses (e.g. wind) activate a generalised stress response can influence interactions of those plants with other environmental stimulations (Cipollini, 1997).

Mechanical stimulation has a significant effect on the mechanical properties of the plant, primarily stems; however, no clear pattern in response was found. A majority of studies indicate that mechanical stimulation causes a reduction in stem stiffness (Pruyn *et al.*, 2000; Henry & Thomas, 2002; Anten *et al.*, 2009; Paul-Victor & Rowe, 2011), while others suggested that stems become more rigid (Goodman & Ennos, 1996). Thus, researchers created two theories presenting opposite plant response strategies, which both lead to an increase in the resistance of plants to mechanical failure. In the first one stems become either longer but more flexible (Cordero, 1999; Pruyn *et al.*, 2000; Anten *et al.*, 2005) while in the second strategy stems become shorter and more rigid and thus less prone to bending (Goodman & Ennos, 1996).

1.2.1.2. ANATOMICAL AND COMPOSITIONAL RESPONSES

Stem anatomy and cell wall composition are well-studied areas, especially in the grasses. Nevertheless, in terms of wind or mechanical stress, the knowledge in these areas is very limited. However, from a scientific point of view, it comes as no surprise to find that morphological changes may be preceded by compositional and anatomical changes. Indeed some compositional and anatomical changes caused by mechanical stimulation have been noticed.

Literature suggests that plants respond to wind by changing lignin accumulation; however, there is no clear consistency in the direction of the response. Increased lignin accumulation was observed in the wind stressed common beans compared with no controls (Cipollini, 1997). Moreover, an increase in lignin content and the number of lignified vessels was observed in *Bryonia dioica* internodes (De Jaegher *et al.*, 1985). On the other hand, a reduction in the density of lignified cells was observed in wind-exposed in *Arabidopsis* plants (Paul-Victor & Rowe, 2011). McArthur et al. noticed that total phenolic concentration was 7% higher in *Eucalyptus tereticornis* seedlings exposed to the chronic wind (McArthur *et al.*, 2010). Moreover, pectins have been implicated in playing an essential role in response to mechanical stimulation in *Arabidopsis* (Verhertbruggen *et al.*, 2013; Rigo, 2016). Researchers found that mechanical stimulation resulted in more abundant pectic galactan in the bottom part of the stem in the parenchyma cells of the pith (Rigo, 2016). Moreover, an increase in the abundance of unbranched (1$\rightarrow$5)-α-L-arabinan epitopes was detected in the epidermis of stress-treated Arabidopsis plants (Verhertbruggen *et al.*, 2013). It was also noted that homogalacturonan does not play a role in response to mechanical stress in *Arabidopsis* (Rigo, 2016).

Mechanical stimulation also affects anatomical and histological features. In dicot plants, research in terms of the effect of mechanical stimulation on plant anatomy and histology is far more detailed compared with studies on monocots. Nevertheless, it was reported that mechanical stimulation has a substantial influence on stem anatomy and geometry. *Arabidopsis* stems responded to mechanical stimulation by developing a lower and more central area of lignified interfascicular tissue, smaller pith, larger cortex

and epidermal tissue (Paul-Victor & Rowe, 2011; Rigo, 2016). On the other hand, pith cells increased in size and number in perturbed bean plants (Biro *et al.*, 1980). An increase in the diameter of cortical cells was also observed in runner bean (*Phaseolus multiflora),* broad bean *(Vicia faba)* (Bunning, 1941) and pea (Goeschl *et al.*, 1966). Generally, changes in the diameter of the cortical parenchyma cells and secondary xylem production accounted for most of the mechanical stress-induced changes in stem diameter (Goeschl *et al.*, 1966; Biro *et al.*, 1980; Biddington, 1986). It has been suggested that mechanical stimulation is positively correlated with the number and amount of vascular bundles in oats (Jellum, 1962) and tall fescue (Grace & Russell, 1977) and rice (Zhang *et al.*, 2013a). Additionally, the response to mechanical stimulation usually includes increased xylem production at the point of flexure (Jaffe, 1973, 1980; Hunt & Jaffe, 1980). Hepworth and Vincent suggested that the cylinder of xylem in the tobacco stems is the most important tissue which determines the stiffness of the whole plant; thus plants respond by increasing the thickness of the xylem tissue cylinder (Jaffe, 1973, 1980; Hunt & Jaffe, 1980; Hepworth & Vincent, 1999). Moreover, it has been suggested that mechanical stimulation affects cell wall thickness; however, the outcome is not very clear. Studies on *Arabidopsis* showed opposite results, one study showed thickening of cell walls (Rigo, 2016), while another study showed thinning of cell walls (Paul-Victor & Rowe, 2011). Thickening of the cell wall was also observed in celery (Venning, 1949; Walker, 1957) and tamarack (*Larix laricina*) (Biddington, 1986), while mechanical stress had no impact on cell wall thickness in tobacco (Hepworth & Vincent, 1999).

1.2.1.3. MOLECULAR RESPONSES

Mechanical stimulation such as touch, rain and wind can rapidly alter gene expression (Braam & Davis, 1990; Lee *et al.*, 2005). In *Arabidopsis,* touch-inducible genes (TCH) have been found to be elicited by the simple bending of the rosette leaves (Braam & Davis, 1990). Further studies on TCH genes in *Arabidopsis* showed that over 2.5% of genes are touch-inducible (Lee *et al.*, 2005). They discovered that genes encoding for Ca2+-binding proteins and cell wall-associated proteins were the most highly

represented functional classes of the touch-regulated genes. Additionally, they identified genes encoding for other putative Ca2+-binding proteins, arabinogalactan proteins, pectin esterases, cellulose synthases, expansins but also genes implicated in disease resistance such as peroxidases, kinases, and transcription factors (Lee *et al.*, 2005). However, there are four main TCH genes: TCH1 encodes one of the *Arabidopsis* calmodulins (CaM2) (Braam & Davis, 1990); TCH2 and TCH3 encode calmodulin-like proteins (CML24 and CML12, respectively) (Braam & Davis, 1990; McCormack & Braam, 2003), and TCH4 is a xyloglucan endotransglucosylase/hydrolase (XTH; XET) (Rose *et al.*, 2002). Unfortunately, little is known about TCH genes in grasses. Mauch *et al.* (1997) demonstrated that the wheat TaLOX1 gene, encoding a lipoxygenase, increases expression after mechanical and wind stimulation. The mechanical strain-regulated lipoxygenase might translate mechanical strain into lipoxygenase pathway-dependent growth responses (Mauch *et al.*, 1997).

1.3. THE GRASS CELL WALL

Cell walls play a very important role in plant growth and development. They are composed of several polymers, which give the whole plant specific features (Carpita, 1996). They determine the shapes of cells and organs and have remarkable mechanical properties to give plants strength and extensibility (Pilling & Höfte, 2003). Cell walls are involved in the response to biotic and abiotic stresses and play an essential role in stress sensing and signal transduction (Sarkar *et al.*, 2009; Seifert & Blaukopf, 2010). Additionally, cell walls from plants growing in stress environment undergo biochemical changes and reorganisation of components and hence, architecture, which allows the cell walls to adapt to particular conditions (Sarkar *et al.*, 2009).

Cell walls undergo many changes during their development. All cell walls in plants have their origin in dividing cells during cytokinesis, which mainly takes place in specialised regions called meristems. The new-born cells are covered by primary cell walls, which are thin, extensible and mechanically stable. These features of primary cell walls allow cells to expand without rupture under cell turgor pressure (Reiter, 2002). When the cells reach their final shape and size, and the processes of growth are finished, the cell walls are no longer extensible. Secondary cell walls, which are deposited between the primary cell wall and the plasma membrane, are a key factor in stiffening. Secondary cell walls are thicker than primary cell walls, making cells more stable, stiff and strong (Burgert, 2006).

1.3.1. STRUCTURE OF THE GRASS CELL WALLS

There is great diversity in the composition of cell walls depending on family, species, cell types or even over time during cellular differentiation (Carpita & Gibeaut, 1993). The main composition of all plant cell walls in flowering plants is similar, but they differ significantly in the number of particular polymers and their structural architecture (Fincher, 2009). Schematically, the construction of the cell wall can be visualised as an insoluble macromolecular network referred to as the wall matrix, comprising of cellulose and related polymers, of hemicelluloses, pectins, structural proteins and phenolic compounds (Rybka, 1993; Ochoa-Villarreal *et al.*, 2012).

Primary cell walls are divided into two groups. Those from dicots, noncommelinid monocots, and gymnosperms belong to type I cell walls, and they are characterised by cellulose fibres which are surrounded by xyloglucan, pectin and structural proteins (McCann & Carpita, 2008). Type II cell walls are found only in commelinoid monocots (grasses), are composed of cellulose fibres encased in glucuronoarabinoxylans (GAX), high levels of hydroxycinnamates, and low levels of pectin and structural proteins (Vogel, 2008). Additionally and specifically for the Poales members of the commelinid monocots, cell walls contain a special type of glucan hemicellulose, (1→3, 1→4)-β-glucan (MLG) (Carpita, 1996).

Compared to primary cell walls, secondary cell walls of grasses differ significantly in the abundance of the above components. Secondary cell walls are composed mainly of cellulose, xylans and lignin, and the amount of other components decrease significantly (Vogel, 2008). The characteristic thickness of secondary cell walls is caused by the massive deposition of cellulose and hemicelluloses inside primary walls (Le Gall *et al.*, 2015). When the secondary cell wall is forming, monolignols, which are precursors of lignin, are secreted into the cell wall space and randomly cross-linked through oxidative polymerisation (Le Gall *et al.*, 2015). The function of secondary cell walls is to provide structural support and integrity, to maintain the shape of the cell and to strengthen protection against biotic and abiotic factors (Pauly & Keegstra, 2010; Malinovsky *et al.*, 2014) (Table 1.1).

Table 1.1. Cell wall composition in grasses and dicots.

Approximate composition (% dry weight) of typical dicot and grass primary and secondary cell walls (Vogel, 2008).

	Primary wall		**Secondary wall**	
	Grass	**Dicot**	**Grass**	**Dicot**
Cellulose	20-30	15-30	35-45	45-50
Xylans	20-40	5	40-50	20-30
MLG	10-30	Absent	Minor	Absent
XyG	1-5	20-25	Minor	Minor
Mannans & glucomannans	Minor	5-10	Minor	3-5
Lignin	Minor	Minor	20	7-10
Ferulic acid & p-Coumaric acid	1-5	Minor	0.5-1.5	Minor
Pectins	5	20-35	0.1	0.1
Structural proteins	1	10	Minor	Minor

1.3.1.1. CELLULOSE

Cellulose is an abundant plant polymer, which provides tensile strength to the cell walls, and as a result, give support to the plant (Carpita, 1996; Ochoa-Villarreal *et al.*, 2012). This polymer is resistant to enzymatic attack, insoluble and highly crystalline (Ochoa-Villarreal *et al.*, 2012). Only small regions of cellulose are unorganised and create an amorphous form of cellulose, more susceptible to enzymatic degradation (Kumar *et al.*, 2009). A single cellulose chain has a linear structure built of repeated sequences of two glucose particles rotated relative to each other by 180° and stabilised by intramolecular hydrogen bonds and Van der Waals forces (Somerville, 2006). The chains of cellulose aggregate together to form bundles of about 40 cellulose chains, which are called microfibrils and have a tensile strength similar to steel. Microfibrils are organised in layers which are connected by polymers of hemicelluloses (Sarkar *et al.*, 2009) (Figure 1.1).

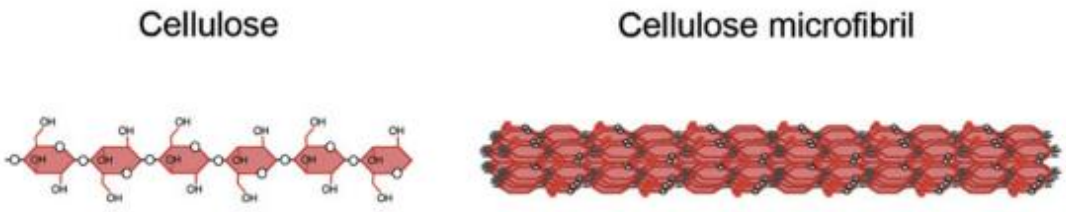

Figure 1.1. Chemical structure of cellulose and cellulose microfibrils.

Source: (Sarkar *et al.*, 2009).

1.3.1.2. HEMICELLULOSE

Hemicelluloses are the second most abundant group of polymers in grass cell walls, and they create a set of short branched β-1,4-linked polysaccharides with a degree of polymerisation of around 500 to 3000. Typical hemicelluloses are composed of a heterogeneous mix of hexoses (D-glucose, D-galactose, D-mannose), pentoses (D-xylose, L-arabinose) and sugar acids (D-glucuronic, D-galacturonic and methylgalacturonic acids) (Donohoe *et al.*, 2008; Limayem & Ricke, 2012). In contrast to cellulose, hemicellulose polymers do not form crystalline structures, and they are

easily hydrolyzable (Kumar *et al.*, 2009). In addition, they tend to form an association or strengthening network at specific junctions of the cellulose (Busse-Wicher *et al.*, 2014; Park & Cosgrove, 2015). Hemicellulose has various side chains, for example, glucogalactomannan is a mixed backbone of β-1,4-linked glucose and mannose with galactosyl side chains that make up the major hemicellulose in softwood species such as pine (Willför *et al.*, 2005).

Xylans are the dominant group of polysaccharides in grass cell walls; they comprise 20%-40% of the dry mass of the primary cell walls and 40%-50% of secondary cell walls (Vogel, 2008). Xylans are more complex than cellulose, as they consist of heteropolymers with (1→4)-β-xylan backbones substituted by arabinose (Ara) and glucuronic acid (GlcA) units, attached to some backbone xylose (Xyl) residues (Carpita, 1996), and are therefore named: arabinoxylan (AX) and glucuronoarabinoxylan (GAX). In the grasses, the major xylans are glucuronoarabinoxylan (GAX), which occupy a similar role in cell wall type II as xyloglucan (XyG) in cell wall type-I (Vogel, 2008). GAX is composed of a β1,4-linked xylose backbone with single arabinose and glucuronic acid side chains primarily attached at the O-3 and O-2 positions, respectively (Ebringerova *et al.*, 2005) and cross-links cellulose microfibrils and is therefore considered a linkage structure in cell walls architecture (McCann & Carpita, 2008). Additionally, Ferulic acid (FA) is attached to the arabinose side chains through various linkages (Vogel, 2008) (Figure 1.2).

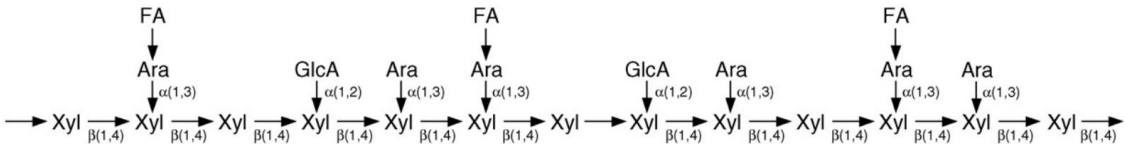

Figure 1.2. Chemical structure of glucuronoarabinoxylan (GAX).

Source: (Vogel, 2008).

Mixed-linkage glucan (MLG) is a linear polymer exclusive only for grasses cell walls, (Carpita *et al.*, 2001) which comprise of 20%-40% of the dry weight of primary cell walls (Vogel, 2008). MLG is an unbranched polymer of glucose, but its mixed linkage effectively results in distinct domains within the molecule composed of β-glucopyranosyl monomers linked by β-glycosidic linkages where most of these linkages are (1,4) and only one third are (1,3) (Gibeaut *et al.*, 2005; Kiemle *et al.*, 2014) (Figure 1.3). The structure, architecture and role of MLG are still poorly understood. However, it was suggested that MLG is linked to cellulose and arabinoxylan, forming a gel-like filler structure between cellulose and GAX (Kozlova *et al.*, 2014). Additionally, Kiemle et al. proposed that MLG acts as a gel-like matrix forming a thick hydrogel onto amorphous regenerated cellulose (Kiemle *et al.*, 2014). That formation provides flexibility, meanwhile strengthening the cell wall in growing tissues such as seedlings (Buckeridge et al. 2004; Vega-Sánchez et al. 2012). Moreover, MLG in the grasses is also thought to act also as storage carbohydrate because of its high concentration in the endosperm of grains (Buckeridge *et al.*, 2004) such as barley and *Brachypodium* (Roulin *et al.*, 2002; Wilson *et al.*, 2006; Guillon *et al.*, 2012).

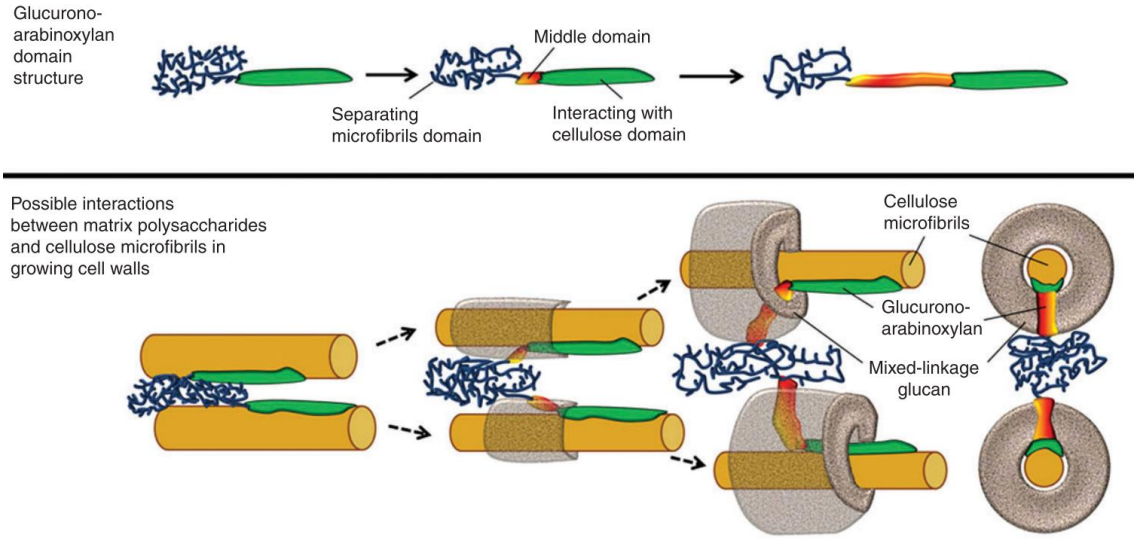

Figure 1.3. A gel-like matrix of MLG, cellulose and GAX.

Glucuronoarabinoxylan structure (top) and its arrangement in the cell walls in relation to mixed-linkage glucan and cellulose at different stages of cell development (Kozlova *et al.*, 2014).

XyG is much less abundant in grass cell walls than in dicots, comprise only 1-5% of grass cell walls (Vogel, 2008). XyG contains a β(1,4) linked glucose backbone substituted in a repeating pattern of four glucose units (Wilder & Albersheim, 1973). Up to 75% of these glucose residues are substituted at O6 with mono-, di-, or triglycosyl side chains, with xylose directly linked to glucose molecules (Carpita, 1996).

1.3.1.3. LIGNIN

Lignin is the most abundant component after cellulose in the plants (Boerjan *et al.*, 2003). In the primary cell walls of grasses, lignin is present in very low concentrations, but in secondary cell walls, it comprises approximately 20% of the dry mass (Vogel, 2008). Composition and content of lignin vary among plants and during development and growth (Chen *et al.*, 2002; Grabber *et al.*, 2004; Mattinen *et al.*, 2008). This polymer is essential for the structural integrity of cell walls (Boerjan *et al.*, 2003). Even though this polymer is much weaker than cellulose, lignin provides additional reinforcement resulting in increased tensile strength (Gibson, 2012; Barros *et al.*, 2015). Additionally, lignin is involved in defence reactions, e.g. during insect and microorganism attack, and water transport by crosslinking with cellulose and hemicellulose and increasing hydrophobicity (Holladay *et al.*, 2007).

Lignin is a polyaromatic and amorphous polymer with a complex chemical structure (Jongerius, 2013). Lignin at its most basic level is composed mostly of three phenolic monomers called monolignols: non-methoxylated p-coumaryl, monomethoxylated coniferyl alcohol and dimethoxylated sinapyl alcohol which respectively form H-(hydroxyphenyl), G-(guaicyl) and S-(syringyl) units in the lignin polymer (Limayem & Ricke, 2012; Barros *et al.*, 2015). The most common form of lignin in grasses is composed of G-(guaicyl) and S-(syringyl) while H-(hydroxyphenyl) units occur as a minor component of lignin (Grabber *et al.*, 2004; Sarkar *et al.*, 2009) (Figure 1.4). The monomers are linked by several types of linkages β-O-4, 5-5, β-5, 4-O-5, β-1, α-O-4 and β-β linkages, but linkage β-O-4 comprises more than half of all linkages which makes it the most abundant (Pandey & Kim, 2011). Aggregates of monolignols are created by several chemical bonds including ether, ester, phenyl and covalent bonds which gives

lignin rigidity, compactness but also fill the gaps in the cellulose-hemicellulose matrix (Boerjan *et al.*, 2003).

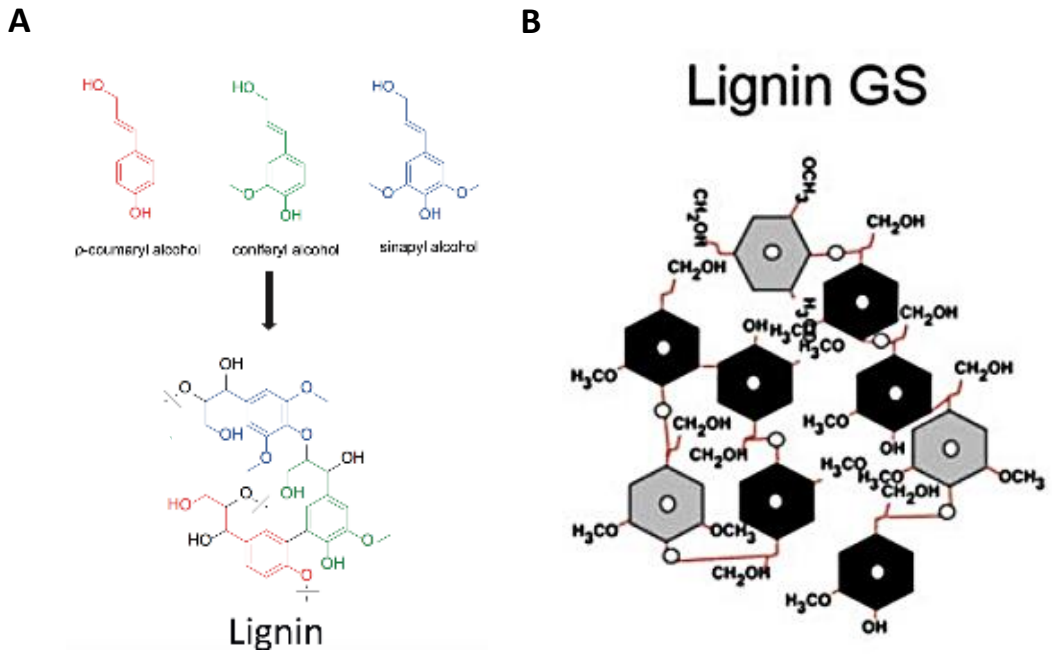

Figure 1.4. Lignin composition.

A. The three monolignols-lignin precursors: p-coumaryl alcohol, coniferyl alcohol and sinapyl alcohol (Jongerius, 2013); B. Lignin composed of G-(guaicyl) (black) and S-(syringyl) units (grey) (Sarkar *et al.*, 2009).

1.3.1.4. CELL WALL-BOUND HYDROXYCINNAMIC ACIDS

The grass cell walls contain two phenolic acids, both being hydroxycinnamates: ferulic acid (FA) and p-coumaric acid (*p*-CA) (Vogel, 2008). Interestingly, these two compounds probably play entirely different roles in grass cell walls. Arabinoxylans mainly attach FA in grasses by an ester linkage to the C5 carbon of arabinofuranosyl branches to the main xylan backbone. The dimerisation of such ferulate esters provides a pathway for cross-linking polysaccharide chains (Ralph *et al.*, 1994). Moreover, FA also binds to monolignols of the lignin polymer. This results in a highly cross-linked matrix involving both carbohydrates and lignin (Grabber *et al.*, 2004; Hatfield & Marita, 2010), which means that FA is involved in mechanical properties of cell walls such as giving strength to plants (Hatfield & Marita, 2010). Casler and Jung demonstrated that reduced content of FA in cell walls increased the digestibility of cell wall polysaccharides (Casler & Jung,

1999). Though present in substantial amounts, the function of *p*-CA in grass cell walls is less clear (Hatfield & Marita, 2010). It is proposed that *p*-CA remains unincorporated other than its attachment to monolignols via an ester linkage. Therefore, *p*-CA does not function as a cross-linking agent between wall matrix polymers, at least between different lignin polymers or between lignin and polysaccharides. It has been suggested that *p*-CA may function as a radical transfer agent to aid in the formation of sinapyl alcohol (SA) and lignin radicals so it may be involved in the lignification process (Hatfield *et al.*, 2008, 2009; Hatfield & Marita, 2010).

1.3.1.5. PECTINS

Although pectins are more abundant in type I cell walls; they are also found in grass cell walls (approximately 5% of the cell wall) (Carpita, 1996; Vogel, 2008). Pectins are the polysaccharides which are rich in α-galacturonate and mainly consist of three interconnected domains linked together by glycosidic bonds: homogalacturonan (HG), rhamnogalacturonan I (RG-I) and rhamnogalacturonan II (RG-II) (Caffall & Mohnen, 2009). Homogalacturonan (HG) frequently makes up the major portion of cell wall pectins (up to 60%) and is comprised of α-1,4-linked-D-galacturonic acid units (Caffall & Mohnen, 2009). HG is usually synthesised in a largely methyl-esterified form and regulation of methyl-esterification status is controlled by pectin methylesterases (PMEs), which catalyses the de-methyl esterification of the C6 linked methyl ester group of HG (Clausen *et al.*, 2003; Pelloux *et al.*, 2007; Mohnen, 2008; Verhertbruggen *et al.*, 2009a; Volpi *et al.*, 2011). Rhamnogalacturonan I (RG-I) is a heteropolymer of repeating (1→2)-α-L-rhamnosyl-(1→4)-α-D-GalA disaccharide units (Carpita, 1996). The structure of rhamnogalacturonan II (RG-II) is highly complex with 12 different types of glycosyl residues, including the rare sugar species 2-O-methyl xylose, 2-O-methyl fucose, 32 aceric acid, 33 2-keto-3-deoxy-D-lyxo heptulosaric acid (Dha), 34 and 2-keto-3-deoxy-D-manno octulosonic acid (Caffall & Mohnen, 2009) (Figure 1.5). These pectins are covalently crosslinked until digestion by pectin-degrading enzymes, which are required to isolate HG, RG-I, and RG-II from each other and cell walls (Mohnen, 2008). Pectins optimise the matrix for deposition, slippage and extension of the cellulosic-glycan network (Willats *et al.*, 2001).

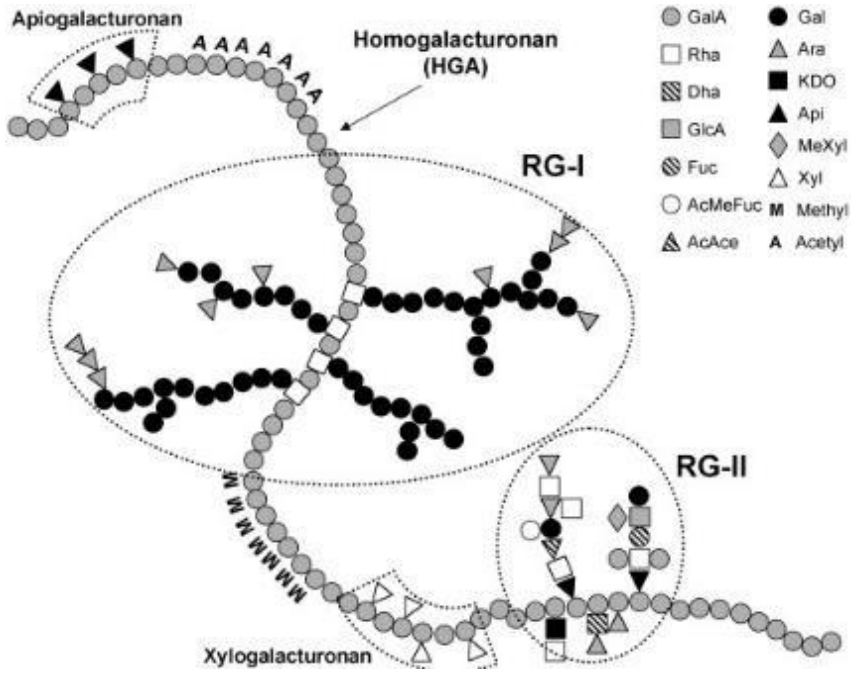

Figure 1.5. Schematic illustration of the primary structure of pectins.

Homogalacturonan (HG), Rhamnogalacturonan I (RG-I) and Rhamnogalacturonan II (RG-II) (Pérez *et al.*, 2003).

Pectins play a number of very important roles in growth, development, and structure of cell walls (Mohnen, 2008). Although they are structurally diverse, they contribute to primary wall functions with regard to cell strength, cell adhesion, stomatal function, and defence response (Caffall & Mohnen, 2009), wall porosity, binding of ions, growth factors and enzymes, pollen tube growth, seed hydration, leaf abscission, and fruit development (Mohnen, 2008). Additionally, it was reported that pectins play a significant role in response to stresses such as drought, cold, salt and heavy metals (Le Gall *et al.*, 2015).

1.3.1.6. STRUCTURAL PROTEINS

Cell wall proteins (CWP) are most abundant in type I cell walls, but they comprise about 1% of grasses cell walls (Vogel, 2008). They are mainly localised in specialised cells in the plants, e.g. in the xylem, epidermis, phloem (Showalter, 1993). Most of them are attached to polysaccharides, but they can also occur independently (Zhu *et al.*, 2006).

Grass structural proteins are divided into four main groups, hydroxyproline-rich glycoproteins (HRGPs), proline-rich proteins (PRP), glycine-rich proteins (GRPs) and arabinogalactan proteins (AGPs) (Carpita, 1996; Pilling & Höfte, 2003; Deepak *et al.*, 2010). HRGPs, due to their oxidative cross-linking property play an essential role in responses biotic and abiotic stress such as cold stress (Deepak *et al.*, 2010; Le Gall *et al.*, 2015). Glycine-rich proteins (GRPs) are a group of proteins which have cytosolic and cell-wall functions (Showalter, 1993). Arabinogalactan proteins (AGPs), seem to be a mediator in the interactions between cells and are also important in cell growth and development, cell division and differentiation and also in the strengthening of the cell wall (Majewska-Sawka & Nothnagel, 2000; Deepak *et al.*, 2010; Le Gall *et al.*, 2015). They are involved in preventing water loss during desiccation and response to cold stress and together with PRP and GPP are involved in salt tolerance.

1.4. *BRACHYPODIUM DISTACHYON*

Brachypodium distachyon, commonly called purple false brome, belongs to the tribe Brachypodieae, which consists solely of the genus *Brachypodium* (Bevan *et al.*, 2010). Various molecular phylogenetic analyses have demonstrated that the genus *Brachypodium* diverged from the ancestral stock of Pooideae immediately prior to the radiation of the modern "core pooids" (Triticeae, Bromeae, Poeae, and Aveneae); which includes the majority of important temperate cereals and forage grasses including wheat (*Triticum aestivum*), barley (*Hordeum vulgare*), rye (*Secale cereale*), triticale (*Triticosecale*) and oats (*Avena sativa*) (Draper *et al.*, 2001).

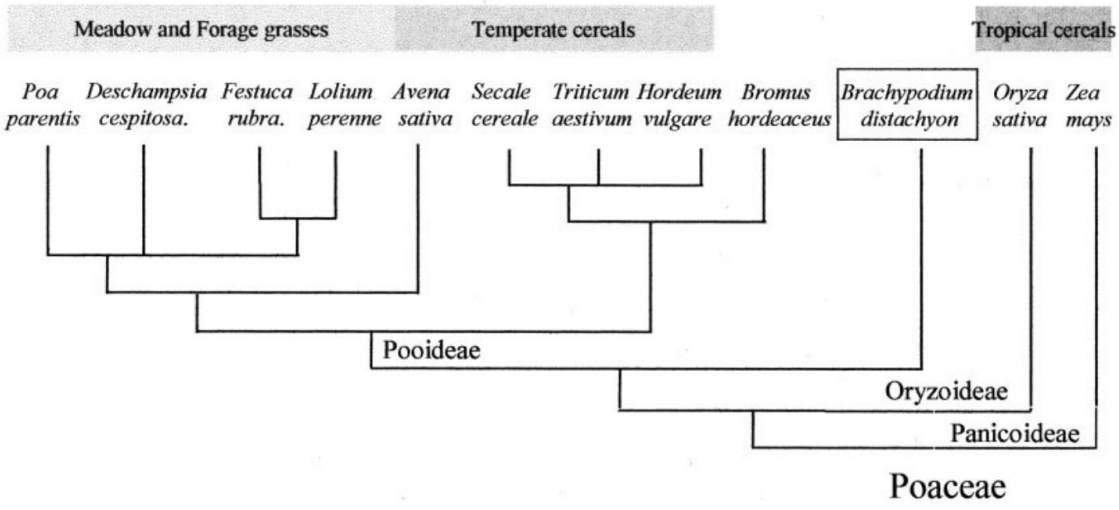

Figure 1.6. Schematic phylogenetic relationship of *Brachypodium distachyon* to other Poaceae.

Source: (Draper *et al.*, 2001).

The grass family (Poaceae) is one of the most important taxonomic groups within the kingdom of flowering plants with over 10,000 species (Kellogg, 1998). Representatives of this family are distributed on all continents and occupy nearly 1/3 of the Earth's surface creating a variety of vegetation formations, such as grasslands, savannahs, prairies and pampas (Frey, 2007). Due to the phenomenon of gene collinearity (synteny) in species closely related, there has been the possibility to introduce model organisms

with a relatively small genome and qualities conducive to research and breeding in the laboratory environment (Feuillet & Keller, 2002). The international scientific community currently accepts *Brachypodium distachyon* as a model for temperate cereals and forage grasses (Draper *et al.*, 2001; Hasterok *et al.*, 2004; Garvin *et al.*, 2008; Mur *et al.*, 2011). *Brachypodium distachyon* has been demonstrated to bea perfect model plant for studying abiotic and biotic stresses (Catalan *et al.*, 2014) such as cold, heat, salt, drought and flooding (Priest *et al.*, 2014). *Brachypodium distachyon* has also been used to study responses to pathogen attack in the Poaceae. The growing importance of renewable energy has led researches to learn more about genetic and molecular mechanisms which control traits such as cell wall composition and biomass yield (Bevan *et al.*, 2010).

The geographic range of natural occurrence of *Brachypodium distachyon* ranges in the circum-Mediterranean region, from the Macaronesian islands to central Asia, and from southern Europe to northern Africa and Ethiopia. It has been introduced and distributed in areas of central Europe, North and South America, Australia and South Africa (Garvin *et al.*, 2008; Catalan *et al.*, 2012). *Brachypodium* is widely adapted to many habitats, being able to survive at both high and low altitudes, explaining its tolerance to varying environmental conditions. However, most ecotypes prefer a dry environment, and they often grow in open areas, pastures and mountain regions, at an altitude of 300 to 1700 m above sea level (Catalan *et al.*, 2012).

1.4.1. MORPHOLOGY

Brachypodium distachyon is a monocotyledon plant. Depending on genotype, mature individuals are small-sized, mostly about 20 to 50 cm high and develop 1-8 reproductive tillers (Hong *et al.*, 2011). *Brachypodium distachyon* has two or three anthers. The number of flowers per spikelet also varies in *B. distachyon*. Although most spikelets have seven flowers, the number can be as few as five or as many as nine. There is a variation in the number of seeds per spikelet, although it typically contains around 7-10 seeds (Catalan *et al.*, 2012). *Brachypodium distachyon* grain is typical of the Poaceae family with a caryopsis size of 8mm by 2mm, and there is a lack of seed shattering (Draper *et al.*, 2001; Garvin *et al.*, 2008; Opanowicz *et al.*, 2008). Many accessions

require an extended period of cold (at least six weeks) to saturate their vernalisation requirement (Woods *et al.*, 2016).

1.4.2. LIFE CYCLE

Brachypodium distachyon is an annual plant with a short life cycle lasting from 7 to 12 weeks (Filiz *et al.*, 2014) and requires simple growing conditions (Draper *et al.*, 2001). *Brachypodium distachyon* initiates flowering around 35 days after sowing, and physiologically mature seeds are harvested at 70 days after sowing. The chronological progression of *Brachypodium distachyon* growth is split into 48 discrete growth stages. However, ten principal stages occur throughout plant development (Hong *et al.*, 2011) (Figure 1.7). Also, a very important feature is self-fertilisation, which allows the transmission of homozygosity to future generations (Draper *et al.*, 2001).

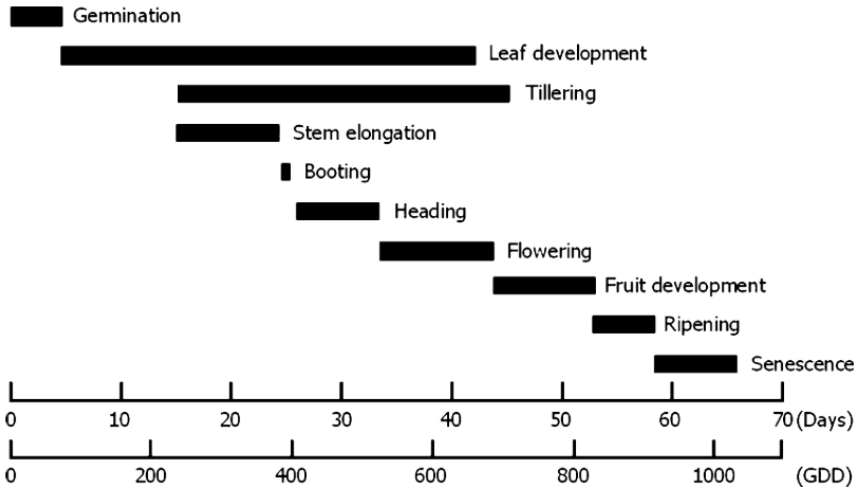

Figure 1.7. *Brachypodium distachyon* growth stages.

Scheme of the chronological progression of principal growth stages in *Brachypodium distachyon*. Horizontal bars indicate the periods of individual growth stages (Hong *et al.*, 2011).

1.4.3. CELL WALL COMPOSITION

The overall organ-specific cell wall composition of *Brachypodium distachyon* is similar in composition to other agronomical important species which belong to the C3 forage grass group including tall fescue (*Festuca arundinacea*), bromegrass (*Bromus inermis*), orchardgrass (*Dactylis glomerata),* reed canarygrass (*Phalaris arundinacea),* winter wheat (*Triticum aestivum*), and oats (*Avena sativa)* (Hatfield *et al.*, 2009; Rancour *et al.*, 2012). The difference in cell wall composition between *Brachypodium distachyon* and these species was found only in lignin and glucose concentration. More mature *Brachypodium* stem cell walls show a relative increase in glucose of 48% and a decrease in lignin of 36% compared to other grasses in this C3 group. This discrepancy may be explained by the relative small *Brachypodium* structure compared with other C3 grasses. As a result, *Brachypodium* may not need lignin to the same extent as the larger C3 grasses for structural support. Therefore, carbohydrate polymer replacement for lignin might be sufficient for it to reach its full developmental stature (Opanowicz *et al.*, 2008; Christensen *et al.*, 2010; Guillon *et al.*, 2012; Rancour *et al.*, 2012).

Generally, cell wall composition differs throughout development in all grasses, including *Brachypodium distachyon*. The difference can be found either between developmental stages, but also between plant organs (Carpita, 1996; Hatfield *et al.*, 2009). The overall characteristic of the cell wall in *Brachypodium distachyon* showed that on average (all developmental stages) cell walls are composed of about 52% of neutral sugars, 5.9% of uronosyls, 1.7% Phenolics, 11.2% lignin and 14.4% protein. The detailed analysis is shown in (Figure 1.8) based on (Rancour *et al.*, 2012). Neutral sugars in *Brachypodium* are divided in major sugars – glucose, xylose, arabinose and galactose, and minor sugars are rhamnose, mannose and fucose. The content of both major and minor sugars differs between developmental stage and organs (Table 1.2).

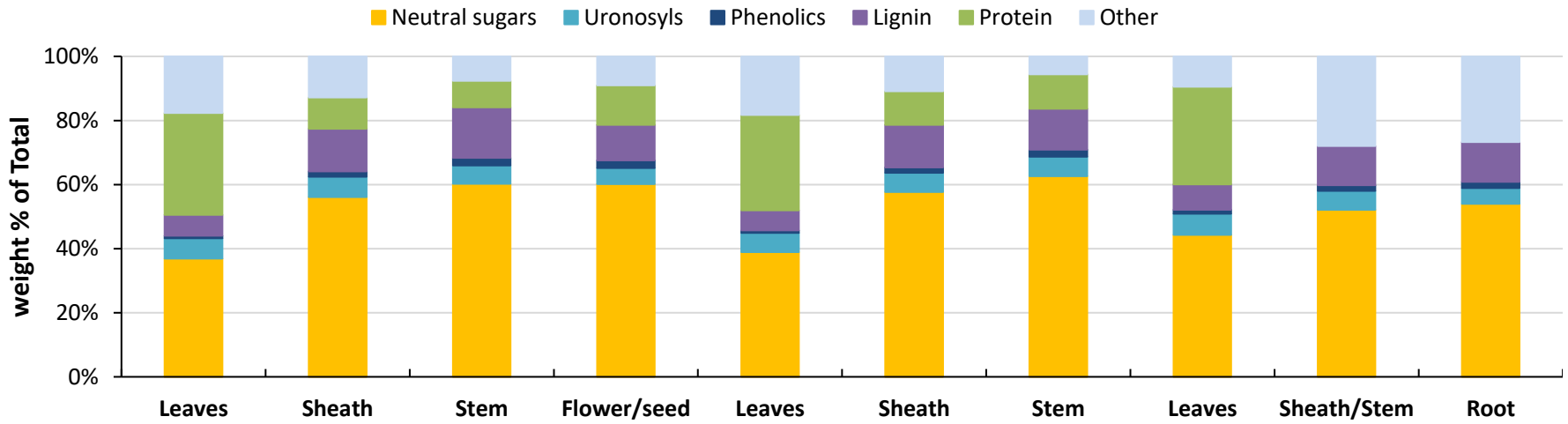

	Mature				Expanding			Seedling		
	Leaves	**Sheath**	**Stem**	**Flower/seed**	**Leaves**	**Sheath**	**Stem**	**Leaves**	**Sheath/Stem**	**Root**
Other	176.7	127.8	76.1	89.8	182.7	109	56.2	94.5	279.6	266.8
Protein	318.2	98.4	82.7	123.8	297.4	104.4	106.9	304.7	0	0
Lignin	64.8	132.9	157.6	110.7	62.5	132.9	127.8	79.2	122.6	124.6
Phenolics	8	16.8	24	24.1	7.7	16.9	22.5	12.5	17.6	19.4
Uronosyls	63.7	63.5	57.7	50.1	60.3	60.1	60.3	66.2	58.6	49.3
Neutral sugars	368.6	560.6	602	601.3	389.3	576.7	626.3	442.9	521.7	539.8

Figure 1.8. Contribution of *Brachypodium distachyon* cell wall components to the total cell wall composition.

The consolidation of cell wall weight percentages of neutral sugars (light blue), uronosyls (red), phenolics (yellow), lignin (purple), protein (green), and other (tan) to equal 100% is given for each tissue from each developmental stage. Numbers in table are in the units of mg/g cell wall. Source (Rancour *et al.*, 2012).

Table 1.2. The neutral sugar content of *Brachypodium distachyon* cell walls.

Neutral sugar content given in mg/g of cell wall ± standard deviation; averaged over two replicates, adapted from (Rancour *et al.*, 2012).

	Organ	Rhamnose	Fucose	Mannose	Galactose	Arabinose	Xylose	Glucose
Mature	Leaves	2.9 ± 0.3	0.6 ± 0.2	1.4 ± 0.2	6.1 ± 1.1	20.2 ± 2.4	96.9 ± 3.2	240.4 ± 15.8
	Sheath	2.9 ± 0	0.6 ± 0.1	2 ± 0.1	6.5 ± 0.8	33.5 ± 0.8	204 ± 1.3	311.1 ± 3.4
	Stem	2.7 ± 0.1	1.2 ± 0.1	1.8 ± 0.2	4.9 ± 0.3	24.7 ± 1.2	212.4 ± 6.3	354.3 ± 17.2
	Flowers/Seed	2.4 ± 0	0.6 ± 0.1	1.5 ± 0.2	5.4 ± 0.3	30.6 ± 0.6	245 ± 2.6	315.8 ± 9.4
Expanding	Leaves	2.8 ± 0.3	0.4 ± 0	1.5 ± 0.2	4.9 ± 0.4	20.8 ± 5.8	103.7 ± 33.8	255.2 ± 43.9
	Sheath	2.7 ± 0.1	0.6 ± 0.3	2.1 ± 0.3	6.9 ± 1.7	33.4 ± 4.6	213.7 ± 30.2	317.2 ± 35.5
	Stem	2.8 ± 0	0.7 ± 0.7	2.4 ± 0	6.3 ± 0.7	30.4 ± 1.4	236.1 ± 24.2	347.6 ± 22.1
Seedling	Leaves	2.9 ± 0	0.3 ± 0	2 ± 0.1	6 ± 1.8	29 ± 2.4	11.9 ± 7.2	293.8 ± 4.5
	Sheath/Seed	2.7 ± 0.1	0.4 ± 0	3.4 ± 0.1	15.7 ± 3.4	42.9 ± 0.4	159.5 ± 3	297 ± 4
	Root	2.7 ± 0.2	0.6 ± 0.1	4.1 ± 0.3	34.3 ± 1.8	46.2 ± 2.5	160.4 ± 2.7	291.6 ± 5

1.4.4. GENETICS

Brachypodium distachyon has one of the smallest grass nuclear genomes 272 Mbp/1C DNA, comprising mostly single- or low-copy repetitive DNA (Shi *et al.*, 1993; Garvin *et al.*, 2008; The International Brachypodium Initiative, 2010). *Brachypodium distachyon* is a diploid species with chromosome numbers of 10, 20, and 30 depending on ecotype (Draper *et al.*, 2001; Hasterok *et al.*, 2004, 2006). It was initially thought that a simple polyploid series cause increased chromosome numbers. Nevertheless, both 2n = 10 and 2n = 20 cytotypes appear to be diploids and the 2n = 30 cytotype seems to be an allotetraploid with genomes similar to those of the 2n = 10 and 2n = 20 cytotypes. As a model organism, 2n = 10 diploid cytotype is primarily being used (Hasterok *et al.*, 2004, 2006).

The broad genetic infrastructure for *Brachypodium distachyon* has been developed including BAC libraries (Huo *et al.*, 2006), BAC-end sequences (Huo *et al.*, 2008), EST libraries and sequences (Vogel *et al.*, 2006), physical maps (Gu *et al.*, 2009), germplasm collections (Mur *et al.*, 2011), genetic markers (Vogel *et al.*, 2009), sequence-indexed T-DNA populations, microarrays, conserved miRNAs and their targets (Unver & Budak, 2009) and most importantly, the complete genome sequence (The International Brachypodium Initiative, 2010).

1.5. AIMS AND OBJECTIVES

Various abiotic stress affecting plants growth and development have been intensively studied in past years, but relatively little research has been done in terms of mechanical stimulation. Nevertheless, the literature suggests, that after mechanical stimulation, plants undergo significant architectural changes across multiple scales, from the whole plant to organ, tissue and cellular level (Chehab *et al.*, 2009). Nonetheless, plant responses to mechanical stimulation focus on studies in dicots, while relatively little research has been done with monocots creating a gap in knowledge of how grasses respond to mechanical stimulation. Thus, this project aims to fulfil the lack of complete studies of the response to mechanical stimulation of the grasses family. This study presents the response to wind and mechanical stress of the model plant for grasses – *Brachypodium distachyon*.

It has been suggested that wind and mechanical stress such as brushing can lead to different plant response, so this study aims to establish if the responses vary between wind and mechanical stress. Moreover, it has been implicated that response can be different between species, but more importantly within species. This study provides a comparison of response between two ecotypes of *Brachypodium distachyon* Bd21 and ABR6, as Aberystwyth University has a recombinant inbred line (RIL) populations of these parents.

The main aim of this study is to characterise the response of *Brachypodium distachyon* stems to the wind and mechanical stress at various levels. In particular, this study focuses on the consequences of WS and MS on stem phenotypic traits, mechanical properties, cell wall composition and anatomy and molecular and metabolic responses. The first aim of this project is to determine if there are any differences in phenotypic traits between plants exposed to wind and mechanical stress compared with the control plant. Because of the importance of cell walls in response to abiotic stress, this project will also focus on the analysis of changes in cell wall composition and anatomy after WS/MS treatment. Modification in cell wall composition and anatomy may have a direct effect on stem mechanical properties; therefore, an attempt to provide reliable data in terms of how wind and mechanical stress influence mechanical properties will be made.

Collectively these experiments will help to characterise stem adaptations to mechanical stimulation and therefore will explain how the plant stem sustain their robustness to wind stress. Moreover, the knowledge gained on the effects of WS on stem cell wall composition and mechanical properties will apply to understand wind stress in an agricultural environment. The last part of this project will involve molecular analysis, including studies on changes of expression of potential TCH genes in grasses and cell wall-related genes upon WS/MS treatment. Moreover, the pathways involved in response to WS/MS will be identified.

Ultimately, the data generated in this project will contribute to the identification of traits favourable for growing plants in environments subject to severe wind.

The main objectives of this study are:

- To characterise the response of *Brachypodium distachyon* plants (Bd21 and ABR6) to wind and mechanical stress assessing phenotypic features such as: reproduction, changes in biomass weight, stem length, number of leaf, tillers and nodes.
- To asses mechanical properies of a stem after mechanical stimulation using the 3 point-bending test for Young's modulus calculations.
- To identify histological, anatomical and composiotonal changes that may occur after mechanical stimulation in stem tissue.
- To identify changes in cell wall composition of *Brachypodium* stems after mechanical stimulation including: lignin, monosaccharides, hydroxycinnamic acids content, and enzymatic sugar release.
- To develop an understanding of molecular response to mechanical stimulation in Brachypodium distachyon.
- To identify metabolite pathways involved in response to mechanical stimulation.

CHAPTER 2

CHAPTER 2 : MORPHOLOGICAL RESPONSE TO WIND AND MECHANICAL STRESS OF *BRACHYPODIUM DISTACHYON* STEMS

2.1. INTRODUCTION

In a plant's life, mechanical stimulation generated by direct interactions with animals, water, snow, insects, and flexure caused by wind is a very frequent event. To prevent potential damage caused by all these factors, plants have evolved many response mechanisms (Biddington, 1986; Bossdorf & Pigliucci, 2009). Developmental responses to mechanical stimulation have been termed thigmomorphogenesis (Jaffe, 1973). These morphogenetic changes occur slowly over time and are, therefore often not readily apparent; however, these responses can be quite dramatic (Braam, 2005). From an evolutionary point of view, thigmomorphogenesis is likely to have evolved as an adaptation for plants to survive in a windy environment and to cope with other forms of mechanical stress (Jaffe *et al.*, 2002; Pigliucci, 2002). There are also suggestions that plants respond differently to wind stress and to mechanical stimulation such as brushing and flexing, and these two factors should be treated separately (Henry & Thomas, 2002; Smith & Ennos, 2003; Anten *et al.*, 2010). Moreover, the differences in response could differ even within species (Bossdorf & Pigliucci, 2009), which is probably caused because of different mechanical plant architectures (Speck & Rowe, 2003).

Nevertheless, the most typical features of thigmomorphogenesis include a decrease in shoot elongation and a general reduction in size, thereby decreasing in total aboveground biomass and yield (Jaffe & Forbes, 1993; Speck, 2003; Chehab *et al.*, 2009; Onoda & Anten, 2011). Usually leaves become smaller and thinner (Grace & Russell, 1977; Niklas, 1996; Cleugh *et al.*, 1998; Telewski & Pruyn, 1998; McArthur *et al.*, 2010), and plants seem to allocate more biomass into roots than shoots (Goodman & Ennos 1996; Crook & Ennos 1994; Niklas 1996; Clemente 2001; Marler 2011; Niklas 1998), which indicates that larger root systems increase the anchorage strength of plants thus preventing plants from being uprooted under mechanical stress (Goodman & Ennos, 1996). There is no other clear response to mechanical stimulation in plant morphology. However, changes in traits such as stem diameter, tillering, and flowering time have

been mentioned (Retuerto & Woodward, 1992; Pruyn *et al.*, 2000; Murren & Pigliucci, 2005; Paul-Victor & Rowe, 2011).

Modification of mechanical properties of plant material after mechanical stimulation have also been described; however, there is no clear pattern of response. Researchers created two theories presenting opposite plant responses, which both led to an increase in the resistance of plants to mechanical failure. The first one is connected with developing more flexible and less rigid stems (Cordero 1999; Anten et al. 2005; Pruyn et al. 2000) while for the second strategy stems become more rigid and thus less prone to bending (Goodman & Ennos, 1996). Nevertheless, even proven theories do have their exceptions. One of the best ways to determine the mechanical properties of plant material such as stems is the use of the three-point bending test. It provides values for the modulus of elasticity, breaking stress and tensile strength (Jin *et al.*, 2009).

It is worth mentioning that although the thigmomorphogenesis response has been described for various species in the literature including herbs (Anten *et al.*, 2009), plants of medical importance (Anten *et al.*, 2010), trees (Cleugh *et al.*, 1998; Cordero, 1999; Kern *et al.*, 2005) and vegetables such as common bean and broccoli (Biro *et al.*, 1980; Latimer, 1990), relatively little research has been done on grasses or crops especially (Biddington & Dearman, 1985; Garner & Björkman, 1996). Cereals are the most important from an economic point of view (Vogel *et al.*, 2006; Bevan *et al.*, 2010). Moreover, there is very limited and research on model plants for grasses, while for a model plant outside the grass family, response to mechanical stimulation is broadly studied (Bossdorf & Pigliucci, 2009).

Therefore, the primary objective of this chapter was to compare phenotypic responses of *Brachypodium distachyon* to both wind stress and mechanical stimulation separately. Furthermore, the comparison of the reaction of two genotypes of *Brachypodium* (Bd21 and ABR6) was also included as these represent the parents of a recombinant inbred line (RIL) population available within IBERS. The selection of stems as material in this research is dictated by the fact that stems represent the plant organs most affected by wind exposure, as they give plants their stability and provide a lever to hold the plant upright (Tripathi *et al.*, 2003). Changes in the plants' phenotypic traits were assessed through a variety of physiological and growth measurements and observations taken

during a greenhouse experiment in which plants were exposed to controlled mechanical stimulation. Moreover, the mechanical properties of stems, as an important factor in plant responses to mechanical stimulation, were also considered in this chapter.

2.2. MATERIALS AND METHODS

2.2.1. *BRACHYPODIUM DISTACHYON* CULTIVATION

In this study, two accessions of *Brachypodium distachyon* were used: Bd21 and ABR6. Florets of both genotypes were peeled from the lemma and palea and transferred into 6-cm diameter pots with a mixture of 20% grit sand and 80% Levington F2 compost. Individual seeds were placed in 1cm deep holes covered lightly with soil so that the seed lies just below the surface of the soil, and then watered with water containing insect pest control (GNAT OFF, Fungus). Plants were germinated in controlled greenhouse conditions operating at 16 h/8 h (day/night), 20-21°C, (natural light supplemented with artificial light from 400-W sodium lamps) with 50%-60% relative humidity. Vernalisation was initiated 14 days after germination to synchronise plant development and to induce the flowering process. Plants were placed in a cold room set at 5°C with 16 h day length for seven weeks. During this process, plants were covered with plastic lids to minimise exposure to air movement or mechanical stress. Soil moisture was monitored weekly, and plants were watered when needed. After vernalisation, plants were transferred to the greenhouse in a strictly controlled and monitored environment operated at 16 h/8 h; 21-22°C/18-20°C day/night. To eliminate the influence of temperature and humidity on plant development between treatments, temperature and humidity were measured every five minutes throughout the experiment. Thirty or sixty plants (depending on the experiment, see details below) at a similar developmental stage for each genotype (Bd21, ABR6) were selected for the stress experiment.

2.2.2. STRESS EXPERIMENT DESIGN

Five independent experiments (Pilot plus four proper experiments) were carried out in a similar manner. Around 100 plants of each genotype per each experiment were sown to select plants at the same developmental stage. For the Pilot and first experiment, 30 from a total number of 100 plants from both genotypes were selected whereas for the rest of the experiments (second, third and fourth) 60 from 100 plants for both genotypes were selected. Three treatment groups were created for each experiment

for Bd21 and ABR6: control, wind stress (WS) and mechanical stress (MS). For the pilot and first experiment, groups were composed of 10 plants, whereas for the remaining experiments, groups were composed of 20 plants per treatment.

Bd21 stress treatments were initiated one day after the vernalisation process, while the stress treatments for ABR6 were initiated three weeks after the vernalisation process. The reason for this was the difference in plant development between the two genotypes. ABR6 started growing stems only three weeks after the transfer from the cold room to the greenhouse environment, while stem elongation for Bd21 had already begun before the vernalisation process and started to flower quickly following transfer from the cold room to greenhouse conditions. During this three-week period, all ABR6 plants were treated as control plants (described below). The duration of stress exposure was established at two weeks for all experiments.

Control treated plants were kept in calm conditions. Air movement or mechanical stress were eliminated by placing these plants in the calmer area of the greenhouse room and by surrounding them with a plastic wall no higher than the plants' height.

Wind stress was created by subjecting plants to the simulated wind produced by a velocity fan (Advent, AVAC 18x). Plants were placed in front of a fan at a mean distance of 1.5 m where wind speed reaches 2-3 m/s measured with an anemometer (Omega). In the natural environment, average wind speed 10-20 cm above the ground is 2-3 m/s (Bossdorf & Pigliucci, 2009), which would be relevant to small plants like *Brachypodium distachyon*. The wind exposure time was 8 h/day and plants were rotated daily to ensure that wind exposure was similar in all directions.

Mechanical stress was created by brushing plants at ¾ of the mean plant height (making sure the stems were bent no further than 45° from the vertical stem position) by the rapid front to back movements all around each stem. Plants were brushed for two periods per day lasting for about 3 minutes (first at 8 am, second at 6 pm). Each period consisted of 40 flexures, so at the end of the day, the plants were brushed 80 times – 40 times in each direction. This treatment was chosen as it simulates the mechanical effect of wind but with minimal air movement (Telewski & Pruyn, 1998; Paul-Victor &

Rowe, 2011). Between those two periods of stress induction, the mechanical stress group was treated the same as the control group.

2.2.3. PHENOTYPIC OBSERVATION

To determine phenotypic changes and differences between treatments, plant development parameters were taken every two days. This process started before stress initiation to make sure that all plants were at the same developmental stage. At the end of the experiment (after 14 days), final more detailed measurements and photographic documentation were taken, including tiller number, leaf number, number of nodes, water consumption, flowering time, stem length, internode length, and stem diameter (Figure 2.1).

After each experiment, stem material was collected for further analysis. Additionally, after the fourth greenhouse experiment, 5 plants per each treatment of both genotypes were left to reach full maturity, and measurements such as above-ground mass, yield, number and weight of seeds were noted and calculated. Seed weight measurements were determined for 25 seeds harvested from 5 plants (5 seeds from each replicate plant). Seeds were harvested from basal florets of spikelets from the main spike, and the lemma and palea were removed before weighing. For yield and a total number of seeds measurements, all seeds from the plant were collected (n=5) (Boden *et al.*, 2013). Above-ground biomass was oven dried to constant mass at 70°C.

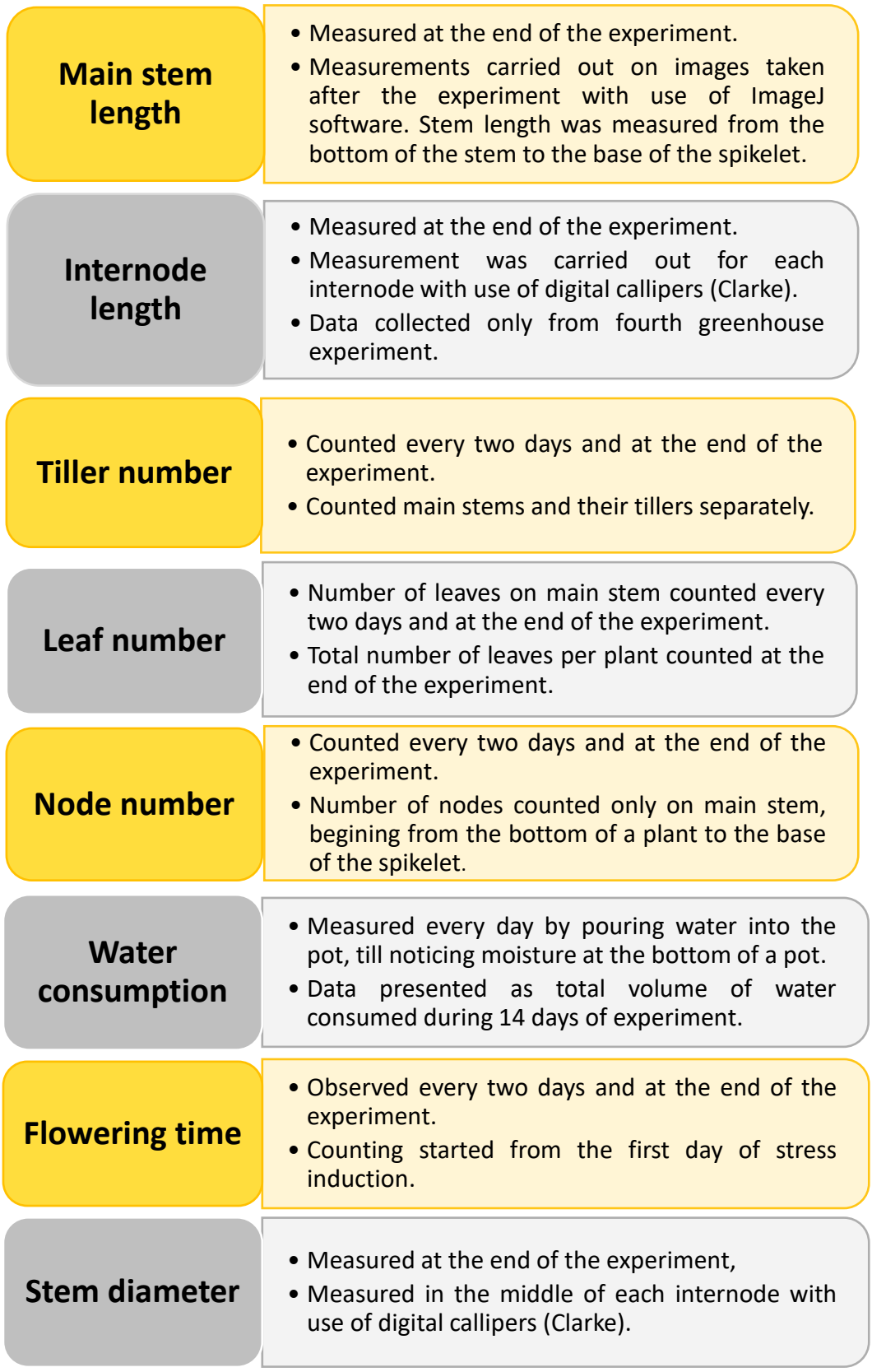

Figure 2.1. Methods used for characterisation of observed phenotypic traits.

2.2.4. MECHANICAL MEASUREMENTS

For the determination of mechanical properties of stems, the three-point bending test (3PBT) was selected following the procedure as described by (Anten *et al.*, 2009; Jin *et al.*, 2009) with some modifications. The three-point bending test was performed using a mechanical texture analyser (TA.XT plus, Stable Micro Systems) equipped with a 50N loading cell. 2.5cm long sections from the middle of the second and third internode were carefully cut with a razor blade without disruption of tissues. An internode section was placed horizontally over two supports positioned 2cm apart, and a vertical force was applied (Figure 2.2). For measurements on fresh tissue, ten plants from each treatment (control, WS, and MS) for both genotypes after the third greenhouse stress experiment were chosen. Measurements of senesced material were performed on five plants from each treatment (control, WS, and MS) after the third experiment. Second and third internode of the main stem (counted from the bottom) were selected as test material for 3PBT.

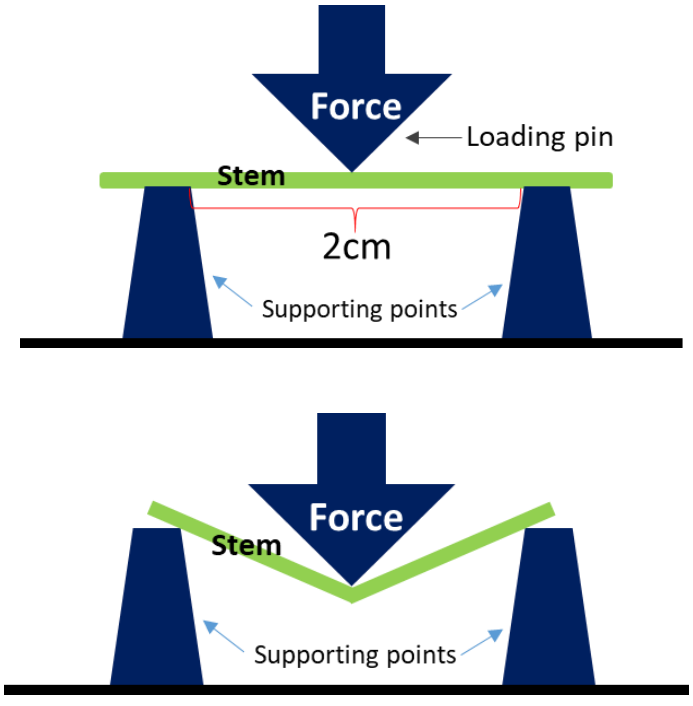

Figure 2.2. Stem under three-point bending test.

The instrument applied the vertical force automatically, and loading pin was stopped after stem rupture.

The load cell was attached to a crosshead located at the midpoint between the two metal supports and moved down at a speed of 15 mm/min. A force (F) and deflection (δ) graph were simultaneously recorded during the bending test with the use of Exponent-TEE32 software. The Young's modulus was calculated from initial linear slope of the force/deflection curve (Figure 2.3).

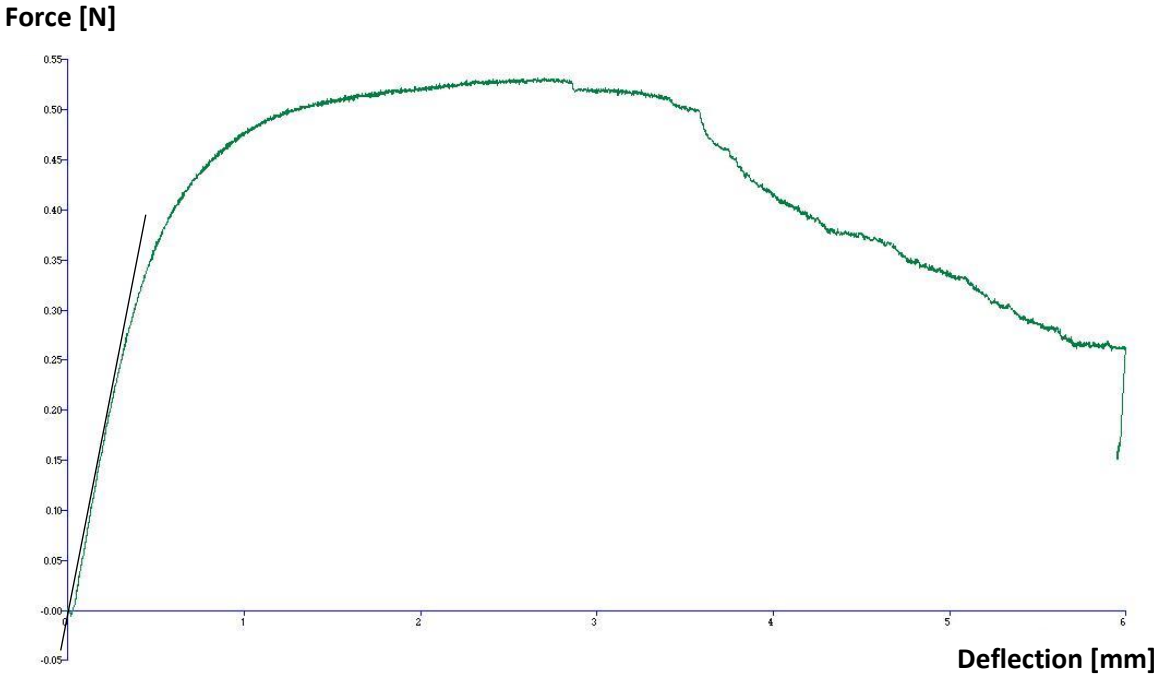

Figure 2.3. A force (F) and deflection (δ) graph.

Example of a graph generated by Exponent-TEE32 software showing stem rupture point (cross) and Force and deflection value.

The elastic modulus – Young's modulus (E) was determined from the force-displacement (F–δ) curve as:

$$\mathbf{E} = \frac{\mathbf{FL^3}}{\mathbf{48\delta I}} \qquad \left[\frac{\mathrm{N}}{\mathrm{mm^2}} = \mathrm{MPa}\right]$$

Where **L** is the length between the supports (mm), and **I** is the second moment of area (m^4). The cross-sectional dimensions of the stems were used to calculate **I**.

For senesced material the equation for the circle was used (Gere, 2004):

$$\boldsymbol{I = \frac{\pi r^4}{4}} \quad [\mathrm{mm}^4]$$

For fresh material, we also used the equation taking into account the fact that stems are hollow (Gere, 2004):

$$\mathbf{I = \frac{1}{4\pi}\left(R_{out}^4 - R_{in}^4\right)} \quad [\mathrm{mm}^4]$$

Where $\mathbf{R_{out}}$ is the outer radius of the stem and $\mathbf{R_{in}}$ is the radius of the internal hollow part.

2.2.5. STATISTICAL ANALYSIS

Measurements and calculations were performed on all plants (20 plants per treatment for both genotypes; 10 plants (fresh) and 5 plants (senesced) per treatment for 3PBT). All values are expressed as mean ±SD. All analyses were performed using SPSS software (version 24). Statistical differences were determined from ANOVA tests at the 5% level ($P \leq 0.05$) of significance, for all parameters evaluated. Where ANOVA indicated a significant difference, pair-wise comparison of means by Tukey's HSD (honestly significant difference) test was carried out at the 5% level ($P \leq 0.05$) of significance. If data did not meet the assumptions of ANOVA, a non-parametric Kruskal-Wallis test was performed at 5% level ($P \leq 0.05$) of significance.

2.3. RESULTS

The morphological measurements and the phenotypic and mechanical characterisation presented in this chapter are mostly analysed and described based on the results from the fourth greenhouse stress experiment. This is because experimental procedures have been further refined in the course of the different experiments; hence, experiment four represents the most robust dataset. There are also phenotypic traits such as internode length, total yield, aboveground mass, and seed weight for which data was collected and analysed only after the fourth greenhouse stress experiment. The three-point bending test was only performed on the third greenhouse stress experiment (Table 2.1). However, it is important to note that the observed differences in phenotypic traits as a result of the stress treatments were consistent across the different experiments and, where available, the data from the other experiments are also presented.

Table 2.1. Summary of all greenhouse stress experiments.

✓ Indicate that analysis was done on a particular experiment.

Trait	#1	#2	#3	#4
Tiller number	✓	✓	✓	✓
Nodes number	✓	✓	✓	✓
Leaves number	✓	✓	✓	✓
Water consumption	✓	✓	✓	✓
Flowering time	✓	✓	✓	✓
Stem diameter	✓	✓	✓	✓
Stem length	✓	✓	✓	✓
Internode length				✓
Above-ground mass				✓
Yield				✓
Seed weight				✓
Seed number				✓
3PBT			✓	

In the next subsections, results of phenotypic measurements and calculation taken during and after experiments will be presented.

2.3.1. PILOT EXPERIMENT

The purpose of the pilot experiment was to provide insight into the response of the *Brachypodium* plants to the wind and mechanical stress conditions for the chosen design of the greenhouse stress experiment. The knowledge gained from this experiment helped to improve the technical design and plant observation for the subsequent experiments. Furthermore, thanks to this experiment, I learned how to eliminate factors that can have a possible influence on plant development, such as temperature, air movement, sun exposition, etc. Treatments in this experiment were not appropriately separated; control plants experienced a little movement because of the closely placed fan. Moreover, control plants were placed near the heater, which could have an impact on the growth and development of the plants. Exposure to stress started for both genotypes one day after transferring plants from the vernalisation room to the greenhouse environment and lasted for two weeks. Plants were analysed in detail only after the experiment, which included tiller number, leaves on the main stem, the total number of leaves, number of nodes on the main stem, and stem length. Plants were also analysed before the experiment, which is essential for selecting plants for an experiment that are at the same developmental stage. Only flowering time was noted during the experiment. This experiment showed that ABR6 plants do not develop stems during vernalisation or ever during two weeks of treatment; thus, no data could be collected. I learned that ABR6 plants need precisely three weeks in the greenhouse environment to start producing stems after vernalisation, which helped me to design the next experiments. Treatments for Bd21 showed no significant difference in tiller number, leaves on the main stem, the total number of leaves, and the number of nodes on the main stem ($P \geq 0.05$). However, both stress treatments resulted in a significant reduction in stem length ($P \leq 0.05$) (Table 2.2) and flowering was delayed by two to four days (Figure 2.4).

Table 2.2. Phenotypic traits observed after a pilot experiment in Bd21 plants.

Results are based on measurements on ten biological replicates per each treatment (C, WS, and MS). Data presented as a mean with standard deviation (±SD). * Statistically significant difference from control, (Kruskal-Wallis test ($P \leq 0.05$); ANOVA test; $P \leq 0.05$).

Treatment	Tiller number	Leaves on the main stem	Leaves - total	Nodes on the main stem	Stem length (cm)
Control	4 ± 0.44	2.5 ± 0.5	12.4 ± 1.35	4.7 ± 0.46	21.61 ± 1.98
WS	4.2 ± 0.4	2.5 ± 0.5	12.3 ± 1	4.6 ± 0.49	11.53 ± 1.46*
MS	4 ± 0	2.4 ± 0.49	12.1 ± 0.83	4.6 ± 0.49	12.23 ± 1.02*

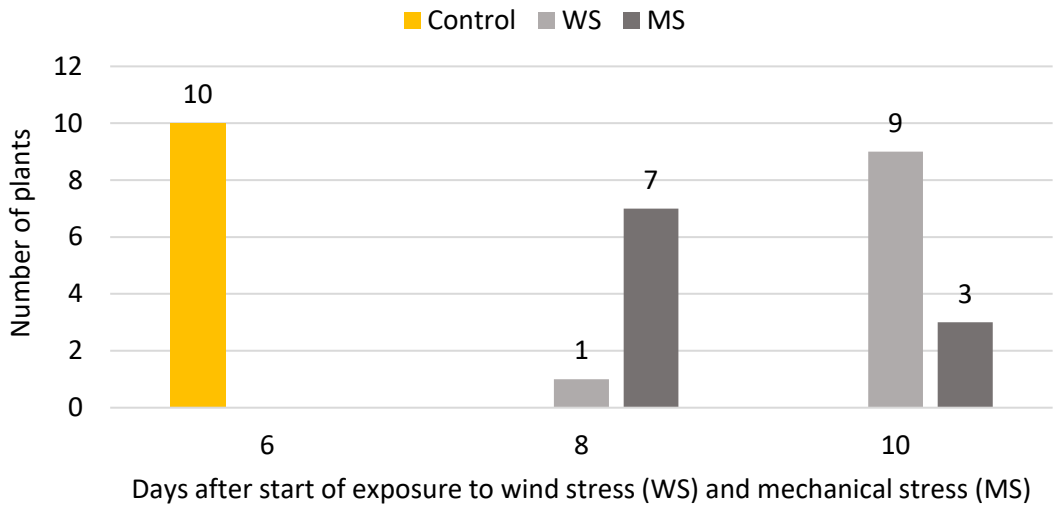

Figure 2.4. Flowering time for Bd21 plants during the pilot experiment.

2.3.2. TILLER NUMBER

The tiller number was counted every two days during the experiments and at the very end of the experiments (after 14 days of stress treatment). The results in Table 2.3 show the tiller number at the end of eachexperiment. Wind and mechanical stimulation did not significantly affect the tiller number for both Bd21 ($P = 0.580$) and ABR6 ($P = 0.899$) after the fourth experiment. Nevertheless, it should be noted that after the first experiment, a statistically significant ($P \leq 0.05$) increase in tiller number in WS treated plants were observed for Bd21 when compared with control plants. Furthermore, the second experiment revealed a significant ($P \leq 0.05$) increase in Bd21 tillering after WS

treatment compared with MS plants, while there was no difference compared with Bd21 control plants. Moreover, after the third experiment, opposite results were obtained, with WS Bd21 plants showing significantly ($P \leq 0.05$) less tillers than MS treated plants, and no difference compared with control (Table 2.3). Summarising the results from all experiments, there is no consistency in the stress-induced changes in tiller number for Bd21 plants, while data collected for ABR6 consistently show no effect on tiller number across all experiments performed.

Table 2.3. Tiller number after stress treatment for Bd21 and ABR6.

Data represent mean tiller number with standard deviation (±SD) of the mean for the four experiments (#1 and #2 (n=10); #3 and #4 (n=20). For statistical significance, the ANOVA test ($P \leq 0.05$) was performed, and if the test showed a significant difference, a post-hoc Tukey's test ($P \leq 0.05$) was also performed. * Statistically significant difference from control; * Statistically significant difference between WS and MS.

Genotype	Treatment	#1	#2	#3	#4
Bd21	Control	4.3 ± 0.46	6.6 ± 0.8	5.65 ± 1.24	3.25 ± 0.49
	WS	6.2 ± 0.75*	7.7 ± 1.01*	4.9 ± 1.09*	3.15 ± 0.48
	MS	5.4 ± 1.11	6.4 ± 0.66	6.35 ± 1.59	3.1 ± 0.43
ABR6	Control	7.7 ± 1.55	15.5 ± 5.46	11.9 ± 1.48	6.5 ± 1.19
	WS	8.8 ± 2.79	21.2 ± 3.89	11.4 ± 1.36	6.3 ± 1.53
	MS	7.9 ± 2.47	18.7 ± 4.73	11.4 ± 1.77	6.45 ± 1.41

2.3.3. LEAF NUMBER

2.3.3.1. NUMBER OF LEAVES ON THE MAIN STEM

Since the stress treatments can affect the main stem development and growth process, the leaf number on the main stem was determined. Leaf numbers were counted every two days during the experiment and at the end of the experiment. Since the set of data is not normally distributed, a non-parametric Kruskal-Wallis test was conducted. No statistically significant difference between treatments was found for Bd21 ($P = 0.465$) and for ABR6 ($P = 0.231$). The average number of leaves in the fourth experiment for

Bd21 control was 4.1 ± 0.48, for WS 4.15 ± 0.57 and MS 4.1 ± 0.44. ABR6 control plants had 5.3 ± 0.46 leaves on average, WS 5.1 ± 0.3 and MS 5.3 ± 0.46 (Table 2.4). Considering the results from all experiments for both genotypes, the WS and MS treatments had no effect on the number of leaves on the main stem.

Table 2.4. The number of leaves on the main stem for Bd21 and ABR6.

Data represent mean number of leaves on main stem with standard deviation (±SD) of the mean (#1 and #2 (n=10); #3 and #4 (n=20). For statistical significance, the non-parametric Kruskal-Wallis test ($P \leq 0.05$) was performed.

Genotype	Treatment	#1	#2	#3	#4
Bd21	Control	2.8 ± 0.6	2.1 ± 0.54	2.35 ± 0.47	4.1 ± 0.48
	WS	2.5 ± 0.5	2.1 ± 0.7	2.55 ± 0.36	4.15 ± 0.57
	MS	2.6 ± 0.66	2 ± 0.44	2.36 ± 0.79	4.1 ± 0.44
ABR6	Control	5.1 ± 0.3	6 ± 0	5 ± 0	5.3 ± 0.46
	WS	5 ± 0.45	5.9 ± 0.54	4.95 ± 0.49	5.1 ± 0.3
	MS	5.2 ± 0.4	5.6 ± 0.49	5.05 ± 0.22	5.3 ± 0.46

2.3.3.2. TOTAL NUMBER OF LEAVES

The total number of leaves was counted after 14 days of stress treatment. Similar to the results for the number of leaves on the main stem, no statistically significant differences were found between treatments in Bd21 ($P = 0.167$) and ABR6 ($P = 0.641$) genotypes. A general observation is that ABR6 plants developed many more leaves than Bd21 in all treatments (Table 2.5). This is probably because ABR6 produces much more stems than Bd21. Considering the results from all experiments for both genotypes stress treatments do not affect the total number of leaves.

Table 2.5. The total number of leaves after stress treatment for Bd21 and ABR6.

Data represent mean of total number of leaves with standard deviation (±SD) of the mean (#1 and #2 (n=10); #3 and #4 (n=20). For statistical significance, the ANOVA test ($P \leq 0.05$) was performed.

Genotype	Treatment	#1	#2	#3	#4
Bd21	Control	14.3 ± 1.1	16.3 ± 1.68	15.5 ± 2.46	13.95 ± 2.67
	WS	15.9 ± 2.02	16.9 ± 1.58	14.15 ± 2.39	12.85 ± 1.9
	MS	15.8 ± 2.27	16.3 ± 1.27	16 ± 3.21	12.95 ± 1.63
ABR6	Control	62.6 ± 10.27	97.5 ± 27.22	73.45 ± 7.92	45.15 ± 6.2
	WS	63.1 ± 15.88	127.4 ± 21.7	67 ± 9.28	45.85 ± 8.36
	MS	60.8 ± 11.6	115.9 ± 26.03	66.5 ± 10.47	47.35 ± 7.79

2.3.4. NODE NUMBER

The number of nodes was monitored every two days, and the results presented in Table 2.6 shows the number of nodes at the end of the each greenhouse experiments. Because the data did not meet the assumption for a parametric test, a non-parametric Kruskal-Wallis test was performed. There was no statistically significant difference between treatments in Bd21 ($P = 0.067$) and in ABR6 ($P = 0.112$). Control Bd21 plants developed on average 5.25 ± 0.43 nodes, WS plants 5.2 ± 0.4 and MS plants 5.3 ± 0.55. ABR6 plants developed more nodes in general than Bd21 plants; control plants produced on average 5.9 ± 0.3 nodes, WS 5.8 ± 0.41 and MS 5.9 ± 0.2 (Table 2.6). In conclusion, none of the stress treatments affected the node number of the main stem.

Table 2.6. Node number after stress treatment for Bd21 and ABR6.

Data represent mean node number on main stem with standard deviation (±SD) of the mean (#1 and #2 (n=10); #3 and #4 (n=20). For statistical significance, the non-parametric Kruskal-Wallis test ($P \leq 0.05$) was performed.

Genotype	Treatment	#1	#2	#3	#4
Bd21	Control	5 ± 0	5 ± 0	4.9 ± 0.3	5.25 ± 0.43
	WS	4.9 ± 0.3	4.7 ± 0.46	4.8 ± 0.4	5.2 ± 0.4
	MS	4.8 ± 0.4	4.8 ± 0.4	4.7 ± 0.46	5.3 ± 0.55
ABR6	Control	5.7 ± 0.46	6.2 ± 0.4	5 ± 0	5.9 ± 0.3
	WS	5.3 ± 0.46	5.8 ± 0.4	5 ± 0	5.8 ± 0.41
	MS	5.6 ± 0.66	5.9 ± 0.3	5 ± 0	5.9 ± 0.2

2.3.5. WATER CONSUMPTION

It is commonly believed that exposure to wind increases the transpiration rate from plant leaves (McVicar *et al.*, 2012). Indeed, water consumption was significantly affected by wind stress, but not by mechanical stimulation. The same response pattern was observed in both genotypes, where plants exposed to wind stress consumed much more water than control and MS plants. The results were consistent for the four greenhouse experiments; thus, the analysis was done based on the results from the fourth experiment and results for the other experiments can be found in Appendix 1. WS plants consumed about 15 mL more water per day for Bd21 and about 10 mL for ABR6 when compared with control and MS plants (Figure 2.5A). Hence, the total volume of consumed water throughout the experiment was significantly higher in WS plants for both genotypes (Figure 2.5B).

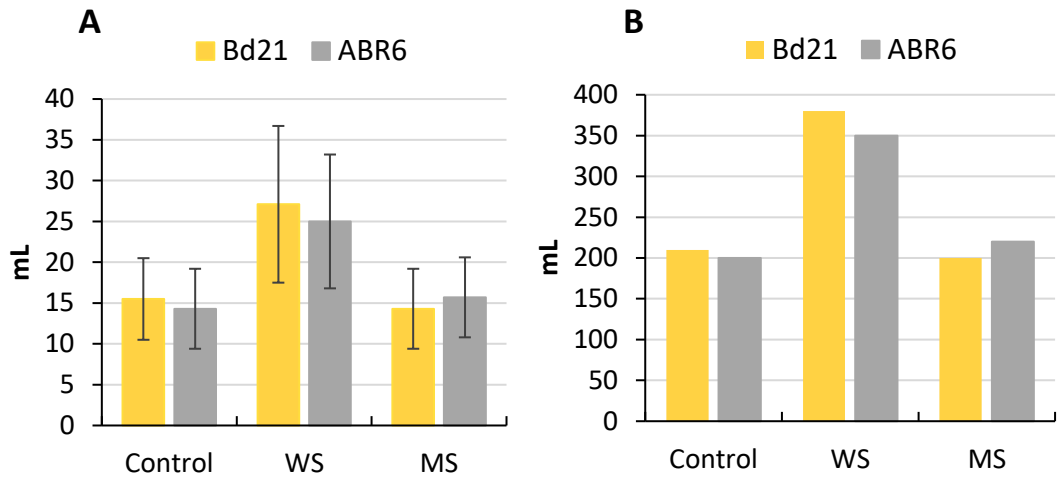

Figure 2.5. Water consumption

Figures present average of water intake (mL) per plant per day (A) and total water consumed per plant during the whole greenhouse stress experiment (14 days) (B).

2.3.6. FLOWERING TIME

Flowering time was counted from the first day of stress treatment. Both genotypes showed a significant delay in flowering time by both stress treatments. The results described below are based on the fourth greenhouse experiment (Figure 2.6). The flowering time results of the other experiments can be found in Appendix 2; the response pattern is the same for all conducted experiments. For Bd21, flowering time was delayed two to four days in WS and MS treated plants compared with Bd21 control, which mostly started flowering at day six from the beginning of the stress treatment. Some of WS and MS plants started flowering at day eight, but the majority of plants at day ten after initiation of the stress treatment (Figure 2.6A). The response pattern for ABR6 was similar to that of Bd21; however, in general, ABR6 plants started flowering two days later than Bd21 plants. Most of the ABR6 control plants started flowering on day eight from the beginning of the stress treatment. There were two to six days of delay in WS plants, the majority of plants flowering on the 12th day and only two plants flowering on the 14th day. In MS plants, flowering was delayed by two to six days compared with control, the majority started flowering on the 12th, and few plants began flowering on the 14th day (Figure 2.6B).

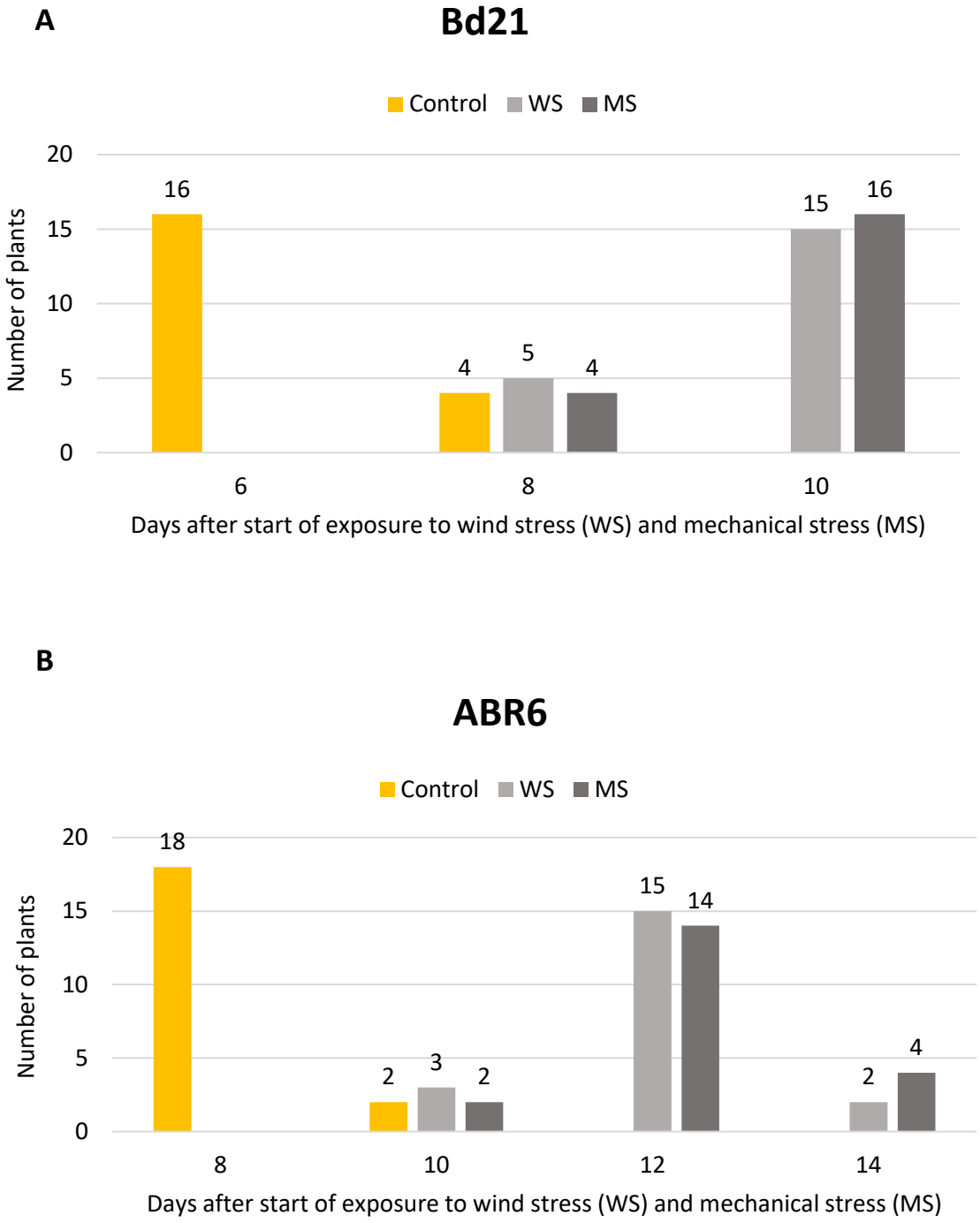

Figure 2.6. Flowering time.

Flowering time was monitored every other day during stress treatments. A. Bd21, B. ABR6.

2.3.7. STEM LENGTH

Stem length was measured at the end of the stress. The overall conclusion is that both stress treatments negatively affected stem elongation resulting in a shorter main stem when compared with control plants. Stem length measurements indicated a statistically significant reduction in WS and MS treated plants in both genotypes ($P \leq 0.05$). Bd21 plants exposed to WS and MS were about 17 cm shorter, reaching less than half the length of the control plants, which were 30.15 ± 1.88 cm long (Table 2.7, Figure 2.10A). Similar results were obtained for ABR6 plants, where WS plants were about 17 cm, and MS plants were 14.5 cm shorter than control plants which were 34.43 cm ± 1.09 long (Table 2.7, Figure 2.B).

Table 2.7. Stem length.

Data represent mean of stem length (cm) with standard deviation (±SD) of the mean for the four experiments (#1 and #2 (n=10); #3 and #4 (n=20). For statistical significance, the ANOVA test ($P \leq 0.05$) was performed, and if the test showed a significant difference, a post-hoc Tukey's test ($P \leq 0.05$) was also performed. * Statistically significant difference from control.

Genotype	Treatment	#1	#2	#3	#4
Bd21	Control	22.19 ± 1.35	23.77 ± 2.55	27.34 ± 2.04	30.15 ± 1.88
	WS	16.93 ± 1.85*	16.39 ± 2.23*	17.36 ± 2.02*	12.93 ± 0.67*
	MS	16.87 ± 2.05*	15.84 ± 2.12*	15.97 ± 1.18*	13.41 ± 1.04*
ABR6	Control	13.03 ± 2.05	19.56 ± 2.48	31.28 ± 3.4	34.43 ± 1.09
	WS	9.67 ± 1.27*	14.18 ± 2.07*	18.07 ± 1.7*	17.73 ± 1.19*
	MS	8.91 ± 1.27*	12.64 ± 1.26*	17.85 ± 1.81*	19.97 ± 0.98*

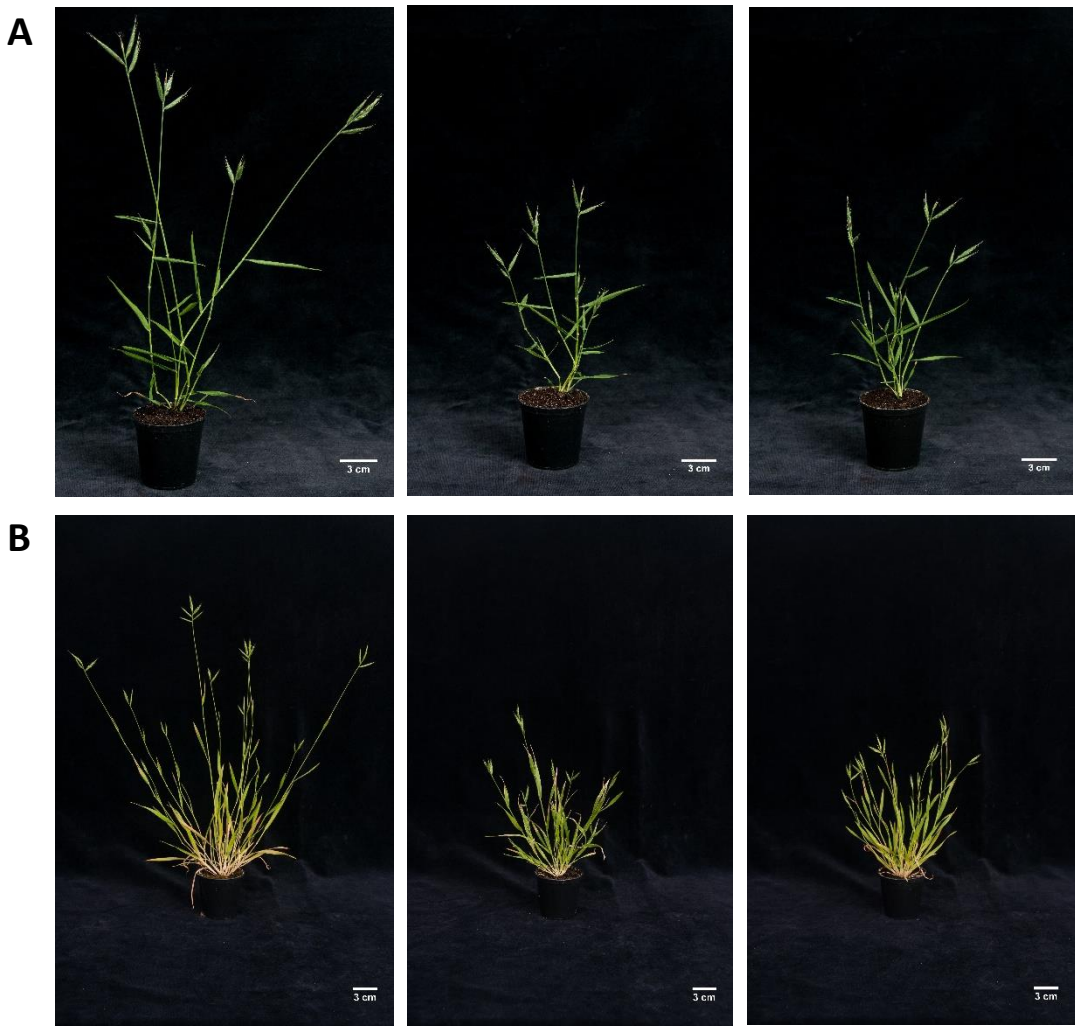

Figure 2.7. Images of A. Bd21 and B. ABR6 plants after treatment.

Images show representative plants for each treatment (control, WS, and MS) for both genotypes. Bar = 6 cm.

2.3.8. INTERNODE LENGTH

To investigate aspects that relate to the length of stems in more detail, measurements of internode (IN) length were performed after the stress treatments. Internode shortening was observed in three internodes: IN3, IN4, IN5 in stress-treated plants (WS and MS) of Bd21 genotype ($P \leq 0.05$), while no statistically significant differences in length of stems were observed in IN1 ($P = 0.181$) and IN2 ($P = 0.082$) between treatments. In ABR6 plants, a statistically significant reduction in internode length was

observed in all of the internodes in WS and MS plants compared with control ($P \leq 0.05$). Moreover, a statistically significant difference was also found in IN3, and IN6 between MS and WS stressed plants, both internodes being significantly shorter for WS compared with MS (Table 2.8). In conclusion, reduction of plant height after stress treatment was caused by a reduction in length of particular internodes for Bd21 while all internodes contributed to the height reduction in ABR6.

Table 2.8. Stress effect on internode length.

Data represent mean of internode length (cm) with standard deviation (±SD) of the mean (n=20). For statistical significance the ANOVA test ($P \leq 0.05$) was performed, and if the test showed a significant difference, a post-hoc Tukey's test ($P \leq 0.05$) was also performed. * Statistically significant difference from control; * Statistically significant difference between WS and MS.

Genotype	Internode	Control	WS	MS
Bd21	IN1	0.53 ± 0.12	0.52 ± 0.09	0.46 ± 0.1
	IN2	1.33 ± 0.59	1.67 ± 0.26	1.26 ± 0.51
	IN3	4.55 ± 0.65	2.8 ± 0.31*	3.09 ± 0.48*
	IN4	6.75 ± 1.09	3.4 ± 0.31*	3.65 ± 0.48*
	IN5	11.83 ± 0.08	4.26 ± 0.49*	4.94 ± 0.83*
ABR6	IN1	2.56 ± 0.81	1.23 ± 0.75*	0.79 ± 0.25*
	IN2	6.14 ± 0.95	4.03 ± 0.58*	3.74 ± 0.86*
	IN3	6.73 ± 0.82	3.59 ± 0.53**	4.81 ± 0.44**
	IN4	6.54 ± 0.74	3.67 ± 0.48*	3.79 ± 0.42*
	IN5	6.91 ± 1.59	3.56 ± 0.56*	3.48 ± 0.49*
	IN6	6.13 ± 0.78	2.53 ± 0.3**	3.35 ± 0.98**

2.3.9. STEM DIAMETER

Stem diameter was measured in the middle of every internode at the end of every experiment in both genotypes. Analysis of data is based on all four experiments because data was inconsistent across all experiments performed.

Stem diameter measurement in Bd21 revealed that there was no statistically significant difference ($P \geq 0.05$) in stem diameter in IN1, IN2, and IN4 in all four experiments. A significant difference ($P \leq 0.05$) was found in IN3 and IN5; however, that was observed only after the third greenhouse stress experiment, while in the other three experiments, no such change was found. Statistically significant ($P \leq 0.05$) thinning was observed after WS and MS treatment in IN3 and after WS in IN5. There was no indication in other experiments suggesting such a tendency of change in IN3 diameter after stress treatments. Moreover, in the first two experiments, an opposite trend was observed showing thickening of internode diameter; however, the difference is to slight to be confirmed statistically. In contrast to IN3, the thinning tendency after stress treatment was observed in IN5 in the other three experiments. A statistically significant difference ($P \leq 0.05$) was only observed after WS in the third experiment.

Results for ABR6 genotype are much more complicated and showing no consistency in most of internodes diameter across four experiments performed. The difference in diameter of IN1 was found only after the third greenhouse experiment ($P \leq 0.05$), and it showed thickening after MS treatment. No such trend was observed in other experiments. The diameter of the second internode and changes after stress treatments vary between all four experiments. Briefly, after the first and fourth experiment, stem thinning was observed in WS and MS plants, while after the second and third experiment, the opposite resulting in thickening of internode was observed. Data for IN3 and IN4 is more consistent across experiments performed compared with previous IN1 and IN2. Increase in IN3 diameter was observed almost in all experiments after WS and MS stress. Some of the differences are only a trend, but some are statistically significant ($P \leq 0.05$). Data for IN4 showed thinning in diameter after MS treatment across all experiments, while after WS treatment, mostly thinning was noted. Increase in diameter was observed after WS and MS treatments in IN5 in three of four experiments. Only the third experiment revealed the opposite trend for both stress

treatments resulting in a statistically significant decrease ($P \leq 0.05$) in diameter. In the last developed internode IN6, differences in diameter were also clearly visible. Plants during the third experiment did not grow IN6; therefore, analysis is based on data from only three other experiments. Results are consistent across all experiments performed and showed statistically significant ($P \leq 0.05$) increases in diameter after both WS and MS treatments.

Table 2.9. Internode diameter

Data represent mean of internode diameter (mm) IN1-IN6 with standard deviation (±SD) of the mean for both genotypes for all four experiments performed. For statistical significance ANOVA test ($P \leq 0.05$) was performed, and if the test showed a significant difference, a post-hoc Tukey's test ($P \leq 0.05$) was also performed. * Statistically significant difference from control; * Statistically significant difference between WS and MS.

		Bd21				ABR6			
		Control	**WS**	**MS**	***P* value**	**Control**	**WS**	**MS**	***P* value**
#1	IN1	0.725 ± 0.017	0.721± 0.022	0.719 ± 0.041	0.227	0.812 ± 0.009	0.814 ± 0.016	0.809 ± 0.02	0.782
	IN2	0.794 ± 0.04	0.799 ± 0.072	0.823 ± 0.046	0.456	0.801 ± 0.023	0.732 ± 0.019***	0.791 ± 0.021*	≤ 0.05
	IN3	0.934 ± 0.03	1.008 ± 0.061	0.99 ± 0.01	0.063	0.754 ± 0.027	0.77 ± 0.016	0.778 ± 0.015*	≤ 0.05
	IN4	1.045 ± 0.066	1.03 ± 0.089	0.982 ± 0.152	0.413	0.71 ± 0.016	0.754 ± 0.021***	0.665 ± 0.018***	≤ 0.05
	IN5	0.969 ± 0.072	0.962 ± 0.072	0.966 ± 0.075	0.982	0.67 ± 0.018	0.704 ± 0.014*	0.71 ± 0.027*	≤ 0.05
	IN6					0.556 ± 0.025	0.64 ± 0.01*	0.647 ± 0.013*	≤ 0.05
#2	IN1	0.728 ± 0.022	0.735 ± 0.031	0.746 ± 0.022	0.269	0.823 ± 0.033	0.811 ± 0.039	0.822 ± 0.013	0.630
	IN2	0.82 ± 0.065	0.842 ± 0.08	0.862 ± 0.062	0.411	0.804 ± 0.049	0.841 ± 0.036	0.818 ± 0.033	0.129
	IN3	0.877 ± 0.058	0.925 ± 0.083	0.927 ± 0.088	0.283	0.755 ± 0.036	0.771± 0.039	0.788 ± 0.022	0.081
	IN4	0.89 ± 0.047	0.88 ± 0.035	0.882 ± 0.017	0.881	0.705 ± 0.05	0.759 ± 0.053***	0.675 ± 0.031*	≤ 0.05
	IN5	0.882 ± 0.041	0.852 ± 0.035	0.861 ± 0.05	0.222	0.676 ± 0.044	0.736 ± 0.076	0.712 ± 0.048	0.085
	IN6					0.565 ± 0.049	0.664 ± 0.05*	0.656 ± 0.013*	≤ 0.05
#3	IN1	0.784 ± 0.023	0.785 ± 0.048	0.773 ± 0.026	0.471	0.791 ± 0.033	0.807 ± 0.039	0.822 ± 0.013*	≤ 0.05
	IN2	0.861 ± 0.034	0.863 ± 0.054	0.853 ± 0.034	0.750	0.848 ± 0.058	0.881 ± 0.038	0.905 ± 0.033*	≤ 0.05
	IN3	0.94 ± 0.044	0.908 ± 0.027*	0.896 ± 0.048*	≤ 0.05	0.873 ± 0.043	0.853 ± 0.049	0.846 ± 0.036	0.142
	IN4	0.928 ± 0.068	0.894 ± 0.048	0.891 ± 0.053	0.079	0.851 ± 0.052	0.773 ± 0.064*	0.797 ± 0.02*	≤ 0.05
	IN5	0.906 ± 0.084	0.843 ± 0.054*	0.854 ± 0.035	≤ 0.05	0.664 ± 0.047	0.66 ± 0.039	0.687 ± 0.048	0.127
#4	IN1	0.732 ± 0.005	0.736 ± 0.043	0.735 ± 0.035	0.124	0.812± 0.015	0.81 ± 0.018	0.813 ± 0.016	0.265
	IN2	0.833 ± 0.008	0.831 ± 0.007	0.833 ± 0.009	0.723	0.801 ± 0.014	0.812 ± 0.008	0.806 ± 0.012	0.247
	IN3	0.916 ± 0.017	0.919 ± 0.015	0.911 ± 0.014	0.255	0.760 ± 0.012	0.762 ± 0.012	0.77 ± 0.01*	≤ 0.05
	IN4	0.899 ± 0.016	0.901± 0.018	0.902 ± 0.016	0.856	0.708 ± 0.007	0.713 ± 0.011*	0.682 ± 0.017***	≤ 0.05
	IN5	0.853 ± 0.013	0.848 ± 0.01	0.851 ± 0.012	0.364	0.707 ± 0.018	0.728 ± 0.019*	0.733 ± 0.019*	≤ 0.05
	IN6					0.556 ± 0.015	0.642 ± 0.017***	0.652 ± 0.019***	≤ 0.05

2.3.10. ABOVEGROUND BIOMASS YIELD

To determine the effect of the stress treatments on aboveground biomass, the weight of mature plants (leaf and stem material, without heads) was measured (Table 2.10; n=5 per each treatment, both genotypes). Bd21 and ABR6 showed the same response pattern resulting in a statistically significant ($P \leq 0.05$) reduction of aboveground biomass after WS and MS treatment compared with control. In Bd21 the strongest response was caused by WS, where the WS weight (0.203 g ± 0.014) was reduced to almost half that of the control weight (0.371 g ± 0.022), and MS weight (0.224 g ± 0.011) was reduced by one-third that of the control weight. In ABR6, WS treatment similarly had the most potent effect (WS 0.429 g ± 0.013 versus control 0.655 ± 0.022); moreover, there was a statistically significant difference between the biomass yield in WS and MS treated ABR6 plants (0.429 ± 0.013 and 0.515 g ± 0.008, respectively) (Table 2.10).

Table 2.10. Stress effect on aboveground mass.

Data represent mean of aboveground biomass (g) with standard deviation (±SD) of the mean (n=5) for both genotypes. For statistical significance the ANOVA test ($P \leq 0.05$)was performed, and if the test showed difference, a post-hoc Tukey's test ($P \leq 0.05$) was also performed. * Statistically significant difference from control; * Statistically significant difference between WS and MS.

Treatment	Bd21	ABR6
Control	0.371 ± 0.022	0.655 ± 0.022
WS	0.203 ± 0.014*	0.429 ± 0.013**
MS	0.224 ± 0.011*	0.515 ± 0.008**

2.3.11. SEED YIELD, NUMBER, AND WEIGHT

To determine if seed yield, number, and weight were affected by WS and MS, five mature plants for each treatment after the fourth greenhouse experiment were analysed (Table 2.11).

The same pattern of response for both genotypes in seed yield was observed: a significant reduction ($P \leq 0.05$) after stress treatment (WS and MS) compared with control. In addition, a significant difference between WS and MS treatments was also observed ($P \leq 0.05$), with WS plants showing the strongest response in seed yield decrease (Table 2.11).

For seed weight, five seeds from the main tiller from five plants were weighed, and data was analysed (n=25). A significant decrease in seed weight in both genotypes was observed after both stress treatments compared with control ($P \leq 0.05$; Table 2.11), except for Bd21 MS plants where the observed decrease in seed weight was not statistically significant. Similarly, as with seed yield, the most significant reduction in seed weight was observed in WS treated plants, which for both genotypes was significantly lower compared with MS treated plants (Table 2.11).

Seed number was scored for five plants per each treatment; all seeds per plant were counted. Seed number was significantly reduced ($P \leq 0.05$) by both stresses for both genotypes compared with control. Generally, the response of plants exposed to WS was the strongest, especially in ABR6, where there was a statistically significant difference ($P \leq 0.05$) between WS and MS, while for Bd21 there was no significant difference between WS and MS (Table 2.11).

Table 2.11. Stress effect on yield, seed weight, and number

Data represent mean of seed yield (g), seed weight (mg) and seed number with standard deviation (±SD) of the mean (n=5; n=25; n=5) for both genotypes. For statistical significance the ANOVA test ($P \leq 0.05$) was performed, and if the test showed difference, a post-hoc Tukey's test ($P \leq 0.05$) was also performed. * Statistically significant difference from control; * Statistically significant difference between WS and MS.

Genotype	Treatment	Yield (g)	Seed weight (mg)	Seed number
Bd21	Control	0.215 ± 0.008	3.74 ± 0.03	57.6 ± 2.3
	WS	0.168 ± 0.004**	3.36 ± 0.02**	50.2 ± 1.2*
	MS	0.194 ± 0.009**	3.61 ± 0.02*	53.8 ± 2.2*
ABR6	Control	0.559 ± 0.023	3.44 ± 0.02	161.8 ± 5.4
	WS	0.349 ± 0.006**	2.85 ± 0.02**	123.2 ± 2.9**
	MS	0.459 ± 0.011**	2.99 ± 0.03**	153.6 ± 3.4**

2.3.12. MECHANICAL PROPERTIES

The mechanical properties of stems exposed to the stress treatments were evaluated with the three-point bending test, which generates data suitable for calculating Young's modulus. Ten biological replicates for fresh material measurements of each treatment for both genotypes were selected for the analysis, with the three-point bending test performed on the second and third internode of the main stem. Selected internodes were vertically stable, and none of them showed observable deformation, creep or failure. Similarly, to previous analyses, the mechanical tests also revealed differences in the response between treatments as well as between genotypes.

The analysis for Bd21 revealed that after stress treatments the second internode had a significantly ($P \leq 0.05$) higher Young's modulus compared with control plants (WS 1785 MPa, MS 1586 MPa, and control 1295 MPa); thus, the stress treatments made the second internode stiffer. Moreover, the response was significantly stronger in WS plants than in MS plants, which means that internode 2 in WS plants are more rigid than those from plants exposed to MS (Figure 2.8A). Wind and mechanical stress had no effect on

Young's modulus values of the third internode of Bd21 (P = 0.921) compared with control (Figure 2.8A).

Analysis of the mechanical properties of ABR6 stem material showed a statistically significant difference ($P \leq 0.05$) in Young's modulus in the second internode. Similarly, to Bd21, there was an increase in Young's modulus after WS (1739 MPa) and MS treatment (1867 MPa) compared with control (1560 MPa) (Figure 2.8B). Significant increase in Young's modulus in internode 3 was observed only after WS treatment (1890 MPa) compared with control (1691 MPa) with an upward tendency after MS (1765 MPa) (Figure 2.8B).

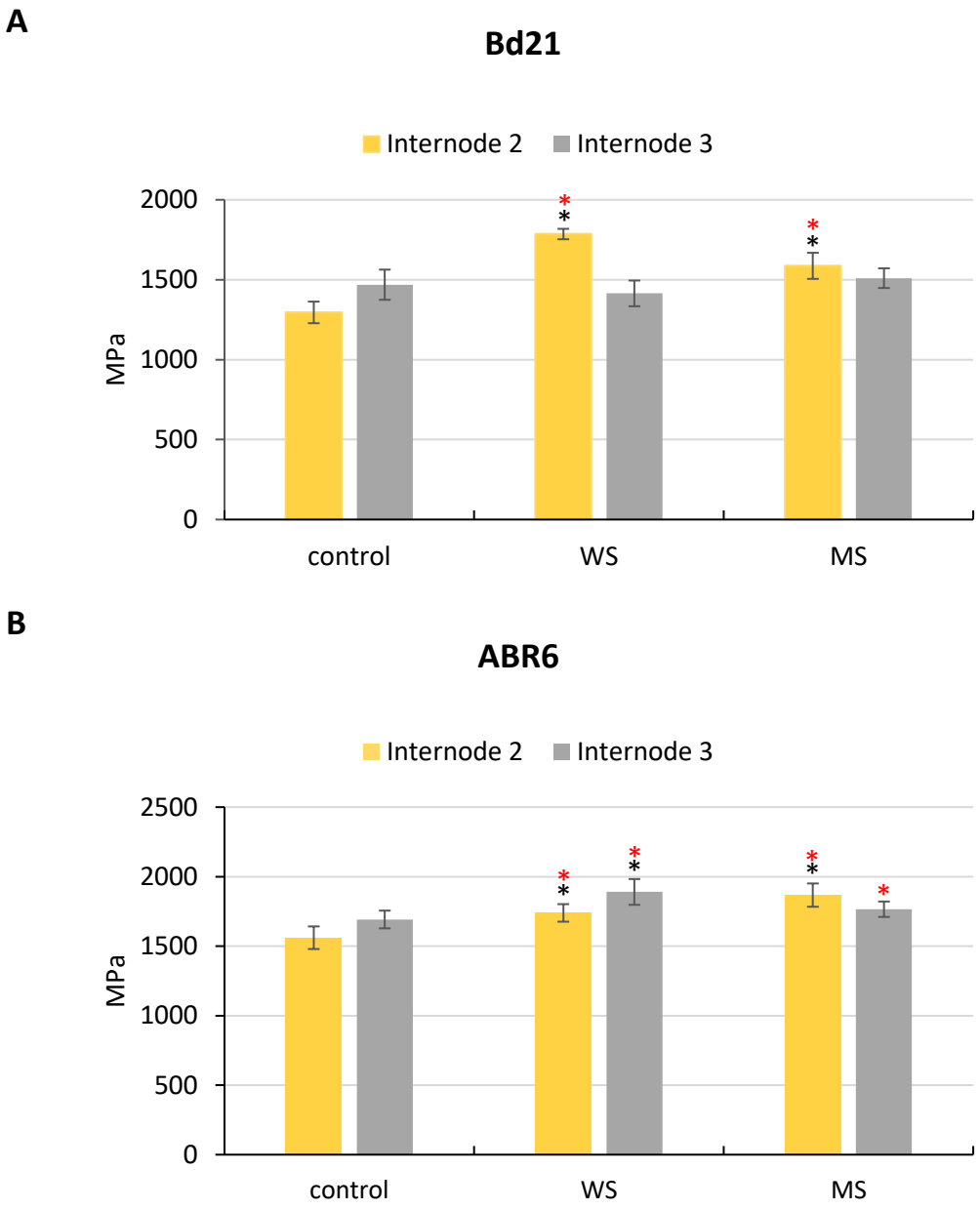

Figure 2.8. Mechanical properties of the stem – Young's modulus.

Data represent mean of Young's modulus (MPa) of the second and third internode with standard deviation (±SD) of the mean (n=10) for Bd21 (A) and ABR6 (B). Values are based on measurements on fresh material. For statistical significance the ANOVA test ($P \leq 0.05$) was performed, and if the test showed a significant difference, a post-hoc Tukey's test ($P \leq 0.05$) was also performed. * Statistically significant difference from control; * Statistically significant difference between WS and MS.

The mechanical properties of *Brachypodium* stems were also assessed on senesced material. Five biological replicates of each treatment for both genotypes were selected for the analysis, with the three-point bending test performed on the second and third internode of the main stem. Compared to results obtained after measurements performed on fresh material results obtained for senesced material were consistent across stress treatment but also genotype. Importantly all internodes ruptured during the 3PBT.

The analysis of both (IN2 and IN3) for Bd21 revealed significant ($P \leq 0.05$) increase in Young's modulus after both stresses compared with control plants. Moreover, for IN2 responses were stronger after MS; thus, the difference between WS and MS was noted (Table 2.12).

Similar response pattern was recorded for ABR6 genotype. Plants exposed to WS and MS showed significantly ($P \leq 0.05$) higher Young's modulus value in IN2 and IN3 compared with control. No differences between WS and MS was observed (Table 2.12).

Table 2.12. Mechanical properties of the stem – Young's modulus.

Data represent mean of Young's modulus (GPa) of the second and third internode with standard deviation (±SD) of the mean (n=5) for both genotypes. Values are based on measurements on senesced material. For statistical significance the ANOVA test ($P \leq 0.05$) was performed, and if the test showed a significant difference, a post-hoc Tukey's test ($P \leq 0.05$) was also performed. * Statistically significant difference from control; * Statistically significant difference between WS and MS.

Genotype	Treatment	IN2	IN3
Bd21	Control	8.67 ± 0.24	8.9 ± 0.53
	WS	9.91 ± 0.16**	10.2 ± 0.29*
	MS	10.29 ± 0.13**	9.96 ± 0.15*
ABR6	Control	10.38 ± 0.37	11.16 ± 0.1
	WS	11.36 ± 0.21*	12.05 ± 0.23*
	MS	11.8 ± 0.42*	12.04 ± 0.41*

2.4. DISCUSSION

Summarising the results obtained in this chapter, no profound differences between stress treatments (WS and MS) and genotypes (Bd21 and ABR6) at the phenotypic level was found. Such outcomes were expected based on the results presented by pioneers in this research area (Jaffe, 1980). Changes in growth and development allow plants to withstand and improve resistance to mechanical stimulation (Whitehead, 1963; Jaffe & Telewski, 1984; Biddington, 1986; Retuerto & Woodward, 1992). Despite that, there were also suggestions that WS and MS can have different effects on stems (Smith & Ennos, 2003) and leaves (Anten *et al.*, 2010) of the same species. Taking these facts into consideration and the general lack in the literature on comparing the effect of both stresses independently on the same species, it was worth examination of both stresses separately. It was also proposed that plants within the same species may respond differently regarding some phenotypical aspects (Murren & Pigliucci, 2005; Bossdorf & Pigliucci, 2009). However, in this study, no such differences were found; both WS and MS affected all of the observed and measured morphological traits in the same manner. Mechanical stimulation through wind and brushing significantly delayed the onset of the flowering of plants, and it reduced their overall growth and reproduction. The main differences compared with control were found in stem length, internode length, seed yield, seed number and weight, aboveground biomass and flowering time and Young's modulus.

It is worth mentioning that plants' phenotypic response to mechanical stimulation is broadly studied. However, there is very limited knowledge about the response of species that belong to the grass family. Moreover, research performed on such species is mostly very old, even in the review paper with the title "Direct mechanical effects of wind on crops" (Cleugh *et al.*, 1998) the majority of examples are dicot plants. Currently, very extensive research is carried out on grasses resistance to lodging, which is defined as the displacement of stems or roots from their vertical and proper placement caused partially by the wind. The wind range of analyses due to lodging resistance was done on barley (Berry *et al.*, 2006; Chen *et al.*, 2014), Miscanthus (Kaack & Schwarz, 2001; Kaack *et al.*, 2003), corn (Hondroyianni *et al.*, 2000; Robertson *et al.*, 2015), with the main focus on rice (Rani Sinniah *et al.*, 2012; Zhang *et al.*, 2016; Fan *et al.*, 2017) and wheat

(Wang *et al.*, 2012; Kong *et al.*, 2013; Peng *et al.*, 2014). Therefore, the discussion presented in this chapter is based on various species from different families response to wind and mechanical stimulation.

Reduction in stem height was the most marked phenotypic change observed after mechanical stimulation in this research by WS and MS. This concurs well with previous findings after mechanical stress generated by brushing, flexing, vibrations and touching (Biro *et al.*, 1980; Niklas, 1998; Telewski & Pruyn, 1998; Paul-Victor & Rowe, 2011; Verhertbruggen *et al.*, 2013) and after wind stress (Hunt & Jaffe, 1980; Retuerto & Woodward, 1992; Bossdorf & Pigliucci, 2009; McArthur *et al.*, 2010). Most importantly, reduction in stem height was observed in two varieties of wheat seedlings *(Triticum aestivum)* after mechanical stimulation. A variety with excellent resistance to lodging, responded to the treatment by a significant reduction, whereas a variety more susceptible to lodging, was not significantly reduced (Steucek & Gordon, 1975). Moreover, the same response was observed after stem rubbing of rice (*Oryza sativa*) (Zhao *et al.*, 2018). Even though most of the studies showed a reduction in stem height similarly as reported in this chapter, there are also reports that mechanical stress leads to a decrease and wind stress to an increase in stem height (Smith & Ennos, 2003). Generally, a taller stature will lead to lower mechanical stability unless it is associated with a concomitant increase in stem diameter, tissue strength, or tissue rigidity (Niklas, 1992). Also, a study performed on different species of *Brassica* led to the conclusion that wind stress affected each species differently, either resulting in an increase or decrease in stem length (Murren & Pigliucci, 2005). The difference in response may be caused by different growth pattern between species (Goodman & Ennos, 1996), but also wind speed is a very important factor with a direct phenotypic result. Such response after wind stress probably is connected with very low wind speed used in both studies, far below 2 m/s, which may not elicit a dramatic phenotypic response (Johnson et al., 1998; Pigliucci, 2002; Retuerto and Woodward, 1992). Another interesting factor, which affects a plant's response to mechanical stimulation is age. Specifically, young tissues show a stronger thigmomorpho-genetic response compared with older ones. The explanation for this is that young plants are more vulnerable to stresses, and thus, their response is more rapid and stronger for them to survive in tough environmental

conditions (Biddington, 1986). Generally, development of shorter stems is consistent with the concept that reduced height will limit the bending moment of the stem and lower the risk of a range of excessive mechanical strains, plastic deformation, uprooting, stem buckling and failure (Paul-Victor & Rowe, 2011).

Reduction in stem height was in strong correlation with a decrease in particular internode lengths which is consistent with previously reported data (Biro *et al.*, 1980; Cleugh *et al.*, 1998; Anten *et al.*, 2009). Moreover, the decrease in second internode length was observed after rubbing of rice stems; however, no differences were found in third and fourth internode compared with control (Zhao *et al.*, 2018). Nevertheless, the response observed in this study revealed the small difference between genotypes. After WS and MS in Bd21, a reduction in length was found only in IN3, IN4 and IN5, while in ABR6 all internodes were reduced in size compared with control. This dissimilarity is probably caused by differences in the development process between genotypes. Bd21 starts to develop stems from the beginning of growth, while ABR6 plants have a more 'bushy' phenotype and need vernalisation and then three weeks to start to develop stems. This means that Bd21 has more time to develop the first two internodes without the disruption caused by mechanical stimulation. ABR6 plants did not have this possibility, because the stress was applied just after stems started to develop.

Grass stems are composed of internodes, which are separated by nodes. An important query in this study was to determine if a reduction in node number accompanied the stress-induced a reduction in stem height. However, this phenotypic trait was not affected in both genotypes after mechanical stimulation. There is not much evidence in the literature on mechanical stimulation inducing changes in the number of nodes/internodes and most of them performed on dicots. Stem anatomy in monocots and dicots differ significantly; however both are based on phytomers. Mechanical stimulation had significant effect on node and internodes in dicots, for instance, a study performed on *Impatiens capensis* (jewelweed) showed no change in node number, resulting in the conclusion that node number is not affected after mechanical stimulation (Anten *et al.*, 2009). This is in contradiction to a very early study done on the tree *Liquidambar* (sweetgum), where a decrease in node number was observed

(Neel & Harris, 1971). Results presented in this study suggests that there is no correlation between a reduction in stem height and internodes length with node number. Unfortunately, no studies were done previously, including analysis of this trait in any species of the grass family.

Measurements of stem diameter in this study revealed no clear pattern of response to mechanical stimulation. Generally, Bd21 showed no differences in stem diameter across all experiments performed, with minor variations. Whereas the response for ABR6 was variable depending on the experiment, treatment and internode; however, no conclusive pattern of decrease or increase in stem diameter could be observed. Only IN6 of ABR6 plant showed an increase in diameter across all experiments (when present) after WS as well as after MS. These results show many similarities with those from previous studies. No clear consistency of response pattern related to stem diameter was found for wind stress across various species, but responses observed after mechanical stress are mostly consistent. Thus, it seems that there could be a difference in response to wind and mechanical stress in what concerns stem diameter (Smith & Ennos, 2003), however, in this study no confirmation for that conclusion was found. A number of studies showed an increase in stem diameter after mechanical stress such as in rice (Zhao *et al.*, 2018) and dicots plants (Biro *et al.*, 1980; Telewski & Pruyn, 1998; Pruyn *et al.*, 2000; Anten *et al.*, 2005, 2009; Kern *et al.*, 2005) or no difference (Goodman & Ennos, 1996), with little evidence for a decrease in stem diameter (Paul-Victor & Rowe, 2011). The stem diameter response to wind stress varies depending on species, a reduction in stem diameter was found in *Abutilon theophrasti* (velvetleaf) (Henry & Thomas, 2002) and *Helianthus annuus* (sunflower) (Smith & Ennos, 2003) and an increase in *Phaseolus vulgaris* (common bean) (Hunt & Jaffe, 1980), while no differences were found in *Arabidopsis* (Bossdorf & Pigliucci, 2009). Moreover, it is suggested that even within species, the response in stem diameter to wind stress can vary (Murren & Pigliucci, 2005). All changes in stem diameter may be connected with anatomical changes in internal tissues such as the cortex and vascular bundles (Jaffe, 1973, 1980; Biro *et al.*, 1980; Kern *et al.*, 2005) (see chapter 3).

Tiller number is one of the phenotypic traits that can be affected by mechanical stimulation. Though in this study, this feature was not affected by stress treatment in

both genotypes. Depending on the experiment, some tendencies were visible; however, some of them were contradictory to each other. Interestingly, the most significant variation was observed after WS compared with control but also to MS. A study done in *Arabidopsis* showed an increase in the number of basal and lateral branches, but only at high wind speed above 5 m/s, however, responses varied depending on ecotype (Bossdorf & Pigliucci, 2009). In addition, an increase in basal branches in *Arabidopsis* was observed after an extended time of wind stress exposition to 16 h/day with a constant wind speed of 1.8 m/s. No differences were found after the shorter exposure (6 h/day) with the same wind speed (Pigliucci, 2002). This indicates that tillering after wind stress may be associated directly with wind speed but also with the exposure time (Pigliucci, 2002). The mechanical stress applied to *Liquidambar* trees resulted in a decrease in the number of lateral branches (Neel & Harris, 1971), while in rice increase of tiller number was observed (Zhao *et al.*, 2018). Overall, the results obtained for tiller number was not affected by stress treatments; however, exposure time and wind speed may be the main factor responsible for such changes or lack of them.

Numerous studies have shown that mechanical stimulation affects several leaf properties, including changes in shape, size, mechanical properties, but also photosynthesis (Anten *et al.*, 2010). Nevertheless, the main focus of this research was on stems; thus, only stress-induced differences in leaf number was assessed. Results obtained after WS and MS in both genotypes revealed no significant differences when compared with their respective control plants, analogous to the results obtained in eucalyptus tree seedlings after WS (McArthur *et al.*, 2010). However, these findings differ significantly from results observed in white mustard, where wind stress-induced a decrease in leaf number (Retuerto and Woodward, 1992). In contrast, wind stress affected various genotypes of the *Arabidopsis* and *Brassica* genus differently, resulting in an increase or decrease in leaf number. Similarly to findings with tillering, this may indicate that the type of responses to mechanical stimulation is species and genotype-dependent (Murren & Pigliucci, 2005; Bossdorf & Pigliucci, 2009).

The aboveground biomass of both genotypes analysed in this study showed a significant reduction after WS and MS, with the most substantial effect after WS. A decrease in biomass is consistent with findings from other species after wind stress (Retuerto &

Woodward, 1992; Goodman & Ennos, 1996; Henry & Thomas, 2002; Anten *et al.*, 2005, 2009; Kern *et al.*, 2005) and also after mechanical stress (Murren & Pigliucci, 2005; Bossdorf & Pigliucci, 2009; Zhao *et al.*, 2018). The observed reduction in biomass is likely associated with a reduction in stem height but may also be connected with a decrease in leaf size. Unfortunately, the leaf analysis in this study was limited only to leaf number; thus based on the literature, it may only be hypothesised that leaf size may contribute to the overall reduction in total aboveground biomass (Jaffe, 1973; Biddington & Dearman, 1985; Anten *et al.*, 2010).

Interestingly, both stresses significantly affected the reproduction of both genotypes, with the most substantial effect after WS. This is clearly expressed in the delay of flowering, but also a reduction of total seed yield, seed number and average seed weight. These findings are in agreement with the findings of most other studies. For instance, mechanical stimulation considerably delayed the onset of flowering in tobacco (Anten *et al.*, 2005), *Capsella bursa-pastoris* (Niklas, 1998), white mustard (Retuerto & Woodward, 1992), *Brassica napus* (Cipollini, 1999) and *Arabidopsis thaliana* (Bossdorf and Pigliucci, 2009; Johnson et al., 1998). In contrast, Pigliucci did not observe a delay in flowering in *Arabidopsis* plants, possibly due to the very low wind speed used in this study. Also, it is suggested that the flowering response is connected with genotype (Pigliucci, 2002). Moreover, anthesis was significantly delayed in *P. vulgaris* (Jaffe, 1976), marigold (Mitchell *et al.*, 1975) and pea (Akers & Mitchell, 1983). Reproductive success not only depends on flowering time but also on developing reproductive structures such as flowering buds, which was significantly reduced after mechanical stimulation in *Mimosa pudica* (Jaffe, 1973). Reduction in seed number, seed weight and thus total yield after mechanical stimulation is also a widespread response to mechanical stimulation in plants (Niklas, 1998; Bossdorf & Pigliucci, 2009; Zhang *et al.*, 2013b). Surprisingly, no study on any species from Poaceae family was undertaken on the reproduction process. Taking into consideration all the above, there is an indication that mechanical stimulation may significantly reduce plant reproduction success and thus make it affect fitness. However, others have argued that it should not be considered as a deficit for the plants and the species, but rather as a necessary mechanism to ensure the continuation of the species in that environment, and

therefore, a beneficial adaptation. Plants are doing everything to stabilise their structure, and still, they reproduce (Jaffe & Forbes, 1993; Cipollini, 1999).

Results from the calculation of the elastic modulus (Young's modulus) revealed that mechanical stimulation has a direct effect on mechanical properties of Brachypodium stems. Statistical analysis of fresh material showed an increase in Young's modulus for IN2 after both stress tretaments in both genotypes. Results obtained for IN3 vary between stresses and genotypes. In Bd21 both WS and MS had no effect on Young's modulus in IN3. In ABR6, WS significantly increased Young's modulus, while after MS only increased trend was observed. Nonetheless, the obtained results do not give clear answer due to the mechanical properties of the stem. Probably performing a test with a higher number of replicates and extension of test for all internodes would give a better idea for this matter. Nevertheless, results obtained after measurements on senesced material revealed an increase in Young's modulus, suggesting that stems are more rigid after WS and MS in both genotypes. Nevertheless, in this study, we mostly focus on plant response noted just after two weeks of stress exposition and fresh material. Thus, results obtained with senesced material may implicate that some processes need a longer time to develop. Generally, a lower elastic modulus of the tissues in stems might be linked to resistance to failure and lodging of stems (Niklas, 1992). A reduction in stiffness of the stem after mechanical stimulation was observed in various plants including conifers such as *Abies fraseri* (Telewski & Jaffe, 1986a) and *Pinus* (Telewski & Jaffe, 1986b), deciduous trees such as *Populus* (Pruyn *et al.*, 2000) as well as herbaceous species such as *Phaseolus* (Jaffe & Telewski, 1984), *Nicotiana tabacum* (Hepworth & Vincent, 1999; Anten *et al.*, 2005), *Abutilon theophrasti* (Henry & Thomas, 2002), *Impatiens capensis* (Anten *et al.*, 2009), *Helianthus annuus* (Goodman & Ennos, 1996) and also *Arabidopsis thaliana* (Paul-Victor & Rowe, 2011). Nevertheless, none of those species belongs to grasses as *Brachypodium distachyon* does and therefore their stems do not have internodes. The detailed study performed on *Zea mays,* which belong to the Poaceae family showed the opposite reaction to mechanical stress resulting in a small increase in Young's modulus (Goodman & Ennos, 1996). This may indicate that species, which belong to the grasses family, may have a different response method to mechanical stimulation, though it needs to be taken into account that data in this area

is very confined. Nonetheless, this is in agreement with results obtained for senesced material. Moreover, the literature showed limited data separating wind and mechanical stress in relation to stem mechanical properties. Nevertheless, Smith and Ennos (2003) suggested that wind stress and mechanical stress affect *Helianthus* differently. Wind stress caused a decrease in Young's modulus but also an increase in stem height was observed, while mechanical stress led to an increase in modulus and shortening of the stem. Such results are indicative of two different response strategies: stems become either longer but more flexible or shorter and more rigid (Smith & Ennos, 2003). Taking into account all the above results presented in this study partially may fit the suggestion that stems after mechanical stimulation become shorter and more rigid. That was visible in both internodes of ABR6 genotype and IN2 of Bd21 for measurements on fresh material and in both internodes in both genotypes for measurements of senesced material. Such results also match with the study performed on *Zea mays*, which is the closest related species to *Brachypodium*.

In this research, WS plants consumed significantly more water compared with control and MS plants. Given that, my findings are based on a rather imprecise measurement system, the results from such analyses should, therefore, be treated with considerable caution. The higher water requirement undoubtedly is connected with higher water evaporation in a windy environment. There is surprisingly little evidence in the recent literature for differences in water usage after mechanical stimulation. However, almost 100 years ago, Finnell found that wind stress increased water usage (Finnell, 1928).

Morphological responses to wind and mechanical stress in this chapter mostly coincide with results presented in the literature. The plant morphology is significantly affected by both stress treatments with the biggest emphasis on reduction in plant height, size, plant reproduction as well as mechanical properties. Almost complete lack of evidence for morphological changes after mechanical stimulation in grasses makes this study more valuable, as performed on the model plant for grass crops. Thus, data presented in this chapter can be utilised as a good starting point for further analysis in grasses, such as maize, wheat or Miscanthus.

CHAPTER 3

CHAPTER 3 : IMPACT OF WIND STRESS AND MECHANICAL STRESS ON THE HISTOLOGY, ANATOMY AND COMPOSITION OF *BRACHYPODIUM DISTACHYON* STEMS

3.1. INTRODUCTION

While in the previous chapter, the main focus was on phenotypic changes occurring after mechanical stimulation, in this chapter, deeper insights into the effect of mechanical stimulation on plant growth and development are discussed. The previous chapter focuses on the phenotypic response of *Brachypodium* stems, while this chapter focusses on the influence of mechanical stress and wind stress on histological, anatomical, and compositional features of cell walls of two genotypes Bd21 and ABR6 of *Brachypodium distachyon* stems.

Cell walls play a very important role in plant growth and development. They are composed of several polymers, which give the whole plant specific features (Carpita, 1996). They determine the shapes of plant cells and organs and have remarkable mechanical properties to give plants strength and extensibility (Pilling & Höfte, 2003). Cell walls are a physical barrier to biotic and abiotic stresses and play an essential role in stress sensing, and signal transduction (Sarkar *et al.*, 2009; Seifert & Blaukopf, 2010). Additionally, in a stressed environment, cell walls incur biochemical changes such as a reorganization of components and hence, architecture, which allows the cell walls to adapt to particular conditions (Sarkar *et al.*, 2009).

While many studies in the area of mechanical stimulation have examined its effect on phenotypic traits, little attention has been given to how such mechanical stimulations may change anatomical and histological features of the cell wall. The structure and composition of cell walls in grasses significantly differ from cell walls of dicots with significant differences in their mechanical properties and development (McCann & Carpita, 2008). Research performed on grasses in terms of the impact of mechanical stimulation on histology and anatomy is very limited and often performed many years ago, when techniques and methodologies were limited. In addition, more recent studies focussing on the analysis of dicots plants such as *Arabidopsis thaliana or* beans.

Nevertheless, technologies available now such as immunological tests (e.g. ELISA) or immunolocalisations detecting specific cell wall components are of great value and can give deep insight into cell wall histology and anatomy. Generally, rearrangements in geometry, architecture and changes in the developed area of particular tissues were observed after mechanical stimulation (Biro *et al.*, 1980; Hunt & Jaffe, 1980; Paul-Victor & Rowe, 2011; Rigo, 2016). Histological analysis performed on mechanically stressed rice stems revealed no differences in anatomical characteristics; however, the analysis included only cell area, stomatal conductance and vascular bundle area (Zhao *et al.*, 2018). While old studies performed on maize (Whitehead, 1963) and tall fescue (Grace & Russell, 1977) after mechanical stimulation showed significant histological and anatomical differences.

There is extensive research and documented changes in the histology and anatomy of grasses after exposure to abiotic stresses such as drought (Mostajeran & Rahimi-Eichi, 2008), water stress (Assem *et al.*, 2017), and salt stress (Céccoli *et al.*, 2011). Because of such noted changes in the histology and anatomy of plants in response to abiotic and biotic stresses, this could represent an important aspect when evaluating the response of *Brachypodium* growth and development to mechanical stimulation.

Therefore, the primary aim of this chapter was to compare growth and developmental response to wind and mechanical stress of *Brachypodium distachyon*. The study involved histological, anatomical and compositional analysis of stems of two *Brachypodium* genotypes, Bd21 and ABR6. The study included tissue composition, cell size and cell wall thickness analysis. Moreover, immuno-localisation of cell-wall components with various monoclonal antibodies, histochemical localisation of lignin and analysis of pectin methylesterase activity was performed.

3.2. MATERIALS AND METHODS

3.2.1. PREPARATION OF PLANT MATERIAL FOR IMMUNO-LOCALISATION

The analysis was carried out only on plants after the first stress greenhouse experiment. Three plants from each treatment (control, WS, MS) for the two *Brachypodium* genotypes Bd21 and ABR6 were selected for the immuno-labelling experiment. All the analyses focused on main stem material obtained from the middle of the second internode, counting from the base. The procedure was carried out according to (Xue *et al.*, 2013) with minor modification.

3.2.1.1. FIXATION

Fixation was performed on 0.5 cm regions excised from the second internodes. Fragments were fixed in PEM buffer (50 mM piperazine-N,N'-bis[2-ethane-sulfonic acid] (PIPES), 5 mM methylene glycol bis(β-aminoethyl ether)-N,N,N',N'-tetraacetic acid (EGTA), 5 mM $MgSO_4$ (pH 6.9)) containing 4% paraformaldehyde and vacuum infiltrated using a vacuum pump for 3 h.

3.2.1.2. EMBEDDING

The fixed internode material was dehydrated with a graded ethanol series starting from 30% and followed by 50%, 70%, 90%, and 100%. Those steps were carried out at 4°C for 40 min each. Subsequently, stems were incubated at 37°C overnight in 1:1 Steedman's wax and 100% ethanol and followed by two changes of 100% wax for 1 h at 37°C. Steedman's wax was prepared by mixing 900 g of polyethylene glycol 400 distearate (Sigma 30, 541-3) with 100 g 1-hexadecanol (Sigma, C7882) and incubation at 65°C until melted. A few drops of melted wax were poured into moulds, and internode fragments were placed on partially congealed wax. Wax was quickly poured over the sample until a convex surface was visible. Moulds were left to set for a few days at room temperature.

3.2.1.3. SECTIONING

Transverse cross-sections were cut to a thickness of 12 µm and placed onto glass slides coated with polylysine (Sigma-Aldrich) with the use of a microtome (Bright, NB500). Prepared samples were air-dried for at least 24 hours. Subsequently, slides were dewaxed in a graded ethanol series: 3x 97%, 90%, 70%, 50%, 30%, and 10% (each dilution – 20 min) and after the ethanol series dipped in water for a few seconds. Slides were allowed to dry for an hour before immuno-labelling procedures.

3.2.1.4. IMMUNO-LOCALISATION PROCEDURE

Cross-sections of stems adhering to microscope slides were incubated for 30 min with 5% (w/v) MP/PBS (milk protein/1x phosphate-buffered saline) and then washed for 5min with PBS. This step was carried out to prevent non-specific binding. Primary rat monoclonal antibodies (LM1, LM2, LM5, LM6, LM10, LM12, LM13, LM19, LM20, LM25, LM28, and JIM7) (Table 3.1) were used at 5-fold dilutions in 5% MP/PBS and incubated at room temperature for 90 min. Primary mouse antibody (BG1) was used at 5 µg/mL and incubated at the same time and conditions. On each cross-section, 20 µL of the prepared solution was added and incubated. Sections were then washed 3X with PBS for 5 min. The secondary antibodies anti-rat IgG-FITC (Sigma-Aldrich, UK) at a 100-fold dilution for the rat primary antibodies and anti-mouse IgG-FITC (Sigma-Aldrich, UK) at a 50-fold dilution for the BG1 MLG primary antibody were added in 5% MP/PBS and incubated for 90 min in the dark. On each cross-section, 20 µL of the prepared solution was added and incubated. Subsequently, sections were washed 3X with PBS (each wash 5 min) to remove unlabelled secondary antibodies. To diminish sample auto-fluorescence, sections were stained with Toluidine blue (0.1% in 0.2 M phosphate pH 5.5) for 5 min. The immuno-labelled sections were then washed thoroughly with 1X PBS to remove any excess toluidine blue stain. Samples were observed with a fluorescence microscope (Leica, DMi8) and images of at least three sections for each sample were captured with a High-end Scientific Fluorescence CCD Camera (Leica, DFC365 FX) using Leica Application Suite X software. The exposure time was set automatically.

Table 3.1. List of monoclonal antibodies used in the study

Monoclonal Antibody	Epitope
Pectin - related	
LM5	(1→4)-β-D-galactans
LM6	(1→5)-α-L-arabinans
LM13	Linearised (1→5)-α-L-arabinan
LM19	Un-esterified homogalacturonan
LM20	Methyl-esterified homogalacturonan
JIM7	Partially methyl-esterified homogalacturonan
Hemicellulose - related	
LM25	XXXG/galactosylated xyloglucan
LM28	Glucuronoxylan
LM10	(1→4)-β-D-xylan
Glycoprotein - related	
LM1	Extensin
LM2	β-linked-GlcA in AGP glycan
Other	
BG1	Mixed-linked glucan
LM12	Anti-feruloylated polymers

3.2.1.5. CALCOFLUOR WHITE STAINING

For cellulose visualisation, staining with Calcofluor White (CFW) was used (0.2mg/mL in PBS). A few drops of the solution were placed on each slide and incubated for 10min at room temperature. Slides were then washed 3X in PBS for 5min each wash and allowed to air dry. To prevent fluorescence fading one drop per section of anti-fade reagent Citifluor glycerol/PBS (Agar Scientific) was added on a microscopic slide before placing a coverslip. After mounting, the slides were stored in a microscope slide box at 4°C in darkness until use. Samples were observed with a fluorescence microscope (Leica, DMi8) and images of at least three sections for each sample were captured with a High-end Scientific Fluorescence CCD Camera (Leica, DFC365 FX) using Leica Application Suite X software. The exposure time was set automatically.

3.2.2. ANATOMICAL AND MORPHOLOGICAL MEASUREMENTS BASED ON CALCOFLUOR STAINING

Anatomical and morphological measurements were carried out according to (Matos *et al.*, 2013) with minor modifications. Three cross-sections from three plants per each treatment for both genotypes Bd21 and ABR6 were analysed. ImageJ software was used to analyse images by automatically measuring selected areas of interest: outer vascular bundles, inner vascular bundles, interfascicular region, pith, cortex, and epidermis (Figure 3.1). Measured areas were presented as a percentage of the total area of cross-section. Whole stem cross-section images were used for the inner, outer and total vascular bundle count. Additionally, measurement of cell wall thickness and cell wall size was performed. Similarly, for this analysis, three plants per each treatment of both genotypes were taken, and three sections for each plant were analysed. The area of interest for measuring cell size and cell wall thickness is localised above vascular bundles. In order to measure cell wall thickness, lines were drawn across the adjacent cell walls of the first four rows of cells above the bundle sheath of a vascular bundle (five cells per row). The same cells were also analysed for a proxy for cell size.

All of the anatomical and morphological measurements were made based on cross-sections stained with Calcofluor White (see 3.2.1.4.).

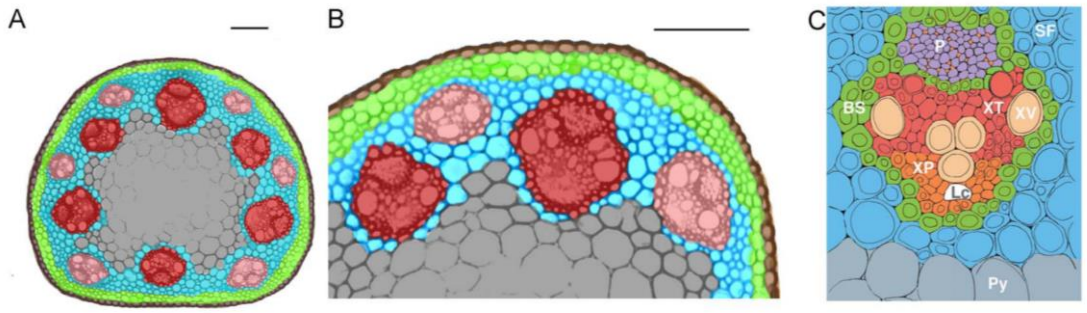

Figure 3.1. Brachypodium distachyon internal stem internode anatomy.

(A) Cross-section of the whole stem and (B) higher magnification of the first stem internode. Red, inner vascular bundles; pink, outer vascular bundles; cyan, interfascicular region comprised mostly of sclerenchyma fibres; grey, pith; lime green, chlorenchyma and sclerenchyma cells comprise the cortex; brown, epidermis. (C) Vascular bundle illustration at high magnification. Green, bundle sheath (BS); purple, phloem (P); Vermilion, companion cells; tan, xylem vessels (XV); red, xylem tracheids (XT); white, lacuna (Lc); orange, xylem parenchyma cells (XP); gray, parenchyma cells (Py); blue, sclerenchyma fibers (SF). (A-B) Bar = 0.1 mm, (C) bar = 0.01 mm. Adapted from (Matos *et al.*, 2013).

3.2.3. SCANNING ELECTRON MICROSCOPY

A middle part of the second internode from three biological replicates per each treatment after the second greenhouse experiment was taken for analysis. The stem pieces were cut to 1 mm in length and embedded in MEADE resin (Methacrylate Embedding & Acetone De-Embedding resin). The resin mixture consisted of 80% butyl-methacrylate, 20% methyl methacrylate, 0.5% (w/v) benzoin ethyl ether (Agar Scientific Ltd). Stem pieces were first dehydrated in an aqueous alcohol series (30%, 50%, 70%, 95% & 100%) for at least an hour in each mixture and left in 100% overnight at 4°C. Subsequently, sections were passed through mixtures of MEADE resin and ethanol (1:2, 1:1 and 2:1) for at least an hour in each mixture and 100% resin overnight at 4°C. The stem pieces were transferred to BEEM capsule polyethylene moulds (Agar Scientific Ltd) in fresh resin and securely capped. The moulds were covered with six sheets of Parafilm M (Agar Scientific Ltd) to slow the polymerisation and discourage brittleness. The resin was polymerised overnight by a UV light source consisting of two 6W UV lamps at a distance of 10 cm. The resulting blocks were cut from the moulds with a single-bladed razor, rinsed in ethanol to remove any unpolymerised resin, aired in a fume hood and

labelled. Sections were cut at a 1-2 µm thickness on a Reichert-Jung Ultracut E Ultramicrotome with glass knives. The sections were collected in 100% acetone in glass vials to solubilise the resin, swirled regularly then left overnight to ensure that the resin was dissolved and removed from the section structure. They were then attached in a drop of acetone to 1" aluminium specimen stubs with 12 mm diameter carbon self-adhesive pads (Agar Scientific, Stansted, UK). The mounted stem sections were gold-coated for 5 min in a Polaron E5000 SEM Coating Unit and imaged using a Hitachi S-4700 FESEM microscope using the Ultra-High-Resolution mode and an accelerating voltage of 3.0 kV at a working distance of 5.0 mm and images were captured at 2560 x 1920 resolution. Areas above the vascular bundles were analysed in order to measure cell wall thickness.

3.2.3.1. MEASUREMENTS BASED ON SEM IMAGES

Based on SEM images, measurements of cell wall thickness were performed with the use of ImageJ software. Similarly, to measurements performed on sections stained with Calcofluor White, cell wall thickness was measured on cells in the area of interest localised above vascular bundles. In order to measure cell wall thickness, lines were drawn across the adjacent cell walls of the first four rows of cells above the bundle sheath of a vascular bundle (five cells per row). In some cases, a line was drawn on two cell walls, and the thickness obtained after measurement was divided to receive two single measurements. In addition to cell wall thickness measurements, SEM images were evaluated for apparent differences caused by the different treatments.

3.2.4. HISTOCHEMICAL STAINING OF LIGNIN IN STEM TISSUE

The second internode of the main stem from three *Brachypodium* plants (Bd21 and ABR6) per each treatment (control, WS, MS) were used as sectioning material. Plants from the second experiment were used in this analysis. Transverse stem cross-sections were hand-cut with a clean razor blade under microscope loupe to obtain good quality and similar thickness sections. Cross-sections were stained with 5% (w/v) phloroglucinol (1,3,5-trihydroxybenzene) (Sigma-Aldrich) in 75% EtOH for 5min in darkness.

Phloroglucinol stains lignified cell walls red-brown as a reaction with aldehyde end groups of lignin (Pomar et al., 2002). The stained sections were transferred onto glass slides and then flooded with a few drops of 12 N HCl. All stained transverse stem cross-sections were mounted on glass slides with 30% glycerol. Immediately after staining samples were observed, and analysed under a bright-field light on a Leica LMD6000 microscope. Images were taken with a Hitachi HV-D20 camera and captured with the Leica LMD V6.5 software. Three cross-sections for each plant were analysed.

3.2.5. ENZYME-LINKED IMMUNOSORBENT ASSAY (ELISA) ASSAY PROCEDURE

3.2.5.1. CELL WALL RESIDUE PREPARATION

Stem material from three plants from the third greenhouse experiment per each treatment – control, WS, and MS (both genotypes) was harvested, and leaf/sheaths and seed heads were carefully removed and discarded. Lignocellulosic biomass was collected and frozen at -80°C, and then freeze-dried. Dry biomass was then milled with use of biomass grinding and loading robot (Labman Automation Ltd.). Biomass material was then fractionated to an alcohol insoluble residue (AIR) according to a protocol adapted from (Foster *et al.*, 2010; da Costa *et al.*, 2014) with some modifications. For each sample, approximately 60-70 mg of dry biomass was weighted, and 1.5 mL of 70% aqueous ethanol was added. Samples were then incubated first for 12 h in a shaking incubator set at 25°C and 150 rpm and then twice for 30 min at 40°C. Subsequently, biomass was extracted three times with 1.5 mL of chloroform/methanol solution (1:1 v/v) at 25°C/ 150 rpm and finally twice with 500 μL of acetone at 25°C/ 150 rpm after which samples were air-dried for at least two days in a laminar fume hood at room temperature. Between each extraction, samples were thoroughly vortexed before incubation and centrifuged at 3,000 rpm for 10 min to aspirate the supernatant containing extractives.

De-starching of extracted biomass was initiated by resuspending the samples in 1 mL of 0.1 M sodium acetate buffer (pH 5) and heating them in a water bath at 80°C for 20 min to induce starch gelatinisation. Samples were subsequently cooled to room temperature and centrifuged at 1000 rpm. After the supernatants were discarded, the

pellet was washed twice with 1.5 mL of deionised water with resuspension, centrifugation and supernatant discarding. To inhibit microbial growth sodium azide was added at 0.0002% (w/v) and starch was removed by incubation with a saturating amount of type-I porcine α-amylase (Sigma-Aldrich; 47 units per 100 mg cell wall) in 0.5 mL of 0.1 M ammonium acetate buffer (pH 5). To ensure complete starch hydrolysis samples were then placed in a shaking incubator set at 25°C (150 rpm) for an extended incubation period of 48 h. α-amylase digestion was terminated by heating samples in the water bath for 15 min at 95°C and samples were cooled at room temperature. The supernatant containing solubilised starch was aspirated, and the pellet was then washed three times in 1.5 mL of deionised water and twice with 1.5 mL of acetone, with centrifugation, vortexing and supernatant removal between each step. De-starched AIR was air-dried in a laminar flow bench until moisture content was ≤10%.

3.2.5.2. EXTRACTION OF MONOSACCHARIDES FOR ELISA ASSAY

The extraction of monosaccharides for ELISA assays was performed on previously prepared cell wall biomass – AIR for three treatments and both genotypes based on the protocol described by (Pattathil *et al.*, 2010, 2012) with modifications. Briefly, 10 mg of AIR sample was extracted with 1 mL of 4 M KOH containing 1% (w/v) $NaBH_4$ for 24 h in shaking incubator set at 25°C and 200 rpm. KOH extracts were neutralised on ice, using acetic acid. To prevent foaming, three drops of 2-octanol were added. All extracts were dialysed against distilled water with a sample: water ratio ≈1:60 for 48 h at room temperature (3.5 kDa molecular weight cut-off tubing, no. S632724; Spectrum Laboratories Inc., California, USA) and left at 4°C until use.

3.2.5.3. PHENOL-SULPHURIC ACID METHOD FOR TOTAL CARBOHYDRATE ESTIMATION

Total carbohydrate content was estimated using the phenol-sulphuric acid method in a 96-well microplate format as described by (Masuko *et al.*, 2005) with minor modifications. Briefly, assays were performed in triplicates in Eppendorf tubes.

Extracted carbohydrates were diluted 1:10 with distilled water. 50 µL of the diluted extract was pipetted into a 96-well microplate, and rapidly 150 µL of concentrated sulfuric acid was added. Immediately after that, 30 µL of 5% (w/v) phenol was added, and the plate was kept in a static water bath for 5 min at 90°C. After cooling to room temperature, the microplate was wiped dry, and the absorbance at 490 nm was measured with a plate reader (µQuant; Bio-Tek Instruments, Winooski, Vermont, USA) using KC4 software (v. 3.3; Bio-Tek). A standard curve was prepared using solutions with varying glucose concentrations to determine glucose equivalents of the sugars in each extract. Negative controls without cell wall extract samples were included in all plates, and their absorbance at 490 nm was read.

3.2.5.4. ENZYME-LINKED IMMUNOSORBENT ASSAY (ELISA)

Extracted samples for ELISA assay were diluted in PBS to a final carbohydrate concentration of 25 µg/mL or 50 µg/mL in PBS. Subsequently, ELISA microtitre plates (NUNC Maxisorp, Thermo Fisher Scientific) were coated with 100 µL of diluted sample and incubated overnight at 4°C. Plates were then washed three times with distilled water. Non-specific binding sites in the previously coated plates were blocked with 200 µL of 7% (w/v) milk powder in PBS for 3 h at room temperature. Plates were then washed 15 times by filling wells with distilled water, shaking and then forcibly throwing water out. Plates were then coated with 100 µL of primary antibody (LM1, LM2, LM5, LM6, LM10, LM12, LM13, LM19, LM20, LM25, LM28, JIM7) at 1:10 dilution in 7% milk powder/PBS and incubated for 90 min at room temperature. Plates were washed as described previously and then were incubated with 100 µL of secondary antibody anti-rat IgG-HRP (A9542, Sigma-Aldrich) at a concentration of 1: 1000 in 7% milk powder/PBS for 1 h. Plates were shaken dry and 100 µL of a freshly prepared substrate composed of 18 mL of water; 2 mL of 1 M sodium acetate buffer, pH 6.0; 200 µL of Tetramethyl Benzidine (10 mg/mL in DMSO) (3,3,5'5'-TetramethylBenzidine, Sigma T-2885); and 20 µL of 6% (v/v) hydrogen peroxide was added to each well and left incubating for blue colour development. After 15 min, the reaction was terminated by the addition 50 µL of 2.5 M H_2SO_4. Immediately after, net OD values of the colour formation in the wells

were measured at 450 nm, subtracting a background reading at 655 nm. Additionally, negative controls consisting of water and the same primary and secondary antibodies were included in all assays, and their absorbance was subtracted from the readings.

3.2.6. THE PECTIN METHYLESTERASE ACTIVITY GEL DIFFUSION ASSAY PROCEDURE

Analysis of pectin methylesterase (PME) activity was performed for both *Brachypodium* genotypes Bd21 and ABR6 for all three treatments (control, WS and MS). The analysis was carried out on leaves and stems from a third greenhouse experiment.

3.2.6.1. PROTEIN EXTRACTION FOR PME ASSAY

Proteins were extracted from leaves and stem material. The procedure was performed as described by (Pinzon-Latorre & Deyholos, 2014) with modifications. Total protein extract was obtained by grinding tissue in liquid nitrogen and then transferred to extraction buffer, containing 1 M NaCl, 12.5 mM Citric Acid, 50 mM Na_2HPO_4 plus one tablet per 10 mL of cOmplete ULTRA protease inhibitor (Roche), pH 6.5 (1 mL of extraction buffer per 1 g of plant tissue). The homogenate was then shaken for 2 h at 4°C, subsequently centrifuged at 14,000 rpm for 15 min, and the supernatant was collected. Protein concentration was determined using the Bradford protein assay method (Biorad reagent) and bovine serum albumin as standard. For stem material, an additional step was introduced because of its low pectin concentration. Stem extract was transferred into Microcon Centrifugal Filter Device (Micon, YM-10) and centrifuged twice at 13,000 rpm for 30 min. Protein concentration was determined once again using the Bradford method based on a standard curve.

3.2.6.2. RADIAL DIFFUSION ASSAY

The PME activity was quantified by radial diffusion assay as described (Downie *et al.*, 1998), with modifications. Briefly, 2% (w/v) agarose gel containing 0.1% (w/v) of 85% methylesterified pectin from citrus fruit (P956, Sigma-Aldrich); 12.5 mM citric acid, and 50 mM Na_2HPO_4, pH 6.5 was prepared. Approximately 25 mL of the mixture was poured

into square 90 mm Petri dishes and allowed to polymerise at room temperature. After cooling, wells with a diameter of 4 mm were obtained with a micropipette tip, and equal amounts of protein samples were dispensed into each well (50 μg of total protein for leaves extract and 100 μg for stem extract in 20 μL). All samples were tested into three technical replicates. Plates were incubated at 30°C for 16 h. The gel was stained with an aqueous solution of 0.05% (w/v) ruthenium red for 1 h and washed a few times with distilled water. The halo resulting from the hydrolysis of esterified pectin in the gel was photographed immediately, and the area of the halo was measured using ImageJ. A standard curve was prepared using commercial orange peel PME (Sigma-Aldrich) with activity range going from 0.005 units to 0.05 units (1 unit – 16.67 nanokatals). PME activity was calculated based on this standard curve.

3.2.7. STATISTICAL ANALYSIS

Values in this chapter are expressed as a mean ±SD. All analyses were performed using SPSS software (version 24). Statistical differences were estimated from ANOVA tests at the 5% level ($P \leq 0.05$) of significance, for all parameters evaluated. Where ANOVA indicated a significant difference, pair-wise comparison of means by Tukey's HSD (honestly significant difference) test was carried out at the 5% ($P \leq 0.05$) of significance.

3.3. RESULTS

Results presented in this chapter are based on material collected after various greenhouse stress experiments (Table 3.2). The reason for that is a limited amount of plant material generated after each greenhouse experiment in which a maximal number of plants per each treatment was 20. Repeatability of phenotypic traits in each experiment (previous chapter) indicates that changes and differences between treatments are stable across experiments performed. Thus, further analysis of the morphological and anatomical level should be constant.

Table 3.2. Summary of all analysis performed in this chapter.

✓ Indicate that analysis was done on a particular experiment.

	#1	#2	#3	#4
Tissue area	✓			
Vascular bundles	✓			
Cell size	✓			
Cell wall thickness (Calcofluor)	✓			
Cell wall thickness (SEM)		✓		
Cell walls distinguishability (SEM)		✓		
Immuno-labelling	✓			
ELISA			✓	
PME assay			✓	
Phloroglucinol staining	✓			

3.3.1. TISSUE AREA

Analysis of tissue area is based on stem material of Bd21, and ABR6 collected after the first greenhouse experiment. Likewise, for measurements of anatomical properties, the second internode (IN2) from the main stem was selected for evaluating possible differences between treatments (control, WS and MS). The analysis is based on cross-sectional anatomy obtained from three plants for each treatment based on Calcofluor White staining. Obtained measurements of each particular tissue type are presented as

a percentage of the area of the whole cross-section. Results indicate that WS and MS treatment changed the anatomy of cross-sections. Moreover, there was a slight difference in the response between WS and MS treatment. The difference in response patterns to MS and WS treatment varies significantly within the genotypes used in this study (Table 3.3).

Table 3.3. Cross-section anatomy.

Stem cross-section anatomy (IN2) of Bd21 and ABR6 plants of all treatments (control, WS and MS) (3 cross-sections per plant; n=3). The Area of a particular tissue is presented as a percentage of the area of the whole cross-section with standard deviation (±SD). Data were normalised to a summative area closure of 100%. For statistical significance the ANOVA test ($P \leq 0.05$) was performed, and if the test showed a significant difference, a post-hoc Tukey's test ($P \leq 0.05$) was also performed. * Statistically significant difference from control; * Statistically significant different between WS and MS.

	Bd21			ABR6		
	Control	**WS**	**MS**	**Control**	**WS**	**MS**
Epidermis	6.75 ± 0.56	6.55 ± 0.27	7.45 ± 0.16	6.49 ± 0.71	4.86 ± 0.58*	4.84 ± 0.06*
Cortex	13.82 ± 0.74	9.37 ± 0.19**	13.77 ± 0.45*	11.91 ± 0.89	10.62 ± 0.44*	12.48 ± 0.48*
Vascular bundle	21.21 ± 0.22	19.39 ± 0.1**	16.92 ± 0.13**	14.84 ± 0.45	19.39 ± 0.1**	22.05 ± 0.73**
Interfascicular region	32.42 ± 0.81	30.68 ± 0.44**	33.4 ± 0.76*	29.91 ± 0.78	30.25 ± 0.15*	28.25 ± 0.47*
Pith	25.8 ± 1.33	34.01 ± 0.71*	28.46 ± 1.14	36.85 ± 1.78	34.13 ± 0.71	32.38 ± 0.14*

3.3.1.1. EPIDERMIS

Bd21 genotype measurements showed that after both stress treatments, no difference in epidermis area was found ($P = 0.054$) compared with control. A slight increase was observed after MS; however, this was not statistically significant. ABR6 responded differently to the treatments compared to Bd21, with both WS and MS treatments resulting in a significant ($P \leq 0.05$) decrease of about 25% in the epidermis area developed in ABR6 compared with controls (Table 3.3).

3.3.1.2. CORTEX

While MS treatment had no effect on the cortex area of Bd21 when compared with control, WS had a significant effect ($P \leq 0.05$) with the cortex area being reduced by more than 30% compared with both control and MS treatment. ABR6 showed a different response, with a decrease after WS and increase after MS compared with control (both were not statistically significant). Because of these opposite tendencies, a significant difference was found between the cortex area after WS and MS in ABR6.

3.3.1.3. VASCULAR BUNDLE

A significant difference ($P \leq 0.05$) was found in the percentage area of the inner, outer and total area of vascular bundles (VB) in Bd21 genotype (Table 3.4). MS treatment resulted in a decrease in the area of both inner and outer VB. After WS, a decrease in the area was found only for the outer VB, while no difference was found for the inner VB when compared with control plants. Taking the total developed area of both inner and outer VB into consideration, wind stress plants showed a significant decrease of about 8.5%, while after mechanical treatment the area decreased about 20% compared with control. Statistically, the difference in the VB area between WS and MS treatment is also significant (Table 3.4). ABR6 showed a very different response compared with that of Bd21. A significant difference ($P \leq 0.05$) was found for the inner, outer and total area of VB; however, the response was in the opposite direction compared with that seen for Bd21. WS and MS plants showed an increase in the area of inner VB of 23% and

36%, respectively compared with control plants. The area of outer VB increased even more with 65% after WS and 78% after MS treatment compared with control. Therefore, as expected from the increases seen for inner and outer VB, the total area of VB was increased by 30% after WS and almost 50% after MS compared with control plants, and a significant difference between WS and MS treatment was also found. Needs to be mentioned that a big difference in the contribution of the VB between Bd21 and ABR6 was observed (Table 3.4).

Table 3.4. Vascular bundle area.

Vascular bundle area (IN2) developed by Bd21 and ABR6 plants after stress treatments (control, WS and MS) (three cross-sections per plant; n=3). The area of a particular tissue is presented as a percentage of the area of the whole cross-section with standard deviation (±SD). For statistical significance the ANOVA test ($P \leq 0.05$) was performed, and if the test showed a significant difference, a post-hoc Tukey's test ($P \leq 0.05$) was also performed. * Statistically significant from control; * Statistically significant difference between WS and MS.

		Outer VB	Inner VB	Total VB
Bd21	Control	7.4 ± 0.57	13.81 ± 0.34	21.21 ± 0.22
	WS	5.93 ± 0.2*	13.46 ± 0.11*	19.39 ± 0.1**
	MS	5.18 ± 0.18*	11.75 ± 0.12**	16.92 ± 0.13**
ABR6	Control	4.4 ± 0.21	10.44 ± 0.43	14.84 ± 0.45
	WS	7.24 ± 0.11*	12.9 ± 0.63*	19.39 ± 0.1**
	MS	7.85 ± 0.09*	14.2 ± 0.71*	22.05 ± 0.73**

3.3.1.4. INTERFASCICULAR REGION

The area of the interfascicular region was significantly reduced by 5% ($P \leq 0.05$) in Bd21 plants exposed to WS compared with control and to MS treated plants. Although a slight increase in the interfascicular area was observed after MS treatment, this was not statistically significant. The interfascicular area developed by ABR6 plants showed an increase after WS and a decrease after MS compared with control; however, a significant difference ($P \leq 0.05$) was found only between WS and MS treatment (Table 3.3).

3.3.1.5. PITH

Bd21 plants exposed to WS developed significantly ($P \leq 0.05$) more pith area than control plants but also more than MS plants. No significant differences between MS and control were found, although a slight increase after MS was observed. Measurements for ABR6 revealed an opposite response to the stress treatments compared with Bd21, with a decrease of the pith area after both MS and WS treatment, although this decrease was only significant ($P \leq 0.05$) after MS treatment when compared with control.

3.3.1.6. VASCULAR BUNDLE NUMBER

The number of vascular bundles was determined for three plants from each treatment for both genotypes. Bd21 analysis showed no significant difference in number of inner ($P = 0.630$), outer ($P = 0.171$), and total number of VB ($P = 0.140$). Similar to Bd21 there was no difference in inner ($P = 0.959$), outer ($P = 0.142$), and total ($P = 0.194$) number of VB in ABR6 plants (Table 3.5).

Table 3.5. Number of vascular bundles after stress treatments of Bd21 and ABR6.

Data represent mean of inner, outer and total vascular bundle number with standard deviation (±SD) of a mean (n=3). For statistical significance the ANOVA test ($P \leq 0.05$) was performed.

		Outer VB	Inner VB	Total VB
Bd21	Control	9.67 ± 1.53	7.67 ± 0.58	17.33 ± 1.15
	WS	9.67 ± 1.53	7.67 ± 0.58	17.33 ± 1.15
	MS	7.67 ± 0.58	8 ± 0	15.67 ± 0.58
ABR6	Control	9.33 ± 0.58	9 ± 0	18.33 ± 1.53
	WS	12 ± 3	9 ± 0	21 ± 2.65
	MS	13.67 ± 2.52	9 ± 1	22.67 ± 3.21

3.3.2. CELL WALL THICKNESS

Considering the differences found in tissue distribution, the decision was made to undertake the further anatomical analysis. Also, based on the analysis of immuno-labelling images (see section 3.3.6), there was an impression that cells above the vascular bundles in perturbed plants (WS and MS) had thicker cell walls. Because of this, the cell wall thickness in this particular region of interest (Figure 3.2) was measured.

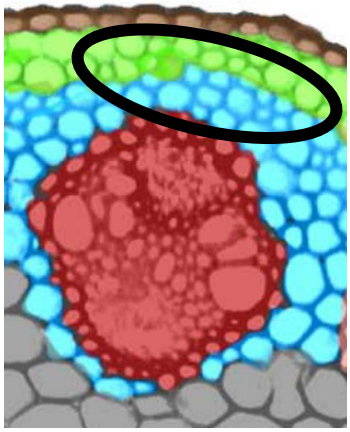

Figure 3.2. Area of cross-sections anatomy taken into consideration for cell wall thickness measurements.

The black ellipse indicates the region of interest. Adapted from (Matos *et al.*, 2013).

First, measurements for cell wall thickness were performed on Calcofluor White stained cross-sections of all treatments (control, WS and MS) after the first greenhouse experiment. Both genotypes showed the same response pattern, namely an increase in cell wall thickness. Cell walls of WS and MS treated Bd21 plants were significantly ($P \leq 0.05$) thicker compared with control by 0.37 µm in WS plants and 0.04 µm in MS plants. Similarly, ABR6 WS cell walls were significantly ($P \leq 0.05$) thicker by 0.35 µm and MS by 0.14 µm compared with control. These results indicated that the response after WS was much stronger than MS (Table 3.6).

To confirm these finding on mechanical stimulation induced increases in cell wall thickness, additional measurements were made using higher magnification images

produced after scanning electron microscopy (SEM). All measurements are based on cross-sections cut from IN2 after the second greenhouse experiment. The results differ significantly from those obtained from Calcofluor White stained cross-sections. Measurements on Bd21 (WS and MS) and ABR6 (WS) showed significant ($P \leq 0.05$) thinning of the cell wall, and therefore, the opposite results compared with the measurements obtained based on Calcofluor White staining. For Bd21 WS and MS, cell walls were significantly ($P \leq 0.05$) thinner compared with control by 0.142 µm and 0.264 µm, respectively and in ABR6 WS by 0.2 µm. In contracts, the cell wall of the measured cells in ABR6 after MS treatment were on average 0.1 µm thicker, similar to the results based on Calcofluor White staining (Table 3.6).

Table 3.6. Cell wall thickness.

Data represent mean of the cell wall thickness (µm) measurements, based on Calcofluor White staining and SEM images, with standard deviation (±SD) of a mean (3 cross-sections per plant; n=3) after treatments (control, WS and MS) for both genotypes. For statistical significance the ANOVA test ($P \leq 0.05$) was performed, and if the test showed a significant difference, a post-hoc Tukey's test ($P \leq 0.05$) was also performed. * Statistically significant difference from control; * Statistically significant difference between WS and MS.

		Calcofluor	SEM
Bd21	Control	1.91 ± 0.11	2.04 ± 0.19
	WS	2.28 ± 0.13**	1.9 ± 0.17**
	MS	1.95 ± 0.12**	1.78 ± 0.17**
ABR6	Control	1.86 ± 0.13	2.06 ± 0.26
	WS	2.12 ± 0.15**	1.86 ± 0.26**
	MS	1.98 ± 0.11**	2.17 ± 0.22**

3.3.3. CELL SIZE

Cell size was measured on the same cells as those used for cell wall thickness measurements (see 3.3.3.) to preserve the continuity of anatomical analysis. Cell size measurements showed no statistical differences between treatments in Bd21 (P = 0.157) and ABR6 (P = 0.223). This is probably related to the sizeable standard deviation

for all measurements. However, measurements showed a slightly different tendency in the response between genotypes. ABR6 plants after wind exposition developed smaller cells than in control or MS, while in Bd21 cells were smaller only in MS plants (Figure 3.3).

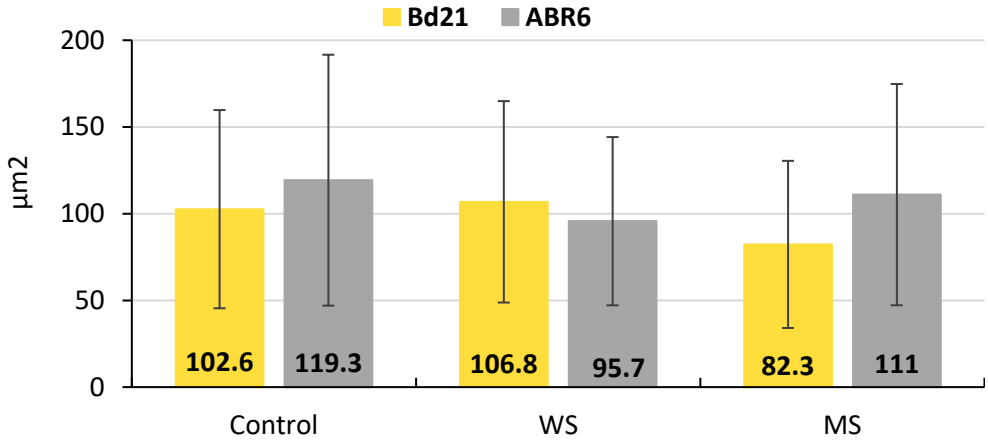

Figure 3.3. Cell size after WS and MS treatment.

Data represent a mean cell size comparison with standard deviation (±SD) of the mean (3 cross-sections per plant; n=3) for both genotypes. For statistical significance, ANOVA test, ($P \leq 0.05$) was performed.

3.3.4. CELL WALL ANALYSIS BY SEM

Besides differences in cell wall thickness, the SEM images revealed one more interesting feature. In some of the cross-sections, cell walls were separated from each other and had a very sharp edge line, thus those were well defined. These cells were distinguishable from each other and obtaining results for cell wall thickness was very simple, allowing the measurement of the cell wall thickness for each cell separately. The visual effect of these type of cross-section may be compared with the effect of cutting metal. In the second category of cross-sections, cell walls were indistinguishable from each other, thus were nondefined. For sections in this category, the cell wall thickness was determined by measuring the thickness of the two cell walls of neighbouring cells and dividing the result by two. Generally, images make an impression that they are made from very soft material, like “cheese”. Lower magnification images of whole cross-section did not reveal any of these differences (Appendix 3). However, images

with higher magnification, which were used for cell wall thickness measurements showed that the difference is very noticeable in Bd21 (Figure 3.4) and ABR6 (Figure 3.5). It is also important to mention that the preparation of stem material for SEM was double-checked and could be eliminated from being the reason for the observed differences seen in the cross-section.

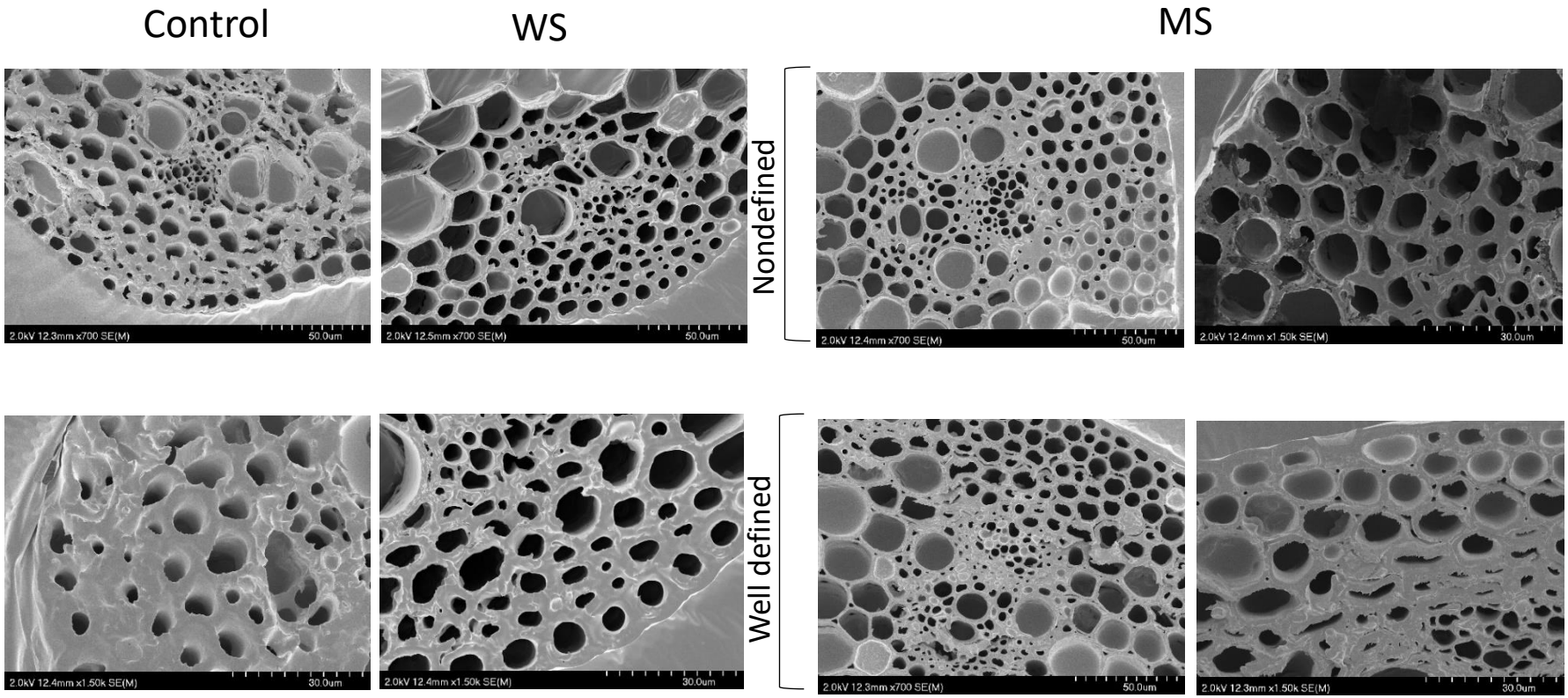

Figure 3.4. SEM images of cell wall in Bd21.

Scanning electron microscope images with various magnification factors showing the difference between well defined and nondefined cell walls of Bd21 cross-sections for all three treatments: control, WS, and MS.

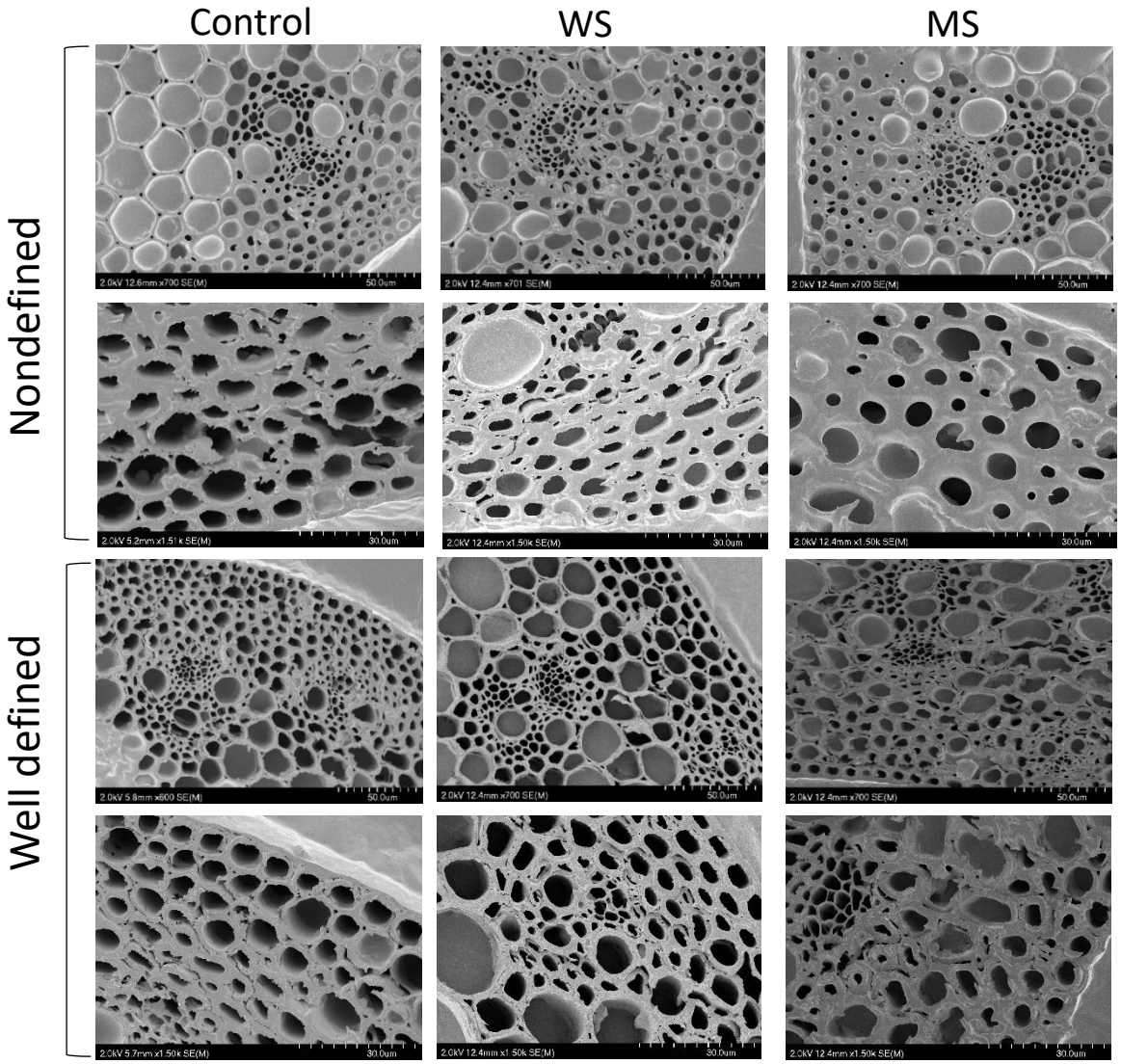

Figure 3.5. SEM images of cell wall in ABR6.

Scanning electron microscope images with various magnification factors showing the difference between well defined and nondefined cell walls of ABR6 cross-sections for all three treatments: control, WS, and MS.

Since it may have a significant impact on cell wall thickness measurements, the number of cross-sections having well defined cell walls were counted. For this analysis, three plants from each treatment (control, WS, and MS) for both genotypes were used. Moreover, for each plant, five cross-sections were analysed. The counts revealed that all (n=15) of the cross-sections of Bd21 control and WS plants were nondefined. Only five of the fifteen cross-sections after MS were well defined. In the control of the ABR6 genotype, all of the cross-sections (n=15) were nondefined, while after WS and MS treatment only five out of fifteen not clear (Figure 3.6).

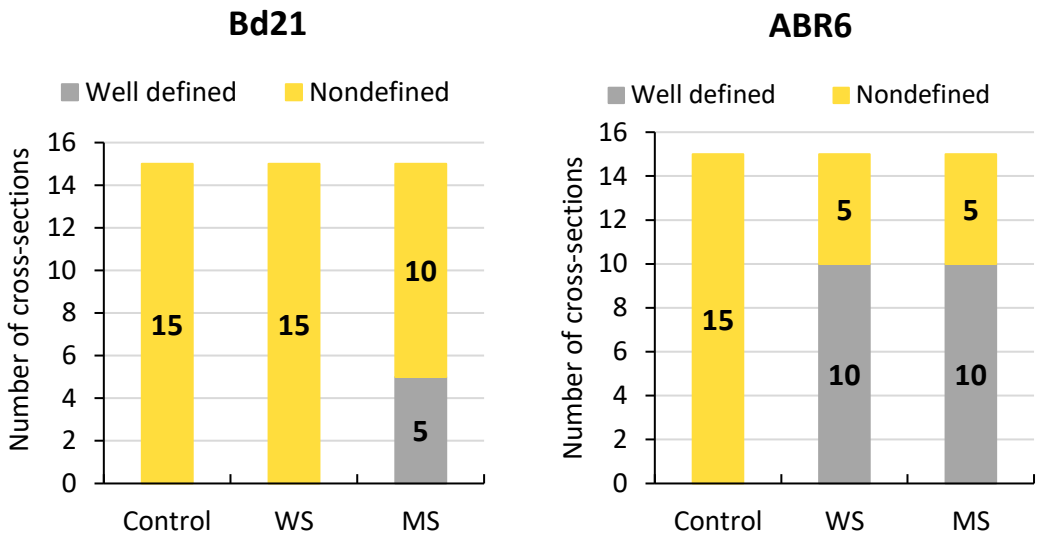

Figure 3.6. Cell wall analysis by SEM.

Analysis of cell walls showing the difference in number of images in which cell walls were well defined and nondefined in cross-sections between treatments: control, WS and MS for both genotypes of *Brachypodium distachyon*; Bd21 and ABR6. Calculations based on three plants, and five sections per plant, thus 15 sections per each treatment.

3.3.5. IMMUNO-LOCALISATION

The effect of the wind and mechanical stress on hemicellulose, pectin, glycoprotein and other cell wall components was examined by immunofluorescence using a range of different monoclonal antibodies directed against different cell wall epitopes (listed in Table 3.1). The main differences between treatments and controls were found in the

distribution of epitopes related to pectins (LM5, LM13, JIM7, LM19). It is important to mention that staining patterns also differed between genotypes.

The LM5 antibody recognises a linear tetra-saccharide in (1-4)-β-D-galactans, and it was strongly detected in bundle sheath cells under xylem cells in control Bd21 plants (Figure 3.7A), while this was not the case for WS and MS treatment (Figure 3.7B-C). In ABR6 plants LM5 showed a different labelling pattern, with a lack of signal in cortex cells in cross-sections of control plants (Figure 3.7D), while after WS and MS treatment there were only small regions with a lack of signal localised in cortical regions between vascular bundles (Figure 3.7E-F). For all samples, irrespective of the treatment, a strong signal was detected in phloem cells.

Labelling with LM13, which binds to an unbranched (1→5)-α-L-arabinan only revealed subtle differences after WS treatment compared with control and MS in Bd21 (Figure 3.8). In all of the three treatments, the LM13 epitope was detected in xylem tracheids, and xylem parenchyma cells localised close to xylem vessels (Figure 3.8A2, B2, C2). In control and MS plants, the LM13 epitope was also detected in cortex cells between VB while no such epitope was found in WS plants (Figure 3.8A1, B1, C1). No differences between treatments were found in ABR6, showing a similar distribution of the LM13 epitope as observed for Bd21; visible in xylem tracheids, and xylem parenchyma cells localised close to xylem vessels (Appendix 4A).

Labelling with JIM7, which bind to partially methyl-esterified homogalacturonan were detected in pith cells of Bd21 for each of the treatments (Figure 3.9). In control and WS plants, JIM7 signals covered all phloem and xylem cells in the VB, but there was no signal observed in these areas in MS plants. Moreover, signals in the cortical region between VB close to the epidermis was much stronger in control and WS treatments compared with MS treatment (Figure 3.9A-C). No differences in labelling pattern between treatments were found in ABR6, with JIM7 epitopes detected in pith and phloem cells (Appendix 4B).

Additionally, some observations suggested a treatment-induced difference in the labelling pattern of the LM19 epitope in ABR6, which binds to un-esterified homogalacturonan. In two out of the three WS plants analysed, the LM19 epitope was

localised in parenchyma xylem cells next to xylem vessels, while no labelling was detected in control and MS plants (Figure 3.10). However, since not all of the analysed plants showed the same labelling pattern, these observations need to be treated with caution. In Bd21, no LM19 epitopes could be detected (Appendix 4C).

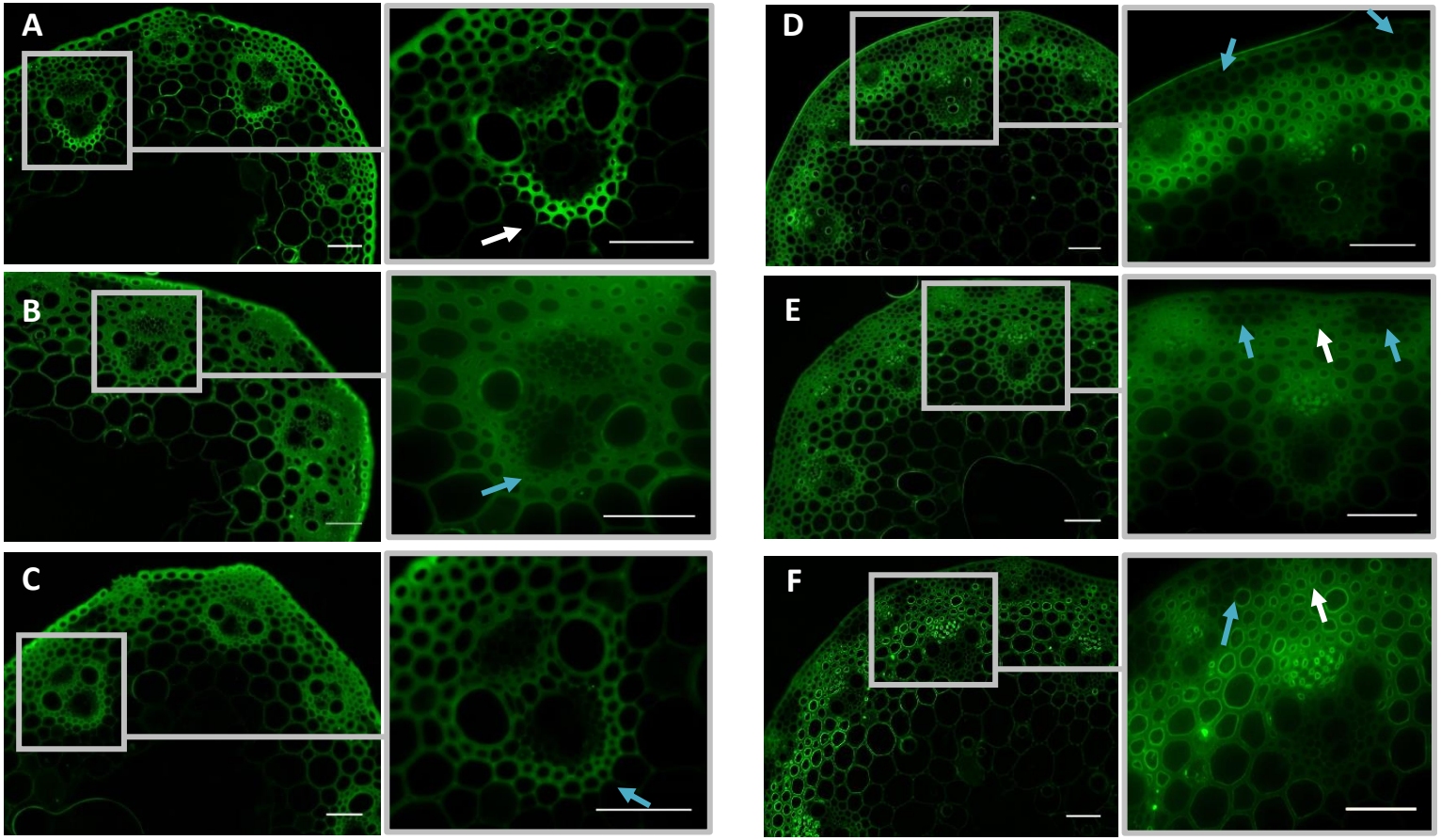

Figure 3.7. Comparison of immuno-localisation of LM5 epitope in Bd21 and ABR6 between treatments.

Indirect immunofluorescence analysis of LM5 binding to transverse sections of *Brachypodium distachyon* second internode of Bd21 and ABR6 for three treatments control, WS and MS. Transverse cross-section visualising labelling pattern for LM5 epitope detection in a selected region of cross-sections with higher magnification images of the selected area in the rectangle: Bd21: control (A), WS (B), MS (C); ABR6: control (D), WS (E), MS (F). White arrows indicate the presence of a signal; blue arrows indicate lack of signal. Scale bar = 50 µm.

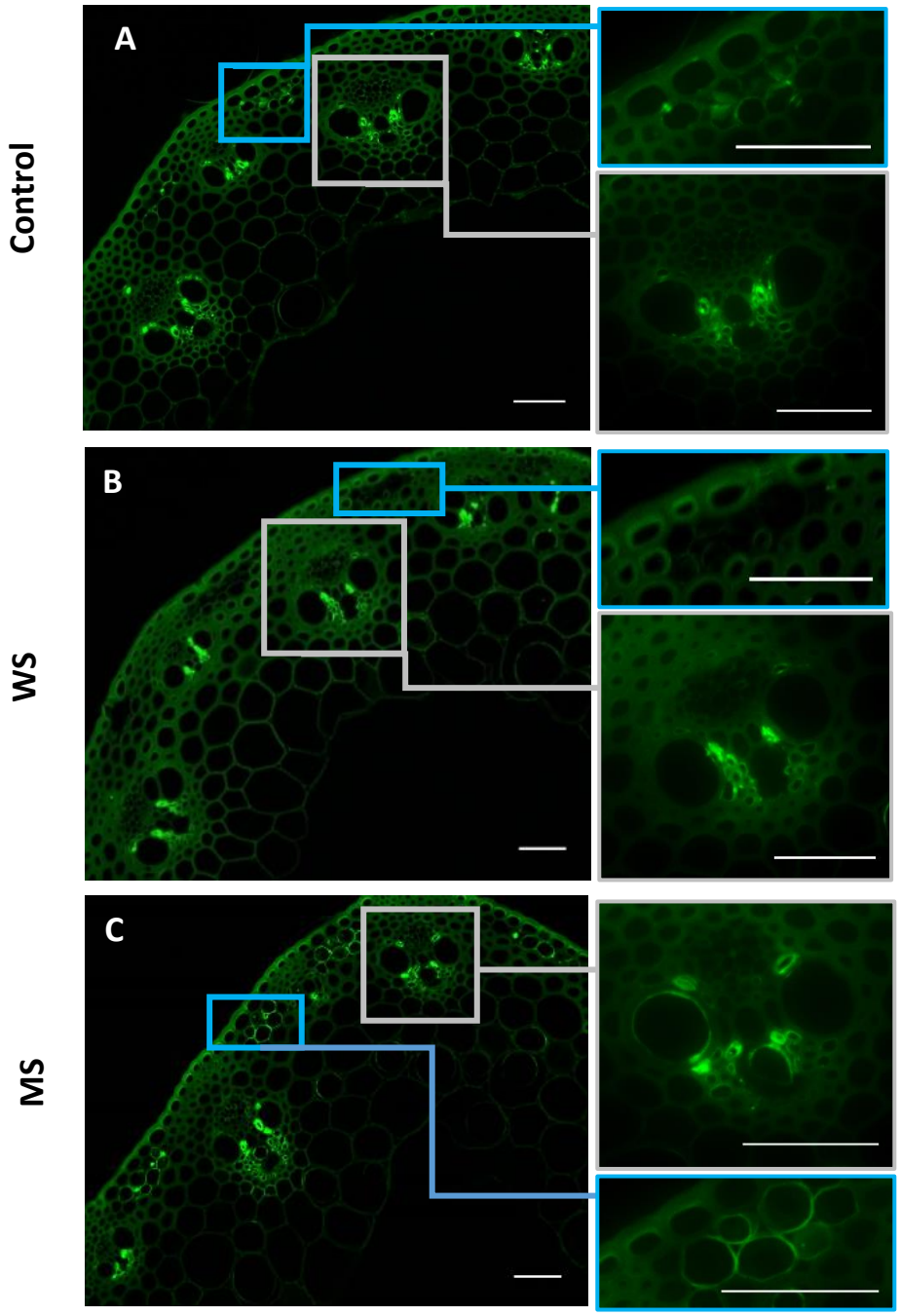

Figure 3.8. Comparison of immuno-localisation of LM13 epitope in Bd21 between treatments.

Indirect immunofluorescence analysis of LM13 binding to transverse sections of Bd21 second internode for three treatments: control (A), WS (B), MS (C) with higher magnification inserts of the selected area in the rectangle: Cortex area – 1, inner vascular bundle area – 2. Scale bar = 50 µm.

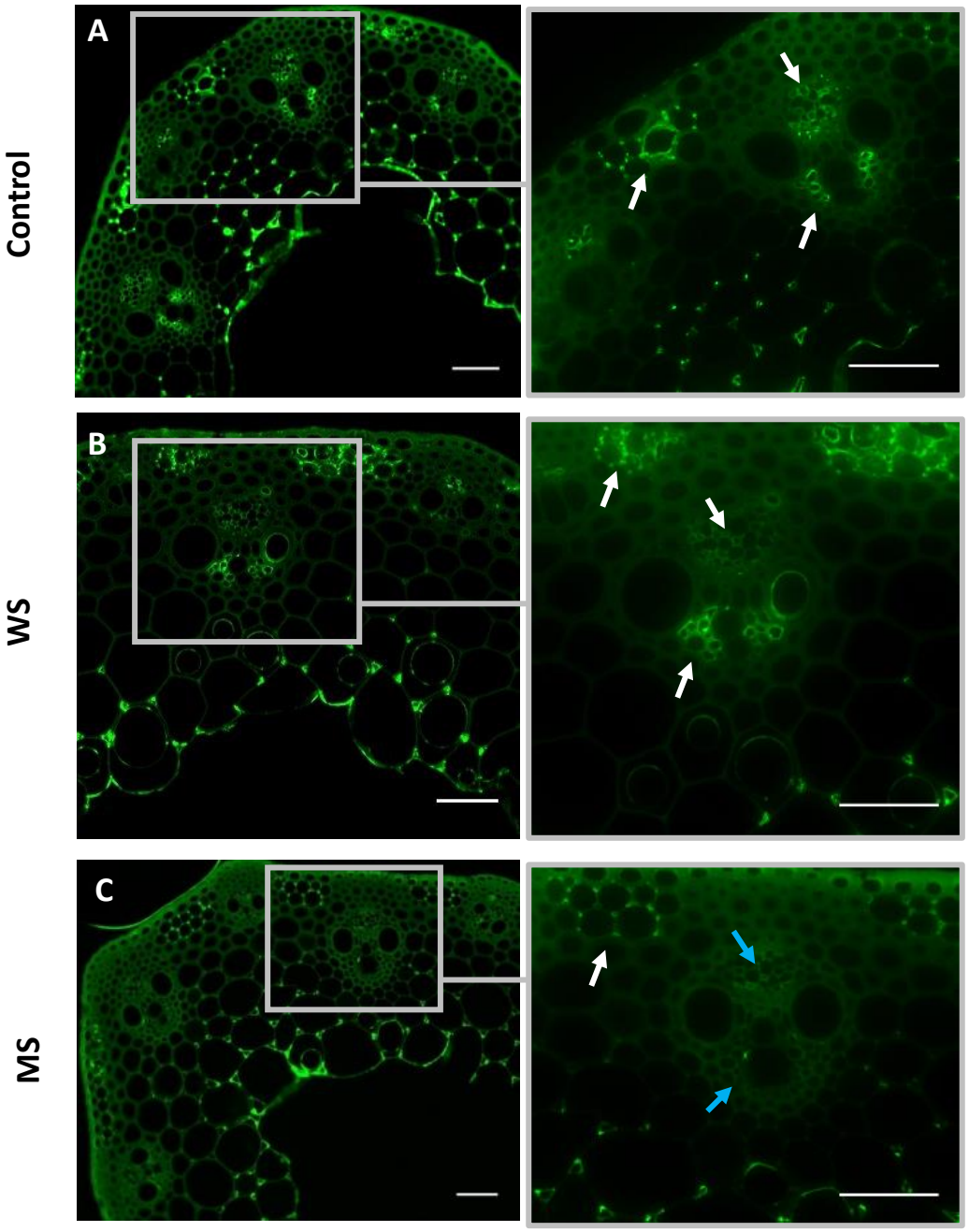

Figure 3.9. Comparison of immuno-localisation of JIM7 epitope in Bd21 between treatments.

Indirect immunofluorescence analysis of JIM7 binding to transverse sections of Bd21 second internode for three treatments: control (A), WS (B), MS (C) with higher magnification inserts of the selected area in the rectangle. Blue arrows indicate cells with a difference in labelling pattern between treatment and control. White arrows indicate the presence of signal; blue arrows indicate lack of signal. Scale bar = 50 µm.

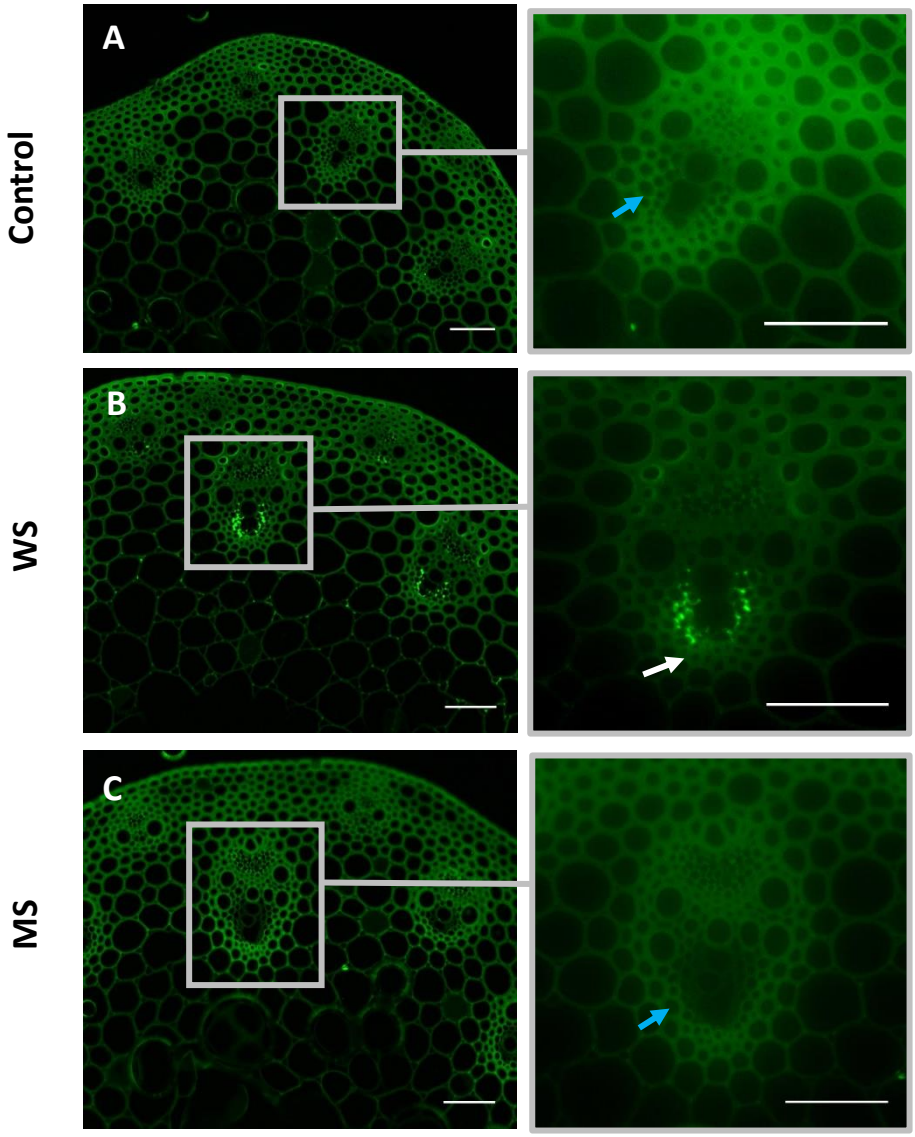

Figure 3.10. Comparison of immuno-localisation of LM19 epitope in ABR6 between treatments.

Immunofluorescence analysis of LM19 binding to transverse sections of ABR6 second internode for three treatments control (A), WS (B), MS (C) with higher magnification inserts of the selected area in the rectangle. White arrows indicate the presence of signal; blue arrows indicate lack of signal. Scale bar = 50 µm.

The LM6 antibody, which binds to (1→5)-α-L-arabinan epitopes were detected in phloem and xylem cell walls in both genotypes in all of the treatments. There was a genotypic difference, as only in Bd21 a signal was detected in cortex cells between VB under the epidermis. No differences between treatments were detected (Appendix 4D). Labelling with LM20, which detects methyl-esterified homogalacturonan, revealed no differences between treatments in both genotypes. Epitopes were visible in the pith, and additionally in Bd21 in cortex cells between VB under the epidermis (Appendix 4E).

No difference between treatments was found in the labelling pattern when using hemicellulose related antibodies (LM25, LM28, LM10). LM25 epitopes were detected in xylem tracheids, and xylem parenchyma cells localised close to xylem vessels. Also, very light signals were visible in phloem cells in both genotypes (Appendix 4F). LM28 which binds to glucuronoxylan was poorly detected in single cells in xylem tracheids, and xylem parenchyma cells localised close to xylem vessels and phloem in all treatments of both genotypes (Appendix 4G). LM10 ((1→4)-β-D-xylan) epitopes were not detected in Bd21, and not in ABR6 control and WS. Epitopes were detected in xylem parenchyma cell walls in only one of three ABR6 plants after MS (Appendix 4H).

No differences between treatments in the labelling pattern were detected in glycoprotein related antibodies (LM1 and LM2). Labelling with LM1, which binds to extensin, was not detected in both genotypes (Appendix 4I). Signals of LM2, which detects β-linked-GlcA in AGP glycan was localised in phloem cell walls, and single signals were observed in xylem cells around xylem vessels (Appendix 4J).

LM12 which binds to ferulic acid showed very light signals in the phloem of Bd21 for all treatments, while no epitope was detected in ABR6 (Appendix 4K).

Labelling with BG1 (mixed-linkage glucan) showed no differences between treatments, and also no differences between genotypes. Epitopes were localised in phloem and pith cell walls. In some of the vascular bundles, signals were also detected in xylem cells (Appendix 4L).

Calcofluor White staining showed more intense labelling of cellulose in pith cell walls and also in the cell walls of the phloem and xylem in both genotypes. No differences were found between treatments (Figure 3.11).

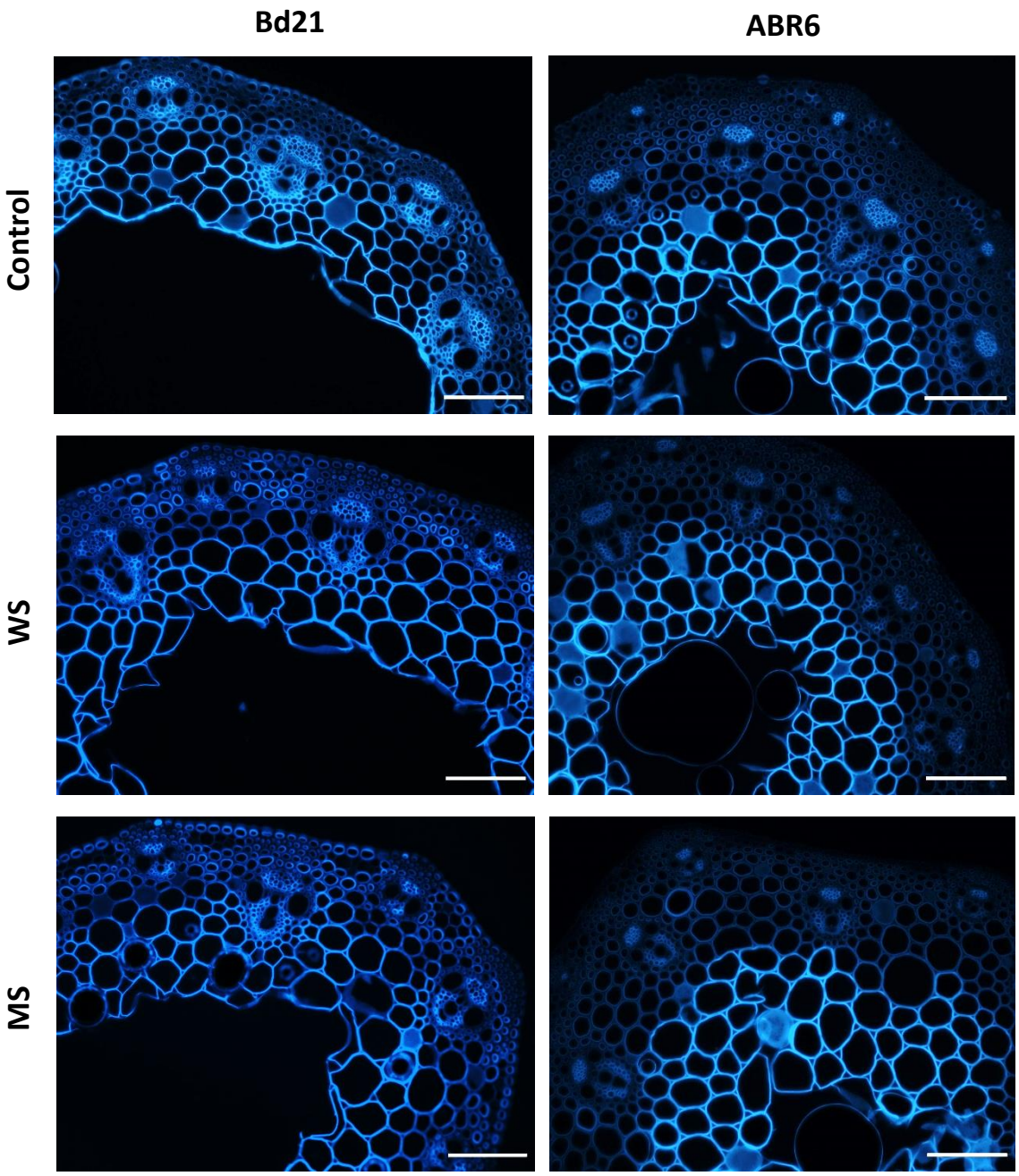

Figure 3.11. Comparison of Calcofluor White staining between treatments in Bd21 and ABR6.

Calcofluor White staining of cell walls of both genotypes in control, WS, and MS treatment. Scale bar = 100 µm.

3.3.6. ENZYME-LINKED IMMUNOSORBENT ASSAY (ELISA)

All anti-hemicellulose, anti-pectin and anti-glycoprotein antibodies used for immuno-localisations were also used for ELISA assays to verify the results and also to obtain quantitative data about the relative abundance of the different epitopes following the different treatments. Results from this assay confirm results obtained from immuno-labelling. No differences were found for LM1, LM2, LM6, LM10, LM12, LM20, LM25, LM28, while a statistically significant difference was found in LM5, LM13, LM19 and JIM7 (Figure 3.12). The OD values of LM19 were significantly higher in ABR6 after WS treatment, which might confirm the additional signals observed in the immuno-localisation study (Figure 3.10). The lower OD value obtained with JIM7 after MS treatment in Bd21 confirms the apparent lower abundance and distribution observed in JIM7 immuno-localisations for MS compared with control and WS treatment (Figure 3.9). A clear labelling pattern for LM5 was observed in Bd21 control, that was absent in WS, and MS (Figure 3.7) and the lower OD value for WS and MS is in agreement with this observation. In ABR6 controls, a lack of signals close to the epidermis was observed (Figure 3.7), and the lower OD value for ABR6 control compared with those of WS and MS samples are in agreement. Moreover, the lower OD obtained for LM13 after WS treatment of Bd21 is in agreement with the lack of signals observed in some cells when compared with the labelling pattern observed for control and MS treatment (Figure 3.8).

		Homogalacturonan - related			Rhamnogalacturonan I - related			Hemicellulose - related			Glycoprotein - related		Other
Genotype	**Treatment**	**LM19**	**LM20**	**JIM7**	**LM5**	**LM6**	**LM13**	**LM25**	**LM10**	**LM28**	**LM2**	**LM1**	**LM12**
Bd21	Control	0.24	0.31	0.72	0.25	0.46	0.24	0.91	0.91	1.09	0.15	0.22	0.51
	WS	0.24	0.31	0.72*	0.22*	0.47	0.17**	0.93	0.91	1.08	0.16	0.22	0.51
	MS	0.25	0.31	0.64**	0.22*	0.47	0.23*	0.89	0.92	1.08	0.15	0.23	0.53
ABR6	Control	0.26	0.34	0.65	0.23	0.51	0.10	0.94	0.87	1.06	0.18	0.25	0.52
	WS	0.28**	0.33	0.65	0.29*	0.52	0.10	0.94	0.89	1.08	0.17	0.24	0.52
	MS	0.24*	0.33	0.65	0.30*	0.51	0.11	0.94	0.87	1.08	0.17	0.24	0.53

Figure 3.12. Heat map-presenting confirmation of immuno-localisation.

Heat map showing the relative abundance of the particular antibody epitopes in cell wall extract of three treatments (control, WS and MS) for both Bd21 and ABR6. Relative intensity shading is applied separately for all antibodies. For the statistical significance of results and differences between treatments the ANOVA test ($P \leq 0.05$) was performed, and if the test showed a significant difference, a post-hoc Tukey's test ($P \leq 0.05$) was also performed. * Statistically significant difference from control; * Statistically significant difference between WS and MS.

3.3.7. PME ASSAY

Radial gel diffusion assays were performed to quantify the pectin methylesterase activity in stems and leaves after both stress treatments in Bd21 and ABR6. Proteins extracted from plant material were allowed to radially diffuse from the well into an agarose gel rich in pectin. PME activity was detected by the development of fuchsia-stained haloes, resulting from de-methylesterification of highly methylesterified pectin present in the gel. Measurement of the area of the halo allowed for a semi-quantitative estimate of PME activity (Pinzon-Latorre & Deyholos, 2014; Lionetti, 2015). Obtained results were calculated based on a standard curve and further transformed to the unit of catalytic activity – nkat.

The area of the formed haloes was much greater after WS and MS in an extract from stems and leaves for both genotypes, compared with controls, which indicated higher PME activity after stress treatments (Figure 3.13). PME activity in Bd21 stems was significantly different between treatments ($P \leq 0.05$). The lowest activity was observed in control – 0.347 nkat, while after WS treatment, the activity was 0.44 nkat, and the highest activity was measured after MS treatment – 0.629 nkat. In ABR6, the response pattern was the same, but generally, PME activity was lower than in Bd21. PME activity in ABR6 control was 0.282 nkat, increasing after WS treatment to 0.476, and the highest activity was again measured after MS treatment – 0.597 nkat (Figure 3.13A). Summarising the results, PME activity was the highest after MS treatment in both genotypes, and a significant difference between WS and MS was also found. Likewise, in the leaves, a statistically significant ($P \leq 0.05$) increase after WS and MS treatment in both genotypes was observed. Bd21 control samples had a PME activity of 0.324 nkat, while for WS this was 0.476 nkat and for MS 0.473 nkat. In ABR6 control the activity was 0.228 nkat, for WS 0.372 nkat, and for MS 0.381 nkat. For the leaf samples, no significant difference between WS and MS in PME activity in both genotypes was found (Figure 3.13B).

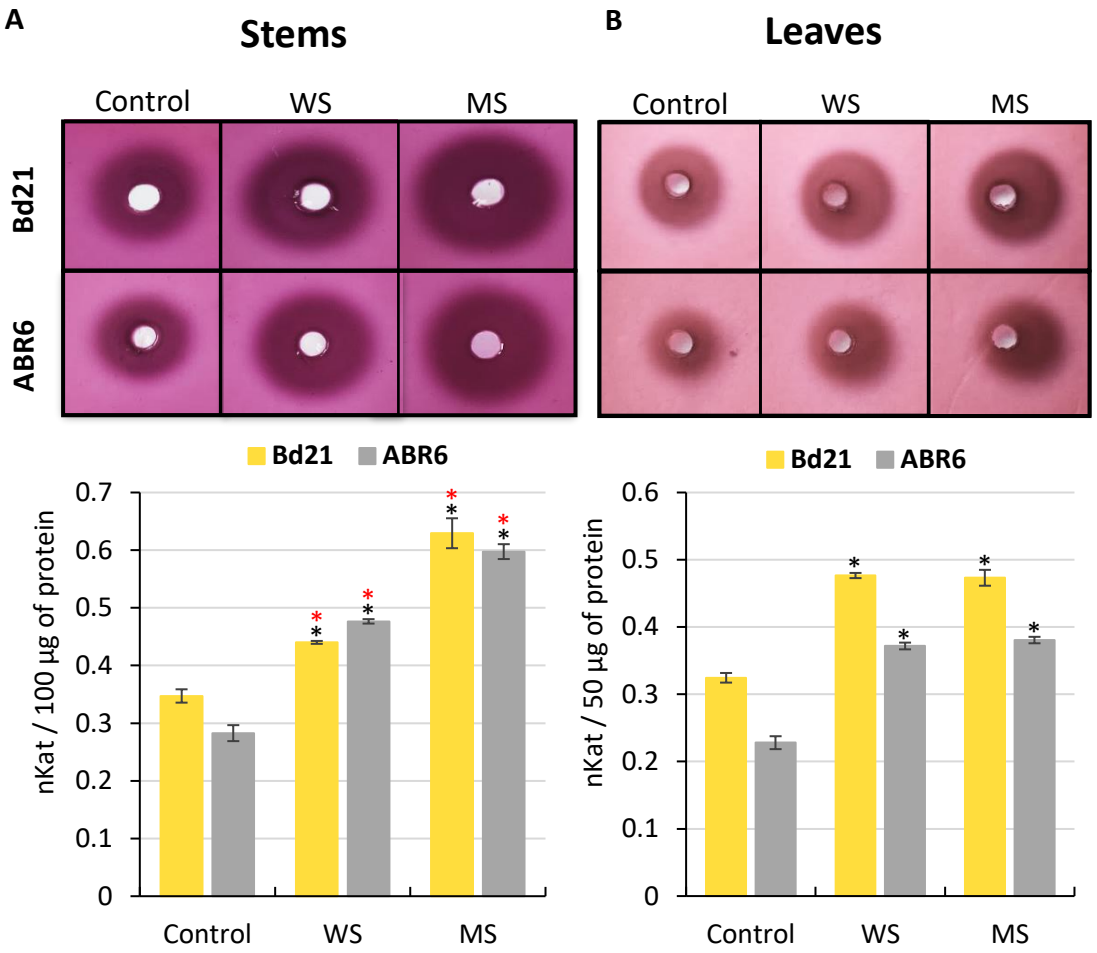

Figure 3.13. PME activity in total protein extract for two genotypes Bd21 and ABR6 of three treatments (control, WS, MS).

A. Radial gel diffusion assay showing PME (halo) activities in protein extracts and quantification of PME activity in stems B. Radial gel diffusion assay showing PME activities and quantification of PME activity in leaves. Data are presented as a mean with standard deviation (±SD). For statistical significance the ANOVA test ($P \leq 0.05$) was performed, and if the test ahowed a significant difference, a post-hoc Tukey's test ($P \leq 0.05$) was also performed. * Statistically significant difference from control; * Statistically significant difference between WS and MS.

3.3.8. PHLOROGLUCINOL STAINING OF STEM TISSUE

Stem cross-sections were stained with phloroglucinol to determine the lignin distribution in stems of both *Brachypodium* genotypes and evaluate if these are different between treatments (control, WS and MS). The phloroglucinol staining clearly showed a more intense signal for stem sections after the WS and MS treatments compared with controls. The colour difference occurred mostly in the sclerenchyma cells below the epidermis (cortex) and in the interfascicular region between VB. The cells below the

epidermis and in the interfascicular region between VB in WS and MS treatment were red-stained, while in control plants appeared pink in both genotypes. Moreover, xylem tracheid's cells were stained brown in WS and MS plants, while in control, the colour was less intense and occurred dark red (Figure 3.14). To conclude, histochemical analysis for lignin showed a clear difference in colour distribution, suggesting that WS and MS stems were more lignified than control plants in both genotypes.

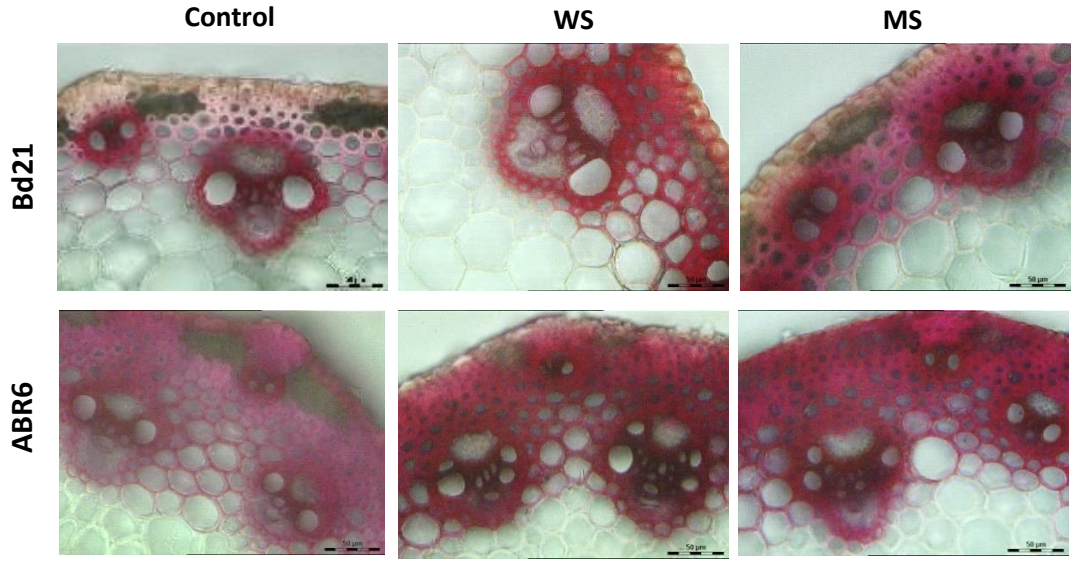

Figure 3.14. Comparison of histochemical staining of lignin between treatments in Bd21 and ABR6 genotype.

Representative images of hand-cut transverse cross-sections of stem second internode for lignin staining with phloroglucinol for all three treatments: control, WS and MS for both genotypes Bd21 and ABR6. Scale bar = 100 µm.

3.4. DISCUSSION

Results presented in this chapter indicate that wind stress and mechanical stress have a significant impact on anatomy, histology and composition of *Brachypodium distachyon* stems. The greater differences between treatments were noted in the localisation of pectic epitopes, PME activity, an organisation of tissues, as well as cell wall thickness and lignin distribution.

Wind stress and mechanical stress induces changes in pectins

Immuno-labelling with specific cell wall antibodies showed differences in the labelling pattern between treatments only with some of the used pectin-related antibodies. The substantial differences were found in the distribution of epitopes related to pectins. Alteration after stress treatments in labelling pattern with RG-I related antibodies (LM5: (1→4)-β-D-galactans, LM13: linearised (1→5)-α-L-arabinan), and HG related antibodies (JIM7: partially methyl-esterified homogalacturonan, LM19: un-esterified homogalacturonan) were observed. Differences were observed not only between control and stress treatment but also between the two stress treatments, indicating that WS and MS may affect plants differently. Although some differences between genotypes were also detected, generally the labelling pattern for most of the antibodies used in this study was very similar between Bd21 and ABR6. Pectins comprise only 5% of the cell wall content in grasses (Vogel, 2008); however, they play a very important part in the complex cell wall matrix. Pectins have been shown to be involved in many different processes, including in plant growth, development, morphogenesis, defence, cell-cell adhesion, wall structure, signalling, cell expansion, wall porosity, binding of ions, growth factors and enzymes, pollen tube growth, seed hydration, leaf abscission, and fruit development (Ridley *et al.*, 2001; Mohnen, 2008). There are three main structural classes of pectins in cell walls, including those of grasses, namely homogalacturonan (HG), rhamnogalacturonan II (RG-II), and rhamnogalacturonan I (RG-I). In functional terms, RG-I is not well defined, although both galactan and arabinan polymers are implicated in contributing to cell wall mechanical properties and to cell wall flexibility (Jones *et al.*, 2003, 2005; Ulvskov *et al.*, 2005; Moore *et al.*, 2008).

(1-4)-β-D-galactans are abundant pectic polysaccharides in plant cell walls and are a significant part of RG-I side chains along with arabinans. The overall function of galactans is poorly understood; however, in the literature, a few possible functions are suggested. Hypotheses were made that galactans retain water and thus may have an impact on modulating the mechanical properties of cell walls (McCartney *et al.*, 2000; Liwanag *et al.*, 2012). Moreover, there are indications that (1-4)-β-D-galactan is essential for the mechanical properties in flax during the development of the fibres (Roach *et al.*, 2011; Liwanag *et al.*, 2012). Pectins are generally most abundant in primary cell walls of expanding cells, but in flax (1-4)-β-D-galactan is relatively abundant in secondary walls, especially in tension wood that forms in response to mechanical stress (Liwanag *et al.*, 2012). Galactans were also found to take part in creating a contractile cell wall in flax by specific entrapment within cellulose microfibrils (Gorshkova *et al.*, 2015). Moreover, galactans may play an important role during cell elongation in *Arabidopsis* seedlings (McCartney *et al.*, 2003). Suggestions were made that (1-4)-β-D-galactan do not affect phenotype (Oxenboll Sorensen *et al.*, 2000; Martín *et al.*, 2005; Ulvskov *et al.*, 2005), but on the other hand the galactan deficient potato tubers were found to be slightly more brittle, indicating that galactan may play a role in transmitting stresses to cellulose microfibrils (Ulvskov *et al.*, 2005). Furthermore, in *Arabidopsis* plants with reduced galactan content, no strong difference in phenotype was noted; however, the stems were thinner compared with the wild type (Øbro *et al.*, 2009).

LM5 antibodies were developed to detect the neutral side chains of RG-I and thus for a better understanding of the role of galactans associated with RG-I (Jones *et al.*, 1997). In this study, LM5 epitopes were detected in the bundle sheath in control plants of Bd21, while no such signals were detected after WS and MS treatments. Moreover, ABR6 showed a different labelling pattern, with no signal in the cortex in control plants. In WS and MS treated plants, only small areas of sub-epidermal parenchyma regions of the cortex were not labelled. Mechanically stressed *Arabidopsis* plants showed that pectic galactan (using LM5) was found to be more abundant in the parenchyma – especially in the pith – of the stressed plant, but only in the bottom part of the stem, while the middle part showed no differences in labelling pattern compared with control

plants (Rigo, 2016). The author suggested that the higher LM5-binding in stressed plants is probably not the result of increased biosynthesis and deposition of galactan in the cell wall as a response to mechanical stress (which would imply a direct effect of mechanical stress), but rather a consequence of galactan not being redistributed in cell walls in stress conditions, because of inhibited cell elongation (Rigo, 2016). These results are different from those obtained for *Brachypodium* in this study, which showed a completely different labelling pattern of cross-sections. One of the reasons for that may be the different cell wall type between these two species. Nevertheless, lack of signals in ABR6 control plants may indicate that these suggestions may be correct indeed. On the other hand, the study performed on *Arabidopsis* seedlings indicated that galactan plays a critical role during the elongation process and as such remains abundant in the cell wall as long as the cell elongates (McCartney *et al.*, 2003). In this study, mechanical stimulation inhibits the elongation of stems compared with control plants. Nevertheless, both studies are performed on different species, with the different cell wall construction and on different tissue type.

Pectic arabinans are a complex set of cell wall polysaccharides in which the (1→5)-α-L-arabinans backbones can variously be branched to RG-I at O-2 or O-3 by single arabinosyl residues or short side chains (Caffall & Mohnen, 2009; Verhertbruggen *et al.*, 2013). It is suggested that arabinans are highly developmentally regulated in terms of their fine structures but also have been shown to integrate within cell wall structures and thus participate in the mechanical and functional properties of plant cell walls (Jones *et al.*, 2003; Ha *et al.*, 2005; Verhertbruggen *et al.*, 2013). Unfortunately, how arabinans act to modulate the mechanical properties and flexibility of cell walls is not understood (Verhertbruggen *et al.*, 2013). LM13 is an antibody that detects unbranched (1→5)-α-L-arabinan epitopes and its binding is highly sensitive to arabinanase action, indicating the recognition of a longer linearised arabinan epitope (Verhertbruggen *et al.*, 2009b, 2013). In *Arabidopsis,* the LM13 epitope is restricted to epidermal cell walls of inflorescence stem and its abundance is relatively stable during development (Verhertbruggen *et al.*, 2013). After exposure to mechanical stress, an increase in the detection of LM13 epitopes in the epidermis was observed compared with *Arabidopsis* control plants (Verhertbruggen *et al.*, 2013). In this study, the labelling pattern is

different from *Arabidopsis*; for all of the treatments, LM13 epitopes were detected in xylem tracheids, and xylem parenchyma cells localised close to xylem vessels. Additionally, in control and MS treatment of Bd21 LM13 epitopes were detected in cortex cells between VB while no such epitope was found in WS plants. No differences in LM13 labelling patterns were found for ABR6. It has been demonstrated that arabinans are extremely variable between species in terms of precise structure (Nakamura *et al.*, 2002; Caffall & Mohnen, 2009). Moreover, there is evidence for heterogeneity of arabinans even between cell types from the same species (Guillemin *et al.*, 2005; Verhertbruggen *et al.*, 2009a). It was suggested that a reduction in the occurrence of the LM13 linear arabinan epitopes could be associated with increased stem stiffness (Verhertbruggen *et al.*, 2013); nevertheless, this study cannot fully demonstrate that. Moreover, in *Arabidopsis,* the occurrence of the LM13 epitope is restricted to epidermal cell walls of younger, elongating regions of inflorescence stems and the authors have indicated that in these areas, greater organ flexibility is required. Additionally, the authors considered that there is a structural requirement for stretches of arabinan that can be acted upon by arabinanase enzymes during elongation growth (Verhertbruggen *et al.*, 2013). The current hypothesis is that the arabinan side chains create highly flexible, space-filling structures that can intervene between nearby HG chains that otherwise would cross-link by means of calcium ions (Jones *et al.*, 2003). Unfortunately, the structure of these arabinan side-chains is still poorly known and understood. Moreover, in the context of linking pectin arabinans, or other cell wall epitopes for that matter, it has been implicated that the key issue in understanding the biomechanical performance of plants from the cell to the tissue and to the organ level is to study the orientation of matrix polymers in relation to cellulose microfibrils or their interplay during mechanical deformation (Burgert, 2006; Thompson, 2008).

Homogalacturonan is the most abundant pectic polysaccharide in cell walls and consists of 1,4-linked galacturonosyl residues. HG is a multifunctional domain of pectin and has many roles relating to primary cell wall assembly and cell extension, cell wall matrix porosity and plant defence responses (Mohnen, 2008; Verhertbruggen *et al.*, 2009a). HG is usually synthesised in a largely methyl-esterified form and regulation of methyl-esterification status is controlled by pectin methylesterases (PMEs), which catalyses the

de-methyl esterification of the C6 linked methyl ester group of HG (Clausen *et al.*, 2003; Pelloux *et al.*, 2007; Mohnen, 2008; Verhertbruggen *et al.*, 2009a; Volpi *et al.*, 2011). The pattern of methylation of HG affects the functional characteristics of the pectic polysaccharides (Caffall & Mohnen, 2009). A number of antibodies are available that can visualise the methyl-esterified and de-esterified forms of HG. In this study, JIM7 and LM20, which both detect methyl-esterified HG and LM19, which detects un-esterified HG were used (Verhertbruggen *et al.*, 2009a). No differences in labelling pattern were found for LM20 between treatments in both genotypes, while JIM7 showed differences only between treatments in Bd21. Compared with WS and control, there was a little to no signal in the phloem and xylem after mechanical stress in Bd21. It is suggested that JIM7 can be used to give a view of the overall methyl-esterification status of HG, while LM20 gives more solid results (Verhertbruggen *et al.*, 2009a) and detects high levels of methyl-esterification (Rigo, 2016). Thus, as no differences in LM20 labelling were found, this may indicate that the amount of methyl-esterified HG is not affected by stress treatments in Bd21 and ABR6. Moreover, labelling with LM19 (un-esterified HG) did not clearly alter in response to mechanical stimulation, suggesting that the treatments did not affect the abundance of pectic de-esterified homogalacturonan. This is in agreement with studies showing no differences in the pattern of LM19 labelling in stems of mechanically stressed *Arabidopsis* plants when compared with controls (Rigo, 2016). In this study, both WS and MS increased the PME activity in both genotypes, suggesting that HG in stress-treated plants contained a lower level of methyl-esterification than control plants. Nevertheless, WS and MS treated plants showed higher PME activity, which would suggest a lower abundance of JIM7/LM20 and higher abundance of LM19. ELISA assays showed no effect for LM20 in both genotypes, and localisation with JIM7 showed only a decrease for MS in Bd21. LM19 was only increased for WS in Bd21 but not for MS. Therefore, ELISA assays could only partly confirm what would be expected based on the radial diffusion assays.

It is known that HG with low levels of methyl-esterification takes part in creating calcium-mediated gels, causing cell wall stiffening and playing a role in regulating the porosity and mechanical properties of cell walls (Ridley *et al.*, 2001; Willats *et al.*, 2001; Hongo *et al.*, 2012). In addition, it may affect intercellular adhesion via the middle

lamella between cell walls (Pelloux *et al.*, 2007; Wolf *et al.*, 2009). Moreover, the level of methyl esterification of cell wall pectin can have a great impact on several physiological processes including stem development (Hongo *et al.*, 2012), cell adhesion (Willatts *et al.*, 2001), fiber elongation (Pinzon-Latorre & Deyholos, 2014), pollen tube growth (Bosch *et al.*, 2005) phyllotaxis (Peaucelle *et al.*, 2008) and cell elongation (Pelletier *et al.*, 2010), but can also influence plant response to fungal and bacterial pathogens (Lionetti *et al.*, 2007; Volpi *et al.*, 2011). Taking all the above into consideration, the results presented in this study suggest that PMEs are involved in the plant response to mechanical stimulation.

The Enzyme-linked immunosorbent assay (ELISA) is a highly versatile and sensitive analytical test for the qualitative or quantitative determination of antibodies or virtually any kind of antigenically active molecule (Engvall & Perlmann, 1971). It has been widely used to detect structurally defined plant cell wall polysaccharide epitopes with use of cell wall antibodies (Verhertbruggen *et al.*, 2009b; Andersen *et al.*, 2016; Posé *et al.*, 2018). In this study, ELISA assays were performed with the same antibodies, which were used for immuno-localisation of cell-wall related antibodies. As the immuno-localisation gives only information about the distribution of the antibodies, ELISA assays were used for additional a semi-quantitative measure of the epitope abundance. In this study, differences found after the immuno-localisation experiment was confirmed by ELISA assays. The differences were found in RG-I related antibodies LM13 in Bd21 and LM5 in both genotypes. Differences were also observed in HG-related antibodies LM19 in ABR6 and JIM7 in Bd21.

Wind stress and mechanical stress induces anatomical and histological changes of stems

Mechanically stimulated plants in this study differed significantly in terms of tissue organisation compared with controls. Moreover, the response differed between the two treatments as well as between the two genotypes. Bd21 WS treated plants developed proportionally more pith, while the area of the cortex, interfascicular region and vascular bundles was reduced. The area of vascular bundles was also reduced in response to MS treatments, but the area of cortex, interfascicular region and pith were similar compared with control. Whereas the area of the cortex and the interfascicular

region was not affected in ABR6, stress-treated plants developed a smaller area of the epidermis and bigger area of vascular bundles. The pith area decreased significantly after MS, with only a slight decrease upon WS treatment compared with controls. Despite these changes in tissue organisation, there was no difference in cell size and number of vascular bundles. Recent studies on *Arabidopsis thaliana* inflorescence showed that mechanical stress has a substantial influence on stem anatomy, resulting in a smaller and more central area of lignified interfascicular tissue. This may suggest a delay in procambial differentiation and expansion prior to the onset of lignification (Paul-Victor & Rowe, 2011; Rigo, 2016). The monocots stems, such as *Brachypodium* do not contain cambium, and their anatomy and development differ significantly. Moreover, during *Brachypodium* stem development, the most drastic changes are visible in the interfascicular region, with the area of this region increasing significantly over time (Matos *et al.*, 2013). As no substantial differences between treatments in terms of area of the interfascicular region was found in both genotypes, this may indicate that plants are at similar development stages and therefore stem development is not affected by mechanical stimulation. Mechanical treatment resulted in a change in tissue geometry and a smaller pith in *Arabidopsis* (Paul-Victor & Rowe, 2011; Rigo, 2016). On the other hand, pith cells increased in size and number in perturbed bean plants; however, this change only tends to fill in the hollow core of the stem and does not significantly contribute to the thickness of the stem and thus its mechanical properties (Biro *et al.*, 1980). In this study, ABR6 and Bd21 responded differently in terms of developed pith area. Bd21 WS plants developed dramatically more pith compared with control and MS, while a small decrease in the pith area was observed after MS in ABR6 plants. *Arabidopsis* mechanical stress-treated plants developed larger cortex and epidermal tissue (Paul-Victor & Rowe, 2011; Rigo, 2016). Increase in the diameter of cortical cells was also observed in runner bean (*Phaseolus multiflora),* broad bean *(Vicia faba)* (Bunning, 1941) and pea (Goeschl *et al.*, 1966). On the other hand, it was suggested that decreased elongation in common bean is due to reduced cell elongation in the outer tissues (epidermis and cortex) (Biro *et al.*, 1980; Biddington, 1986). Generally, changes in the diameter of the cortical parenchyma cells and secondary xylem production accounted for most of the mechanical stress-induced

changes in stem diameter (Goeschl *et al.*, 1966; Biro *et al.*, 1980; Biddington, 1986). In this study, no clear evidence for changes in stem diameter was obtained. On the other hand wind stress reduced the size of tall fescue (*Festuca arundinacea*) leaves, however epidermal cells of the leaves were of similar size compared with control, suggesting that wind reduced the number and not the size of the epidermal cells in the leaves (Grace & Russell, 1977; Biddington, 1986). For oats, the response to windy conditions may be positively correlated with the number and amount of vascular bundles (Jellum, 1962). Old studies on tall fescue showed that the vascular bundles of the control plants were larger but were spaced further apart than in the leaves of wind stressed plants (Grace & Russell, 1977). However, the most recent study on rice (genotype Shengbasimiao) revealed no significant difference in the area of vascular bundles in stem after rubbing (Zhao *et al.*, 2018). In contrast to this finding, mechanically stressed rice stems of a different genotype (Simiaoxuan) developed greater areas of vascular bundles (Zhang *et al.*, 2013a). All the above indicate that response may be connected with species, but also may differ within species between genotypes. This suggestion is in agreement with this study, as results showed a different response to stress treatments between genotypes. Thus Bd21 stressed plants reacted with decrease and ABR6 with an increase of vascular bundle area. All of the vascular bundles in *Brachypodium distachyon* are formed at or before the point of elongation, as the number and size do not significantly change over the time during development and growth (Matos *et al.*, 2013); thus any changes in their area may suggest a direct effect of mechanical stimulation. In dicot plants, research in terms of the effect of mechanical stimulation on plants anatomy and histology is more detailed compared with studies on monocots. Hepworth and Vincent suggested that the cylinder of xylem in the tobacco stems is the most important tissue which determines the stiffness of the whole plant; thus plants respond by increasing the thickness of the xylem tissue cylinder (Jaffe, 1973, 1980; Hunt & Jaffe, 1980; Hepworth & Vincent, 1999). Although the reason for such anatomical structure changes of *Brachypodium* stems presented in this chapter in terms of vascular bundle area remains unknown, it is suggested that obtained results are caused by the direct impact of mechanical stimulation.

Cell wall thickness measurements of the particular region of interest (localised between inner vascular bundle and epidermis) performed in this study were not easy to interpret due to different results obtained by two different techniques used for sample preparation and visualisation. Analysis based on Calcofluor White staining revealed thickening of cell walls after both stresses (both genotypes), while analysis based on scanning electron microscopy (SEM) images showed the opposite. Thinning of cell walls was observed after wind stress in both genotypes and after MS in Bd21, while for ABR6 thickening was observed after MS compared with control. Both procedures have their limitations and advantages. It is difficult to say clearly, which measurements are better and correct. Limited literature, especially for the grasses in terms of changes in cell wall thickness after mechanical stimulation, makes this even more difficult to interpret. Mechanically stressed *Arabidopsis* stems, on the one hand, showed thickening of cell walls of the interfascicular tissue (Rigo, 2016); however, another study showed thinning of the cell wall in the three outer cell layers of the interfascicular tissue (Paul-Victor & Rowe, 2011). It has been suggested that these contrasting findings may be caused by the fact that Paul-Victor and Rowe did not observe a difference in stem diameter and lignification and therefore compared absolute measurements, while in the Rigo study relative proportions were compared because of the varying diameters between stressed and non-stressed inflorescence stems (Rigo, 2016). Moreover, Rigo did not clearly explained which type of staining the cell wall thickness measurements was performed. An increase in cell wall thickness of collenchyma tissue in petioles was observed in mechanically-stressed and wind-stressed celery (Venning, 1949; Walker, 1957). Thickening of cell walls of tracheids was also observed in wind-stressed tamarack (*Larix laricina*) (Biddington, 1986), while mechanical stress had no impact on cell wall thickness in tobacco (Hepworth & Vincent, 1999). Cell wall thickness and lignification of most of the tissues in developing *Brachypodium distachyon* plants increases dramatically over time (Matos *et al.*, 2013). Thus the other aspect that may help with analysis of the cell wall thickness are results from Phloroglucinol – lignin staining. These clearly showed more intense staining in the interfascicular tissue and cortex of wind and mechanically stressed plants. Moreover, higher lignin content after wind and mechanical stress was confirmed by composition analysis (Chapter 4). Lignification is

often connected with thickening of cell walls (Matos *et al.*, 2013), which was clearly observed in *Arabidopsis* stems (Rigo, 2016). This may indicate that measurements based on Calcofluor White staining more accurately reflect the true cell wall thickness compared with those based on SEM. In addition, a substantial part of cell walls in the SEM images was indistinguishable from each other. It might significantly affect measurements, making them less adequate and burdened of greater error compared with measurements based on Calcofluor White.

In conclusion, histological and anatomical features analysed in this chapter are significantly affected by both wind and mechanical stress. The greater changes were observed in tissue geometry, cell wall thickness, pectin polysaccharide distribution, as well as PME activity. Moreover, taking into account the very limited literature in terms of such changes, especially in grasses, makes these finding even more important. This study may be a good indicator for histological and anatomical research connected with lodging resistance in grasses as well as more detailed studies of the response of grasses to the wind and mechanical stress.

CHAPTER 4

CHAPTER 4 : IMPACT OF WIND AND MECHANICAL STRESS ON THE CELL WALL COMPOSITION OF *BRACHYPODIUM DISTACHYON* STEMS

4.1. INTRODUCTION

Grasses are very important from an economic point of view; they provide the majority of calories consumed by humans either directly through the consumption of grains or indirectly through animals fed a diet of grains and forage (Vogel, 2008). Moreover, beyond providing calories, grass cell walls offer essential health benefits through a high content of dietary fibre (Harris & Smith, 2006). Furthermore, polysaccharides of grass cell walls are a significant source of renewable energy because they can be converted into liquid fuel (e.g. ethanol, butanol) and the entire cell wall can be burned to produce heat or electricity (Service, 2007; Vogel, 2008).

The cell walls of monocotyledonous (monocot) plants such as grasses including *Brachypodium distachyon* differ from those of dicotyledonous (dicot) plants as represented by *Arabidopsis thaliana*. Generally, the overall construction of grass and dicot cell walls is alike; a matrix of non-cellulosic polysaccharides surrounds cellulose fibres; nevertheless, cell wall composition differs substantially (Wang *et al.*, 2014). The typical monocot cell walls consist of the three main heterogeneous polymeric components: cellulose, hemicelluloses and lignin, but also other minor components such as pectins, proteins and hydroxycinnamic acids and hydrophobic compounds such as waxes, cutins, and suberins (Carpita, 1996; Rancour *et al.*, 2012). The relative proportion of these chemical subgroups may vary within a single species throughout its development (Carpita, 1996; Fincher, 2009), but also differ substantially between various grass species (Hatfield *et al.*, 2009).

The plant cell walls are the most external layer of a plant cell, which gives shape, controlling growth, and also have remarkable mechanical properties to give plants strength and extensibility (Pilling & Höfte, 2003). Moreover, cell walls provide carbohydrate storage and are the basis for many fundamental functions such as creating defensive barriers for many environmental factors and also play an essential

role in stress sensing and signal transduction (Sarkar et al. 2009; Seifert & Blaukopf 2010).

Cell walls from plants growing in stress environment undergo biochemical changes and reorganisation of components and hence, architecture, which allows the cell walls to adapt to particular conditions (Sarkar *et al.*, 2009). However, there is remarkably little knowledge of the effect of mechanical stimulation on cell wall composition. Cell wall composition is intensively studied in analyses with a focus on plants adaptation to a windy environment and in analyses of lodging resistance. Nevertheless, even in this area of research, the outcome is still not very well understood. Thus, this chapter presents results for compositional changes and alterations in monosaccharides, lignin and hydroxycinnamic acids content as well as differences in saccharification after wind and mechanical stress treatments in *Brachypodium distachyon* stems. Together with phenotypic, histological and anatomical changes, it gives a broader overview of the effect of mechanical stimulation on plants.

4.2. MATERIALS AND METHODS

4.2.1. CELL WALL RESIDUE PREPARATION

Stem material from five plants per each treatment (both genotypes) was harvested and pooled together, and leaf/sheaths and seed heads were carefully removed and discarded. For biological replicates material from first, a second and third experiment was selected (control, WS, and MS). Lignocellulosic biomass was prepared according to the NREL LAP "Preparation of samples for compositional analysis" (Hames *et al.*, 2008). Biomass preparation includes oven-drying biomass at 45°C until moisture content was ≤10%. Dry biomass was then milled with the use of a biomass grinding and loading robot (Labman Automation Ltd.). Biomass material was then fractionated to an alcohol insoluble residue (AIR) according to a protocol adapted from (Foster *et al.*, 2010; da Costa *et al.*, 2014) with some modifications. For each sample, approximately 60-70 mg of dry biomass was weighed, and 1.5 mL of 70% aqueous ethanol was added. Samples were then incubated first for 12 h in a shaking incubator set at 25°C and 150 rpm and then twice for 30 min at 40°C. Subsequently, biomass was extracted three times with 1.5 mL of chloroform/methanol solution (1:1 v/v) at 25°C/150 rpm and finally twice with 500µL of acetone at 25°C/150 rpm after which samples were air-dried for at least two days in a laminar fume hood at room temperature. Between each of the extraction, step samples were thoroughly vortexed before incubation and centrifuged at 3000 rpm for 10 min to aspirate the supernatant containing extractives.

De-starching of extracted biomass was initiated by re-suspending samples in 1 mL of 0.1 M sodium acetate buffer (pH 5) and heating samples in a water bath at 80°C for 20 min to induce starch gelatinisation. After the samples were cooled down to room temperature, they were centrifuged at 1000 rpm, supernatants were discarded, and the pellet was washed twice with 1.5 mL of deionised water with resuspension, centrifugation and supernatant discarding. To inhibit microbial growth, sodium azide was added at 0.0002% (w/v), and starch was removed by incubation with a saturating amount of type-I porcine α-amylase (Sigma-Aldrich; 47 units per 100 mg cell wall) in 0.5 mL of 0.1 M ammonium acetate buffer (pH 5). To ensure complete starch hydrolysis samples were then placed in a shaking incubator set at 25°C (150 rpm) for an extended

incubation period of 48 h. α-amylase digestion was terminated by heating samples in a water bath for 15 min at 95°C and samples were then cooled down at room temperature. The supernatant containing solubilised starch was aspirated, and the pellet was then washed three times in 1.5 mL of deionised water and twice with 1.5 mL of acetone, with centrifugation, vortexing and supernatant removal between each step. De-starched AIR was air-dried in a laminar flow bench until moisture content was ≤10%.

4.2.2. DETERMINATION OF ACETYL BROMIDE SOLUBLE LIGNIN CONTENT

The lignin content of de-starched AIR samples of both genotypes (Bd21, ABR6) was quantified as described by (da Costa *et al.*, 2014) with some modifications. Acetyl bromide soluble lignin (ABSL) content was determined in three technical replicates for each biological replicate (first, second and third experiment) for all of the treatments (control, WS and MS) for both genotypes. Briefly, approximately 7 mg of previously prepared AIR was transferred into 10 mL Pyrex glass tubes, and 500 µL of freshly prepared 25% (v/v) acetyl bromide solution in glacial acetic acid was added to solubilise lignin. Samples were capped with polypropylene caps and placed in a heating block set at 50°C for a total time of 3 h. During the third incubation hour, samples were vortexed thoroughly every 10 min. After incubation, samples were cooled down at room temperature and then diluted by the addition of 2 mL of 2 M NaOH and 350 µL of 0.5 M hydroxylamine hydrochloride and tubes were vortexed. The final volume was adjusted to 10 mL with glacial acetic acid and samples were mixed by inversion, followed by centrifuging at 5,000 rpm for 5 min to produce a particulate-free supernatant. Subsequently, 200 µL of each sample was transferred to UV transparent 96-well plates (UV-Star; Greiner Bio-One), and the absorbance at 280 nm was measured with a µQuant BioTEK plate reader using KC4 software version BioTEK 3.3. A negative control sample without AIR was included to subtract background readings, and a host lab control sample was included as an internal standard. ABSL was calculated using the equation outlined in (Foster *et al.*, 2010).

$$ABSL\% = \left[\left(\frac{A_{280}}{AC \times PL}\right) \times \left(\frac{V_R}{W_S}\right)\right] \times 100\%$$

Where: ABSL% - acetyl bromide soluble lignin percentage content; A280 - absorption reading at 280 nm; PL - path length (0.556cm); V_R - reaction volume (L); W_S - sample weight (g); AC - specific absorption coefficient - 18.126 g^{-1} L cm^{-1}.

4.2.3. DETERMINATION OF MONOSACCHARIDE CONTENT

Composition analysis of previously prepared AIR samples was based on the procedure described by (Sluiter *et al.*, 2012). The analysis was performed on stem samples in two technical replicates for each biological replicate (first, second and third experiment) for all of the treatments (control, WS and MS) for both genotypes. All samples were analysed in duplicates. Briefly, 10 mg of AIR samples was weighed into 10 mL Pyrex glass tubes and 100 µL of 72% (w/w) H_2SO_4 was added. Tubes were capped with polypropylene caps and placed on a heating block set at 30°C for 1 h. Samples were vortexed every 10 min. The acid hydrolysate was diluted to 4% (w/w) H_2SO_4 with 2.5 mL of deionised water and samples were mixed by inversion to eliminate phase separation. Subsequently, tubes were sealed and placed in an autoclave at 121°C for 1 h and then cooled to room temperature and centrifuged to produce a particulate-free supernatant. Samples were diluted ten-fold (1:10) by mixing 100 µL of each sample with 900 µL of deionised water followed by a hundred-fold (1:100) dilution by mixing 50 µL of the 1:10-diluted samples with 950 µL of a solution of 0.015 M KOH. Finally, 400 µL of the 1:100 diluted samples were transferred into 0.45 µm nylon filter-vials (Thomson SINGLE StEP). Monosaccharide concentrations were determined using a Dionex ICS-5000 HPAEC system equipped with a pulsed amperometric detector (PAD) using a gold working electrode and an Ag/AgCl reference electrode. Monosaccharides were separated using the Dionex CarboPac SA10 column set at 45°C and 1 mM KOH for isocratic elution, with a flow rate of 1.5 mL/min for 14 min and 25 µL injection volume. Sugar calibration standards for glucose, xylose, arabinose, galactose, mannose, fructose, sucrose, cellobiose, and fucose were run using serial dilution concentration ranges of 20 µg/mL, 10 µg/mL, 5 µg/mL, 2.5 µg/mL and 1.25 µg/mL. A cellobiose standard was used as an indicator of incomplete hydrolysis. Chromeleon™ 7.2 Chromatography Data System (CDS) software was used for processing and analysing monosaccharide chromatograms.

Finally, the content of each component was estimated as a percentage of cell wall biomass dry weight (Mns%) according to:

$$Mns\% = \frac{C_{Mns} \times V_R}{W_S} \times 100\%$$

Where: C_{Mns} - supernatant concentration (g/L) of the corresponding monosaccharide; V_R - reaction volume (L); W_S - sample weight (g).

4.3.4. ENZYMATIC CELL WALL HYDROLYSIS

The cell wall digestibility was determined using previously prepared un-treated biomass, followed by HPAEC-PAD analysis for all three treatments for both genotypes. Analysis was performed in two technical replicates for each biological replicate (first, second and third experiment). An enzyme cocktail consisting of a mixture of Celluclast (NS 50013; cellulase) and Novozyme 188 (NS 50010; β-glucosidase) was added to approximately 10 mg of cell wall residue (AIR) at a 4:1 ratio. Per sample 997 µL of KOAc buffer at 0.025 M (pH=5.6), 2.4 µL of Celluclast, and 0.6 µL of Novozyme 188, with added sodium azide at 0.04% (w/v) to inhibit microbial growth was used. Samples were incubated for 48 h in a shaking incubator set at 50°C and 150 rpm. After incubation, samples were diluted by adding 9 mL of deionised water (1:10), centrifuged and the supernatant was collected. Immediately before analysis samples were diluted one more time by taking 100 µL of 1:10 diluted samples and 900 µL of distilled water, which resulted in 1:100 dilution factor. Before analysis, 400 µL of diluted samples was transferred into 0.45 µm nylon filter-vials (Thomson, SINGLE StEP) and analysed by HPAEC-PAD on an ICS-5000 ion chromatography system. The analysis was performed with the Dionex CarboPac SA10 column set at 45°C and 1 mM KOH for isocratic elution, with a flow rate of 1.5 mL/min for 14 min and 25 µL injection volume. Results were analysed based on a prepared standard curve with corresponding monosaccharides. From the amount of enzymatically released monosaccharides and the total amount of monosaccharides contained within the cell wall, the percentage of enzymatically released monosaccharides was calculated. All samples were analysed in duplicates.

$$Percentage_{Total\ Mns} = \frac{Enz.\ Mns}{Total\ Mns} \times 100\%\ Total\ Mns$$

Where: Enz. Mns is the amount of enzymatically released monosaccharide from the sample; Total Mns is the total amount of monosaccharide in the sample, previously determined by total acid hydrolysis of the cell wall (Section 4.2.3).

4.2.5. DETERMINATION OF CELL WALL HYDROXYCINNAMOYL ESTERS

The amount of hydroxycinnamic acid (HCA) derivatives *p*-coumaric acid (*p*-CA) and ferulic acid (FA) in AIR were determined using an alkaline saponification method. The analysis was performed in three technical replicates for each biological replicate (first, second and third experiment) for all of the treatments (control, WS and MS) for both genotypes. Approximately 10 mg of AIR was incubated in 500 µL of degassed 1 M NaOH extracting solution for 16 h in a shaking incubator set at 22°C and 200 rpm. After incubation, 490 µL of 1 M hydrochloric acid was added to achieve a pH in the 3-8 range. Samples were then centrifuged, the supernatant was collected, and the pellet was washed with 1 mL of deionised water, and both supernatants were combined. HCAs were then recovered by reverse phase C18 solid-phase extraction (Sep-Pak C^{18} Vac RC cartridges, 500 mg, 3 cm^3, 55-105 µm particle size, Waters Corporation, Milford, Massachusetts, USA), and the resulting samples were centrifugally evaporated at 65°C. Subsequently, samples were reconstituted in 70 µL of 70% (v/v) methanol, and 20 µL were injected for analysis on an RP-HPLC-DAD system (Waters Corp.). For analysis, a radial compression column was used (8.0×100 mm Nova-Pak C^{18} Radial-Pak Cartridge, 4 µm particle size, Waters Corp.), equipped with 100% methanol and 5% (v/v) acetic acid as eluents. Samples were run at 15% isocratic methanol gradient for 15 min, at a flow rate of 2 mL/min. Chromatograms were monitored using a diode array detector (Waters 996 PAD, Waters Corp.) collecting UV/visible spectra at 240 nm – 400 nm and linked to Empower Pro software (Waters Corp.). Amounts of *p*-CA and FA in samples were analysed based on a standard curve prepared with a concentration gradient of the

corresponding HCA. Results are expressed as a percentage of cell wall biomass dry weight.

4.2.6. STATISTICAL ANALYSIS

Values in this chapter are expressed as the mean ± SD. All analyses were performed using SPSS software (version 24). Statistical differences were determined from ANOVA tests at the 5% level ($P \leq 0.05$) of significance, for all parameters evaluated. Where ANOVA indicated a significant difference, pair-wise comparison of means by Tukey's HSD (honestly significant difference) test was carried out at the 5% ($P \leq 0.05$) of significance.

4.3. RESULTS

Results presented in this chapter are based on material collected after three greenhouse stress experiments (Table 4.1). Each experiment represents a biological replicate of a particular treatment. Repeatability of phenotypic traits in each experiment indicates that changes and differences between treatments are stable across experiments performed, thus cell wall composition analysis should also be constant.

Table 4.1. Summary of all analysis performed in this chapter.

✓ Indicates that analysis was done on a particular experiment.

	#1	#2	#3
%ABSL	✓	✓	✓
Monosaccharide analysis	✓	✓	✓
Saccharification	✓	✓	✓
Cell wall-bound hydroxycinnamic acids			✓

4.3.1. LIGNIN CONTENT

Results obtained with phloroglucinol lignin showed changes in staining intensity, indicating differences in lignin content between treatments (see Chapter 3, Figure 3.14). Thus, a more detailed examination of lignin content using the acetyl bromide method was undertaken. The study confirmed histochemical analysis as the lignin content was significantly higher ($P \leq 0.05$) in WS and MS treated plants in both genotypes compared with control plants. For Bd21, WS and MS resulted in a 7.5% and 7.8% higher lignin content, respectively, compared with control plants, and in ABR6 WS plants showed an increase of 6.18% and MS 8.04% in lignin content compared with control plants (Figure 4.1).

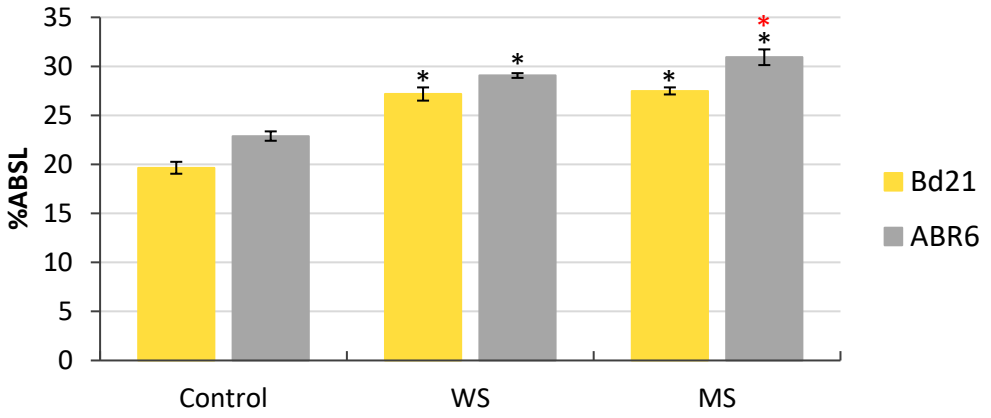

Figure 4.1. Acetyl bromide soluble lignin content.

Comparison of lignin content between treatments (control, WS, MS) for both Bd21 and ABR6 genotypes. Error bars represent standard deviation (SD±) of the mean (n=3). For statistical significance the ANOVA test ($P \leq 0.05$) was performed, and if the test ahowed a significant difference, a post-hoc Tukey's test ($P \leq 0.05$) was also performed. * Statistically significant difference from control; * Statistically significant difference between WS and MS.

4.3.2. CELL WALL MONOSACCHARIDE CONTENT

Cell wall monosaccharide content was characterised for all three treatments (control, WS, and MS) for both genotypes through complete cell wall hydrolysis followed by HPAEC-PAD. Arabinose, galactose, glucose, mannose and xylose were identified and quantified (Table 4.2). The analysis revealed that significant differences ($P \leq 0.05$) between treatments in the content of major cell wall monosaccharides occurred in both genotypes. Arabinose content after MS treatment was significantly lower in both genotypes, moreover, in Bd21, a significant difference between WS and MS was also observed. MS treated plants also showed lower galactose content in both genotypes, WS plants of ABR6 were not affected, while in Bd21 galactose content was significantly higher than control. Both stress treatments resulted in an increased glucose content for ABR6, while in Bd21, a significant increase occurred only after MS treatment. There was no statistically significant difference between treatments in xylose content in Bd21, whereas MS plants of ABR6 had less xylose compared with control and WS treatment. An increase of mannose content was observed in WS treatment in both genotypes, and the same effect was observed after MS treatment but only for ABR6 (Table 4.2).

Table 4.2. Comparison of total monosaccharide content of the cell wall.

Values are expressed as a percentage of cell wall material dry weight (% CWM) for three treatments (control, WS and MS) for each genotype and are presented as the mean (n=3) with standard deviation (SD±). For statistical significance the ANOVA test ($P \leq 0.05$) was performed, and if the test showed a significant difference, a post-hoc Tukey's test ($P \leq 0.05$) was also performed. * Statistically significant difference from control; * Significantly significant difference between WS and MS.

Genotype	Treatment	Arabinose	Galactose	Glucose	Xylose	Mannose
Bd21	Control	3.03 ± 0.1	0.63 ± 0.03	36.99 ± 0.87	22.98 ± 0.48	0.57 ± 0.04
	WS	2.99 ± 0.12*	0.72 ± 0.06**	37.20 ± 0.86*	22.42 ± 0.53	0.64 ± 0.04*
	MS	2.54 ± 0.14**	0.50 ± 0.05**	41.23 ± 1.87**	21.94 ± 1.14	0.60 ± 0.04
ABR6	Control	2.59 ± 0.09	0.55 ± 0.03	40.48 ± 0.4	21.46 ± 0.36	0.45 ± 0.02
	WS	2.47 ± 0.13	0.52 ± 0.04*	42.97 ± 1.07*	21.28 ± 0.74*	0.58 ± 0.06*
	MS	2.33 ± 0.11*	0.45 ± 0.03**	42.81 ± 0.68*	19.74 ± 0.32**	0.61 ± 0.03*

4.3.3. ENZYMATIC CELL WALL HYDROLYSIS

Enzymatic saccharification of two *Brachypodium* genotypes for three treatments (control, WS, and MS) was assessed by extraction with enzymatic cocktail treatment followed by HPAEC-PAD. The analysis revealed that only three major cell wall monosaccharides (glucose, arabinose and xylose) could be detected at substantial amounts after enzymatic hydrolysis of the cell wall. A significant ($P \leq 0.05$) decrease in arabinose and glucose release was observed after both stress treatments for the two genotypes. Arabinose release for Bd21 control was 17.28 ± 0.18, while values for WS and MS were noticeably lower: 14.58 ± 0.53 and 15.71 ± 0.64, respectively (Table 4.3). Similar results were obtained for ABR6 where control showed the highest level of arabinose release (16.04 ± 0.22), while values for WS and MS were lower (14.41 ± 0.81 and 14.51 ± 0.27, respectively). Glucose release for Bd21 was significantly lower after MS treatment (25.81 ± 0.43) and WS treatment (25.87 ± 0.31) when compared with control plants (28.13± 0.59). A similar pattern was observed for ABR6 (WS 23.51 ± 0.49, MS 23.66 ± 0.8, and control 25.97 ± 0.46). The two genotypes showed an opposite response for xylose release: an increase in xylose release was observed for Bd21 plants after WS (18.3 ± 0.27) and MS (17.88 ± 0.63) treatment compared with control (15.89 ± 0.78). While ABR6 plants showed a decrease in xylose release for both stress treatments (WS 14.09 ± 0.24), MS 15.35 ± 0.16) compared with control (16.46 ± 0.25) (Table 4.3).

Table 4.3. Comparison of sugar release after enzymatic hydrolysis.

Values are expressed as a percentage of corresponding monosaccharide content for three treatments (control, WS and MS) for each genotype and are presented as the mean(n=3) with standard deviation (±SD). For statistical significance the ANOVA test ($P \leq 0.05$) was performed, and if the test showed significance difference post-hoc Tukey's test ($P \leq 0.05$) was also performed. * Statistically significant difference from control; * Statistically significant difference between WS and MS.

Genotype	Treatment	Arabinose	Glucose	Xylose
Bd21	Control	17.28 ± 0.18	28.13± 0.59	15.89 ± 0.78
	WS	14.58 ± 0.53*	25.87 ± 0.31*	18.3 ± 0.27*
	MS	15.71 ± 0.64*	25.81 ± 0.43*	17.88 ± 0.63*
ABR6	Control	16.04 ± 0.22	25.97 ± 0.46	16.46 ± 0.25
	WS	14.41 ± 0.81*	23.51 ± 0.49*	14.09 ± 0.24**
	MS	14.51 ± 0.27*	23.66 ± 0.8*	15.35 ± 0.16**

4.3.4. CELL WALL-BOUND HYDROXYCINNAMIC ACIDS

Characterisation of the cell wall-bound hydroxycinnamic acids ferulic acid (FA) and *p*-Coumaric acid (*p*-CA) was performed after extraction with 1 M KOH. The analysis revealed statistically significant ($P \leq 0.05$) differences between treatments in Bd21 and ABR6 for both FA and *p*-CA. An increase in *p*-CA was observed after WS and MS in both genotypes. FA content decreased after both stress treatment in ABR6. The same pattern was observed after MS in Bd21, while after WS, an increase in FA content was noted (Table 4.4).

Genotype	Treatment	*p*-Coumaric acid	Ferulic acid
Bd21	Control	0.336 ± 0.001	0.361 ± 0.002
	WS	0.343 ± 0.001**	0.399 ± 0.004**
	MS	0.364 ± 0.002**	0.321 ± 0.003**
ABR6	Control	0.501 ± 0.006	0.547 ± 0.004
	WS	0.58 ± 0.008**	0.541 ± 0.001*
	MS	0.553 ± 0.004**	0.532 ± 0.002**

Table 4.4. Comparison of cell wall-bound hydroxycinnamic acids.

Values are expressed as a percentage of cell wall material dry weight (% CWM) for three treatments (control, WS and MS) for each genotype and are presented as the mean (n=3) with standard deviation (±SD). For statistical significance, ANOVA test ($P \leq 0.05$) was performed, and if the test showed significance difference, post-hoc Tukey's test ($P \leq 0.05$) was also performed. * Statistically significant difference from control; * Statistically significant difference between WS and MS.

4.4. DISCUSSION

Cell wall composition and associated changes during plant growth and development have been well studied in dicots, in particular, Arabidopsis (Liepman *et al.*, 2010). In addition, with the envisaged utilisation of biomass from grasses (e.g. cereals and dedicated energy grasses), a lot of knowledge has been gathered about cell wall composition in grasses over the last decade (Bhatia *et al.*, 2017). However, knowledge about the impact of environmental stresses, and in particular wind or mechanical stress, on grasses is very limited. This chapter presents various results of changes in cell wall composition of *Brachypodium distachyon* stems after plants were exposed to wind and mechanical stress. In summary, significant stress-induced differences in lignin, monosaccharide content, and ferulic acid and *p*-Coumaric acid content, as well as in saccharification, were obtained.

For quantification of the lignin content, the ABSL method was used. It is a widespread and rapid procedure, which allows determining lignin content in small samples (Hatfield *et al.*, 1999). The extinction coefficients for lignin at a wavelength of 280nm, which is used for the estimation of total lignin content, are very similar for different grass species (Chang *et al.*, 2008). It is known that lignin is essential for the structural integrity of cell walls (Boerjan *et al.*, 2003). Even though this polymer is much weaker than cellulose, lignin provides additional reinforcement resulting in increased tensile strength (Gibson, 2012; Barros *et al.*, 2015). It has been shown that in *Brachypodium distachyon* Bd21 lignin content increases from ~12.8 to 15.8% of the cell wall during the development from expanding to mature developmental stages (Rancour *et al.*, 2012). In this study, lignin content for both Bd21 and ABR6 was significantly increased after plants were exposed to WS or MS with the most substantial effect after MS. There is some evidence in the literature that plants respond to wind by changing lignin accumulation; however, there is no clear consistency in the direction of the response. Wind stressed common bean showed a 25% increase in lignin accumulation compared with non-stressed plants (Cipollini, 1997). Moreover, mechanical stress induced an increase in lignin monomer (sinapylic, coniferylic and p-coumarylic alcohols) content and the number of lignifying vessels in young *Bryonia dioica* internodes (De Jaegher *et al.*, 1985). It has been hypothesised that reduced elongation was related to cell wall rigidification as a result

of accelerated lignification. Authors also suggested that a comparison is possible between accelerated lignification by wind and mechanical stress and induced lignification as a mechanism of disease resistance (De Jaegher *et al.*, 1985). The thigmomorphogenesis response in *Bryonia dioica* can be considered as a mechanism of resistance in order to withstand further environmental, mechanical perturbation (De Jaegher *et al.*, 1985). On the other hand, a reduction in density of lignified cells was found in *Arabidopsis thaliana* plants exposed to wind (Paul-Victor & Rowe, 2011) and no differences in lignin was found in the wind stressed *Abutilon theophrasti* (Henry & Thomas, 2002). Even the relationship between lignin content and lodging resistance is not clear at all. Some studies showed that lignin accumulation is positively correlated with lodging resistance and its higher amounts increase the physical strength of stems (Jones *et al.*, 2001; Berry *et al.*, 2003; Peng *et al.*, 2014). On the other hand, some studies did not observe a correlation between the amount of lignin and lodging resistance (Hondroyianni *et al.*, 2000). There are also suggestions that plants with higher lignin concentration were more prone to stem breakage (Li, 1997). The results presented in this chapter clearly indicate that lignification plays a role in the response of *Brachypodium* plants to mechanical stimulation.

The grass cell walls contain two phenolic acids, both being hydroxycinnamates: ferulic acid (FA) and p-coumaric acid (*p*-CA) (Vogel, 2008). Both FA and *p*-CA content were significantly affected by both wind and mechanical stress treatments in both genotypes. The content of *p*-CA increased after WS and MS in both genotypes, while the response pattern for FA was not the same for both genotypes. In ABR6, a decrease in FA content was observed for both stresses, while for Bd21 WS resulted in an increase and MS in a decrease in FA content compared with control treatment. It needs to be emphasised that observed differences in the content of hydroxycinnamates are small. However, because of the low standard deviation, these small differences in content were identified as being significant by statistical tests. In the literature, there is no evidence of similar studies conducted. Furthermore, the evidence for the analysis of soluble phenolics content after mechanical stimulation, which is not connected with the cell wall, has, to my knowledge, only been described in one paper. McArthur et al. noticed that total soluble phenolic concentration was 7% higher in *Eucalyptus tereticornis*

seedlings exposed to the chronic wind compared with samples from plants from no wind treatment (McArthur *et al.*, 2010). They suggested that their results are consistent with the concept that soluble phenolics, as antioxidants, increase to minimise oxidative pressure that otherwise leads to photo damage and that can occur as a result of a range of abiotic factors, potentially including wind (Close & Mcarthur, 2002; McArthur *et al.*, 2010). Generally, FA and *p*-CA probably play completely different roles in grass cell walls. FA in grasses is mainly by on arabinoxylans attached by an ester linkage to the C5 carbon of arabinofuranosyl branches on the main xylan backbone. Incorporation of FA into the cell wall matrix in most of the grasses is mostly by substitutions upon newly synthesised arabinoxylans (Hatfield & Marita, 2010). The dimerisation of such ferulate esters provides a pathway for cross-linking polysaccharide chains (Ralph *et al.*, 1994). Moreover, FA is also bound to monolignols of the lignin polymer. This results in a highly cross-linked matrix involving both carbohydrates and lignin (Grabber *et al.*, 2004; Hatfield & Marita, 2010). Therefore, FA is involved in the mechanical properties of cell walls, such as giving strength to plants (Hatfield & Marita, 2010). Casler and Jung demonstrated that reduced content of FA in cell walls lead to the enhanced digestibility of cell wall polysaccharides (Casler & Jung, 1999). Structural analysis of feruloylated and lignified grass cell walls revealed that FA might function as nucleation sites for the lignification process, also providing an anchor point to perhaps direct lignification into specific regions of the cell wall (Ralph *et al.*, 1995; Hatfield *et al.*, 1999; Hatfield & Marita, 2010). Though present in substantial amounts, the function of *p*-CA in grass cell walls is less clear, but it has been postulated to be involved in the lignification process (Hatfield & Marita, 2010). The results of this study suggest that ferulic and *p*-CA acids may play a role in response to mechanical stimulation in *Brachypodium distachyon*.

Neutral sugars in the cell wall of *Brachypodium distachyon* were characterised by using a procedure involving total acid hydrolysis of cell wall samples followed by HPAEC-PAD separation and detection. The analysis was performed on stem biomass for three treatments (control, WS and MS) for two genotypes Bd21 and ABR6. The carbohydrates in *Brachypodium distachyon* can be divided into two groups based on abundance: major, including arabinose (Ara), xylose (Xyl), glucose (Glc), galactose (Gal); minor, including rhamnose (Rha), fucose (Fuc), and mannose (Man) (Rancour *et al.*, 2012). In

this study, results for Glu, Xyl, Ara, Gal and Man are presented. Results revealed various differences in neutral sugar content between treatments in both genotypes. Glucose content was significantly higher after both WS and MS in ABR6 compared with control, while in Bd21 a higher glucose content was observed only after MS. Glucose is the most abundant cell wall neutral sugar throughout development and the principal component of cellulose and the mixed-linkage β-glucan and xyloglucan. No differences in labelling pattern with antibodies for MLG and XG and cellulose visualisation with Calcofluor White (chapter 3) were found for such components, but immuno-localisation detect only the specific epitopes, which do not reflect the total content of glucose. Moreover, immuno-localisation was performed only on the second internode of the main stem, while composition analysis was based on overall stem material from plants. Xylose content in Bd21 was not affected by both stress treatments while MS treated plants of ABR6 showed lower xylose content compared with control. Both stresses also affected arabinose, resulting in a lower content after MS in both genotypes. The majority of the xylose found in walls of grasses derives from arabinoxylan, while a smaller contribution arises from xyloglucan. Almost all the arabinose is derived from arabinoxylan, as the contribution from pectic arabinan is very small in grasses (Carpita *et al.*, 2001; Gibeaut *et al.*, 2005; Christensen *et al.*, 2010). Differences found in the content of these two monosaccharides may be at some point connected with differences found in the labelling pattern of RG-I related antibodies used in immuno-localisation (see Chapter 3, Figure 3.7 and 3.8). Galactose content after stress treatment was significantly affected by both stresses. MS treatment led to a lower Gal content compared with control in both genotypes, while WS treatment resulted in higher Gal content for Bd21. Gal, in grass cell walls, is predominantly derived from galactans, mainly in the form of arabinogalactans, which typically occur as side-chains of pectic polysaccharides or as part of AGPs (Carpita, 1996). High Gal content in cell walls was observed during early stages of plant development (seedlings, embryos) in *Brachypodium* rather than in later developmental stages because of more abundant primary cell walls (Rancour *et al.*, 2012). Since galactose occur mostly associated with pectins and AGPs, which are less abundant in secondary cell walls (Ishii, 1997), low Gal contents in stress treatments may be explained by the higher proportion of secondary cell walls after stress exposition. It

would be in agreement with higher lignin content in stress-treated plants of both genotypes. A difference in content was also observed for the minor neutral sugar mannose, resulting in higher mannose content after WS and MS in ABR6 and after WS in Bd21. To my knowledge, there is no data available in the literature on the effect of mechanical stimulation on cell wall monosaccharide content, making it difficult to relate and discuss obtained results with published research. The only analysis of carbohydrate composition was done on soluble sugars, which are not related to the cell wall, however taking into account lack of composition analysis in response to mechanical stimulation, those findings will be discussed. Analysis of the response of seedlings of Eucalyptus tree to wind treatment revealed no significant differences in total soluble carbohydrates (McArthur *et al.*, 2010) while rubbing of rice (*Oryza sativa*) stems did not result in differences in total soluble sugar content compared with control (Zhao *et al.*, 2018). Composition analysis of potential cell wall monosaccharide content alterations after mechanical stimulation was not previously studied. Thus, the results presented in this chapter are novel and may be a good indicator for further and more detailed monosaccharide analyses of the response of grasses to the wind and mechanical stress.

More recently, grasses have been explored as biomass feedstocks for bioenergy production and biorefining into platform chemicals and value-added bio-based products. The inherent recalcitrance of lignocellulosic materials to deconstruction is the most crucial limitation for the commercial viability and economic feasibility of biomass biorefining (Bhatia *et al.*, 2017). Sugar release by enzymatic hydrolysis is one of the most commonly used quality measures for grass biomass quality, as a forage and a bioenergy feedstock. To our knowledge, this is the first data linking mechanical stimulation to differences in saccharification. Enzymatic hydrolysis performed in this study was aimed at comparing potential differences in saccharification (i.e. enzymatic sugar release using an enzyme cocktail) between stress treatments: WS, MS and control. Indeed, significant differences were found, with wind and mechanical stress treatments resulting in lower glucose and arabinose release in both genotypes. Moreover, lower xylose release was observed after both stresses in ABR6, while in Bd21 release of xylose was higher after stresses compared with control treatment. The most likely explanation for lower saccharification after the stress treatments is the higher lignin content observed in

these plants. Lignin is considered to be a major determinant of cell-wall digestibility due to the coating of cell polysaccharides with this complex and insoluble polymer (Marriott *et al.*, 2014). It has been reported that lignin content, as well as lignin structure in cell walls, can have an impact on saccharification (Chen & Dixon, 2007; Studer *et al.*, 2011; Bouvier D'Yvoire *et al.*, 2013; Marriott *et al.*, 2014). There are also reports that modifications in cell wall components other than lignin can affect biomass digestibility such as alteration of production, deposition, or crystallinity of cellulose, which is hard to digest (Harris *et al.*, 2009; Sahoo *et al.*, 2013). Moreover, modification in polysaccharide content and composition can have an impact on saccharification by changing the extractability and/or architecture of the cell wall (Lee *et al.*, 2009; DeMartini *et al.*, 2013; Marriott *et al.*, 2014), but also alteration in linkages between lignin and the polysaccharide matrix via ferulic acid esters may have an effect on saccharification (Marcia, 2009). To my knowledge, this is the first data linking mechanical stimulation to differences in saccharification, which makes this result novel in this area of research.

In conclusion, the results of this chapter provide proof for cell wall compositional alterations in *Brachypodium* stems in response to mechanical stimulation. Cell wall composition changes were detected after both wind and mechanical stress treatment in both genotypes. All of the examined compositional features were significantly affected, resulting in altered monosaccharide, FA and *p*-CA contents, increased lignin content, as well as in lower sugar release. These results indicate that mechanical stimulation affects visual, mechanical and anatomical changes, which may partially originate from changes in cell wall composition.

CHAPTER 5

CHAPTER 5 : THE MOLECULAR AND METABOLIC RESPONSE OF *BRACHYPODIUM DISTACHYON* STEMS TO WIND AND MECHANICAL STRESS

5.1. INTRODUCTION

Despite the sessile nature, plants are very sensitive and responsive to mechanical stimulation, and even seemingly harmless stimulation can provoke reactions in plants. Plants can undergo many changes in terms of their physiology and development to adapt to the surrounding environment, which was clearly visible in previous chapters. Such changes can be noticed some time after stress exposure, but molecular and metabolic changes can occur very quickly after mechanical stimulation. While the phenotypical or developmental alterations are broadly studied and very well documented, especially in dicots, the molecular mechanisms underlying touch perception and mechanotransduction are not well understood (Mauch *et al.*, 1997).

Touch stimulation can rapidly alter gene expression (Lee *et al.*, 2005). The first described touch-induced (TCH) genes in plants were discovered by (Braam & Davis, 1990) in *Arabidopsis thaliana*, which were induced in plants 10 to 30 min following many forms of mechanical stimulation such as touch, rain and wind (Braam & Davis, 1990). A differential cDNA library screen led to the discovery of four TCH genes. The first of these genes, TCH1, encodes a calmodulin (Braam & Davis, 1990; Lee *et al.*, 2005), the next two TCH2 and TCH3 encode calmodulin-like proteins CML24 and CML12, respectively (Braam & Davis, 1990; McCormack *et al.*, 2005; Sistrunk *et al.*, 2007). The TCH4 gene encodes a xyloglucan endotransglucosylase/ hydrolase (XTH), which is involved in cell wall modification (Xu *et al.*, 1996; Rose *et al.*, 2002). Moreover, further genome-wide identification of touch-regulated *Arabidopsis* genes was accomplished (Lee *et al.*, 2005). Researchers found that touch stimulation increased the expression (at least two-fold change) of over 2.5% of genes expressed in *Arabidopsis*. They discovered that genes encoding for Ca^{2+}-binding proteins and cell wall-associated proteins were the most highly represented functional classes of the touch-regulated genes. Additionally, they identified genes encoding for other putative Ca^{2+}-binding proteins, arabinogalactan proteins, pectin esterases, cellulose synthases, expansins but also genes implicated in

disease resistance such as peroxidases, kinases, and transcription factors (Lee *et al.*, 2005). A link between mentioned gene classes and mechanical stimulation has been studied in *Arabidopsis* as well as in other species. For example, genes encoding other CaMs and protein kinases in *Arabidopsis* and in mung bean (*Vigna radiate*) (Perera & Zielinski, 1992; Botella *et al.*, 1996; Mizoguchi *et al.*, 1996), a lipoxygenase in wheat (Mauch *et al.*, 1997), ACC synthases and a cytosolic ascorbate peroxidase in tomato (Gadea *et al.*, 1999; Tatsuki & Mori, 1999), extensins in tobacco (Hirsinger *et al.*, 1999) and xyloglucan endotransglucosylase/ hydrolase in *Arabidopsis* (Xu *et al.*, 1996; Purugganan *et al.*, 1997; Campbell & Braam, 1998). Despite the relatively massive transcriptional reprogramming upon mechanical stimulation, a functional role for the TCH genes in thigmomorphogenesis has yet to be established (Börnke & Rocksch, 2018). Moreover, there is very limited knowledge in terms of the effect of mechanical stimulation on metabolites. Most of the metabolite related studies have focussed on the analysis of cellular signalling involving mostly hormones such as abscisic acid (ABA), auxin (Whitehead, 1963; Chehab *et al.*, 2009), and ethylene (Goeschl *et al.*, 1966; Botella *et al.*, 1995; Johnson *et al.*, 1998; Braam, 2005). Unfortunately, their role in touch-induced changes mostly remains unclear (Börnke & Rocksch, 2018). There is also a hypothesis that the phytohormone jasmonate (JA) might be important for thigmomorphogenesis firstly because of the overlap between genes whose expression is induced by touch and wound-responsive genes induced by JA (Chehab *et al.*, 2012). Secondly, it was reported that jasmonates induce lipoxygenase (LOX) genes and the products of these genes are part of a jasmonate-based signal amplification mechanism (Bell & Mullet, 1991; Mauch *et al.*, 1997). Nevertheless, knowledge in this area of research is still not well established.

The main objective of this study was to investigate if the expression of TCH and cell wall-related genes, identified as being regulated by touch in *Arabidopsis,* is also affected in response to wind and mechanical stress in *Brachypodium distachyon*. The almost complete lack of knowledge of the molecular response in grasses to mechanical stimulation makes this aim even stronger. The study includes analysis of *Brachypodium* orthologues genes established based on over-expressed TCH and cell-wall related genes of *Arabidopsis thaliana* from (Lee *et al.*, 2005). In addition, using the knowledge

acquired in chapter 3 where PME activity was enhanced by mechanical stimulation, it was decided to extend the molecular analysis to PME genes. Additionally, Lipoxygenase genes were analysed, as it was reported that in wheat, the TaLOX1 gene was highly expressed after mechanical stimulation (Mauch *et al.*, 1997). Plants metabolic response to various abiotic stresses is intensively studied, while the metabolic response to mechanical stimulation remains unknown. In the literature no evidence can be found of analysis of pathways involved in response to wind, or other sources of mechanical stress, thus in this chapter, the preliminary metabolic response to wind and mechanical stress was analysed and presented.

5.2. MATERIALS AND METHODS

5.2.1. RNA ISOLATION

Total RNA was isolated from *Brachypodium distachyon* stems of two genotypes, Bd21 and ABR6, for all three treatments (control, WS and MS). For each treatment, stem material from three plants from the first greenhouse experiment was collected and stored at -80^{o}C until use for RNA isolation.

For isolation and purification, the combination of Trizol reagent (Invitrogen) and Qiagen RNAeasy Plant Mini Kit was used. Stem tissue was homogenised to powder in liquid nitrogen with RNase-free mortar and pestle. Around 100 mg of homogenised tissue was transferred to 2 mL Eppendorf tubes and immediately 1 mL of pre-warmed Trizol Reagent was added, and samples were mixed well by vortexing. This is a very crucial step in terms of obtaining pure and high-quality RNA. Addition of Trizol Reagent stabilises RNA from lysis and deactivates intracellular RNases released during the homogenisation. Samples were then incubated at room temperature for 5 min and vortexed frequently. Subsequently, 0.2 mL of chloroform was added, and samples were vortexed for 15 s, incubated at room temperature and again vortexed for 15 s. The chloroform addition is necessary to ensure the partitioning of RNA into aqueous supernatant for isolation and purification. For phase separation, the sample mix was centrifuged at 15,000 rpm for 10 min and RNA was then purified using the Qiagen RNAeasy Mini Kit. Briefly, 200 µL of colourless aqueous RNA supernatant was transferred into a new 2 mL Eppendorf tube, and 700 µL of RNeasy Lysis buffer (RLT) containing 7 µL beta-mercaptoethanol (ß-ME) was added. The remaining aqueous RNA supernatant (±700 µL) was saved as a backup in case of low yield and stored at -20°C. Beta-mercaptoethanol (ß-ME) was supplemented to the RLT buffer, as it is a reducing disulphide bonds agent that irreversibly denatures and inactivates RNases in combination with the guanidinium isothiocyanate (GITC) contained in RLT buffer (Qiagen). To the sample mix composed of sample and buffer, 500 µL of 100% ethanol was added, and samples were vortexed for 15 s. This ethanol step provides the perfect binding conditions for RNA onto the RNeasy silica membrane (Qiagen). Half of the sample was then transferred to the RNeasy MiniElute spin column and centrifuged at

10,000 rpm for 30 s. The flow-through was discarded, and the procedure was repeated with the second half of the sample. An on-column DNase digestion was performed to eliminate genomic DNA contamination. Briefly, 350 µL of RW1 buffer was transferred to the RNeasy MiniElute spin column, incubated for 1min at room temperature, and centrifuged for 30 s at 8,000 rpm. The flow-through was discarded and 80 µL DNase I incubation mix composed of 10 µL of DNase I stock solution and 70 µL of RDD buffer was pipetted directly onto the RNeasy MiniElute spin column. This step must be performed with caution as the digestion may be incomplete if the incubation mix is not on the column. The samples were incubated at room temperature for 15 min, and subsequently, 350 µL of RW1 buffer was added to the column and samples were centrifuged for 30 s at 8,000 rpm. RNeasy MiniElute spin columns were transferred to new 2mL Eppendorf tubes and 500 µL of RPE buffer was added to the column. Samples were centrifuged for 30 s at 10,000 rpm, and the flow-through was discarded. Subsequently, the column was washed twice with 750 µL of 80% ethanol, followed by centrifugation at 10,000 rpm for 15 s after each wash to remove traces of salts on the column due to buffers used earlier in the protocol. RNeasy MiniElute spin columns were again transferred to the new 2 mL Eppendorf tube and spun for 5 min at top speed with the cap off to ensure removal of trace amounts of ethanol that may interfere with downstream applications. Finally, RNA was eluted and dissolved in 30 µL of RNase free water. Following isolation, RNA quality and quantity were assessed using an Epoch Microplate Spectrophotometer (BioTEK). The two ratios were used for checking the purity of RNA sample: A260/230 and A260/280. The nucleic acid is detected at 260 nm, whereas protein, salt and solvents are detected at 230 and 280 nm. Good quality RNA has a value of 1.8 or greater for A260/230 ratio and between 1.8 and 2 for A260/280.

5.2.2. ISOPROPANOL PRECIPITATION OF RNA SAMPLES

For samples with too low RNA yield or purity, isopropanol precipitation was performed. The tube containing aqueous RNA supernatant from the protocol for RNA isolation was defrosted, and the exact volume was determined. An equal volume of 100% isopropanol was added and mixed well by vortexing and incubated at -20°C overnight. The samples

were then centrifuged for 15 min at 14,000 rpm at 4°C and the supernatant was removed without disruption of the pellet. The pellet was washed with 1 mL of 75% ethanol prepared with RNase free water followed by vigorous vortexing. The samples were then centrifuged at max speed for 5 min at 4°C and ethanol was removed. The pellet was left with caps open at room temperature for 5-10 min to air-dry. Finally, the pellet was re-suspended in 200 µL of RNase free water, and the isolation of RNA was continued with RNA isolation protocol from the step of addition of RNeasy Lysis buffer (RLT).

5.2.3. RNA INTEGRITY USING TAE AGAROSE GEL

The integrity and size distribution of total RNA purified with RNeasy Kits can be checked by denaturing agarose gel electrophoresis and GelRed® Nucleic Acid Gel Stain (Biotium). Briefly, the electrophoresis tank, tray, comb, and 100 mL flask were rinsed with 100% ethanol. The gel was prepared with 100 mL of 1xTAE buffer (98 mL ddH_20 + 2 mL 50x TAE stock) and 0.8 g of agarose. The agarose solution was boiled in the microwave, cooled, and GelRed® Nucleic Acid Gel Stain was added, and the solution poured into the tank and solidified. A total of 1.5 µg of RNA was loaded for each sample with 2 µL of 6x loading dye and RNase free water to achieve 12 µL total volume. The gel was run for 30 min at 110 volts. The respective ribosomal RNAs should appear as sharp bands. If the ribosomal bands of a specific sample are not sharp but appear as a smear towards smaller sized RNAs, it is likely that the sample suffered major degradation either before or during RNA purification.

5.2.4. FIRST-STRAND CDNA SYNTHESIS

Synthesis of cDNA was performed with the SuperScript III First-Strand Synthesis SuperMix according to the manufacturer's protocol (Invitrogen). Briefly, obtained RNA was converted into the first-strand cDNA using 1 µg total RNA, 1 µL of 50 µM oligo (dT)20 primer and annealing buffer and RNAse free water to a total reaction volume of 8 µL. The reaction was conducted in aseptic conditions in 100 µL PCR tubes on ice. After

preparing the mix, samples were incubated in a preheated thermal cycler at 65°C for 5 min to anneal template with oligo (dT)20 primers. The reaction was terminated by placing tubes on ice for few minutes immediately after incubation. Subsequently, 10 µL of 2X First-Strand Reaction Mix and 2 µL of Superscript III/RNase OUT Enzyme Mix were then added to the PCR tube on ice. Samples were mixed by vortexing, and the contents of the PCR tube were collected by brief centrifugation and incubated in the thermal cycler at 50°C for 50 min. The reaction was terminated at 85°C for 5 min and stored at -20°C until use.

5.2.5. EXAMINATION OF PCR PRIMERS SPECIFICITY

PCR examinations were performed to check cDNA integrity and primer specificity. PCR reactions consisted of 5 µL of 10x PCR Buffer (Roche), 0.5 µL of 10mM dNTPs, 0.2 µL of FastStart Taq DNA Polymerase (Roche), 0.5 µL of each primer (5 µM) (Forward, Reverse), 0.5 µL of cDNA template and 20.3 µL DEPC treated water. The following PCR thermal cycling conditions were used: 6 min of denaturation at 95°C, subsequently 35 cycles of denaturation (95°C, 30 s), annealing (60°C, 30 s) and elongation (72°C, 1 min), followed by one cycle of final extension (72°C, 7 min). Non-specific amplification, product integrity and specificity, were confirmed by 1% agarose gel with 1x TAE Buffer at an electric field set at 100 V. Primer pairs showing the expected results were then taken into further Real-Time PCR analysis (Table 5.1) and all primers tested are listed in Appendix 5.

For RT-PCR analysis two reference genes were selected based on constitutive expression (Hong *et al.*, 2008; Verelst *et al.*, 2013). S-adenosylmethionine decarboxylase gene (SamDC) was ranked as the most stable in plants grown under various environmental stresses. Ubiquitin-conjugating enzyme 18 gene (UBC18) was validated as a suitable reference gene across all the plant tissues, environmental stresses and various growth conditions (Hong *et al.*, 2008). Reference genes are listed at the bottom of Table 5.1.

Table 5.1. List of primer pairs used for RT-PCR analysis.

Gene name	Gene ID	Designed primer	The sequence of gene-specific primers	Amplicon size (bp)
CaM1	Bradi2g21460	AG01 AG02	F:5'-TCAACGAGGTTGACGCTGAT-3' R:5'-TCTGGTCCTTGTCGAAGACAC-3'	135
		AG03 AG04	F:5'-TTTCTGAACCTGATGGCAAGGA-3' R:5'-CTTCTCCCCGAGGTTGGTCAT-3'	144
CaM5	Bradi1g17237	AG09 AG10	F:5'-TTAAGGAGGCTTTCCGTGTG-3' R:5'-TCACGGATCATCTCATCCAC-3'	127
		AG11 AG12	F:5'-GGCTGAACTCCGTCATGTCA-3' R:5'-TCTGACCGTCACCATCAACG-3'	101
CaM5	Bradi2g10010	AG05 AG06	F:5'-GGCAACGGCACCATTGATTT-3' R:5'-TCAGCAGCAGAGATGAAGCC-3'	137
		AG07 AG08	F:5'-AGTTGGGAACTGTCATGCGT-3' R:5'-AAATCAATGGTGCCGTTGCC-3'	103
CML23	Bradi2g51090	AG19 AG20	F:5'-CATCACTTCGCTGAGCCTGA-3' R:5'-CCCGTTGAGATCAAACCTGC-3'	100
GH	Bradi1g33810	AG21 AG22	F:5'-TGTCGTTCCCAAAGTCGCAG-3' R:5'-CGTTGAAGTCGCGGAAAGAG-3'	135
		AG23 AG24	F:5'-CTCAGCGACATGAGCTACCG-3' R:5'-CGTCGGTGCAGTAGTTGTAGA-3'	73
GH	Bradi1g33840	AG27 AG28	F:5'-AACCTGGAGGGGAAAGGGAT-3' R:5'-GGTAGGATGCCGAGAAGGG-3'	142
ExpA1	Bradi1g76260	AG37 AG38	F:5'-TGTGGGCAGAGAAGGAAGTG-3' R:5'-GTGTCGCAAGGGAAGCAG-3'	109
		AG39 AG40	F:5'-CAAGTGGGTGTGGGCAGAGA-3' R:5'-CACCTCCACTCCTGCGTGTC-3'	132
ExpA1	Bradi1g76270	AG41 AG42	F:5'-TAGGGTCGTCGAACTGGAAG-3' R:5'-ACTTCCTTCTCCACCCACAG-3'	142
		AG43 AG44	F:5'-GGGTGGAGAAGGAAGTGCTG-3' R:5'-GATGTCGGTGATCTGGAGCC-3'	77
ExpA3	Bradi1g28130	AG45 AG46	F:5'-TGGGTGTGGGCTGATAAAG-3' R:5'-GCCACTTTCATTTCCCAGTC-3'	137
CSLD2	Bradi1g50170	AG53 AG54	F:5'-GTATGGCAGCAATGGTGAAG-3' R:5'-TTTCACGGGACACATAGACC-3'	89
b-Glu	Bradi3g03520	AG59 AG60	F:5'-AACTACCTCAACGACGGCTG-3' R:5'-TTTCGGAGGGCAGGAAAAGT-3'	110
Pkinase	Bradi5g24311	AG61 AG62	F:5'-CGGTGGTTGCAAGACTCACA-3' R:5'-TGGAGCATTCTGGCTCACTC-3'	146
PME	Bradi2g11860	AG115 AG116	F:5'-CTTCACCGTGGGATCGTTCA-3' R:5'-TCGCTTGTGACCCTTCAGTC-3'	115
PME	Bradi2g56820	AG71 AG72	F:5'-TATGGCGAGTACGACAGTGC-3' R:5'-TGTATGAAGCTAGCGACGCC-3'	119
		AG117 AG118	F:5'-CGCTAGCTTCATACAGGGGG-3' R:5'-AGTGTTTGCCCAACCTCACA-3'	171
PME	Bradi5g17850	AG75 AG76	F:5'-ATGACGGCGTTCTTTGGGAT-3' R:5'-GAGCCAGTGGAATCCGTTGA-3'	141
		AG119	F:5'-TCAACGGATTCCACTGGCTC-3'	106

		AG120	R:5'-TGCCTGTGCTGTACGAATGA-3'	
		AG121 AG122	F:5'-TCATTCGTACAGCACAGGCA-3' R:5'-GTGGAACTTGTGACCACCCT-3'	140
PMEI	Bradi5g27675	AG129 AG130	F:5'-CTCTTCAGGAGGAAGCGAGTG-3' R:5'-CTTGAGCAGTCGCCATTAGC-3'	143
LOX	Bradi1g11680	AG63 AG64	F:5'-ACAATGATCCCAGCCTCAAG-3' R:5'-TCGGAGGTATTGGGGTAGAG-3'	76
		AG65 AG66	F:5'-TCGAGCAGTACGTGAACGAG-3' R:5'-TCCTTCCACCATGACTGTAGC-3'	91
LOX1/LOX5	Bradi1g09270	AG85 AG86	F:5'-GCAAAAGCGTTGGAGGCATT-3' R:5'-GTATGGAAACTTGGCTGGGC-3'	123
		AG87 AG88	F:5'-CTTCGTCATCGCCACAAGCC-3' R:5'-GGTCATCTCGATGATCCCGC-3'	142
LOX1/LOX5	Bradi1g11670	AG89 AG90	F:5'-AATATCGCCCGTCGGAATCA-3' R:5'-CGCTCAGGAAAAAGGGACCA-3'	143
		AG91 AG92	F:5'-TCAACTTGCCCTTTCCACATG-3' R:5'-GCAAACCGGATTAACTCCTGC-3'	100
LOX2	Bradi3g39980	AG101 AG102	F:5'-GATCCGTTGATCCCGCTAGT-3' R:5'-ACCTCATCTTGTTACCCCTCA-3'	148
LOX3	Bradi1g72690	AG93 AG94	F:5'-ATCTAAGAAGGCGGGGGAGT-3' R:5'-AGATGAGTTTGCAGATAGGCG-3'	96
		AG95 AG96	F:5'-TGATCTCGGCTAAGAATCTGACT-3' R:5'-ACTCCCCCGCCTTCTTAGAT-3'	143
LOX3	Bradi5g11590	AG107 AG108	F:5'-GTGTTCAAGCTGCTCAAGCC-3' R:5'-TCGCCGTTGATGAGGATCTG-3'	80
		AG109 AG110	F:5'-GATCCAGGAGAACAGCGAGG-3' R:5'-GGGAACTCCTGAAGACGCTC-3'	150
LOX5	Bradi3g59942	AG111 AG112	F:5'-CGGCTCAATGAAAACGCCAT-3' R:5'-GACACACATGCCGATGATGC-3'	81
LOX5	Bradi3g59710	AG105 AG106	F:5'-AACGACCTGTACAGCAAGCC-3' R:5'-GGAACTTGACGGGGTTCTCC-3'	133
Gene name	**Reference genes**	**Designed primers**	**Sequence of gene-specific primers**	**Amplicon size (bp)**
SamDC	Bradi5g14640.1	LF72 LF73	F:5'-ATCCATGTGACCCCTGAGGA-3' R:5'-CCTCTTGACAAGGTCGCCAT-3'	87
UBC18	Bradi4g00660.1	LF74 LF76	F:5'-GGAGGCACCTCAGGTCATTT-3' R:5'-CGAGCTAGACAGCATGGACA-3'	157

5.2.6. REAL-TIME PCR ANALYSIS

Real-Time PCR was performed on a Light Cycler® 480 Real-Time Instrument (Roche) with a fluorescence binding dye SYBR® Green PCR Master Mix (Applied Biosystems). SYBR®Green detects specifically the presence of double-stranded DNA (dsDNA) and along with gene-specific primers amplifies a target sequence. The amount of PCR

product doubles after each cycle and hence, the number of SYBR® green molecules incorporated into DNA increases. Therefore, fluorescence intensity increases proportional to the amount of PCR product. The fluorescence signal generated by SYBR®Green was detected and analysed by a Roche Light Cycler® 480 at 530 nm. The Real-Time PCR Instrument monitors the amplification of products in real-time and calculates the amplification efficiency of the products to perform quantitative analysis of gene expression (Figure 5.1). There are two main types of analysis techniques/methods to quantify gene expression by Real-Time PCR: the absolute and the relative quantification.

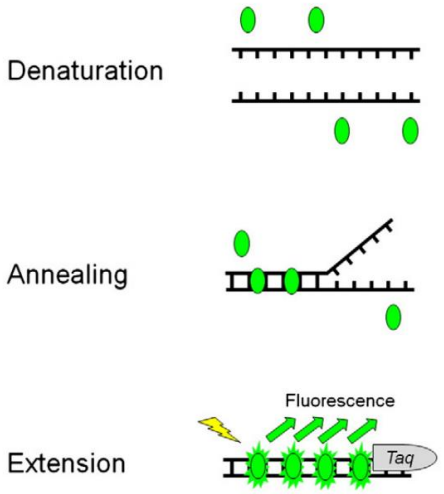

Figure 5.1. SYBR® Green I dye detection chemistries for qPCR.

In the denaturation and annealing phase, the fluorescence signal of the SYBR® Green I dye is absent or very low. Subsequently, during the annealing phase, gene-specific primers hybridize to the target creating short regions of dsDNA. In the extension phase, amount of incorporated SYBR Green I increases as more dsDNA shapes, and therefore signal can be detected and is at its maximum at the end of a PCR cycle (Kim *et al.*, 2013).

5.2.6.1. THE ABSOLUTE QUANTIFICATION

The absolute quantification method was used to evaluate gene-specific primer amplification efficiencies and to quantify a target DNA concentration. In this analysis, a standard curve was used to determine the concentration of unknown samples. In the standard curve, serial dilutions of known concentrations of standard samples are

plotted against the absolute crossing point (Cp) value of the samples. The Cp value is the cycle number at which the fluorescence of a sample becomes detectable by the Roche Light Cycler® 480. Its value depends on the initial DNA concentration in the sample; high initial concentration requires fewer amplification cycles to reach the Cp, while low initial concentration requires more amplification cycles (Figure 5.2). A perfect amplification reaction would produce a standard curve with *Efficiency* of 2.0 because the amount of target DNA doubles with each amplification cycle. Nevertheless, most of the reactions do not show exactly an *Efficiency* of 2.0 due to factors including sample preparation, RNA purity and integrity as well as high GC-content. An *Error* value shows the accuracy of the quantification of the results and should not exceed 0.2 (mean squared error of the single data point fit the regression line). The *Slope* of the standard curve describes the kinetics of the PCR amplification. It indicates how quickly the amount of target DNA can be expected to increase with the amplification cycles, perfect value for the *Slope,* which gives the *Efficiency* of 2.0 is -3.3 (Figure 5.2A). Moreover, Melting Peaks and Amplification Curves generated by the Light Cycler 480® Software were checked for PCR product specificity and the absence of primer-dimers (Figure 5.2B).

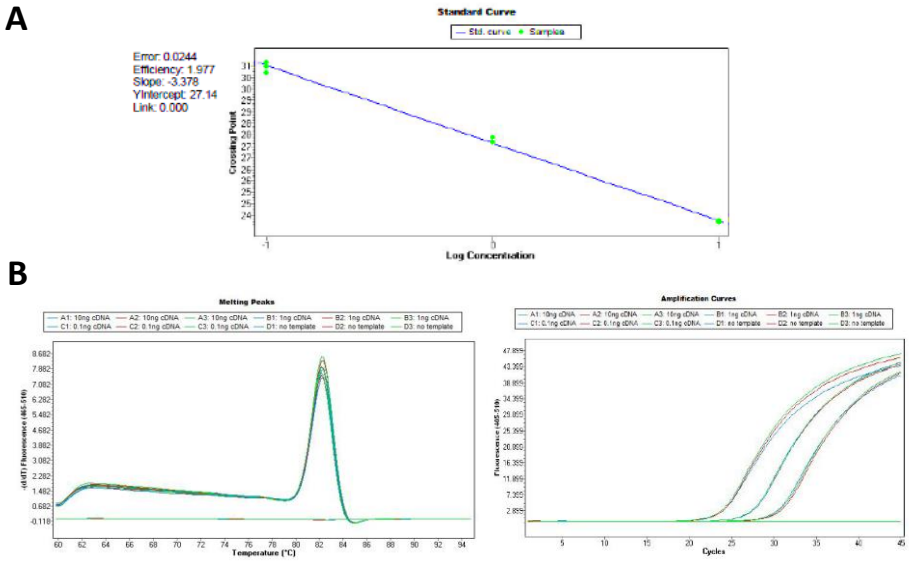

Figure 5.2. Example of Real-Time PCR analysis report on gene-specific primer amplification efficiency.

A. A standard curve, B. Melt Curve and Amplification Curve.

Real-Time PCR reactions were performed in 96-well plates (Roche) with three technical replicates per sample. The reaction mix per sample consisted of 10 µL SYBR Green I Master Mix (Applied Biosystems), 1 µL of each primer (Forward, Reverse) at 5 µM concentration, 3 µL of water and 5 µL of cDNA template from pooled samples diluted to 2 ng/µL, 0.2 ng/µL and 0.02 ng/µL. For each primer set, negative control without template was included. The 96-well plate was sealed with an optical adhesive cover and centrifuged to position PCR reactions into the bottom of the well. 96-well plates with reaction components were assembled on ice until ready to load onto the Light Cycler® 480. Thermal cycling conditions were composed of an initial denaturation step for polymerase activation set at 50°C for 2 min and then 95°C for 10 min, followed by 45 PCR cycles consisting of a denaturation step at 95°C for 15 s, and annealing at 60°C for 1 min. The next step was a melting peak analysis step (1cycle) set at 95°C for 15 s, 60°C for 1 min and 95°C with continuous acquisition mode/monitoring of the fluorescence. A primer amplification efficiency of 1.8 to 2.0 (80%-100%) calculated by the Light Cycler® 480 software was considered satisfactory (Table 5.2). Real-Time PCR reports are presented in Appendix 6.

Table 5.2. Standard curve information for Real-time PCR.

Results of absolute quantification for evaluation of gene-specific primer amplification efficiencies and other parameters are defining primers (slope, error, specificity). Red coloured pairs of primers indicate primers, which matched all criteria, required for being selected for further analysis – relative expression levels. * Indicates pair of primers, which matched all criteria, but other pairs of primers were selected for further analysis. *Specificity* - indicateswhether the pair of primers have non-specific products and/or primer-dimers; + indicates that a pair of primers were specific; - non-specific.

Family	Gene	Designed primer	Slope	LC480 PCR efficiency	Error	Specificity
CaM1	Bradi2g21460	**AG01/AG02**	**-3.085**	**2.110**	**0.071**	**+**
		AG03/AG04*	-3.053	2.126	0.075	+
CaM5	Bradi2g10010	**AG11/AG12**	**-3.249**	**2.032**	**0.06**	**+**
		AG09/AG10	-3.038	2.134	0.056	-
CaM5	Bradi1g17237	**AG07/AG08**	**-3.046**	**2.130**	**0.059**	**+**
		AG05/AG06*	-3.072	2.116	0.055	+
CML23	Bradi2g51090	AG19/AG20	-	-	-	-
GH	Bradi1g33810	AG23/AG24	-2.030	3.109	0.193	+

		AG21AG22	-2.006	3.151	0.178	-
GH	Bradi1g33840	AG27/AG28	-2.831	2.256	0.047	-
ExpA1	Bradi1g76260	AG37/AG38 AG39/AG40	-2.814 -3.660	2.267 1.876	0.244 0.096	- -
ExpA1	Bradi1g76270	**AG43/AG44** AG41/AG42	**-3.652** -2.222	**1.879** 2.819	**0.059** 0.422	**+** -
ExpA3	Bradi1g28130	AG45/AG46	-2.621	2.407	0.25	-
CSLD2	Bradi1g50170	**AG53/AG54**	**-3.137**	**2.083**	**0.094**	**+**
b-Glu	Bradi3g03520	**AG59/AG60**	**-3.247**	**2.032**	**0.044**	**+**
WAK	Bradi5g24311	**AG61/AG62**	**-3.469**	**1.942**	**0.101**	**+**
PME	Bradi2g11860	AG115/AG116	-	-	-	-
PME	Bradi2g56820	**AG71/AG72** AG117/AG118	**-3.432** -2.489	**1.956** 2.522	**0.025** 0.172	**+** +
PME	Bradi5g17850	AG75/AG76 AG119/AG120 AG121/AG122	- -2.170 -3.355	- 2.889 1.986	- 0.024 0.008	- - -
PMEI	Bradi5g27675	AG129/AG130	-	-	-	-
LOX	Bradi1g11680	**AG63/AG64** AG65/AG66*	**-3.378** -2.717	**1.977** 2.334	**0.024** 0.011	**+** +
LOX1/LOX5	Bradi1g09270	**AG85/AG86** AG87/AG88*	**-3.375** -3.249	**1.978** 2.031	**0.015** 0.015	**+** +
LOX1/LOX5	Bradi1g11670	**AG91/AG92** AG89/AG90	**-3.511** -3.874	**1.927** 1.812	**0.028** 0.263	**+** +
LOX2	Bradi3g39980	**AG101/AG102**	**-2.835**	**2.253**	**0.232**	**+**
LOX3	Bradi1g72690	AG93/AG94 AG95/AG96	- -	- -	- -	- -
LOX3	Bradi5g11590	**AG107/AG108** AG109/AG110*	**-3.252** -3.075	**2.030** 2.114	**0.082** 0.027	**+** +
LOX5	Bradi3g59942	**AG111/AG112**	**-3.495**	**1.932**	**0.064**	**+**
LOX5	Bradi3g59710	AG105/AG106	-2.306	2.714	0.015	+

Family	**Reference genes**	**Designed primer**	**Slope**	**LC480 PCR efficiency**	**Error**	**Specificity**
SamDC	Bradi5g14640	**LF72/LF73**	-3.051	2.127	0.110	+
UBC18	Bradi4g00660	**LF74/LF76**	-3.079	2.113	0.107	+

5.2.6.2. THE RELATIVE QUANTIFICATION

The relative quantification was used to verify expression levels of genes of interest. This method compares the Cp value of two different DNA sequences. The first sequence is a reference gene, which should demonstrate a constant Cp value across all samples. This is a very important factor as it provides a basis for normalisation of sample-to-sample differences. The second sequence is a gene of interest. Cp values generated by the Light Cycler® 480 software were then used to calculate the relative fold gene expression with the use of the delta-delta Cp method described by the formula:

$$\text{Fold gene expression} = 2^{-\Delta\Delta\text{Cp}}$$

Where:
ΔΔCp = ΔCp (experimental sample) – ΔCp (control sample)
ΔCp = Cp (gene of interest) – Cp (reference gene)

Once the amplification efficiencies for target and reference genes were confirmed (Absolute quantification), the relative quantification can be conducted. Real-Time PCR reactions were performed in the 96-well plates and consisted of 10 µL of SYBR Green I Master Mix (Applied Biosystems), 1 µL of each primer (Forward, Reverse) at 5 µM concentration, 3 µL of water and 5 µL of cDNA template samples diluted to 2 ng/µL. All samples were analysed in three technical replicates (n=3), and the negative control without cDNA template was incorporated for each sample. The 96-well plate was sealed with an optical adhesive cover and centrifuged to position PCR reactions into the bottom of the well. 96-well plates with reaction components were assembled on ice until ready to load onto the Light Cycler® 480. Thermal cycling conditions were the same as for Absolute quantification. All genes in red in Table 5.2 were analysed for both genotypes Bd21 and ABR6, for all three treatments: control, WS and MS. RT-PCR experiments were performed twice, as independent experiments, and results were tested with the use of the statistical t-student test.

5.2.7. SAMPLE PREPARATION FOR METABOLITE ANALYSIS

For metabolite extraction, six plants per each treatment (control, WS and MS) of both genotypes Bd21 and ABR6 from the second greenhouse experiment were collected. From each plant, the main stem was selected for analysis. Briefly, approximately 40 mg of main stem material was collected and individually placed in Eppendorf microfuge tubes with metal ball bearing before being flash-frozen in liquid nitrogen and stored at -80°C. Samples were then homogenised to a fine powder in a Retch-mill MM300, mixer mill (Retch, Germany) for 2 min. Subsequently, samples were transferred to ice and a 1 mL aliquot of chloroform: methanol: dH_20 (in ratio 1: 2.5: 1) was added to each tube and samples were vortexed and placed in a shaker for 15 min set at 4°C. Samples were again vortexed and subjected to centrifugation for 3 min at 4°C. Particulate free supernatants were then transferred into a new Eppendorf tube and placed on ice. Immediately after this, 80 µL of the extract was transferred into an HPLC vial containing a 0.2 mL flat bottom micro insert and sealed for metabolite analysis. All samples were run in triplicate with no significant differences in the results obtained.

5.2.8. METABOLITE FINGERPRINTING BY FLOW INJECTION ELECTROSPRAY HIGH-RESOLUTION MASS SPECTROMETRY (FIE-HRMS)

Flow injection electrospray high-resolution mass spectrometry (FIE-HRMS) was performed in the High-Resolution Metabolomics Laboratory (HRML) at Aberystwyth University. A Q-Exactive Plus (Thermo-Scientific) mass analyser equipped with an UltiMate 3000 UHPLC system (Thermo-Scientific) consisting of a binary pump and an auto sampler generated metabolite fingerprints in positive-negative polarity switching mode. In the positive ion mode protonated and/or alkali adduct analyte molecules are generally observed in the mass spectra, while in the negative ion mode operation peaks correspond to deprotonated analyte molecules. Ion intensities were acquired between m/z 55 and 1200 in profiling mode at a resolution setting of 280,000 for 3.5 min. An auto sampler injected 20 µL extract into a flow of 100 $\mu L*min^{-1}$ methanol: water (70:30, v/v). Electrospray ionisation (ESI) source parameter settings were according to the manufacturer's recommendations. Mass spectra around the apex of the infusion

maximum were combined into a single mean intensity matrix (runs x m/z) for each ionisation mode using FIEms-pro in R-studio.

5.2.8.1. METABOLOMIC DATA ANALYSIS

Statistical analyses were performed with the R-based MetaboAnalyst 4.0 platform. Data were filtered based on the interquartile range (IQR) to remove variables that were unlikely to be used when modelling the data. Principal component analysis (PCA) was used to distinguish the difference between treatments and genotypes. Statistical differences were estimated from ANOVA tests at the 5% level ($P \leq 0.05$) of significance, and where a significant difference was indicated, pair-wise comparison of means by Tukey's HSD (honestly significant difference) test was carried out at the 5% ($P \leq 0.05$) of significance. For compound and pathway identification, the mummichog algorithm within MetaboAnalyst 4.0 for high-resolution MS peaks was used, without prior peak annotation. Compounds were identified based on mass-to-charge (m/z); the p-values and t-scores, which were used to interrogate the Kyoto Encyclopedia of Genes and Genomes library (KEGG). The targeted metabolites were mapped on to KEGG for pathway analysis. Metabolite Set Enrichment Analysis (MSEA) was performed to identify biologically meaningful pathways.

5.3. RESULTS

Results presented in this chapter are based on material collected after various greenhouse stress experiments (Table 5.3). Repeatability of phenotypic traits in each experiment (Chapter 2) indicates that changes and differences between treatments are stable across experiments performed. Thus, further analysis of the gene expression and metabolomic level should be constant.

Table 5.3. Summary of all analysis performed in this chapter.

✓ Indicates that analysis was done on a particular experiment.

	#1	#2	#3	#4
Gene expression	✓			
Metabolite fingerprinting				✓

5.3.1. THE REAL-TIME PCR ANALYSIS OF GENE EXPRESSION LEVELS

Genetic analysis with the use of Real-Time PCR method was performed to compare gene expression levels between control plants and stress treated plants (WS and MS). The analysis is based on the first greenhouse experiment. The examination includes analysis of cell wall-related and touch-regulated genes (TCH); pectin methylesterase/pectin methylesterase inhibitor genes and lipoxygenase genes.

5.3.1.1. RELATIVE EXPRESSION OF CELL WALL-RELATED GENES

Literature research showed almost no results for the analysis of touch regulated genes in the grass family (one touch-related gene was identified, see section 5.3.1.3); however, a complete analysis was made by Lee et al. on the model plant *Arabidopsis thaliana* (Lee *et al.*, 2005). After careful analysis of their work, it was decided to select cell wall-related genes and touch-regulated genes, which were highly expressed after mechanical stimulation in *Arabidopsis*. The reason for selecting cell wall-related genes was based on the fact that changes in cell wall properties induced by mechanical

stimulation were central to the PhD project. Based on selected *Arabidopsis* genes, the apparent orthologues genes were identified in *Brachypodium distachyon* with use of Phytozyme v.12.1 and EnsemblPlants database (Table 5.4). Unfortunately, many sets of primers were excluded from RT-PCR analysis because of the lack of bands after gel electrophoresis or pairs of primers were not efficient enough for relative quantification analysis. Hence, relative quantification of gene expression levels was performed only on seven genes from the list.

Table 5.4. List of selected *Arabidopsis* genes and *Brachypodium* orthologue genes.

List of selected cell wall-related genes and touch-related genes in *Arabidopsis thaliana* with higher expression level after mechanical stimulation and their orthologue in *Brachypodium distachyon* with a description. Genes were selected and described based on (Lee *et al.*, 2005), supported by information found on the TAIR database. * Indicates information added based on TAIR database. *Brachypodium* gene IDs with a grey background indicates genes that were analysed by RT-PCR; the bold font specifies genes for which the relative quantification was possible to perform. For the remaining genes in the table, the analysis was not performed due to low primer specificity and/or efficiency.

***Arabidopsis thaliana* gene ID**	**Description**	**Orthologue gene ID – *Brachypodium distachyon***	**Description**
At5g37780	CaM1 (TCH1)*	**Bradi2g21460**	Calmodulin-1-related (CAM1)
At2g41110	CaM2 (TCH1)	**Bradi2g10010**	Calmodulin-5-related (CAM5)
At1g66410	CaM4 (TCH1)*	**Bradi1g17237**	Calmodulin-5-related (CAM5)
At3g45970 At4g38400	ExpA1 ExpA2	**Bradi1g76270**	Expansin-like A1-related (ExpA1)
At5g16910	CSLD2	**Bradi1g50170**	Cellulose synthase-like (CSL), Subfamily D2
At5g58090	Glucan endo 1,3beta-glucosidase 6	**Bradi3g03520**	Glycosyl hydrolase (GH), Subfamily GH17, Glucan endo-1,3-beta-D-glucosidase
At1g79680	WAKL10	**Bradi5g24311**	Protein kinase domain (Pkinase), Wall-associated receptor kinase galacturonan-binding (WAK)
At3g01830	CML40	Bradi2g51090	Putative calcium-binding Protein, CML23-related (CML23)
At5g57560	XTH22 (TCH4)	Bradi1g33810	Glycosyl hydrolase (GH), subfamily GH16
		Bradi1g33840	Glycosyl hydrolase (GH), Subfamily GH16' Xyloglucan

			Endotransglucosylase/Hydrolase protein 14-related
At2g41100	CML12 (TCH3)	No orthologue found	
At5g37770	CML24 (TCH2)	Bradi2g02340	Calcium-dependent protein serine/threonine phosphatase activity (CDP)
		Bradi2g31900	Calcium-dependent protein, myosin heavy chain binding, actin filament binding (CDP)
At3g61640	AGP	Bradi2g45510	Arabinogalactan peptide 16-related (AGP)
At3g45970 At4g38400	ExpA1 ExpA2	Bradi1g76260	Expansin-like A1-related (ExpA1)
At3g45970 At4g38400	ExpA1 ExpA2	Bradi1g28130	Expansin-like A3-related (ExpA3)
At4g02330	PME	Bradi2g11850	Pectin methylesterase (PME)
At4g02330	PME	Bradi2g27930	Pectin methylesterase (PME)

Gene expression levels were calculated for seven genes including three encoding calcium-binding proteins: Bradi2g21460, Bradi2g10010, Bradi1g17237; two encoding expansin-related proteins: Bradi1g76260, Bradi1g50170; with the remaining two encoding a glycosyl hydrolase, Bradi3g03520, and a wall-associated receptor kinase, Bradi5g24311. In Bd21, WS and MS treatments resulted in down-regulation of all genes compared with control. A statistically significant difference in expression in Bd21 was found with Bradi2g21460 and Bradi1g76260 after both stresses; Bradi2g10010, Bradi3g03520 and Bradi5g24311 only after WS treatment; Bradi1g50170 only after MS treatment (Table 5.5). Similar results were observed with ABR6; most of the genes after both stress treatments were down-regulated compared with the control. A statistically significant difference after both WS and MS treatment was found for Bradi2g21460, only after MS treatment for Bradi1g17237, Bradi1g76260 and Bradi5g24311, only after WS treatment for Bradi3g03520 and Bradi3g03520. There was one up-regulated gene (Bradi3g03520), although the difference is significant, the fold change increased only by 0.14 compared with control (Table 5.5).

Table 5.5. Comparison of relative expression levels of cell wall-related and touch-related genes between treatments.

RT-PCR analysis to determine the relative expression level of cell wall-related and touch-related genes in three treatments of Brachypodium distachyon stems (control, WS, MS) for two genotypes Bd21 and ABR6. RT-PCR analysis was repeated twice independently with three biological replicates for each treatment; data are expressed as means with standard error means ±SE. The expression level of genes in control was set to 1. For statistical significance t-test, ($P \leq 0.05$) was performed. * Statistically significant difference from control.

Gene	Name	Bd21			ABR6		
		Control	WS	MS	Control	WS	MS
Bradi2g21460	CaM1	1 ± 0.23	0.51 ± 0.03*	0.62 ± 0.07*	1 ± 0.12	0.75 ± 0.08*	0.63 ± 0.06*
Bradi1g17237	CaM5	1 ± 0.26	0.62 ± 0.07*	0.79 ± 0.07	1 ± 0.12	1.14 ± 0.14*	0.64 ± 0.05
Bradi2g10010	CaM5	1 ± 0.28	0.57 ± 0.07	0.78 ± 0.06	1 ± 0.12	0.91 ± 0.05	0.82 ± 0.05*
Bradi1g76270	ExpA1	1 ± 0.31	0.84 ± 0.11*	0.76 ± 0.11*	1 ± 0.19	0.95 ± 0.12	0.76 ± 0.17*
Bradi1g50170	ExpA1	1 ± 0.16	0.89 ± 0.14	0.77 ± 0.15*	1 ± 0.15	0.84 ± 0.05	1.18 ± 0.1
Bradi3g03520	b-Glu	1 ± 0.16	0.59 ± 0.09*	0.67 ± 0.11	1 ± 0.16	0.65 ± 0.07*	0.8 ± 0.08
Bradi5g24311	WAK	1 ± 0.11	0.55 ± 0.09*	0.85 ± 0.19	1 ± 0.14	0.8 ± 0.04	0.66 ± 0.04*

5.3.1.2. RELATIVE EXPRESSION OF PME GENES

Considering the data presented in Chapter 3 in terms of results obtained with immuno-localisation of pectin-related antibodies and PME gel diffusion assay, it was decided that RT-PCR analysis including pectin methylesterase (PME) and pectin methylesterase inhibitor (PMEI) genes should be performed. It may give a deeper insight into the relationship between mechanical stimulation and pectins. Recognition of all PME/PMEI genes identified in *Brachypodium* was performed with the use of Phytozyme v.12.1 and EnsemblPlants database. The approach for the selection of PME/PMEI genes for RT-PCR analysis was to find genes with higher expression, particularly in stem-related plants organs, as the main focus of analysis in this research are stems. For the selection of candidates' genes with the higher expression levels in early inflorescence and/or emerging inflorescence and/or leaves the EnsemblPlants database and EMBL-EBI Expression Atlas was interrogated. List of genes, which show any expression in plant parts listed above is presented in Appendix 7. After choosing genes, which show any expression in these plant organs, six genes with the highest expression levels were selected for further analysis (Table 5.6).

Table 5.6. List of selected PME/PMEI genes.

Pectin methylesterase genes and pectin methylesterase inhibitor genes with the highest expression levels in early inflorescence and/or emerging inflorescence and/or leaves selected for expression analysis. *Brachypodium distachyon* gene IDs on grey background indicate genes that were analysed by RT-PCR; the bold font specifies the PME gene (Bradi2g56820) for which the relative quantification was possible to perform. For the remaining genes in the table, further analysis was not performed due to low primer specificity and/or efficiency.

Gene	Description
Bradi2g56820	Pectin methylesterase
Bradi2g11860	Pectin methylesterase
Bradi5g17850	Pectin methylesterase
Bradi5g27675	Pectin methylesterase inhibitor
Bradi3g30770	Pectin methylesterase inhibitor
Bradi3g45080	Pectin methylesterase inhibitor

Bradi2g56820 showed down-regulation after MS treatment in Bd21, while WS treatment had no effect compared with control (Table 5.7). Results for ABR6 were opposite, with MS treatment resulting in up-regulation of the gene expression, while WS treatment in down-regulation compared with control treatment (Table 5.7).

Table 5.7. Comparison of the relative expression level of the Bradi2g56820 PME gene between treatments.

RT-PCR analysis of the relative expression level of PME (Bradi2g56820) in three treatments of *Brachypodium distachyon* stems (control, WS, MS) for two genotypes Bd21 and ABR6. RT-PCR analysis was repeated twice independently with three biological replicates for each treatment; data are expressed as the mean with a standard error of the mean ±SE. The expression level of genes in control was set to 1. For statistical significance t-test, ($P \leq 0.05$) was performed. * Statistically significant difference from control.

Gene	Name	Bd21			ABR6		
		Control	WS	MS	Control	WS	MS
Bradi2g56820	PME	1 ± 0.14	1.05 ± 0.15*	0.67 ± 0.09**	1 ± 0.35	0.78 ± 0.11**	1.6 ± 0.22**

5.3.1.3. LIPOXYGENASE GENES

To our knowledge, only one touch-related gene, encoding for a lipoxygenase, has been identified in the grasses. Researchers found that after mechanical stimulation, a lipoxygenase gene in wheat (*TaLOX1*, GenBank: U32428.1) was highly expressed (Mauch *et al.*, 1997). Bradi1g11680 was identified as the orthologue for *TaLOX1* in *Brachypodium distachyon*. Real-time PCR analysis showed very high expression levels of Bradi1g11680, especially after MS treatment in ABR6. This result prompted us to continue the analysis of lipoxygenase genes. Two approaches were undertaken. The first approach was to select genes from the pathway that Bradi1g11680 is part of. This analysis was made with the use of the PlantCyc *Brachypodium distachyon* database, and it revealed that Bradi1g11680 is a part of the 9-lipoxygenase and 9-hydroperoxide lyase pathway (Appendix 8A). The five LOX genes out of the seven genes in that pathway were selected for further analysis. Available expression data showed that Bradi1g11680 had by far the highest expression levels of these five LOX genes, especially in the inflorescence (Appendix 8B). In the second approach, similar to what was previously presented (section 5.3.1.2), lipoxygenase genes, not confined to the before-mentioned pathway, were selected based on their expression levels (Appendix 9). All selected genes from the two approaches are listed in Table 5.8.

Table 5.8. List of selected Lipoxygenase genes

List of selected *Brachypodium distachyon* lipoxygenase genes. *Brachypodium* gene IDs on grey background indicate genes that were analysed by RT-PCR; the bold font specifies genes for which the relative quantification was possible to perform. For the remaining genes listed in the table, further analysis was not performed due to low primer specificity and/or efficiency.

Gene	Description
Bradi1g11680	Iron ion binding, lipoxygenase activity / TaLOX1 (wheat)
Bradi1g09270	Iron ion binding, lipoxygenase activity (LOX)
Bradi1g11670	Iron ion binding, lipoxygenase activity (LOX)
Bradi3g39980	Iron ion binding, lipoxygenase 2-related activity (LOX2)
Bradi5g11590	Iron ion binding, lipoxygenase 3-related activity (LOX3)
Bradi3g59942	Iron ion binding, lipoxygenase 5-related activity (LOX5)
Bradi1g72690	Iron ion binding, lipoxygenase 3-related activity (LOX3)
Bradi3g59710	Iron ion binding, lipoxygenase 5-related activity (LOX5)
Bradi3g07000	Iron ion binding, lipoxygenase 2-related activity (LOX2)
Bradi3g07010	Iron ion binding, lipoxygenase 2-related activity (LOX2)
Bradi1g09260	Iron ion binding, lipoxygenase activity (LOX)

As already mentioned, expression of Bradi1g11680, the orthologue to wheat TaLOX1, showed a significant increase in ABR6; ranging from ˜2.5 fold after WS treatment and ˜7.5 fold after MS treatment compared with control (Table 5.9). The lipoxygenase encoding gene Bradi1g09270 was down-regulated after WS treatment in ABR6, while after MS treatment, there was a statistically significant increase in expression by ˜2.5 fold. Analysis of Bradi1g11670 showed a slight increase of expression after both stresses in ABR6; however, these were not significant. Lower expression was observed for Bradi3g39980 after WS treatment, while expression was significantly higher (˜1.7 fold) in MS treated ABR6 plants compared with control. Increased expression in both stresses was also detected for Bradi5g11590, ranging from ˜1.8 fold after MS treatment to ˜1.6 fold after WS. The expression of Bradi3g59942 was significantly lower after both stresses in ABR6 (Table 5.9).

Generally, the results for Bd21 were not consistent with those for ABR6 (Table 5.9). While Bradi1g11680 was highly expressed in ABR6 after both stresses, expression in Bd21 showed a significant down-regulation after both stresses. The same pattern of response (lower expression compared with controls) was also observed for Bradi1g11670, Bradi5g11590 and Bradi3g59942. Bradi1g09270 was down-regulated after WS treatment, while after MS treatment, there was a slight increase in expression (˜1.13 fold); however, this was not significant. No differences in expression levels were found for Bradi3g39980 (Table 5.9).

Table 5.9. Comparison of relative expression levels of lipoxygenase genes between treatments.

RT-PCR analysis to determine the relative expression level of lipoxygenase genes in three treatments of *Brachypodium distachyon* stems (control, WS, MS) for two genotypes Bd21 and ABR6. RT-PCR analysis was repeated twice independently with three biological replicates for each treatment; data are expressed as the mean with a standard error of the mean ±SE. The expression level of genes in control was set to 1. For statistical significance t-test, ($P \leq 0.05$) was performed. * Statistically significant difference from control.

Gene	Name	Bd21			ABR6		
		Control	WS	MS	Control	WS	MS
Bradi1g11680	LOX	1 ± 0.25	0.57 ± 0.07*	0.64 ± 0.09*	1 ± 0.08	2.42 ± 0.26**	7.51 ± 0.72**
Bradi1g09270	LOX	1 ± 0.21	0.61 ± 0.09**	1.13 ± 0.31*	1 ± 0.2	0.31 ± 0.04**	2.56 ± 0.4**
Bradi1g11670	LOX	1 ± 0.21	0.52 ± 0.05*	0.57 ± 0.06*	1 ± 0.24	1.15 ± 0.08	1.36 ± 0.11
Bradi3g39980	LOX	1 ± 0.05	0.57 ± 0.16	0.69 ± 0.09	1 ± 0.2	0.75 ± 0.06**	1.73 ± 0.34**
Bradi5g11590	LOX	1 ± 0.17	0.69 ± 0.07**	0.87 ± 0.13**	1 ± 0.3	1.58 ± 0.13*	1.77 ± 0.09*
Bradi3g59942	LOX	1 ± 0.06	0.82 ± 0.08*	0.9 ± 0.07*	1 ± 0.24	0.6 ± 0.06**	0.44 ± 0.03**

5.3.2. METABOLITE FINGERPRINTING ANALYSIS

Metabolite analysis was performed for all three treatments (control, WS and MS) for both genotypes Bd21 and ABR6 with use of metabolite fingerprinting by flow injection electrospray high-resolution mass spectrometry (FIE-HRMS). The negative and positive ionisation spectra were generated and analysed with principal component analysis (PCA) and Partial Least Squares Discriminant Analysis (PLS-DA). PCA analysis belongs to a so-called unsupervised technique, and PLS-DA is a supervised technique used for metabolite data presentation and analysis. The PCA method focuses on differences between samples rather than differences between groups, which means that the method does not use class label information. On the other hand, PLS-DA highlights the differences between groups (Worley & Powers, 2013).

PCA analysis for the negative ionisation derived spectra showed the well-defined separation of two genotypes (Figure 5.3A). The majority of the variation in Bd21 is between WS treated samples with control and MS treated samples (Figure 5.3B). In ABR6, the variation between treatments is not significantly different (Figure 5.3C). Nevertheless, PLS-DA analysis for metabolites detected in negative ionisation mode showed clear variation between genotypes (Figure 5.3D), but also within each genotype showing separation between all three treatments in both genotypes (Figure 5.3E, F).

Spectra derived in positive ionisation mode analysed by PCA indicates that there is a clear separation between the two genotypes (Figure 5.4A). Moreover, a significant difference was observed in Bd21 clustering between WS with control and MS treatment (Figure 5.4B), while in ABR6, no distinctive clustering was observed (Figure 5.4C). PLS-DA plots similarly as in negative ionisation showed clear distinctive clustering between all three treatments, and between genotypes (Figure 5.4D-F).

The top 20 metabolites showing the biggest differences in concentration between treatments for both genotypes and both ionisation modes were identified and are presented in Appendix 10. Identification of metabolites was based on KEGG and MZedDB databases.

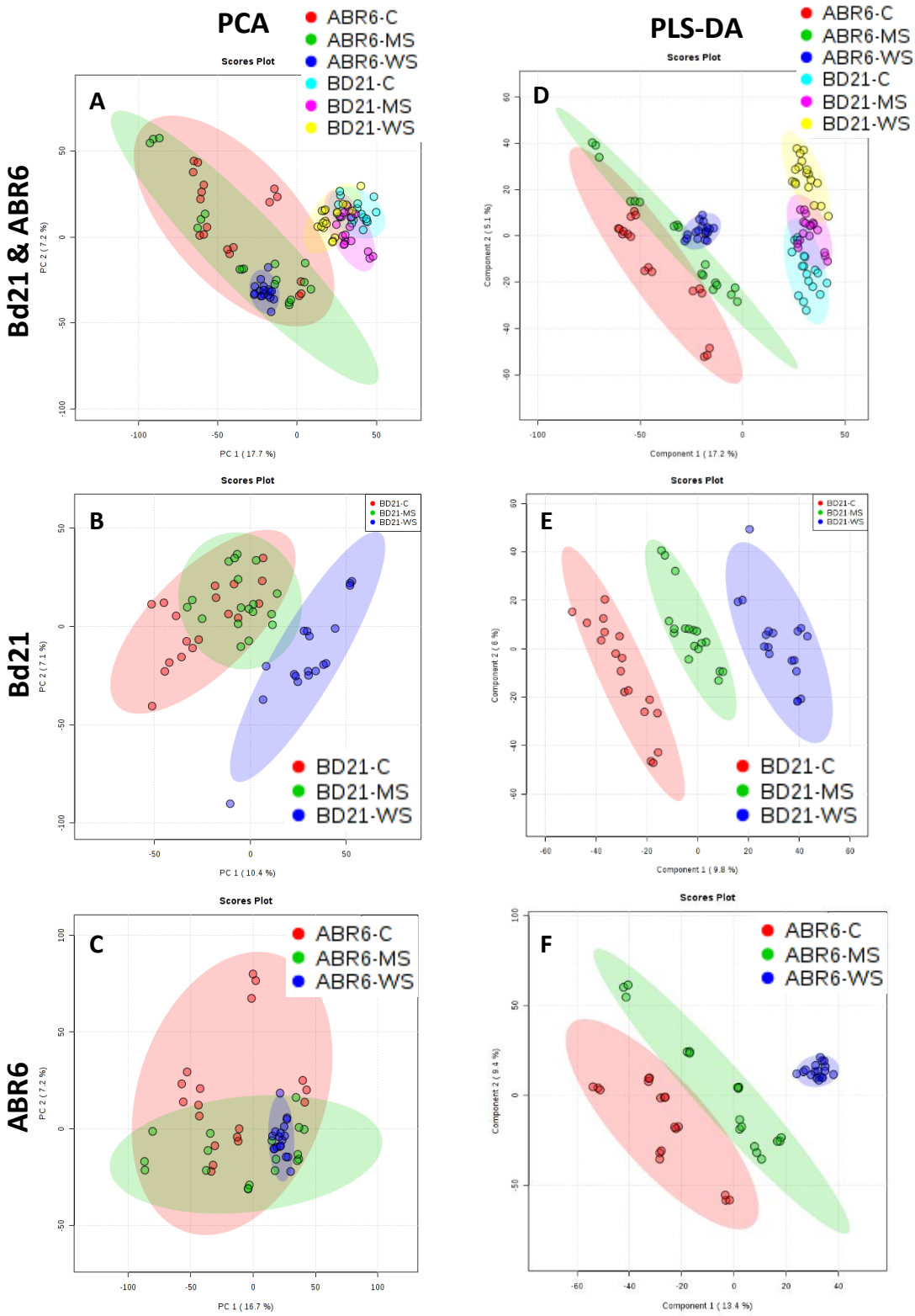

Figure 5.3. PCA and PLS-DA analysis of all metabolites detected by mass spectrometry in negative ionisation mode in Bd21 and ABR6.

Derived spectra were analysed by Principal Components Analysis (PCA) and Partial Least Squares Discriminant Analysis (PLS-DA). Shaded areas indicate 95% confidence intervals. The explained variances for each PC are shown in brackets (C – control; WS – wind stress; MS – mechanical stress). PCA plot for all treatment for both genotypes (A), PCA plot for Bd21 (B), PCA plot for ABR6 (C), PLS-DA plot for all treatments (D), PLS-DA plot for Bd21 (E), PLS-DA plot for ABR6 (F).

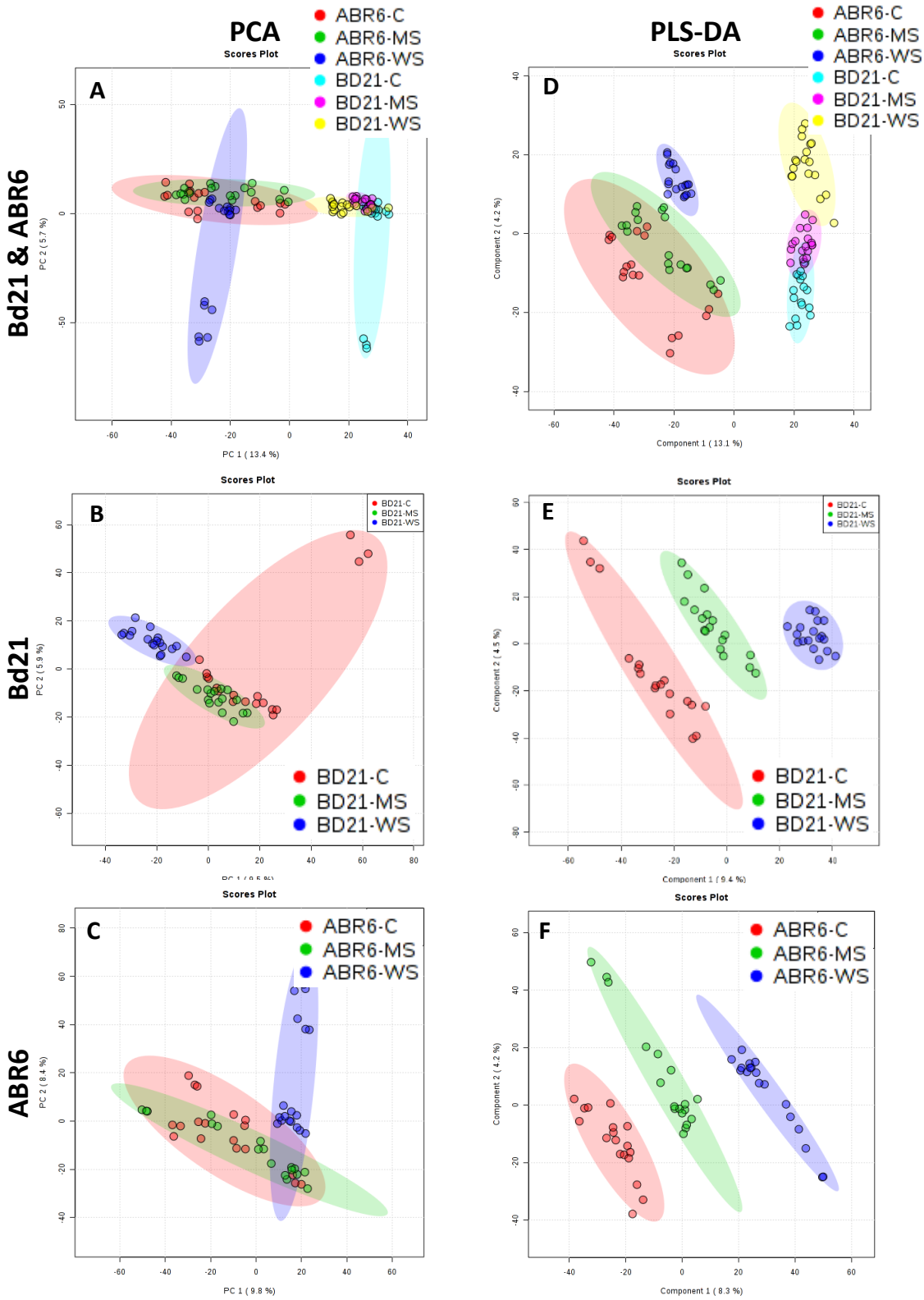

Figure 5.4. PCA and PLS-DA analysis of all metabolites detected by mass spectrometry in positive ionisation mode in Bd21 and ABR6.

Derived spectra were analysed by Principal Components Analysis (PCA) and Partial Least Squares Discriminant Analysis (PLS-DA). Shaded areas indicate 95% confidence intervals. The explained variances for each PC are shown in brackets (C – control; WS – wind stress; MS – mechanical stress). PCA plot for all treatment for both genotypes (A), PCA plot for Bd21 (B), PCA plot for ABR6 (C), PLS-DA plot for all treatments (D), PLS-DA plot for Bd21 (E), PLS-DA plot for ABR6 (F).

5.3.2.1. PATHWAY ENRICHMENT

In an attempt to provide functional information on the responses to mechanical stimulation in each genotype, the significant metabolites ($P \leq 0.05$) were assessed for pathway enrichment for both negative and positive ionisation modes. An overview of the top 50 enriched pathways for positive and negative ionisation mode for both genotypes can be found in Appendix 11. Although none of the enriched pathways exhibited robust statistical validity with satisfactory *P* value ($P \leq 0.05$) and FDR ($P \leq 0.05$), it was decided to accept pathways with $P \leq 0.1$ and flagged it as suggestive and thus to present data analysis for these pathways.

5.3.2.1.1. Pathway enrichment for Bd21

In the case of Bd21 for negative ionisation mode, three pathways were accepted as enriched: Glycolysis, Pentose Phosphate and Gluconeogenesis, while for positive ionisation mode two pathways were enriched: Methylhistidine Metabolism and Galactose Metabolism (Table 5.10).

Table 5.10. Pathway enrichment detected by mass spectrometry in negative and positive ionisation mode in Bd21.

Pathway	Hits	*P* value	FDR
Negative ionisation mode			
Glycolysis	12/25	0.0582	1
Pentose Phosphate Pathway	13/29	0.0856	1
Gluconeogenesis	15/35	0.0974	1
Positive ionisation mode			
Methylhistidine Metabolism	4/4	0.018	1
Galactose Metabolism	19/38	0.0612	1

All metabolites represented in the PCA and PLS-DA analysis were compared for treatment effect by statistical ANOVA test at the 5% level ($P \leq 0.05$) of significance.

Where ANOVA indicated a significant difference, pair-wise comparison of means by Tukey's HSD (honestly significant difference) test was carried out at the 5% level ($P \leq 0.05$) of significance. Metabolites with P value ($P \leq 0.05$) and FDR ($P \leq 0.05$) were considered as significant. Metabolites with the same chemical formula were clustered. Box plots with normalised concentrations of most significant metabolites in each pathway enriched are presented in Appendix 12A-B.

METABOLITES DETECTED BY MASS SPECTROMETRY IN NEGATIVE IONISATION MODE

Glycolysis Pathway

The metabolites tentatively identified as being involved in the Glycolysis Pathway: D-Glucose; Pyruvic acid; Phosphoenolpyruvic acid; Beta-D-Glucose; 3-Phosphoglyceric acid; D-glyceraldehyde 3-phosphate; Glyceric acid 1,3-biphosphate; 2,3-Diphosphoglyceric acid, ADP, Dihydroxyacetone phosphate, NADH and Alpha-D-Glucose were selected for PCA and PLS-DA analysis. Both types of analyses showed a distinctive clustering between treatments, especially between control and WS treatment, while MS treatment clustered mostly with control (Figure 5.5).

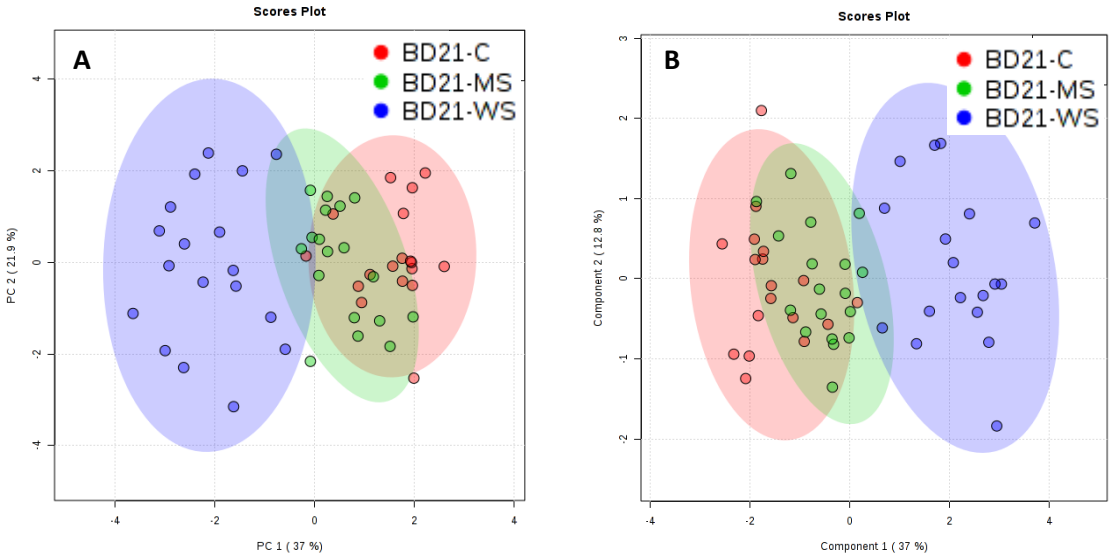

Figure 5.5. PCA and PLS-DA analysis of metabolites linked to the Glycolysis Pathway.

Derived spectra were analysed by A. Principal Components Analysis (PCA) and B. Partial Least Squares Discriminant Analysis (PLS-DA) to assign the profiles to groups based on metabolites tentatively linked to the Glycolysis Pathway. Shaded areas indicate 95% confidence intervals.

The explained variances for PC1 and PC2 are shown in brackets (C – control; WS – wind stress; MS – mechanical stress).

NADH and 3-Phosphoglyceric acid showed decreased concentrations after both WS and MS treatments, with stronger effect after WS treatment. ADP, $C_3H_7O_6P$, and Phosphoenolpyruvic acid displayed the same pattern; however, the difference was found between WS and control as well as MS, with no difference between control and MS. An increased concentration of $C_6H_{12}O_6$ and Pyruvic acid was detected after WS treatment in comparison with control and WS, while for $C_3H_8O_{10}P_2$, a difference was found only between WS and control (Figure 5.6).

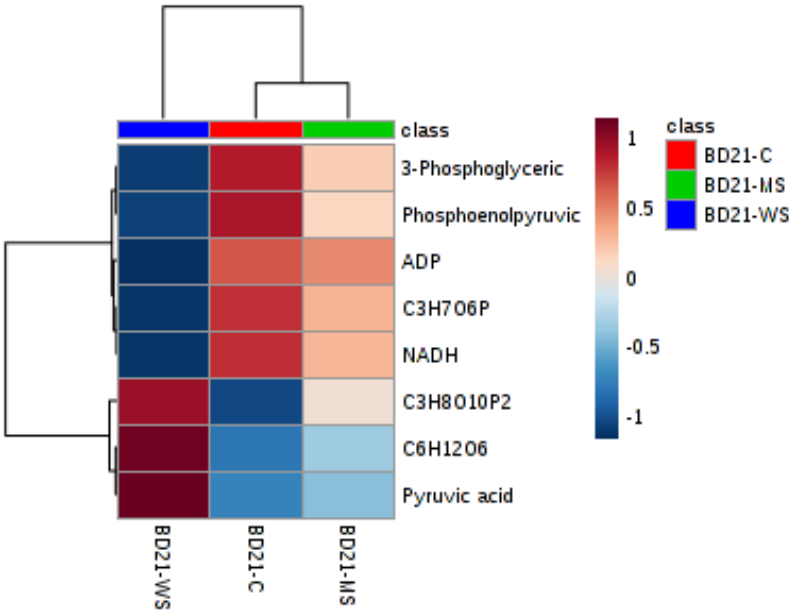

Compound	*P* value	FDR	Differences		
NADH	1.37E-09	1.10E-08	C	WS**	MS**
3-Phosphoglyceric acid	8.23E-08	2.63E-07	C	WS**	MS**
ADP	9.86E-08	2.63E-07	C	WS**	MS*
$C_6H_{12}O_6$	7.46E-05	0.000149	C	WS**	MS*
Pyruvic acid	0.0023646	0.003783	C	WS**	MS*
$C_3H_8O_{10}P_2$	0.0084088	0.011212	C	WS*	MS
Phosphoenolpyruvic acid	0.011975	0.013686	C	WS*	MS
$C_3H_7O_6P$	0.013824	0.013824	C	WS**	MS*

Figure 5.6. Average normalised concentrations of most significant metabolites in the Glycolysis Pathway.

A heat map with an average normalised concentration of metabolites with statistics. ANOVA with a *post hoc* Tukey test was performed to identify statistical differences ($P \leq 0.05$); * Significantly different from control; * Significant difference between WS and MS. $C_3H_7O_6P$ includes D-glyceraldehyde 3-phosphate and Dihydroxyacetone phosphate; $C_6H_{12}O_6$ includes D-Glucose, Alfa-D-Glucose and Beta-D-glucose; $C_3H_8O_{10}P_2$ includes Glyceric acid 1,3-biphosphate and 2,3-Diphosphoglyceric acid.

Pentose Phosphate Pathway

The metabolites tentatively identified as being involved in pentose Phosphate Pathway: Adenosine monophosphate; Gluconolactone; NADPH; D-Ribose; D-Ribulose 5-phosphate; Xylulose 5-phosphate; D-glyceraldehyde 3-phosphate; 6-Phosphogluconic acid; ADP; Dihydroxyacetone phosphate; Ribose 1-phosphate; D-Ribose 5-phosphate and Carbon dioxide were selected for PCA and PLS-DA analysis. Like previously observed for the Glycolysis Pathway, both analyses revealed a distinctive clustering between treatments, especially between control and WS treatment, while MS treatment clustered mostly with control (Figure 5.7).

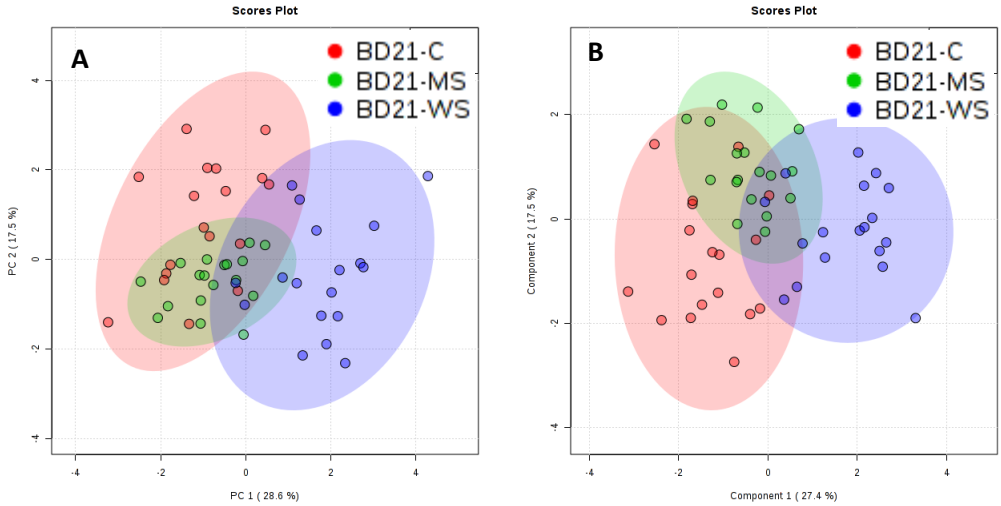

Figure 5.7. PCA and PLS-DA analysis of metabolites linked to the Pentose Phosphate Pathway.

Derived spectra were analysed by A. Principal Components Analysis (PCA) and B. Partial Least Squares Discriminant Analysis (PLS-DA) to assign the profiles to groups based on metabolites tentatively linked to the Pentose Phosphate Pathway. Shaded areas indicate 95% confidence intervals. The explained variances for PC1 and PC2 are shown in brackets (C – control; WS – wind stress; MS – mechanical stress).

ADP, NADPH, 6-Phosphogluconic acid and $C_3H_7O_6P$ showed a decreased concentration after WS treatment compared with control as well as to MS, while for $C_5H_{11}O_8P$, a decrease was observed after both stress treatments. An increase in concentration after both stress treatments was detected for D-Ribose and Gluconolactone with the strongest effect after WS treatment. The concentration of Carbon dioxide was increased

by MS treatment compared with control and MS, while the Adenosine monophosphate concentration increased only after WS treatment compared with control and MS (Figure 5.8).

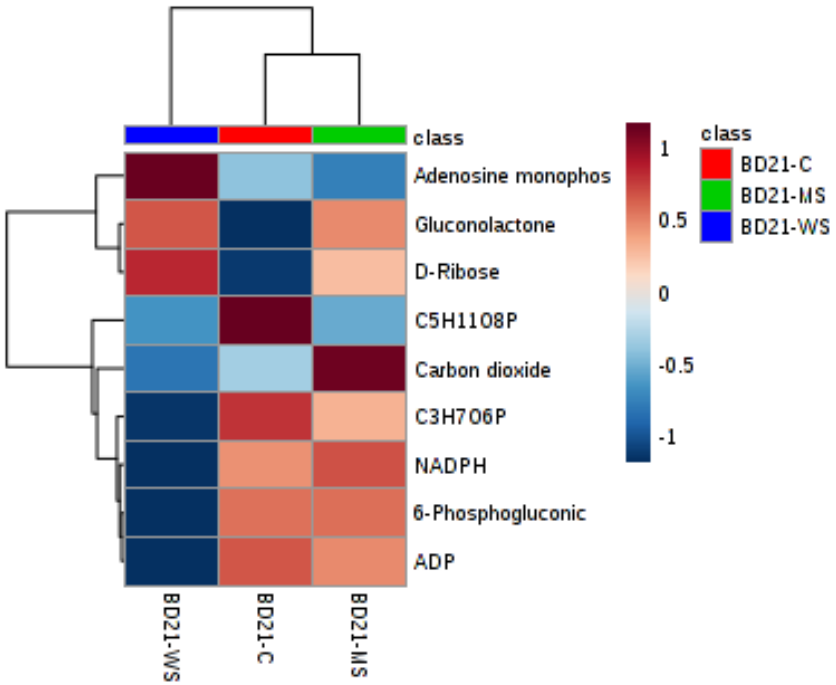

Compound	*P* value	FDR	Differences		
ADP	9.86E-08	8.87E-07	C	WS**	MS*
Carbon dioxide	2.25E-06	1.01E-05	C	WS*	MS**
$C_5H_{11}O_8P$	3.33E-05	9.98E-05	C	WS*	MS*
NADPH	0.000234	0.000527	C	WS**	MS*
6-Phosphogluconic acid	0.001125	0.002025	C	WS**	MS*
D-Ribose	0.005162	0.00754	C	WS*	MS*
Gluconolactone	0.005864	0.00754	C	WS*	MS*
Adenosine monophosphate	0.008505	0.009569	C	WS**	MS*
$C_3H_7O_6P$	0.013824	0.013824	C	WS**	MS*

Figure 5.8. Average normalised concentrations of most significant metabolites in the Pentose Phosphate Pathway.

A heat map with an average normalised concentration of metabolites with statistics. ANOVA with a *post hoc* Tukey test was performed to identify statistical differences ($P \leq 0.05$); * Significantly different from control; * Significant difference between WS and MS. $C_3H_7O_6P$ includes D-glyceraldehyde 3-phosphate and Dihydroxyacetone phosphate; $C_5H_{11}O_8P$ includes D-Ribulose 5-phosphate, Xylulose 5-phosphate, Ribose 1-phosphate and D-Ribose 5-phosphate.

Gluconeogenesis Pathway

The metabolites tentatively identified as being involved in the Gluconeogenesis Pathway: D-Glucose, Beta-D-Glucose, Alpha-D-Glucose, D-Glyceraldehyde 3-phosphate, Dihydroxyacetone phosphate, Glyceric acid 1,3-biphosphate, 2,3-Diphosphoglyceric acid, L-Lactic acid, Pyruvic acid, Phosphoenolpyruvic acid, NADH, Carbon dioxide, Hydrogen carbonate, 3-Phosphoglyceric acid and ADP were selected for PCA and PLS-DA analysis. Again, both analyses showed a similar outcome than seen for the Glycolysis Pathway and Pentose Phosphate Pathway analysis with a distinctive clustering between treatments, especially between control and WS treatment, while MS treatment clustered mostly with control (Figure 5.9).

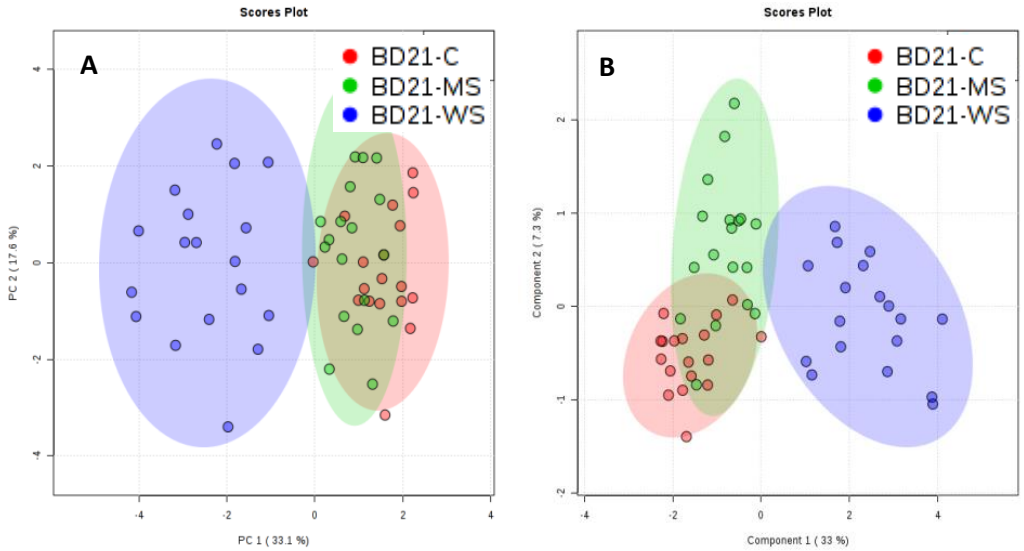

Figure 5.9. PCA and PLS-DA analysis of metabolites linked to the Gluconeogenesis Pathway.

Derived spectra were analysed by A. Principal Components Analysis (PCA) and B. Partial Least Squares Discriminant Analysis (PLS-DA) to assign the profiles to groups based on metabolites tentatively linked to the Gluconeogenesis Pathway. Shaded areas indicate 95% confidence intervals. The explained variances for PC1 and PC2 are shown in brackets (C – control; WS – wind stress; MS – mechanical stress).

NADH and 3-Phosphoglyceric acid showed a lower concentration after both stress treatments, more pronounced for WS, compared with control while a decreased concentration caused by WS treatment was observed for ADP, Phosphoenolpyruvic acid

and $C_3H_7O_6P$. An increased concentration after WS compared with control and MS treatment was observed for Hydrogen carbonate, $C_6H_{12}O_6$, Pyruvic acid and L-Lactic acid. The concentration of $C_3H_8O_{10}P_2$ was also significantly increased by WS treatment compared with control, but additionally, a slightly increasing tendency was observed after MS treatment. Only the concentration of Carbon dioxide was increased by MS with the concentration for control and WS being at the same level (Figure 5.10).

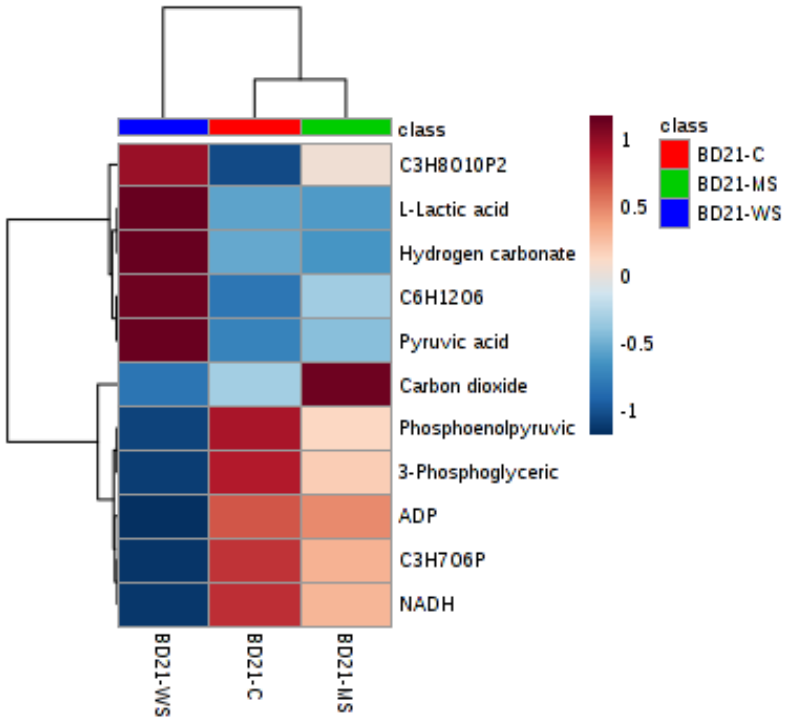

Compound	*P* value	FDR	Differences		
NADH	1.37E-09	1.51E-08	C	WS**	MS**
3-Phosphoglyceric acid	8.23E-08	3.61E-07	C	WS**	MS**
ADP	9.86E-08	3.61E-07	C	WS**	MS*
Hydrogen carbonate	4.71E-07	1.30E-06	C	WS**	MS*
Carbon dioxide	2.25E-06	4.95E-06	C	WS*	MS**
$C_6H_{12}O_6$	7.46E-05	0.000137	C	WS**	MS*
Pyruvic acid	0.002365	0.003716	C	WS**	MS*
$C_3H_8O_{10}P_2$	0.008409	0.011562	C	WS*	MS
Phosphoenolpyruvic acid	0.011975	0.013536	C	WS*	MS
L-Lactic acid	0.012306	0.013536	C	WS**	MS*
$C_3H_7O_6P$	0.013824	0.013824	C	WS**	MS*

Figure 5.10. Average normalised concentrations of most significant metabolites in the Gluconeogenesis Pathway.

A heat map with an average normalised concentration of metabolites with statistics. ANOVA with a *post hoc* Tukey test was performed to identify statistical differences ($P \leq 0.05$); * Significantly different from control; * Significant difference between WS and MS. $C_3H_7O_6P$ includes D-Glyceraldehyde 3-phosphate and Dihydroxyacetone phosphate; $C_6H_{12}O_6$ includes D-Glucose, Beta-D-Glucose, Alpha-D-Glucose; $C_3H_8O_{10}P_2$ includes Glyceric acid 1,3-biphosphate and 2,3-Diphosphoglyceric acid.

METABOLITES DETECTED BY MASS SPECTROMETRY IN POSITIVE IONISATION MODE

Methylhistidine Metabolism

The metabolites tentatively identified as being involved in Methylhistidine Metabolism: L-Histidine, 3-Methylhistidine, S-Adenosylhomocysteine and S-Adenosylmethionine were selected for PCA and PLS-DA analysis. PCA analysis with metabolites associated with Methylhistidine Metabolism revealed no distinctive clustering between treatments (Figure 5.11). PLS-DA analysis could not be performed due to the small number of compounds assigned to this pathway.

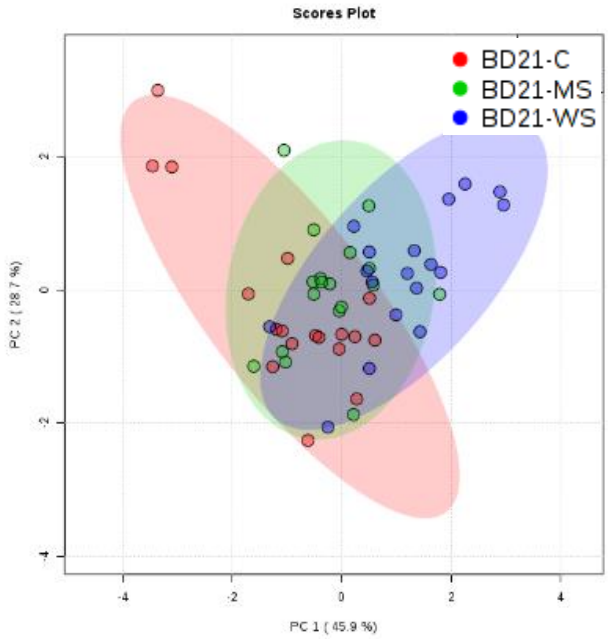

Figure 5.11. PCA analysis of metabolites linked to methylhistidine metabolism.

Derived spectra were analysed by Principal Components Analysis (PCA) to assign the profiles to groups based on metabolites tentatively linked to the Methylhistidine Metabolism. Shaded areas indicate 95% confidence intervals. The explained variances for PC1 and PC2 are shown in brackets (C – control; WS – wind stress; MS – mechanical stress).

3-Methylhistidine showed an increased concentration after WS treatment compared with control and MS, while the L-Histidine concentration increased after both stress treatments. A decreased concentration was detected after WS for S-Adenosylhomocysteine and S-Adenosylmethionine compared with control and MS (Figure 5.12).

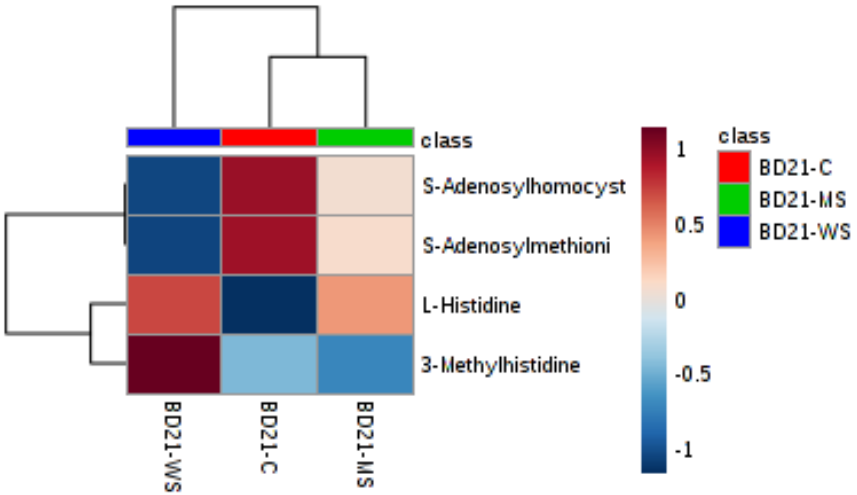

Compound	*P* value	FDR	Differences		
3-Methylhistidine	3.21E-05	0.000128	C	WS**	MS*
L-Histidine	0.00039	0.00078	C	WS*	MS*
S-Adenosylhomocysteine	0.007219	0.008587	C	WS*	MS
S-Adenosylmethionine	0.008587	0.008587	C	WS*	MS

Figure 5.12. Average normalised concentrations of the most significant metabolites linked to methylhistidine metabolism.

A heat map with an average normalised concentration of metabolites with statistics. ANOVA with a *post hoc* Tukey test was performed to identify statistical differences ($P \leq 0.05$); * Significantly different from control; * Significant difference between wind stress (WS) and mechanical stress (MS).

Galactose Metabolism

The metabolites tentatively identified as being involved in Galactose metabolism: D-Glucose, D-Galactose, D-Mannose, Myo-inositol, D-Fructose, Alpha-D-Glucose, Alpha-Lactose, Sucrose, Sorbitol, Galactitol, Adenosine triphosphate, Glycerol, Uridine 5'-diphosphate, NAD, Maltotriose, Phosphate, NADH, Raffinose and Stachyose were selected for PCA and PLS-DA analysis. Both analyses revealed a distinctive clustering between all three treatments (Figure 5.13).

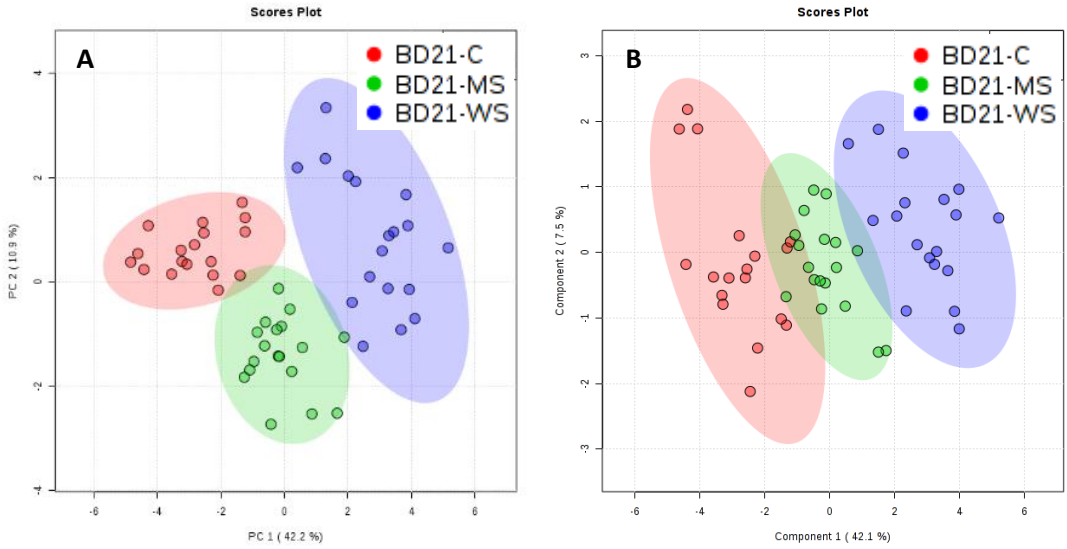

Figure 5.13. PCA and PLS-DA analysis of metabolites linked to galactose metabolism.

Derived spectra were analysed by A. Principal Components Analysis (PCA) and B. Partial Least Squares Discriminant Analysis (PLS-DA) to assign the profiles to groups based on metabolites tentatively linked to Galactose Metabolism. Shaded areas indicate 95% confidence intervals. The explained variances for PC1 and PC2 are shown in brackets (C – control; WS – wind stress; MS – mechanical stress).

The NADH, Raffinose and NAD concentration decreased after both stress treatments compared with control, however, WS had the strongest effect, while for Maltotriose and Phosphate a similar decrease in concentration was observed after both stresses when compared with control. For S-Adenosylhomocysteine, S-Adenosylmethionine and Stachyose, the concentration was only significantly lower after WS treatment compared with control, and for Stachyose a significant difference between WS and MS was also

noted. The concentration of Glycerol decreased by MS only compared with control and WS. An increased concentration was detected after WS treatment for Uridine 5'-diphosphate, 3-Methylhistidine, Adenosine triphosphate and $C_6H_{14}O_6$ compared with control and WS; moreover, a difference between WS and MS was also detected for these metabolites. L-Histidine and $C_6H_{12}O_6$ increased in their concentration by both stresses, while $C_{12}H_{22}O_{11}$ only increased by MS compared with control and WS (Figure 5.14).

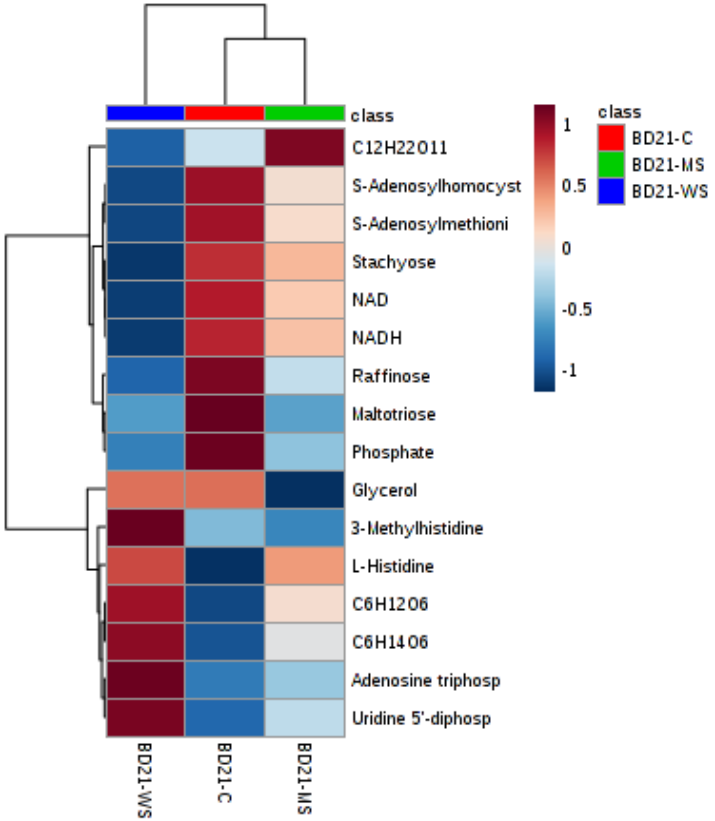

Compound	*P* value	FDR	Differences		
NADH	1.26E-20	2.01E-19	C	WS**	MS**
Raffinose	2.15E-19	1.72E-18	C	WS**	MS**
NAD	4.16E-19	2.22E-18	C	WS**	MS**
Maltotriose	4.40E-12	1.76E-11	C	WS*	MS*
$C_6H_{12}O_6$	1.86E-11	5.97E-11	C	WS**	MS**
Uridine 5'-diphosphate	3.30E-06	8.80E-06	C	WS**	MS*
Glycerol	1.22E-05	2.80E-05	C	WS*	MS**
3-Methylhistidine	3.21E-05	6.42E-05	C	WS**	MS*
Stachyose	5.52E-05	9.75E-05	C	WS**	MS*
Phosphate	6.09E-05	9.75E-05	C	WS*	MS*
$C_{12}H_{22}O_{11}$	0.000165	0.000239	C	WS*	MS**
L-Histidine	0.00039	0.00052	C	WS*	MS*
$C_6H_{14}O_6$	0.000971	0.001195	C	WS**	MS*
S-Adenosylhomocysteine	0.007219	0.00825	C	WS*	MS
S-Adenosylmethionine	0.008587	0.009159	C	WS*	MS
Adenosine triphosphate	0.010087	0.010087	C	WS**	MS*

Figure 5.14. Average normalised concentrations of most significant metabolites linked to galactose metabolism.

A heat map with an average normalised concentration of metabolites with statistics. ANOVA with a *post hoc* Tukey test was performed to identify statistical differences ($P \leq 0.05$); * Significantly different from control; * Significant difference between WS and MS. $C_6H_{14}O_6$ includes Sorbitol and Galactitol; $C_6H_{12}O_6$ includes D-Glucose, D-Galactose, D-Mannose, myo-Inositol, D-Fructose and Alpha-D-Glucose; $C_{12}H_{22}O_{11}$ includes Alpha-Lactose and Sucrose.

5.3.2.1.2. Pathway enrichment of ABR6

In the case of ABR6 six pathways were accepted as enriched for negative ionisation mode: Nucleotide Sugars Metabolism, Galactose Metabolism, Fructose and Mannose Degradation, Glycolysis Pathway, Lactose Synthesis, Starch and Sucrose Metabolism and Gluconeogenesis, while for positive ionisation mode only Galactose Metabolism (Table 5.11).

Table 5.11. Pathway enrichment detected by mass spectrometry in negative and positive ionisations mode in ABR6.

Pathway	Hits	*P* value	FDR
Negative ionisation mode			
Nucleotide Sugars Metabolism	13/20	0.000991	0.0971
Galactose Metabolism	20/38	0.00204	0.1
Fructose and Mannose Degradation	16/32	0.0109	0.357
Glycolysis	12/25	0.0381	0.741
Starch and Sucrose Metabolism	14/31	0.0454	0.741
Gluconeogenesis	15/35	0.0624	0.873
Positive ionisation mode			
Galactose Metabolism	17/38	0.0538	1

All metabolites represented in the PCA and PLS-DA analysis were compared for treatment effect by statistical ANOVA test at the 5% level ($P \leq 0.05$) of significance. Where ANOVA indicated a significant difference, pair-wise comparison of means by Tukey's HSD (honestly significant difference) test was carried out at the 5% level ($P \leq 0.05$) of significance. Metabolites with *P* value ($P \leq 0.05$) and FDR ($P \leq 0.05$) were considered as significant. Metabolites with the same chemical formula were clustered. Box plots with normalised concentrations of most significant metabolites in each pathway enriched are presented in Appendix 13A-B.

METABOLITES DETECTED BY MASS SPECTROMETRY IN NEGATIVE IONISATION MODE

Nucleotide Sugars Metabolism

The metabolites tentatively identified as being involved in the Nucleotide Sugars Metabolism: Galactose 1-phosphate, Glucose 6-phosphate, Glucose 1-phosphate, D-Galactose, Alpha-D-Glucose, Uridine diphosphate glucose, Uridine diphosphate galactose, NADH, Pyrophosphate, Uridine triphosphate, Uridine diphosphate glucuronic acid. UDP-D-Xylose and Zinc (II) ion were selected for PCA and PLS-DA analysis. No clear distinctive clustering between treatments could be observed. Nevertheless, it may be suggested that the cluster for WS treatment is at the very edge of the control cluster (Figure 5.15).

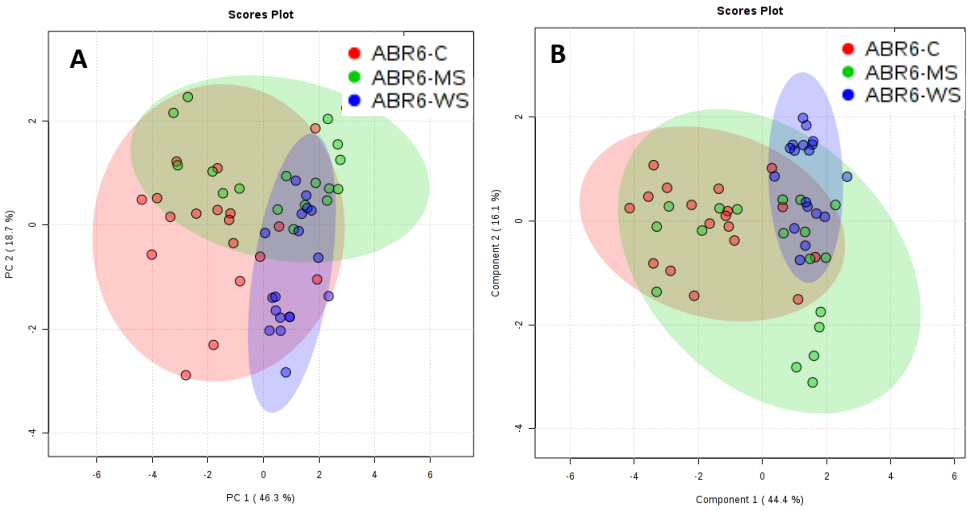

Figure 5.15. PCA and PLS-DA analysis of metabolites linked to nucleotide sugar metabolism.

Derived spectra were analysed by A. Principal Components Analysis (PCA) and B. Partial Least Squares Discriminant Analysis (PLS-DA) to assign the profiles to groups based on metabolites tentatively linked to metabolites forming Nucleotide Sugar Metabolism. Shaded areas indicate 95% confidence intervals. The explained variances for PC1 and PC2 are shown in brackets (C – control; WS – wind stress; MS – mechanical stress).

The NADH and UDP-D-Xylose concentration increased by both stress treatments compared with control while Pyrophosphate increased only after WS treatment. Decreased concentrations were detected for Uridine diphosphate glucuronic acid and $C_{15}H_{24}N_2O_{17}P_2$ after both stresses, while Zinc II ion and $C_6H_{13}O_9P$ only decreased after WS and $C_6H_{12}O_6$ and Uridine triphosphate only after MS (Figure 5.16).

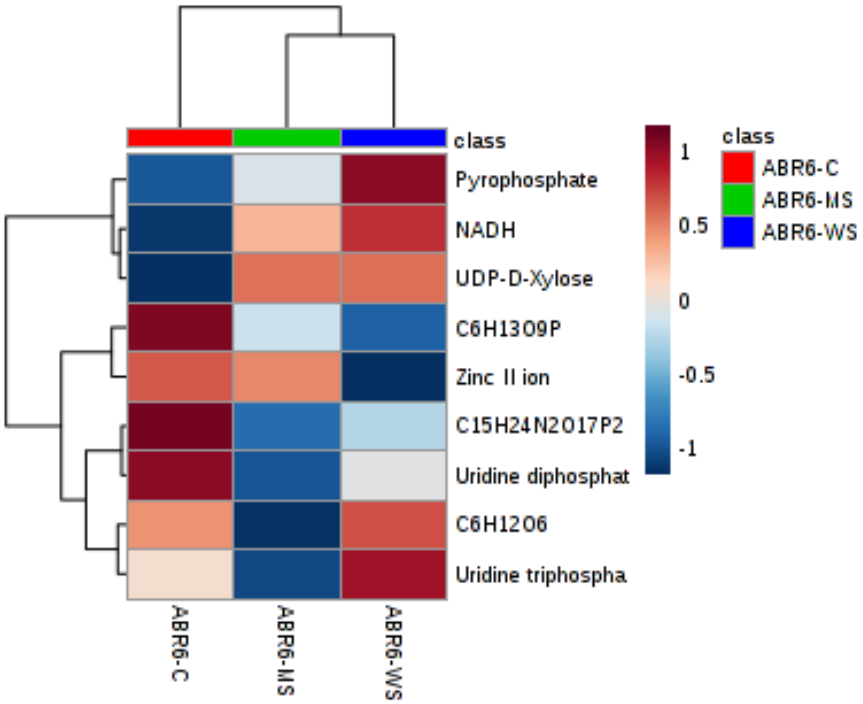

Compound	*P* value	FDR	Differences		
NADH	1.01E-05	7.91E-05	C	WS*	MS*
Zinc II ion	1.76E-05	7.91E-05	C	WS**	MS*
UDP-D-Xylose	0.000455	0.001366	C	WS*	MS*
Pyrophosphate	0.000665	0.001497	C	WS**	MS*
$C_{15}H_{24}N_2O_{17}P_2$	0.001007	0.001813	C	WS*	MS*
Uridine diphosphate glucuronic acid	0.001442	0.002163	C	WS*	MS*
Uridine triphosphate	0.001704	0.002191	C	WS*	MS**
$C_6H_{12}O_6$	0.009471	0.010654	C	WS*	MS**
$C_6H_{13}O_9P$	0.013223	0.013223	C	WS*	MS

Figure 5.16. Average normalised concentrations of most significant metabolites in to nucleotide sugar metabolism.

A heat map with an average normalised concentration of metabolites with statistics. ANOVA with a *post hoc* Tukey test was performed to identify statistical differences ($P \leq 0.05$); * Significantly different from control; * Significant difference between WS and MS. $C_{15}H_{24}N_2O_{17}P_2$ includes Uridine diphosphate glucose and Uridine diphosphate galactose; $C_6H_{13}O_9P$ incudes Galactose 1-phosphate, Glucose 6-phosphate and Glucose 1-phosphate; $C_6H_{12}O_6$ includes D-Galactose and Alpha-D-Glucose.

Galactose Metabolism

The metabolites tentatively identified as being involved in Galactose Metabolism: Galactose 1-phosphate, Glucose 6-phosphate, Glucose 1-phosphate, D-Glucose, D-Galactose, D-Mannose, myo-Inositol, D-Fructose, Alpha-D-Glucose, Alpha-Lactose, Sucrose, Uridine diphosphate glucose, Uridine diphosphate galactose, Maltotriose, NADH, Pyrophosphate. Uridine triphosphate, Zinc (II) ion, Raffinose and Stachyose were selected for PCA and PLS-DA analysis. PCA analysis revealed no significant difference between treatments; however, it can be noted that the WS treatment cluster is much denser compared with control. Moreover, PLS-DA analysis showed distinctive clustering between control and WS treatment (Figure 5.17).

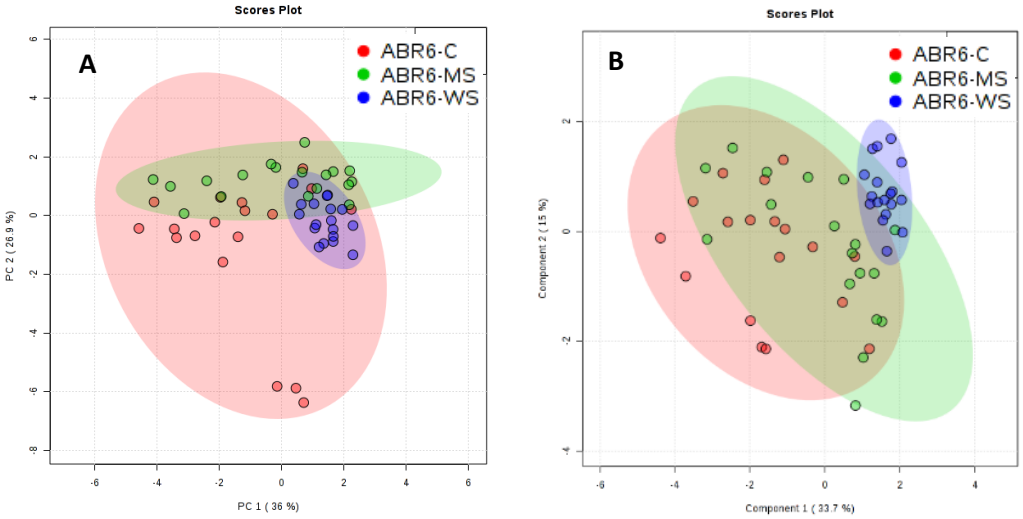

Figure 5.17. PCA and PLS-DA analysis of metabolites linked to galactose metabolism.

Derived spectra were analysed by A. Principal Components Analysis (PCA) and B. Partial Least Squares Discriminant Analysis (PLS-DA) to assign the profiles to groups based on metabolites tentatively linked to metabolites forming Galactose Metabolism. Shaded areas indicate 95% confidence intervals. The explained variances for PC1 and PC2 are shown in brackets (C – control; WS – wind stress; MS – mechanical stress).

The NADH, $C_{12}H_{22}O_{11}$ and Maltotriose concentration was increased by both stress treatments compared with control, while the Pyrophosphate (concentration was increased only by WS. A decreased concentration was detected after both stress

treatments for $C_{15}H_{24}N_2O_{17}P$, while WS treatment resulted in lower Zinc II ion and $C_6H_{13}O_9P$ concentrations. MS treatment caused a decrease in Uridine triphosphate and $C_6H_{12}O_6$ concentration. WS treatment showed a lower concentration of Raffinose, while MS resulted in a higher concentration of this metabolite. A similar situation was observed for Stachyose; however, this difference was not significant, though the difference between WS and MS were significant (Figure 5.18).

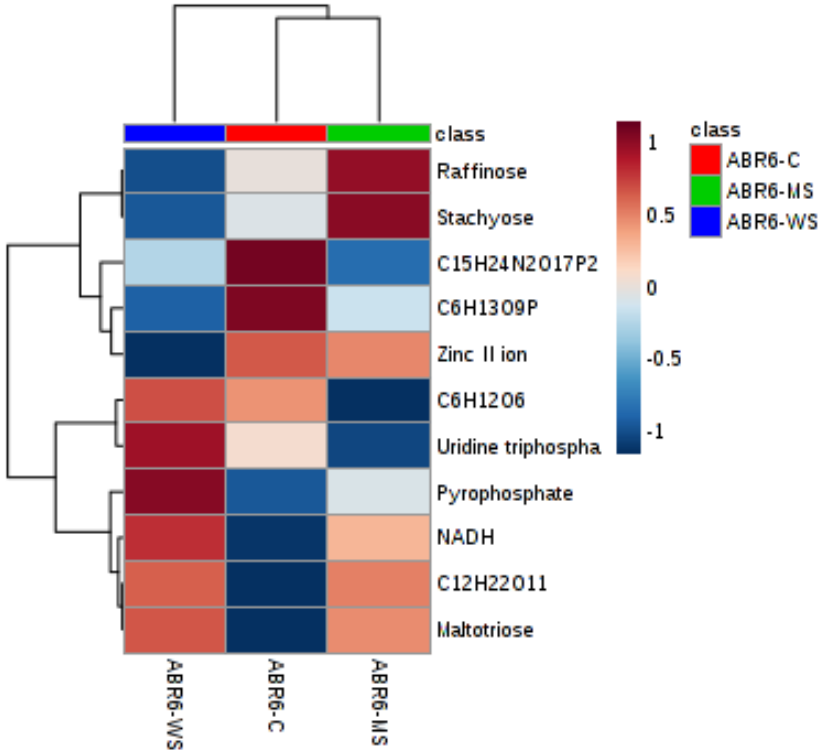

Compound	*P* value	FDR		Differences	
NADH	1.01E-05	9.67E-05	C	WS*	MS*
Zinc II ion	1.76E-05	9.67E-05	C	WS**	MS*
Raffinose	0.000248	0.000711	C	WS**	MS**
$C_{12}H_{22}O_{11}$	0.000258	0.000711	C	WS*	MS*
Pyrophosphate	0.000665	0.001464	C	WS**	MS*
Maltotriose	0.000961	0.001583	C	WS*	MS*
$C_{15}H_{24}N_2O_{17}P_2$	0.001007	0.001583	C	WS*	MS*
Uridine triphosphate	0.001704	0.002343	C	WS*	MS**
Stachyose	0.008162	0.009975	C	WS*	MS*
$C_6H_{12}O_6$	0.009471	0.010418	C	WS*	MS**
$C_6H_{13}O_9P$	0.013223	0.013223	C	WS*	MS

Figure 5.18. Average normalised concentrations of the most significant metabolites in the Galactose Metabolic pathway.

A heat map with an average normalised concentration of metabolites with statistics. ANOVA with a *post hoc* Tukey test was performed to identify statistical differences ($P \leq 0.05$); * Significantly different from control; * Significant difference between WS and MS. $C_{12}H_{22}O_{11}$ includes Alpha-Lactose and Sucrose; $C_{15}H_{24}N_2O_{17}P_2$ includes Uridine diphosphate glucose and Uridine diphosphate galactose; $C_6H_{13}O_9P$ includes Galactose 1-phosphate, Glucose 6-phosphate and Glucose 1-phosphate; $C_6H_{12}O_6$ includes D-Glucose, D-Galactose, D-Mannose, myo-Inositol, D-Fructose and Alpha-D-Glucose.

Fructose and Mannose Degradation

The metabolites tentatively identified as being involved in Fructose and Mannose Degradation: Fructose 1-phosphate, Mannose 6-phosphate, D-Mannose 1-phosphate, Fructose 6-phosphate, D-Mannose, D-Fructose, Alpha-D-Glucose, D-Fructose 2,6-bisphosphate, Fructose 1,6-bisphosphate, D-Glyceraldehyde 3-phosphate, Dihydroxyacetone phosphate, GDP-L-fucose, Guanosine triphosphate, NADH, Pyrophosphate and Zinc (II) ion were selected for further PCA and PLS-DA analysis. Both analyses revealed a significant difference between control and WS clustering, while control and MS clustered comparably (Figure 5.19).

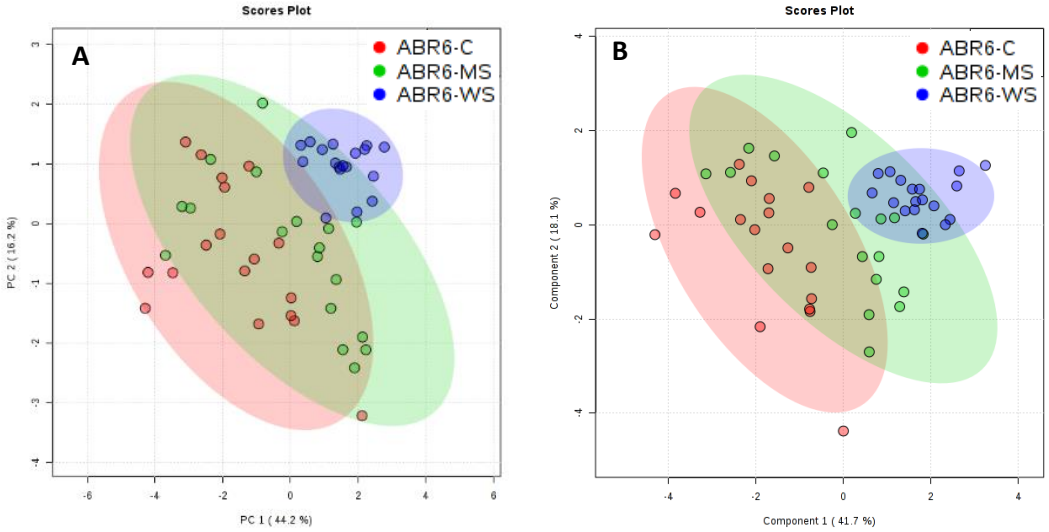

Figure 5.19. PCA and PLS-DA analysis of metabolites linked to fructose and mannose degradation.

Derived spectra were analysed by A. Principal Components Analysis (PCA) and B. Partial Least Squares Discriminant Analysis (PLS-DA) to assign the profiles to groups based on metabolites tentatively linked to metabolites forming Fructose and Mannose Degradation. Shaded areas indicate 95% confidence intervals. The explained variances for PC1 and PC2 are shown in brackets (C – control; WS – wind stress; MS – mechanical stress).

As seen before, the NADH concentration increased by both stress treatments compared with control, while the Guanosine triphosphate and Pyrophosphate concentrations were higher only after WS treatment and GDP-L-Fucose only after MS treatment. Decreased concentrations of $C_3H_7O_6P$ and $C_6H_{14}O_{12}P_2$ were caused by both stresses compared with control. A lower concentration after WS treatment was observed for

$C_6H_{13}O_9P$ and Zinc II ion and after MS treatment for $C_6H_{12}O_6$ compared with control (Figure 5.20).

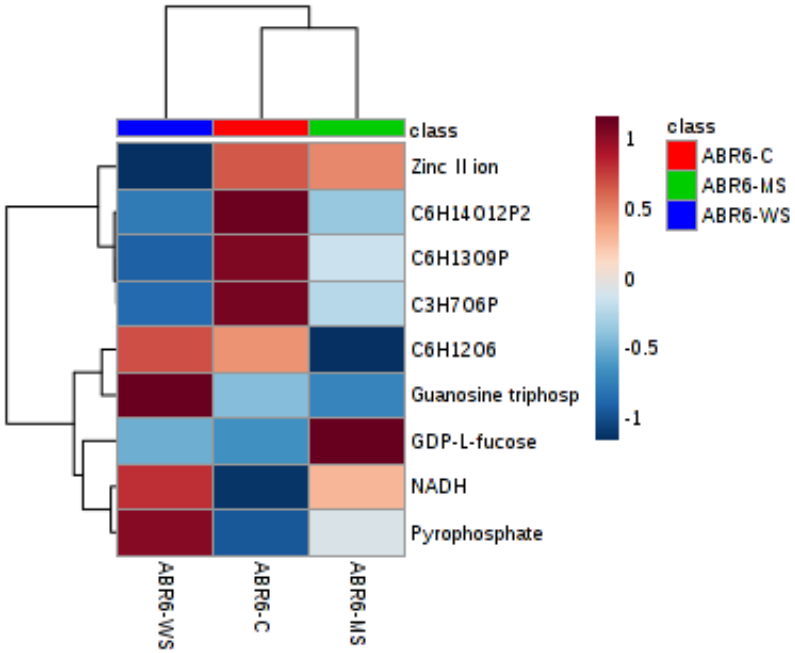

Compound	*P* value	FDR	Differences		
$C_3H_7O_6P$	6.71E-12	6.04E-11	C	WS**	MS**
NADH	1.01E-05	3.53E-05	C	WS*	MS*
Guanosine triphosphate	1.61E-05	3.53E-05	C	WS**	MS*
Zinc II ion	1.76E-05	3.53E-05	C	WS**	MS*
$C_6H_{14}O_{12}P_2$	1.96E-05	3.53E-05	C	WS*	MS*
Pyrophosphate	0.000665	0.000998	C	WS**	MS*
GDP-L-Fucose	0.001971	0.002534	C	WS*	MS**
$C_6H_{12}O_6$	0.009471	0.010654	C	WS*	MS**
$C_6H_{13}O_9P$	0.013223	0.013223	C	WS*	MS

Figure 5.20. Average normalised concentrations of most significant metabolites linked to fructose and mannose degradation.

A heat map with an average normalised concentration of metabolites with statistics. ANOVA with a *post hoc* Tukey test was performed to identify statistical differences ($P \leq 0.05$); * Significantly different from control; * Significant difference between WS and MS. $C_3H_7O_6P$ includes D-Glyceraldehyde 3-phosphate and Dihydroxyacetone phosphate; $C_6H_{14}O_{12}P_2$ includes D-Fructose 2,6-bisphosphate and Fructose 1,6-bisphosphate; $C_6H_{13}O_9P$ includes Fructose 1-phosphate, Mannose 6-phosphate, D-Mannose 1-phosphate and Fructose 6-phosphate.

Glycolysis Pathway

The metabolites tentatively identified as being involved in Glycolysis Pathway: Fructose 6-phosphate, Glucose 6-phosphate, Glucose 1-phosphate, Beta-D-Glucose 6-phosphate, D-Glucose, Beta-D-Glucose, Alpha-D-Glucose, D-Glyceraldehyde 3-phosphate, Dihydroxyacetone phosphate, Fructose 1,6-bisphosphate, NADH and 3-Phosphoglyceric acid were selected for further PCA and PLS-DA analysis. PCA analysis with metabolites associated with Glycolysis Pathway revealed that there is no clear distinctive clustering between treatments. Nevertheless, WS treatment is placed at the edge of a control cluster (Figure 5.21). PLS-DA analysis could not be performed due to a small number of compounds assigned to this pathway.

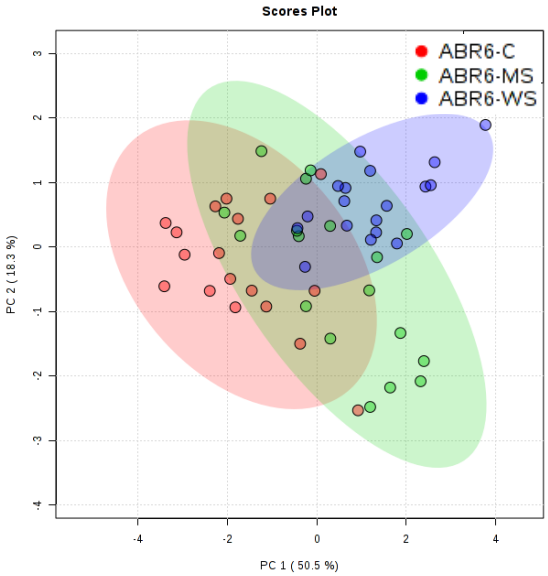

Figure 5.21. PCA analysis of metabolites linked to the Glycolysis Pathway.

Derived spectra were analysed by Principal Components Analysis (PCA) to assign the profiles to groups based on metabolites tentatively linked to metabolites forming the Glycolysis pathway. Shaded areas indicate 95% confidence intervals. The explained variances for PC1 and PC2 are shown in brackets (C – control; WS – wind stress; MS – mechanical stress).

In this pathway, only NADH concentration was increased by both stress treatments compared with control. Decreased concentration after both stresses was observed in $C_3H_7O_6P$ and $C_6H_{14}O_{12}P_2$ and after WS in $C_6H_{13}O_9P$, $C_6H_{12}O_6$ and Phosphoglyceric acid compared with control (Figure 5.22).

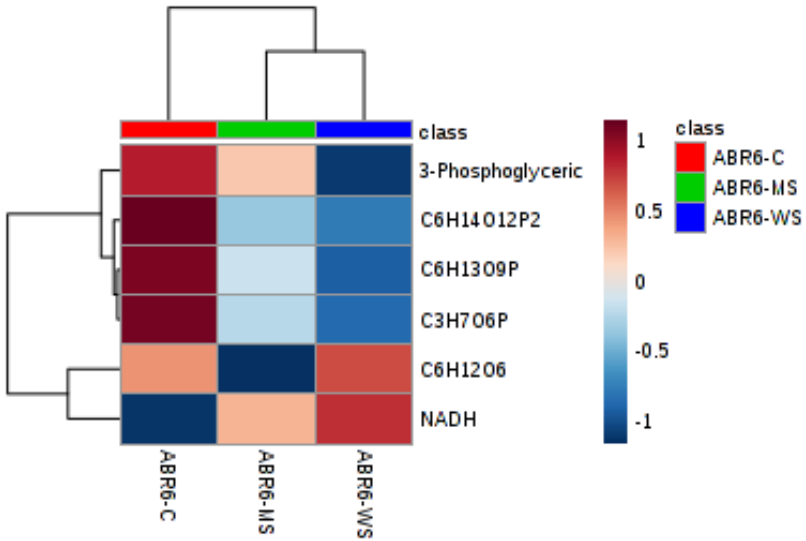

Compound	*P* value	FDR	Differences		
$C_3H_7O_6P$	6.71E-12	4.03E-11	C	WS**	MS**
NADH	1.01E-05	3.02E-05	C	WS*	MS*
$C_6H_{14}O_{12}P_2$	1.96E-05	3.92E-05	C	WS*	MS*
3-Phosphoglyceric acid	0.000445	0.000668	C	WS**	MS*
$C_6H_{12}O_6$	0.009471	0.011365	C	WS**	MS*
$C_6H_{13}O_9P$	0.013223	0.013223	C	WS*	MS

Figure 5.22. Average normalised concentrations of most significant metabolites in the Glycolysis Pathway.

A heat map with an average normalised concentration of metabolites with statistics. ANOVA with a *post hoc* Tukey test was performed to identify statistical differences ($P \leq 0.05$); * Significantly different from control; * Significant difference between WS and MS. $C_3H_7O_6P$ includes D-Glyceraldehyde 3-phosphate and Dihydroxyacetone phosphate; $C_6H_{14}O_{12}P_2$ includes Fructose 1,6-bisphosphate; $C_6H_{13}O_9P$ includes Fructose 6-phosphate, Glucose 6-phosphate, Glucose 1-phosphate and Beta-D-Glucose 6-phosphate; $C_6H_{12}O_6$ includes D-Glucose, Beta-D-Glucose and Alpha-D-Glucose.

Starch and Sucrose Metabolism

The metabolites tentatively identified as being involved in Starch and Sucrose Metabolism: Glucose 6-phosphate, Glucose 1-phosphate, Alpha-D-Glucose, D-Fructose, D-Maltose, Sucrose, Uridine diphosphate glucose, Alpha-D-Glucose 1,6-bisphosphate, 3-Phosphoglyceric acid, Glycogen, NADH, Pyrophosphate, Uridine triphosphate and Uridine diphosphate glucuronic acid were therefore selected for further PCA and PLS-DA analysis. PCA and PLS-DA analysis with metabolites associated with Starch and Sucrose Metabolism was performed. PCA analysis revealed no significant difference between treatments (Figure5.25A), while PLS-DA analysis showed distinctive clustering between control and WS treatment (Figure 5.25B).

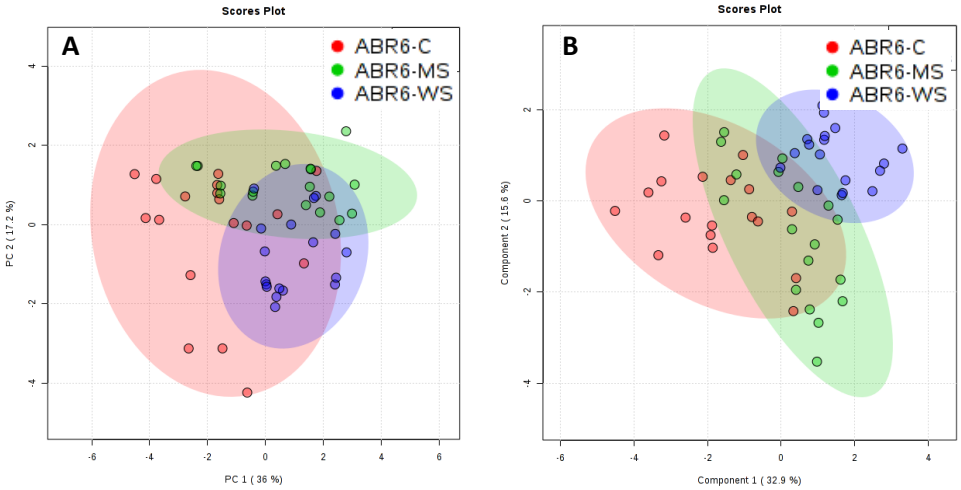

Figure 5.23. PCA and PLS-DA analysis of metabolites linked to starch and sucrose metabolism.

Derived spectra were analysed by A. Principal Components Analysis (PCA) and B. Partial Least Squares Discriminant Analysis (PLS-DA) to assign the profiles to groups based on metabolites tentatively linked to metabolites forming Starch and Sucrose Metabolism. Shaded areas indicate 95% confidence intervals. The explained variances for PC1 and PC2 are shown in brackets (C – control; WS – wind stress; MS – mechanical stress).

In this pathway, NADH and $C_{12}H_{22}O_{11}$ concentrations were increased by both stress treatments compared with control, while Pyrophosphate only by WS. Lower concentration after both stresses was detected in $C_6H_{14}O_{12}P_2$, 3-Phosphoglyceric acid, $C_{15}H_{24}N_2O_{17}P_2$ and Uridine diphosphate glucuronic acid. WS treatment decreased

$C_6H_{13}O_9P$ concentration, and decrease tendency was also observed in Glycogen concentration; however, the difference is not significant. Lower concentration after MS was detected in Uridine triphosphate and $C_6H_{12}O_6$ (Figure 5.26).

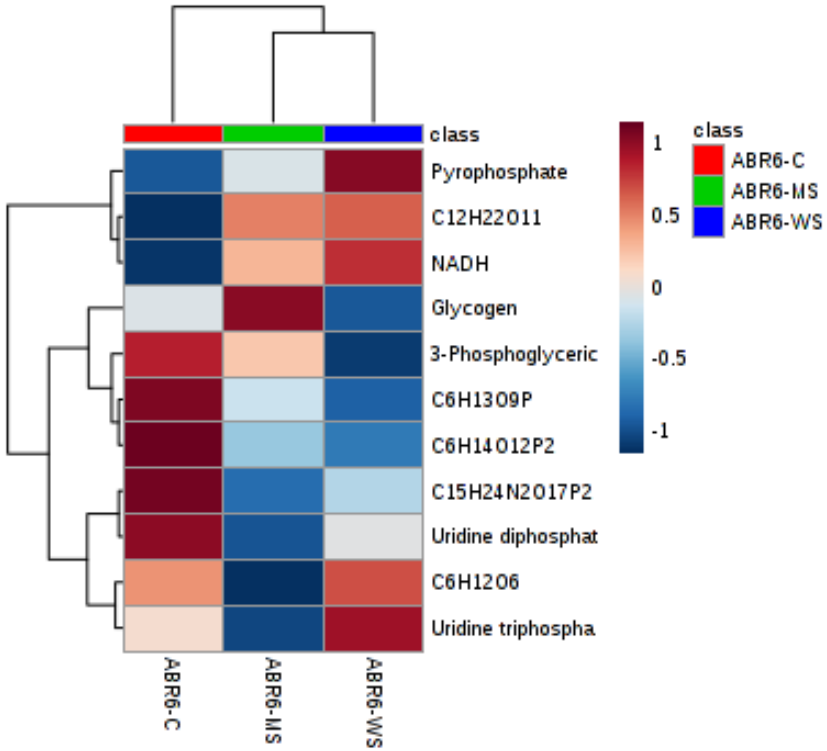

Compound	*P* value	FDR	Differences		
NADH	1.01E-05	0.000108	C	WS*	MS*
$C_6H_{14}O_{12}P_2$	1.96E-05	0.000108	C	WS*	MS*
$C_{12}H_{22}O_{11}$	0.000258	0.000948	C	WS*	MS*
3-Phosphoglyceric acid	0.000445	0.001225	C	WS*	MS*
Pyrophosphate	0.000665	0.001464	C	WS**	MS*
$C_{15}H_{24}N_2O_{17}P_2$	0.001007	0.001847	C	WS*	MS*
Uridine diphosphate glucuronic acid	0.001442	0.002266	C	WS*	MS*
Uridine triphosphate	0.001704	0.002343	C	WS*	MS**
Glycogen	0.008162	0.009975	C	WS*	MS*
$C_6H_{12}O_6$	0.009471	0.010418	C	WS*	MS**
$C_6H_{13}O_9P$	0.013223	0.013223	C	WS*	MS

Figure 5.24. Average normalised concentrations of most significant metabolites linked to starch and sucrose metabolism.

A heat map with an average normalised concentration of metabolites with statistics. ANOVA with a *post hoc* Tukey test was performed to identify statistical differences ($P \leq 0.05$); * Significantly different from control; * Significant difference between WS and MS. $C_{12}H_{22}O_{11}$ includes D-Maltose and Sucrose; $C_6H_{14}O_{12}P_2$ includes Alpha-D-Glucose 1,6-bisphosphate; $C_{15}H_{24}N_2O_{17}P_2$ includes Uridine diphosphate glucose; $C_6H_{13}O_9P$ includes Glucose 6-phosphate and Glucose 1-phosphate; $C_6H_{12}O_6$ includes Alpha-D-Glucose and D-Fructose.

Gluconeogenesis Pathway

The metabolites tentatively identified as being involved in Gluconeogenesis Pathway: Beta-D-Glucose 6-phosphate, Glucose 1-phosphate, Fructose 6-phosphate, Glucose 6-phosphate, Alpha-D-Glucose, D-Glucose, Beta-D-Glucose, D-Glyceraldehyde 3-phosphate, Dihydroxyacetone phosphate, Fructose 1,6-bisphosphate, 3-Phosphoglyceric acid Guanosine triphosphate, NADH, Oxoglutaric acid and Oxalacetic acid were therefore selected for further PCA and PLS-DA analysis. Both analyses revealed a significant difference between control and WS clustering, while control and MS clustered comparably (Figure 5.27).

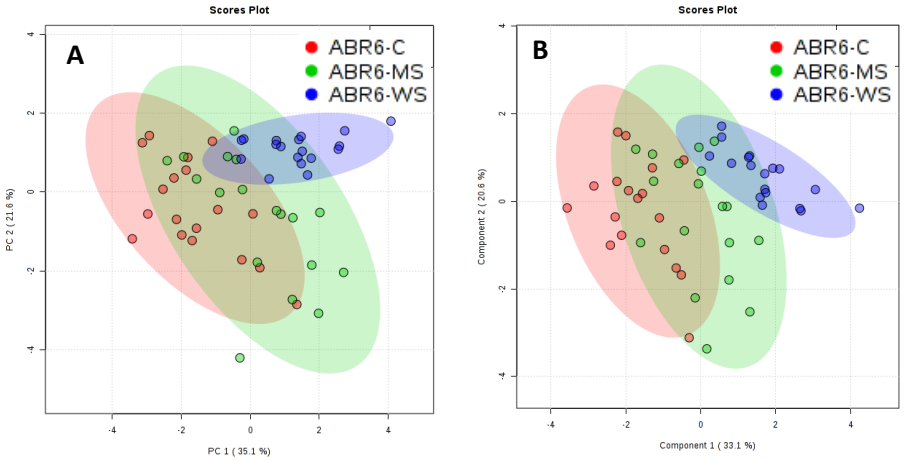

Figure 5.25. PCA and PLS-DA analysis of metabolites linked to the Gluconeogenesis Pathway.

Derived spectra were analysed by A. Principal Components Analysis (PCA) and B. Partial Least Squares Discriminant Analysis (PLS-DA) to assign the profiles to groups based on metabolites tentatively linked to metabolites forming Gluconeogenesis Pathway. Shaded areas indicate 95% confidence intervals. The explained variances for PC1 and PC2 are shown in brackets (C – control; WS – wind stress; MS – mechanical stress).

In this pathway, only NADH concentration was increased by both stress treatments compared with control. Guanosine triphosphate and Oxalacetic acid concentrations were increased by WS treatment, while MS treatment effected in a higher concentration of Oxoglutaric acid. Lower concentration after both stresses was detected in $C_3H_7O_6P$ and $C_6H_{14}O_{12}P_2$ and WS treatment caused a decrease in the

concentration of $C_6H_{13}O_9P$ and 3-Phosphoglyceric acid, while MS treatment caused a lower concentration of $C_6H_{12}O_6$ (Figure 5.28).

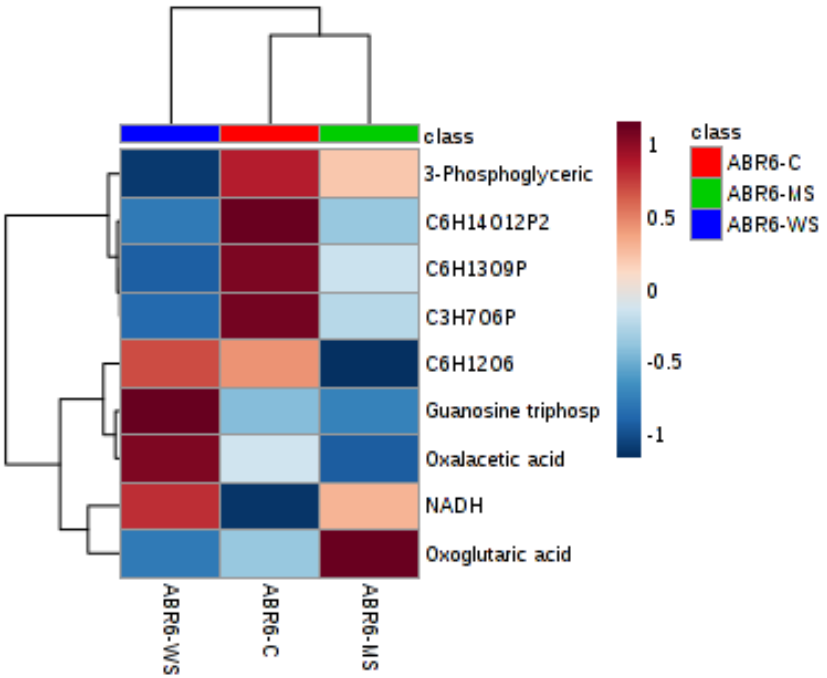

Compound	*P* value	FDR	Differences		
$C_3H_7O_6P$	6.71E-12	6.04E-11	C	WS**	MS**
NADH	1.01E-05	4.41E-05	C	WS*	MS*
Guanosine triphosphate	1.61E-05	4.41E-05	C	WS**	MS*
$C_6H_{14}O_{12}P_2$	1.96E-05	4.41E-05	C	WS*	MS*
3-Phosphoglyceric acid	0.000445	0.000802	C	WS**	MS*
Oxoglutaric acid	0.001416	0.002124	C	WS*	MS**
Oxalacetic acid	0.00256	0.003291	C	WS**	MS*
$C_6H_{12}O_6$	0.009471	0.010654	C	WS*	MS**
$C_6H_{13}O_9P$	0.013223	0.013223	C	WS*	MS

Figure 5.26. Average normalised concentrations of most significant metabolites linked to starch and sucrose Metabolism.

A heat map with an average normalised concentration of metabolites with statistics. ANOVA with a *post hoc* Tukey test was performed to identify statistical differences ($P \leq 0.05$); * Significantly different from control; * Significant difference between WS and MS. $C_3H_7O_6P$ includes D-Glyceraldehyde 3-phosphate and Dihydroxyacetone phosphate; $C_6H_{14}O_{12}P_2$ includes Fructose 1,6-bisphosphate; $C_6H_{13}O_9P$ includes Beta-D-Glucose 6-phosphate, Glucose 1-phosphate, Fructose 6-phosphate and Glucose 6-phosphate; $C_6H_{12}O_6$ includes Alpha-D-Glucose, D-Glucose and Beta-D-Glucose.

DETECTION BY MASS SPECTROMETRY IN POSITIVE IONISATION MODE

Galactose Metabolism

The metabolites tentatively identified as being involved in Galactose Metabolism: D-Glucose, D-Fructose, D-Galactose, D-Mannose, Alpha-Lactose, myo-Inositol, Alpha-D-Glucose, Uridine diphosphate glucose, Uridine diphosphate galactose, Raffinose, Maltotriose, Stachyose, Glycerol, Sucrose, NAD, NADH and ADP were therefore selected for further PCA and PLS-DA analysis. Both analyses revealed a significant difference in WS clustering compared with control and MS, which clustered comparably (Figure 5.29).

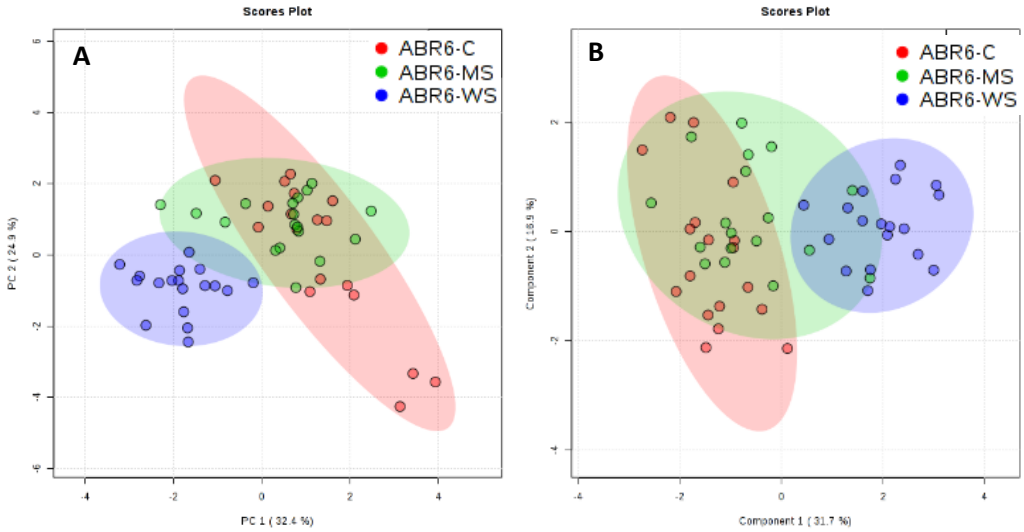

Figure 5.27. PCA and PLS-DA analysis of metabolites linked to galactose metabolism.

Derived spectra were analysed by A. Principal Components Analysis (PCA) and B. Partial Least Squares Discriminant Analysis (PLS-DA) to assign the profiles to groups based on metabolites tentatively linked to metabolites forming Galactose Metabolism. Shaded areas indicate 95% confidence intervals. The explained variances for PC1 and PC2 are shown in brackets (C – control; WS – wind stress; MS – mechanical stress).

$C_{15}H_{24}N_2O_{17}P_2$ concentration was increased by both stress treatments compared with control. WS treatment effected in a higher concentration of NAD, NADH and Stachyose, while MS in Sucrose. Decrease in concentration after WS treatment was observed in $C_{18}H_{32}O_{16}$, ADP and Glycerol, while after MS in $C_6H_{12}O_6$ (Figure 5.30).

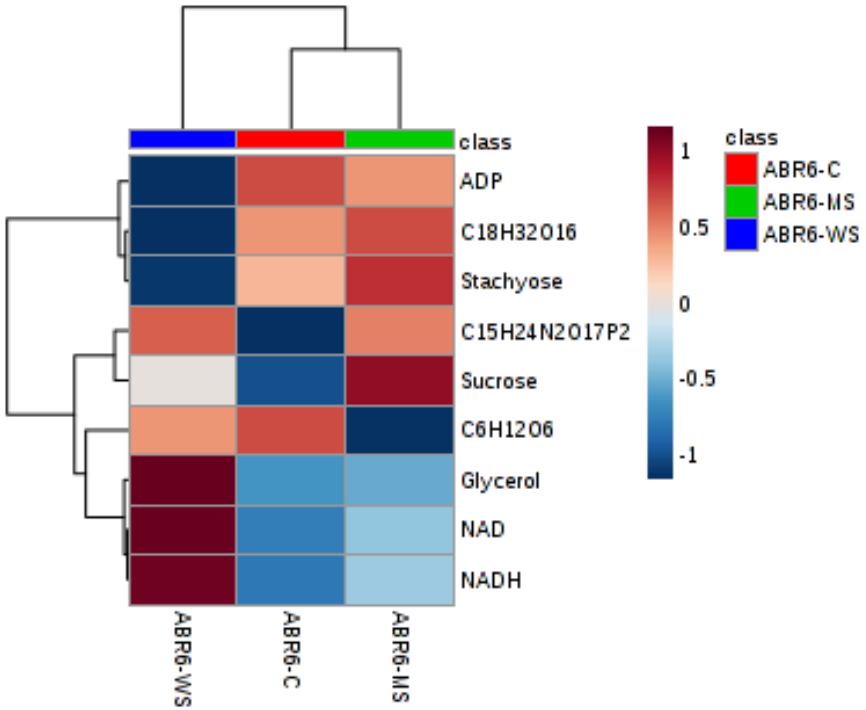

Compound	*P* value	FDR	Differences		
NAD	1.00E-09	9.04E-09	C	WS**	MS*
NADH	2.16E-08	9.70E-08	C	WS**	MS*
$C_{18}H_{32}O_{16}$	2.18E-07	6.54E-07	C	WS**	MS*
Stachyose	0.000851	0.001673	C	WS**	MS*
Sucrose	0.000929	0.001673	C	WS*	MS**
Glycerol	0.001172	0.001759	C	WS**	MS*
$C_6H_{12}O_6$	0.003246	0.004173	C	WS*	MS**
ADP	0.006061	0.006337	C	WS**	MS*
$C_{15}H_{24}N_2O_{17}P_2$	0.006337	0.006337	C	WS*	MS*

Figure 5.28. Average normalised concentrations of most significant metabolites linked to starch and sucrose metabolism.

A heat map with an average normalised concentration of metabolites with statistics. ANOVA with a *post hoc* Tukey test was performed to identify statistical differences ($P \leq 0.05$); * Significantly different from control; * Significant difference between WS and MS. $C_{15}H_{24}N_2O_{17}P_2$ includes Uridine diphosphate glucose and Uridine diphosphate galactose; $C_{18}H_{32}O_{16}$ includes Raffinose and Maltotriose; $C_6H_{12}O_6$ includes D-Glucose, D-Fructose, D-Galactose, D-Mannose, Alpha-Lactose, myo-Inositol and Alpha-D-Glucose.

5.3.2.2. MANUAL SELECTION OF METABOLITES LINKED TO THE PHENYLPROPANOID PATHWAY.

The Phenylpropanoid Pathway is one of the indispensable pathways to plants because of its role in the production of the hydroxycinnamyl alcohols, also known as monolignols. Monolignols serve as the building blocks of lignin, which confers structural support (Fraser & Chapple, 2011). Experiments performed in this project (Chapter 4) revealed that both stress treatments induced changes in the content of cell wall hydroxycinnamoyl esters as well as an impressive increase in lignin content. As the Phenylpropanoid Pathway was not enriched, it was decided to manually select metabolites linked to this pathway and to perform an analysis. This pathway contains 66 metabolites according to the KEGG database. Table 5.12 lists all the metabolites linked to the Phenylpropanoid Pathway found in the samples accompanied by the significance of the difference between three treatments (control, WS and MS) (ANOVA, $P \leq 0.05$). Interestingly all metabolites detected in the samples are located in the first part of this pathway, so the table lists the first 23 metabolites of the Phenylpropanoid Pathway.

PCA analysis with selected metabolites for each genotype and ionisation mode was performed. PLS-DA analysis was performed only for Bd21 positive ionisation mode, for the Bd21 negative and ABR6 positive and negative ionisation mode the number of metabolites assigned was too small. PCA analysis for Bd21 negative and positive ionisation mode shows no cluster separation (Figure 5.31A-B). However, PLS-DA analysis performed on Bd21 positive ionisation mode shows the separation of WS treatment from control, while MS treatment clusters in between these two treatments (Figure 5.31C). No distinctive clustering between treatments in positive and negative ionisation modes was observed in ABR6 (Figure 5.32)

Table 5.12. Metabolites associated with the Phenylpropanoid Pathway

Metabolites associated with Phenylpropanoid Pathway with the statistical significance (ANOVA, $P \leq 0.05$) for both genotypes and both negative and positive ionisation mode. The listed compounds represent the first 23 metabolites of this pathway.

Metabolite	Bd21		ABR6	
	Negative	Positive	Negative	Positive
L-Phenylalanine	-	4.32E-05	-	6.71E-04
L-Tyrosine	-	-	-	-
p-Coumaroyl-CoA	2.22E-04	-	3.97E-04	-
Spermidine	-	-	-	2.92E-04
Caffeoyl-CoA	-	-	-	-
Feruloyl-CoA	-	1.06E-04	-	-
Sinapoyl-CoA	-	-	-	-
trans-Cinnamate	-	5.28E-03	-	8.40E-04
Sinapate	-	-	7.56E-03	3.44E-03
Cinnamoyl-CoA	-	2.31E-03	-	5.01E-04
Coniferyl alcohol	-	1.10E-03	-	9.42E-03
Coniferin	1.53E-02	-	4.12E-03	-
4-Coumarate	-	3.71E-04	-	-
Chlorogenate	-	1.41E-03	9.75E-04	-
Cinnamaldehyde	-	1.24E-03	-	6.62E-05
Sinapine	-	-	-	-
1-O-Sinapoyl-beta-D-glucose	1.14E-04	1.91E-04	1.86E-04	-
Caffeate	5.83E-03	-	-	-
Ferulate	-	-	-	-
Scopolin	-	1.41E-03	9.75E-04	-
Syringin	1.71E-03	-	2.67E-03	-
Scopoletin	-	-	-	-
trans-2-Hydroxycinnamate		3.71E-04	-	-

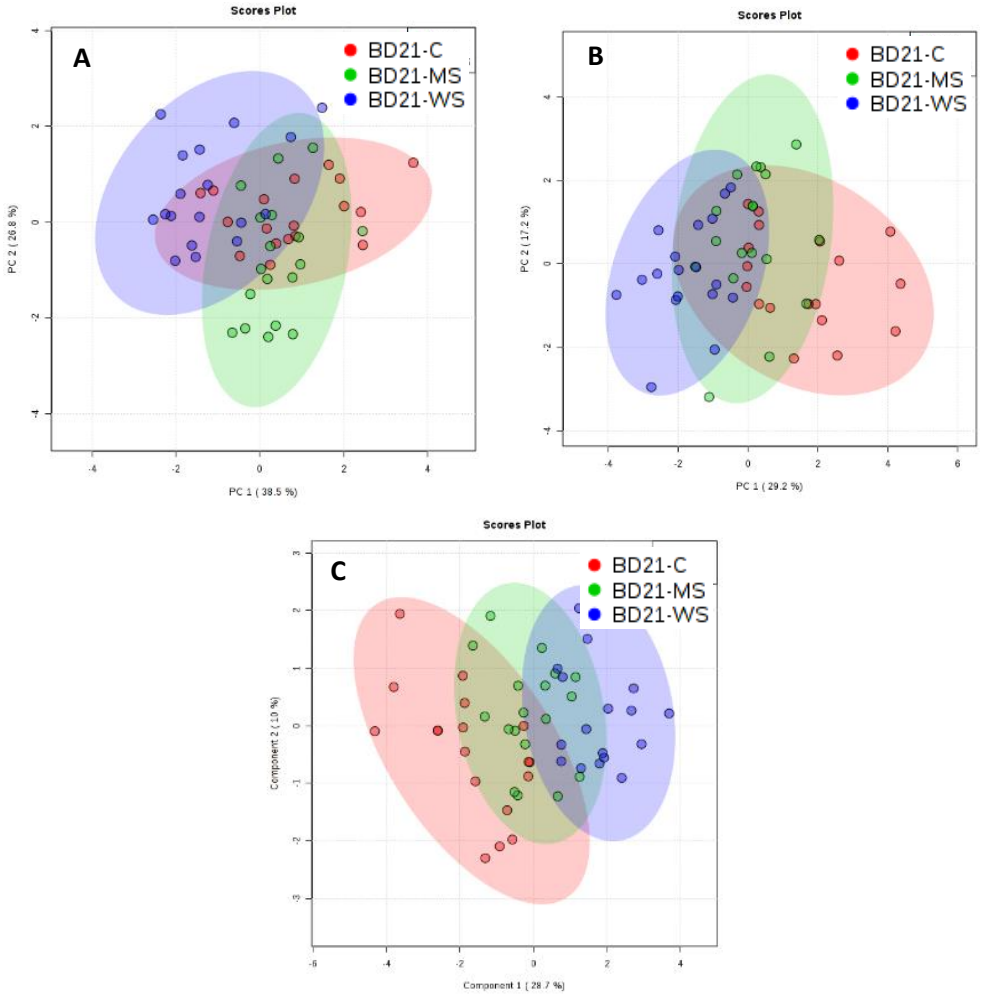

Figure 5.29. PCA and PLS-DA analysis of metabolites linked to the Phenylpropanoid Pathway in Bd21.

Derived spectra were analysed by Principal Components Analysis (PCA) of A. negative ionisation mode, B. Positive ionisation mode, to assign the profiles to groups based on metabolites tentatively linked to the Phenylpropanoid Pathway. C. Partial Least Squares Discriminant Analysis (PLS-DA) analysis of Bd21 positive ionisation mode. Shaded areas indicate 95% confidence intervals. The explained variances for PC1 and PC2 are shown in brackets (C – control; WS – wind stress; MS – mechanical stress).

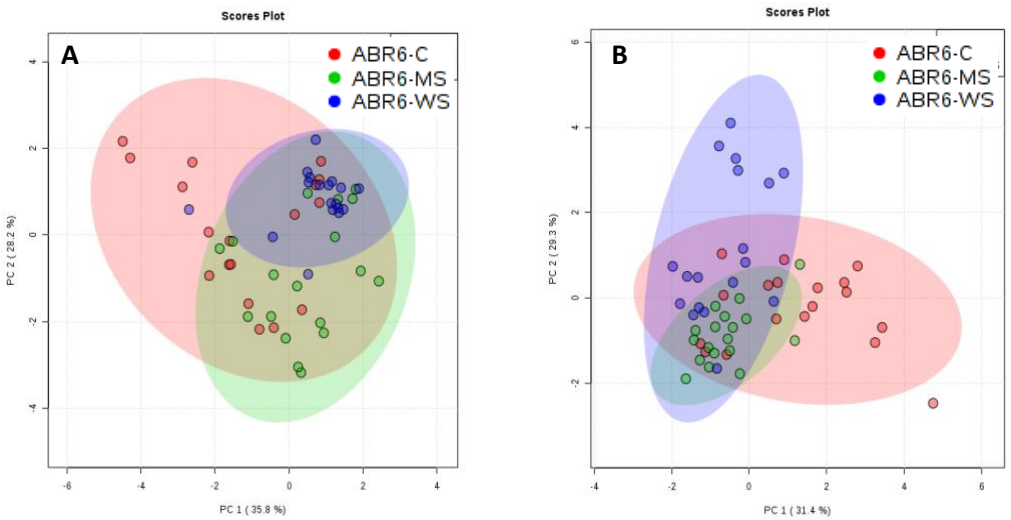

Figure 5.30. PCA analysis of metabolites linked to the Phenylpropanoid Pathway in ABR6.

Derived spectra were analysed by Principal Components Analysis (PCA) of A. negative ionisation mode, B. Positive ionisation mode, to assign the profiles to groups based on metabolites tentatively linked to the Phenylpropanoid Pathway. Shaded areas indicate 95% confidence intervals. The explained variances for PC1 and PC2 are shown in brackets (C – control; WS – wind stress; MS – mechanical stress).

5.4. DISCUSSION

The aim of this chapter was to investigate the influence of wind and mechanical stress on the expression of previously reported touch-inducible geneses and cell wall-related genes. An additional aim was to identify metabolite pathways involved in response to mechanical stimulation.

The response of plants to mechanical stimulation encompasses many phenotypic, histological, physiological and compositional changes, as has been described for many different species, and was presented in the previous chapters of this thesis. These modifications require alterations in gene expression, and indeed, various touch-induced genes were previously reported (Lee *et al.*, 2005).

In the present study, the potential *Brachypodium* orthologs of the touch-inducible and touch responsive cell wall-related genes reported in *Arabidopsis* (Lee *et al.*, 2005) were identified, and the effect of wind and mechanical stress on their gene expression was analysed. Unfortunately, only one of the *Arabidopsis* TCH genes could be analysed, due to problems with primer efficiency and specificity. The three candidate *Brachypodium* ortholog genes (Bradi2g21460, Bradi2g10010 and Bradi1g17237) for the *Arabidopsis* TCH1 gene, which encodes a calmodulin, were analysed by Real-Time PCR. Calmodulins and calmodulin-like proteins are ubiquitous calcium-dependent activators of various enzymes in eukaryotic cells, and their alteration in expression upon mechanical stimulation suggests the involvement of Ca^{2+} in plant mechanosensing (Börnke & Rocksch, 2018). The current study does not support previous findings in Arabidopsis as results indicate a down-regulation of the expression of the TCH-related genes in both *Brachypodium* genotypes and after both stress treatments (WS and MS), while in *Arabidopsis* TCH1 was highly expressed after mechanical stimulation (Braam & Davis, 1990; Lee *et al.*, 2005). Nearly half of the 33 XTH (including TCH4) genes were highly expressed after mechanical stimulation in *Arabidopsis* (Lee *et al.*, 2005). The family of XTH genes is involved in cell wall modifications through alterations of xyloglucan polymers in the plant cell wall, which may affect wall architecture (Campbell & Braam, 1998; Steele *et al.*, 2001). Furthermore, xyloglucans cross-link the cellulose microfibrils, which provides cell wall integrity (Rose *et al.*, 2002). Unfortunately, in this study

expression analysis of these important genes was unsuccessful, due to primer efficiency issues. One of the most important aspects of gene expression analysis by RT-PCR is primer specificity and/or efficiency. Many attempts of changing the RT-PCR parameters and concentrations of reaction components were performed but were unfortunately unsuccessful in overcoming the before-mentioned issues. The expression analyses of other cell wall-related genes in this study could not confirm results from previous studies. While the ExpA-related, CSL, WAK and GH genes were all highly expressed upon mechanical stimulation in *Arabidopsis*, their potential orthologs in *Brachypodium* showed down-regulation. These results may suggest that *Brachypodium* has a different molecular thigmomorphogenesis response pathway compared to *Arabidopsis*. However, it is important to note that the experimental setup for the *Arabidopsis* experiment was different than presented in this research. Mechanically treated *Arabidopsis* rosettes were collected after 30min, while *Brachypodium* stems were collected after two weeks of stress treatment. These two weeks of exposure to stress may cause at some point plant adaptation to particular environmental conditions, and thus, the expression of genes may stabilise and therefore, the overexpression cannot be observed.

Pectin esterases, especially pectin methylesterases (PME), was another group of genes, which were found to be highly expressed after mechanical stimulation in *Arabidopsis*. Two pectin methylesterase genes At4g02330 and At1g53840 were over-expressed with around ˜7.47- and ˜2.09-fold change, respectively after mechanical stimulation. Moreover, two pectin methylesterase inhibitor (PMEI) genes At3g10720 and At5g62360, respectively were also upregulated by ˜4.39- and ˜2.04-fold after mechanical stimulation (Lee *et al.*, 2005). Taking this into consideration and combined with the results presented in Chapter 3 (page 118), which suggested that pectin methylesterase activity was enhanced by wind and mechanical stress, it was decided to perform a more extensive examination of PME and PMEI genes. Expression analysis of the orthologue of Arabidopsis genes in Brachypodium combined with a selection of PME/PMEI genes showing the highest expression levels in “early inflorescence and/or emerging inflorescence and/or leaves” was performed. However, because of similar primer specificity and/or efficiency issues as mentioned before, expression analysis was

possible only for one PME gene - Bradi2g56820, which showed a down-regulation after MS in Bd21 and after WS in ABR6 and a 1.6-increase in expression was obtained after MS in ABR6. The analysis presented in this chapter in terms of expected over-expression of PME genes after mechanical stimulation failed to give an explanation for the increased PME activity (see Chapter 3) after stress treatments.

The analysis of LOX genes presented in this chapter revealed an increased expression of the *Brachypodium* orthologue for wheat TaLOX1 (Bradi1g11680), especially after MS in ABR6 (˜7.5-fold change) and after WS treatment (˜2.5-fold change). This is in agreement with previously reported data in wheat, where researchers found this gene to be highly expressed after brushing (Mauch *et al.*, 1997). The closer relation of *Brachypodium* to wheat than to *Arabidopsis* makes these results even more important, as it suggests that the family of monocot grasses may display a different response to mechanical stimulation than dicot plants. However, the expression analysis in Bd21 showed down-regulation of the expression of this gene after WS and a slight increase in expression after MS (˜1.7-fold change), which may suggest that even within species responses can differ. The analysis of other LOX genes also revealed different responses between genotypes. All analysed LOX genes in Bd21 were down-regulated. In ABR6, WS treatment caused mostly down-regulation of LOX genes; only two genes out of six analysed by Real-Time PCR showed a slightly increased expression (1.15 and 1.58) while MS treatment caused mostly a low increase in expression, ranging between ˜1.36-2.56-fold change. This indicates that WS and MS treatment may affect plants differently on the molecular level. Lipoxygenase genes are an integral part of the jasmonic acid biosynthetic pathway. Jasmonates are a family of cyclopentanone derivatives synthesised from linolenic acid via the octadecanoid pathway. These lipid-derived metabolites, which include jasmonic acid (JA), its methyl ester (MeJA), and 12-oxo-10,15-phytodienoic acid (12-OPDA) (a central intermediate) (Chehab *et al.*, 2009) were previously implicated to play a role in plant thigmomorphogenetic responses to mechanical stimulations (Stelmach *et al.*, 1998; Ellis *et al.*, 2002; Tretner *et al.*, 2008). The metabolic analysis did not reveal enrichment for the JA biosynthesis pathway, linolenic acid pathway or octadecanoid pathway. Manual selection of metabolites was unsuccessful because only one of the metabolites from such pathways was detected.

12-OPDA was detected in negative ionisation mode in Bd21 and displayed a significant difference in concentration between treatments (Appendix 10A, page 305). Nevertheless, based on the literature, it would be expected that the concentration after stresses should be increased, while in this analysis, the 12-OPDA concentration decreased after both stress treatments. The *Arabidopsis* cev1 mutant, with a mutation in the cellulose synthase gene CeSA3, produced constitutively high levels of JA and 12-OPDA and showed a phenotype that resembled those associated with thigmomorphogenetic changes (Ellis *et al.*, 2002). Moreover, it was also reported that in common bean (*Phaseolus vulgaris)* application of the 12-OPDA analogue - coronatine, a - elicits physiological changes reminiscent of thigmomorphogenesis. Furthermore, the levels of *cis*-OPDA were found to increase several-fold well before the development of thigmomorphogenic symptoms (Stelmach *et al.*, 1998). The results obtained for the expression analysis of LOX genes in the current study, which showed either a decrease or a slight increase of expression for the LOX genes tested after both stresses in Bd21, are only partially in agreement with the presented findings in the literature. Although the results of the gene expression data in this study do not provide many new insights about the molecular response of *Brachypodium distachyon* to WS and MS, it should be stressed that this is a novel research area with little to no data on the molecular mechanisms involved in wind and mechanical stress in grasses. As such, albeit limited, this analysis gives some insight into the complexity of the response to mechanical stimulation in grasses and provides a platform for future more detailed analyses.

Plants have developed biochemical, physiological, but also metabolic strategies in order to fight abiotic stresses. Thus, metabolomics plays an important role to gather information about stress-induced changes in plant development (Gupta, 2014). In this study, metabolites were extracted from stem tissue of *Brachypodium distachyon* after exposure to wind and mechanical stress. These were analysed by flow injection electrospray high-resolution mass spectrometry and and metabolite profiles showing a high degree of variation were identified. The metabolites that showed significant changes in response to the treatments were further assessed for pathway enrichment, and pathways involved in response to mechanical stimulation were identified. Although the identified pathways did not exhibit robust statistical validity with satisfactory *P*

value ($P \leq 0.05$) and FDR ($P \leq 0.05$), and therefore cannot be marked as enriched, it was decided to accept pathways with $P \leq 0.1$ and flagged these as suggestive. The reason for that is the novelty of results in this area of research and, to my knowledge, this represents the first data linking mechanical stimulation to metabolite profiling.

The pathways showing tentative enrichment for Bd21 were Glycolysis, Pentose Phosphate and Gluconeogenesis in negative ionisation mode and Methylhistidine Metabolism and Galactose metabolism in positive ionisation mode. There were seven enriched pathways identified in ABR6 in negative ionisation mode, including Nucleotide Sugars Metabolism, Galactose Metabolism, Fructose and Mannose Degradation, Glycolysis, Starch and Sucrose Pathway and Gluconeogenesis, while for positive ionisation mode, only Galactose Metabolism showed enrichment. All the identified enriched ($P \leq 0.1$) pathways in both genotypes belong to the parenting pathway of Carbohydrate Metabolism. The main pathways from Carbohydrate Metabolism are Glycolysis, Gluconeogenesis and Pentose Phosphate pathways. Glycolysis is the process of converting glucose into pyruvate and generating small amounts of ATP (energy) and NADH (reducing power). Moreover, it is a central pathway that produces important precursor metabolites. Glycolysis is thus of crucial importance in plants because it is the predominant pathway that "fuels" plant respiration (Plaxton, 1996). Gluconeogenesis is a synthesis pathway of glucose from noncarbohydrate precursors. It is essentially a reversal of glycolysis with minor variations of alternative paths. The pentose phosphate pathway is a process of glucose turnover that produces NADPH as reducing equivalents and pentoses as essential parts of nucleotides. Indirectly, the sugars play an important role during plant growth and development under abiotic stresses by regulating carbohydrate metabolism (Gupta & Kaur, 2005). Soluble carbohydrates and starch, which accumulates under normal conditions before the stress, constitute the main resources for plants to supply energy during stress condition, as well as during recovery (Khelil *et al.*, 2007). Indeed, many environmental stresses like drought (Pelleschi *et al.*, 1997; Xue *et al.*, 2008), cold (Morsy *et al.*, 2007), salinity (Khodary, 2004; Morsy *et al.*, 2007; Zhang *et al.*, 2012), pollutants like cadmium (Devi *et al.*, 2007) lead to major alterations in Carbohydrate Metabolism.

Metabolic adjustments in response to unfavourable conditions are dynamic and multifaceted and not only depend on the type and strength of the stress, but also on the cultivar and the plant species. Plants respond to stress by a progressive adjustment of their metabolism with sustained, transient, early- and late-responsive metabolic alterations. For example, raffinose and proline accumulate to high levels over the course of several days of salt exposure, drought, or cold, whereas carbohydrate metabolism changes rapidly in a complex, time-dependent manner (Krasensky & Jonak, 2012). Moreover, different species may accumulate different metabolites in response to stress, and sometimes there is no obligation for the accumulation of particular metabolite for adaptation to particular stress environment. In some cases, the flux through a metabolic pathway, rather than the accumulation of a specific metabolite per se, might contribute to stress tolerance (Krasensky & Jonak, 2012).

Nevertheless, in response to various abiotic stresses such as drought, salt and many others, plants alter the accumulation of few classes of metabolites. Many of them belong to Carbohydrate Metabolism, namely: fructans, starch, mono- and disaccharides, trehalose and raffinose family oligosaccharides such as raffinose and stachyose (Krasensky & Jonak, 2012). In this research, *Brachypodium distachyon* responded by enrichment of many pathways involved in carbohydrate metabolism. Generally speaking, accumulation of sugars in response to various abiotic stresses can function as osmolytes to maintain cell turgor and have the ability to protect membranes and proteins from stress damage (Madden *et al.*, 1985; Kaplan & Guy, 2004). Moreover, carbohydrate accumulation may function as storage substances, which can be mobilised in response to abiotic stresses, when limited energy supply is provided, or in the situation of enhanced demands (Hendry, 1993). Carbohydrate storage can be quickly metabolised to provide soluble sugars. Carbohydrate Metabolism is very sensitive to changes in the environment (Kaplan & Guy, 2004; Kempa *et al.*, 2008; Todaka *et al.*, 2017).

Moreover, proline metabolism has been noted to be involved in response to various abiotic stresses. Proline and arginine metabolism is the central pathway for biosynthesis of the amino acids proline and arginine from glutamate (Rizhsky *et al.*, 2004; Dobra *et al.*, 2010). In this research study, proline and arginine metabolism was not observed to

be enriched in response to wind or mechanical stress; however, a few metabolites which are involved in this pathway were in the top 20 of metabolites identified showing the biggest difference between treatments in both genotypes. It has been proposed that proline acts as an osmolyte and therefore contributes to osmotic adjustment within the cells (Delauney & Verma, 1993). Moreover, it was proposed that proline is a molecular companion which helps in the stabilisation of proteins and therefore protect cells from damage caused by environmental stresses (Hare & Cress, 1997; Verbruggen & Hermans, 2008; Szabados & Savouré, 2010).

Hormone metabolism has been linked to the response to mechanical stimulation in plants, namely ethylene, auxin and abscisic acid (ABA). It has been implicated that mechanical stimulation led to an increase in the release of ethylene (Goeschl *et al.*, 1966; Biro & Jaffe, 1984; Onguso *et al.*, 2006), increase in ABA accumulation (Jeong & Ota, 1980; Erner & Jaffe, 1982) and changes in auxin distribution (Mitchell, 1977; Boyer *et al.*, 1979; Hofinger *et al.*, 1979). Brassinosteroids (BR) have also been linked to plant thigmomorphogenesis. Arabidopsis plants exposed to the highly active BR, 24-epibrassinolide showed over-expression of TCH4 (Xu *et al.*, 1995; Iliev *et al.*, 2002), which encodes an enzyme xyloglucan endotransglycosylase predicted to have a role in cell wall modification (Campbell & Braam, 1998; Rose *et al.*, 2002). In this study, we did not perform detailed metabolite profiling; thus, such observation could not be made. Nevertheless, it needs further consideration.

In conclusion, gene expression results in response to mechanical stimulation presented in this chapter are completely novel in this area of research, especially for the grasses. Some alterations in expression were found in cell-wall related genes, LOX and PME genes. Moreover, it is the first study to investigate a plants' response to mechanical stimulation at a metabolic level, where we began to unravel the metabolic response of *Brachypodium distachyon* stems to the wind and mechanical stress. The pathways found to be enriched play a crucial role in Carbohydrate Metabolism, which was previously reported to be involved in response to many abiotic stresses. All these results indicate that mechanical stimulation affects not only visual, mechanical, anatomical and compositional changes of cell walls but also induces changes at the molecular and metabolic level.

CHAPTER 6

CHAPTER 6 : GENERAL DISCUSSION

6.1. AIMS AND BACKGROUND

Plants through their life are exposed to many abiotic stresses. Over the last decade, the climate is constantly changing, and weather anomalies responsible for abiotic stresses in plants become more frequent. This has a direct effect on plant growth and development (Le Gall *et al.*, 2015). While plant responses to abiotic stresses such as drought, cold, air pollutants are intensively studied, there is relatively little research related to the response of plants to mechanical stimulation such as wind, brushing or touching. Nevertheless, it has been previously shown that plants respond to mechanical stimulation by modifications in phenotypic features, alterations in histology and anatomy and mechanical properties (Cleugh *et al.*, 1998; Braam, 2005; Chehab *et al.*, 2009). Furthermore, molecular responses were also noted (Braam & Davis, 1990; Lee *et al.*, 2005). Moreover, investigations of responses to mechanical stimulation are performed mostly on dicots, while there is almost no data for the most economically important plant group, the grasses. Literature suggests that responses may differ between plant species, but most importantly also within populations of the same species (Jaffe & Telewski, 1984; Bossdorf & Pigliucci, 2009). These responses are also determined by the intensity, duration (Retuerto & Woodward, 1992; Johnson *et al.*, 1998; Pigliucci, 2002) but also form of mechanical stimulation (e.g. wind stress, brushing) (Smith & Ennos, 2003; Anten *et al.*, 2010).

The main objective of this study was to characterise the response of two genotypes Bd21 and ABR6 of *Brachypodium distachyon* to wind stress and mechanical stress at various levels with an emphasis on stem cell walls. In particular, the main focus in this study was on consequences of WS and MS on cell wall composition, architectural and histological features of the stems, as well as phenotypic responses and mechanical properties. The molecular changes elicited by WS and MS were identified by analysis of expression of cell-wall related genes as well as metabolic pathways involved in response to mechanical stimulation.

6.2. KEY FINDINGS

Morphological responses:

- Both genotypes showed very similar responses to WS and MS.
- Plants reacted by a reduction in main stem length and aboveground biomass.
- Mechanical stimulation affected reproduction in *Brachypodium distachyon* by a reduction in seed yield, weight and number and also by delay in flowering time.
- WS and MS caused alterations in stem mechanical properties by increasing the stiffness of these tissues.

Anatomical and compositional responses:

- Mechanical stimulation resulted in alterations in stem anatomy
    - Changes in tissue organisation
    - Increased cell wall thickness in specific areas
    - ABR6 reacted to mechanical stimulation by an increase in the area of VB, while in Bd21 B area decreased
- Immuno-localisation with various cell wall related antibodies revealed that pectins are involved in response to MS and WS in both genotypes.
- Both stresses enhance pectin methylesterases activity.
- Cell wall composition analysis revealed alterations in monosaccharides content, increases in lignin and a reduction in recalcitrance to saccharification after WS and MS in both genotypes.
- Lignin distribution assessed by phloroglucinol staining showed increased lignification in the cortex and interfascicular region of stem cross-sections.

Molecular and metabolic responses:

- Results indicate that *Brachypodium distachyon* has a different molecular response to mechanical stimulation compared with *Arabidopsis thaliana.*
- RT-PCR analysis revealed that both treatments increase the expression of a Lipoxygenase gene previously reported in wheat to be touch-inducible.
- Metabolite analysis identified changes in the concentration of metabolites involved in carbohydrate metabolism.

6.3. MORPHOLOGICAL RESPONSES

It was previously established that plants respond to mechanical stimulation by various morphological modifications (Braam, 2005; Börnke & Rocksch, 2018). The responses may vary depending on species, genotypes, age of tissues but also factors such as duration, time and intensity of stress treatment (Jaffe, 1973; Biddington, 1986; Johnson *et al.*, 1998; Bossdorf & Pigliucci, 2009; Anten *et al.*, 2010). In this study, such responses were analysed on the model plant for grasses – *Brachypodium distachyon*. It was shown that exposure of two genotypes (Bd21 and ABR6) to wind and mechanical stress caused alterations in phenotypic traits. The most dramatic changes observed were a reduction of main stem length and aboveground biomass as well as alterations in the reproduction process and mechanical properties.

Reduction in stem height is the most common response to mechanical stimulation, previously reported in various species (Retuerto & Woodward, 1992; Telewski & Pruyn, 1998; Verhertbruggen *et al.*, 2013). Generally, development of shorter stems is consistent with the concept that reduced height will limit the bending moment of the stem and lower the risk of a range of excessive mechanical strains, plastic deformation, uprooting, stem buckling and failure (Paul-Victor & Rowe, 2011). Thus, stem shortening is directly connected with alterations in mechanical properties. Literature suggests that stems after exposure to mechanical stimulation become either longer but more flexible or shorter and more rigid (Smith & Ennos, 2003). Results presented in this study may partially confirm the hypothesis that stems after mechanical stimulation become shorter and more rigid. Such results are also in agreement with the results from a study performed on *Zea mays*, another grass species (Whirehead & Luti, 1962).

Reduction in aboveground biomass in this study is in agreement with previously established data (Goodman & Ennos, 1996; Henry & Thomas, 2002; Kern *et al.*, 2005; Murren & Pigliucci, 2005). It is hypothesised that such reduction may be associated with stem height but most of all with a decrease in leaf size and area, which was broadly documented in many species (Jaffe, 1973; Biddington, 1986; Anten *et al.*, 2010), however, leaves characteristic was not determined in this study.

Plant reproduction was significantly affected by mechanical stimulation in this study. Flowering time was delayed, and seed weight, number and total seed yield were reduced. It was previously noted in various species that mechanical stimulation resulted in delay of flowering (Retuerto & Woodward, 1992; Johnson *et al.*, 1998; Niklas, 1998; Cipollini, 1999; Anten *et al.*, 2005; Bossdorf & Pigliucci, 2009), delay of anthesis (Mitchell *et al.*, 1975; Jaffe, 1976; Akers & Mitchell, 1983), reduction in reproductive structures, seed number, weight and total yield (Jaffe, 1973; Niklas, 1998; Bossdorf & Pigliucci, 2009; Zhang *et al.*, 2013b). Such a response to mechanical stimulation may indicate that mechanical stimulation significantly aggravates plant reproduction success. However, it has been hypothesised that this may be an adaptation mechanism to ensure the continuation of propagation (Jaffe & Forbes, 1993; Cipollini, 1999).

6.4. ANATOMICAL, HISTOLOGICAL AND COMPOSITIONAL RESPONSES

While many studies in the area of mechanical stimulation have examined its effect on phenotypic traits, little attention has been given to how such mechanical stimulation may affect anatomical and histological features of the stem and compositional features of the cell wall. Plant cell walls are the first barrier to abiotic stress, and biochemical changes in its composition and structural reorganisation of its architecture allow cell walls to adapt to particular conditions (Sarkar *et al.*, 2009).

This study clearly shows that stems undergo many histological and anatomical modifications in response to wind and mechanical stress. Such changes were previously studied mostly in dicots, with very limited studies performed in grasses, which have different stem anatomy compared with monocots. Observed anatomical and histological changes caused by both stresses suggest that plant's response to mechanical stimulation may be species-specific or even genotype-specific. This study revealed that wind and mechanical stress caused rearrangements in tissue organisation; however, the response differs between genotypes. The most dramatic response was observed in vascular bundle area developed, which decreased after stresses in Bd21 and increased in ABR6. Moreover, both stresses resulted in an increase in cell wall thickness and increased lignification in the interfascicular region and cortex area. The further histological investigation included of immuno-localisation with cell-wall related

antibodies in the grass family. Such analysis revealed multiple alterations in labelling with pectin-related antibodies. Moreover, this study is the first to our knowledge to examine the pectin involvement in response to mechanical stimulation in the grass family. The outcome of such an analysis did not reveal a clear pattern and did not give consistent results, and therefore, it is difficult to interpret and establish a clear conclusion. Nevertheless, pectins are involved in response to wind and mechanical stress. Such involvement was previously reported in *Arabidopsis*; however, similar to our work, the outcome was not consistent (Verhertbruggen *et al.*, 2013; Rigo, 2016). It is known that HG with low levels of methyl-esterification takes part in creating calcium-mediated gels, causing cell wall stiffening and playing a role in regulating the porosity and mechanical properties of cell walls (Ridley *et al.*, 2001; Willats *et al.*, 2001; Hongo *et al.*, 2012). Also, lignin is known to be essential for the structural integrity of cell walls (Boerjan *et al.*, 2003) and provides additional reinforcement resulting in increased tensile strength (Gibson, 2012; Barros *et al.*, 2015). Thus, both increased levels of lignin and demethylesterified pectin could contribute to the observed increases in stem rigidity.

This study was the first to our knowledge to asses complete cell wall composition analysis of stem responses to mechanical stimulation. The work shows that cell walls undergo many modifications in response do WS and MS treatment. Both stresses in both genotypes led to alterations in monosaccharide and cell wall-bound hydroxycinnamic acids content and composition, increase in lignin content and decreased sugar release. While changes in lignin accumulation in response to mechanical stimulation was previously investigated, there is no information in the literature for other compositional changes of cell wall components. Moreover, there is no clear consistency in the effect on the lignin content response (De Jaegher *et al.*, 1985; Cipollini, 1997; Henry & Thomas, 2002; Paul-Victor & Rowe, 2011).

Summarising histological, anatomical and compositional results obtained in this study, it is clear that the response of Brachypodium to wind and mechanical stress is not limited to morphological changes. WS and MS induce architectural changes across multiple scales, from the whole plant to organ, tissue and cellular level, highlighting the complex nature of how plants respond to wind stress and mechanical stimulation.

6.5. MOLECULAR AND METABOLIC RESPONSES

This work forms the first study to investigate the response of the *Brachypodium distachyon* model for grasses to wind and mechanical stress at the molecular and metabolic level. So far the molecular analysis of touch inducible genes was performed on *Arabidopsis thaliana* and revealed four TCH genes and a range of touch responsive cell-wall related genes which were highly expressed after mechanical stimulation (Braam & Davis, 1990; Lee *et al.*, 2005). This study aimed to investigate orthologues genes in *Brachypodium distachyon*. The analysis revealed that the molecular response of *Brachypodium* to mechanical stimulation might have a difference compared with that of Arabidopsis, as the expression of none of the orthologue genes was induced by either WS or MS. Moreover, small alterations in the expression of PMEs were observed, indicating that indeed pectins may play a role in response to wind and mechanical stress of *Brachypodium distachyon*. High expression of LOX, especially after MS, was noted in this study in ABR6, which is in agreement with previously reported data in wheat, where researchers found this gene to be highly expressed after brushing (Mauch *et al.*, 1997). The higher expression only in ABR6 may indicate that mechanical stimulation may affect genotypes differently on the molecular level. Although the results of the gene expression data in this study do not provide many new insights about the molecular response of *Brachypodium distachyon* to WS and MS, it should be stressed that this is a novel research area with little to no data on the molecular mechanisms involved in wind and mechanical stress in grasses.

This study is the first to investigate a plants' response to wind and mechanical stress at a metabolic level. To obtain insights into the metabolic response, the metabolite fingerprints after treatments was determined with the use of flow injection electrospray high-resolution mass spectrometry. Although analysis revealed no significant pathway enrichment, we decided to accept pathways with $P \leq 0.1$ and flagged these as tentative. The reason for that is the novelty of results in this area of research and, to my knowledge, this represents the first data linking mechanical stimulation to metabolite profiling. It was previously suggested that the jasmonic acid biosynthesis pathway might play a role in plant thigmomorphogenetic responses to mechanical stimulations (Stelmach *et al.*, 1998; Ellis *et al.*, 2002; Tretner *et al.*, 2008). However, this study does

not confirm such theories. The present work suggests that pathways involved in carbohydrate metabolism play an important role in response to wind and mechanical stress, which were previously also reported to be involved in response to many other abiotic stresses (Devi *et al.*, 2007; Morsy *et al.*, 2007; Xue *et al.*, 2008).

6.6. CONCLUSIONS AND FUTURE WORK

This study has begun to unravel the response to wind and mechanical stress in the model plant for grasses – *Brachypodium distachyon*. Moreover, the two factors of mechanical stimulation, wind and mechanical stress, were analysed separately, as it was proposed that both stresses may cause different plant responses. Two genotypes of *Brachypodium* were used in this study as Aberystwyth University has a RIL population of these parents, and more importantly, as these lines have contrasting properties, to evaluate if there are differences in response within species.

Both stresses had the same effect on phenotypic changes in *Brachypodium distachyon* resulting in shortening of the main stem, alterations in the reproductive process and mechanical properties. Based on previously reported studies from dicots, such an outcome was to some extend expected. However, the fact that this represents the most extensive study on mechanical stimulation on a grass makes this work a very good indicator and reference for further studies on economically important grasses such as maize, Miscanthus or rice. Moreover, it would be important to get a deeper insight into reproductive features, as the study suggests that seed yield was drastically decreased after both stresses.

The detailed cell wall compositional analysis alongside with histological and anatomical analysis generated in this study provides a platform for the future integration of events associated with cell wall properties in response to mechanical stimulation. This study is first to our knowledge to present changes in cell wall composition in response to wind and mechanical stress in grasses. *Brachypodium* reacted to WS and MS by an increase in lignin content, alterations in monosaccharide and cell wall-bound hydroxycinnamic acids and decrease in sugar release. Such analysis can be used as a starting point for analysis in other grass family members. Moreover, as analysis in this study only focused

on stems, it would be of interest to also characterise cell wall compositional features of leaves, as they present a substantial amount of plant tissues. Such a complete analysis of stem and leaf material would be useful as grasses have been explored as biomass feedstock for bioenergy production and biorefining into platform chemicals and value-added bio-based products. The main feedstock explored to date are agricultural residues and the harvestable biomass of dedicated perennial biomass crops, including Miscanthus and switchgrass (*Panicum virgatum)* (Bhatia *et al.*, 2017). Reduction of aboveground mass and changes in cell wall composition may significantly affect such processes. Thus, further analysis should focus on detailed lignin analysis, as its composition and content directly affect sugar release.

Anatomical and histological analyses revealed changes in tissue organisation after exposure to the wind and mechanical stress. Moreover, the cell wall thickness was significantly thicker after WS and MS in both genotypes. Our measurements of cell wall thickness have their limitations; thus, it would be interesting to pursue measurements with other technique (e.g. Transmission electron microscopy - TEM), which would give more reliable results. This work reports the first data on changes in the distribution and abundance of certain cell wall epitopes in response to mechanical stimulation using immuno-localisation methods. Such analysis showed differences in the labelling pattern between treatments only with some of the pectin-related antibodies. Moreover, it was noted that WS and MS resulted in enhanced pectin methylesterase activity. Such results indicate that pectins are involved in response to mechanical stimulation. Nevertheless, results obtained in this work do not give a clear answer of pectin involvement. Further validation of the role of pectins in plant response to mechanical stimulation is needed. This will enable further, more detailed studies of pectins association with obtaining more quantitative data. It would also be of interest to perform immuno-localisations with other internodes, as the distribution of epitopes may vary between internodes. Such comparison will enable a much fuller picture of the response to mechanical stimulation of *Brachypodium distachyon* stems.

Genetics and metabolomics are an important area that should not be overlooked when attempting to understand the response of plants to mechanical stimulation. Nevertheless, the knowledge in this area is extremely poor, and not very well

understood. This study is the first to start to unravel molecular and metabolic response to mechanical stimulation in grasses based on the model plant *Brachypodium distachyon*. The genome-wide analysis of such response was previously performed on *Arabidopsis*, which led to the discovery of four touch inducible genes and the range of touch responsive cell-wall related genes. This study aimed to compare if the response to mechanical stimulation in *Brachypodium* have similarities. The expression analysis presented in this study does not provide strong evidence for a conserved set of touch inducible genes between Arabidopsis and *Brachypodium*. Thus, the molecular response to mechanical stimulation needs further attention. This should include genome-wide identification of genes involved in response to mechanical stimulation. Moreover, the design of plant exposure to stress should also be considered, as for *Arabidopsis* touch induced expression was noted 30 min after stress treatment. In our study, the molecular response was examined after two weeks of stress treatment, which may lead to stabilisation of genes expression, and thus, results may be misleading.

Moreover, *Brachypodium distachyon* as a model plant for grasses may be used as a system to dissect treatment- and genotype-specific responses to mechanical stimulation. This may be achieved by use of the RIL population, which is available at Aberystwyth University. One of the important features, which showed an opposite response after mechanical stimulation, is vascular bundle area. This trait may be utilised for mapping studies.

Metabolomics plays an important role to gather information about stress-induced changes in plant development (Gupta, 2014). Analysis of the metabolite response to mechanical stimulation presented in this work is completely novel in this area of research, especially for the grasses. Metabolite fingerprinting analysis revealed that pathways involved in carbohydrate metabolism are significantly enriched. Initial analysis and results of the metabolic data provided in this study present important information, but they also provide a basis for further analysis. Further detailed analysis of pathways enriched is needed. Moreover, in-depth analysis and accurate mass determination of the highly significant metabolites is necessary to validate the findings described in this work. Moreover, more detailed data may be used in the future to provide insight into the genetic basis of plant response to mechanical stimulation

Selection of the most responsive metabolites after mechanical stimulation may be used to identify genes, which are up-regulated after stress treatment. Such an approach led to the identification of genes, which are involved in response to drought in wheat. Moreover, the transcriptomic analysis combined with metabolomics may also be useful for understanding the molecular mechanism underlying responses to mechanical stimulation in grasses.

REFERENCES

Akers SW, Mitchell CA. **1983**. Seismic stress effects on vegetative and reproductive development of 'Alaska' pea. *Canadian Journal of Botany* **62**: 2011–2015.

Andersen MCF, Boos I, Marcus SE, Kračun SK, Rydahl MG, Willats WGT, Knox JP, Clausen MH. **2016**. Characterization of the LM5 pectic galactan epitope with synthetic analogues of β-1,4-D-galactotetraose. *Carbohydrate Research* **436**: 36–40.

Anten NPR, Alcalá-Herrera R, Schieving F, Onoda Y. **2010**. Wind and mechanical stimuli differentially affect leaf traits in *Plantago major*. *New Phytologist* **188**: 554–564.

Anten NPR, Casado-Garcia R, Nagashima H. **2005**. Effects of mechanical stress and plant density on mechanical characteristics, growth, and lifetime reproduction of tobacco plants. *The American Naturalist* **166**: 650–660.

Anten NPR, von Wettberg EJ, Pawlowski M, Huber H. **2009**. Interactive effects of spectral shading and mechanical stress on the expression and costs of shade avoidance. *The American Naturalist* **173**: 241–255.

Asensi-Fabado MA, Amtmann A, Perrella G. **2017**. Plant responses to abiotic stress: The chromatin context of transcriptional regulation. *Biochimica et Biophysica Acta - Gene Regulatory Mechanisms* **1860**: 106–122.

Assem N, El Hafid L, Lamchouri F. **2017**. Impact of water stress on the leaf tissues of two Moroccan varieties of durum wheat (*Triticum durum* Desf). *Journal of Materials and Environmental Science* **8**: 3583–3487.

Baker CJ, Sterling M, Berry P. **2014**. A generalised model of crop lodging. *Journal of Theoretical Biology* **363**: 1–12.

Barros J, Serk H, Granlund I, Pesquet E. **2015**. The cell biology of lignification in higher plants. *Annals of Botany* **115**: 1053–1074.

Bell E, Mullet JE. **1991**. Lipoxygenase gene expression is modulated in plants by water deficit, wounding, and methyl jasmonate. *Molecular and General Genetics MGG* **230**: 456–462.

Berry PM, Sterling M, Baker CJ, Spink J, Sparkes DL. **2003**. A calibrated model of wheat lodging compared with field measurements. *Agricultural and Forest Meteorology* **119**: 167–180.

Berry PM, Sterling M, Mooney SJ. **2006**. Development of a model of lodging for barley. *Journal of Agronomy and Crop Science* **192**: 151–158.

Bevan MW, Garvin DF, Vogel JP. **2010**. *Brachypodium distachyon* genomics for sustainable food and fuel production. *Current Opinion in Biotechnology* **21**: 211–

217.

Bhatia R, Gallagher JA, Gomez LD, Bosch M. **2017**. Genetic engineering of grass cell wall polysaccharides for biorefining. *Plant Biotechnology Journal* **15**: 1071–1092.

Biddington NL. **1986**. The effects of mechanically-induced stress in plants - a review. *Plant Growth Regulation* **4**: 103–123.

Biddington NL, Dearman AS. **1985**. The effect of mechanically induced stress on the growth of cauliflower, lettuce and celery seedlings. *Annals of Botany* **55**: 109–119.

Biro RL, Hunt ER, Erner Y, Jaffe MJ. **1980**. Thigmomorphogenesis: Changes in cell division and elongation in the internodes of mechanically-perturbed or ethrel-treated bean plants. *Annals of Botany* **45**: 655–664.

Biro RL, Jaffe MJ. **1984**. Thigmomorphogensis: ethylene evolution and its role in the changes observed in mechanically perturbed bean plants. *Physiologia Plantarum* **62**: 289–296.

Boden SA, Kavanová M, Finnegan E, Wigge PA, Wardlaw I, Dawson I, Wallwork M, Jenner C, Logue S, Sedgley M, *et al.* 2013. Thermal stress effects on grain yield in *Brachypodium distachyon* occur via H2A.Z-nucleosomes. *Genome Biology* **14**: R65.

Boerjan W, Ralph J, Baucher M. **2003**. Lignin Biosynthesis. *Annual Review of Plant Biology* **54**: 519–546.

Börnke F, Rocksch T. **2018**. Thigmomorphogenesis – Control of plant growth by mechanical stimulation. *Scientia Horticulturae* **234**: 344–353.

Bosch M, Cheung AY, Hepler PK. **2005**. Pectin methylesterase, a regulator of pollen tube growth. *Plant Physiology* **138**: 1334–1346.

Bossdorf O, Pigliucci M. **2009**. Plasticity to wind is modular and genetically variable in *Arabidopsis thaliana*. *Evolutionary Ecology* **23**: 669–685.

Botella JR, Arteca RN, Frangosts JA. **1995**. A mechanical strain-induced 1-aminocyclopropane-1carboxylic acid synthase gene. *Proceedings of the National Academy of Sciences of the United States of America* **92**: 1595–1598.

Botella JR, Arteca JM, Somodevilla M, Arteca RN. **1996**. Calcium-dependent protein kinase gene expression in response to physical and chemical stimuli in mungbean (*Vigna radiata*). *Plant Molecular Biology* **30**: 1129–1137.

Bouvier D'Yvoire M, Bouchabke-Coussa O, Voorend W, Antelme S, Cezard L, Legee F, Lebris P, Legay S, Whitehead C, McQueen-Mason SJ, *et al.* 2013. Disrupting the cinnamyl alcohol dehydrogenase 1 gene (BdCAD1) leads to altered lignification and improved saccharification in *Brachypodium distachyon*. *Plant Journal* **73**: 496–508.

Boyer N, Chapelle B, Gaspar T. **1979**. Lithium inhibition of the thigmomorphogenetic

response in *Bryonia diocia*. *Plant Physiology* **63**: 1215–1216.

Braam J. **2005**. In touch: Plant responses to mechanical stimuli. *New Phytologist* **165**: 373–389.

Braam J, Davis RW. **1990**. Rain-, wind- and touch-induced expression of calmodulin and calmodulin- related genes in Arabidopsis. *Cell Press* **60**: 357–364.

Buckeridge MS, Rayon C, Urbanowicz B, Tine MAS, Carpita NC. **2004**. Mixed linkage (1→3),(1→4)-β-D- glucans of grasses. *Cereal Chemistry* **81**: 115−127.

Bunning E. **1941**. Uber die Verhinderung des Etiolements. *Ber Dt Bot Ges* **59**: 2–9.

Burgert I. **2006**. Exploring the micromechanical design of plant cell walls. *American Journal of Botany* **93**: 1391–1401.

Busse-Wicher M, Gomes TCF, Tryfona T, Nikolovski N, Stott K, Grantham NJ, Bolam DN, Skaf MS, Dupree P. **2014**. The pattern of xylan acetylation suggests xylan may interact with cellulose microfibrils as a twofold helical screw in the secondary plant cell wall of *Arabidopsis thaliana*. *Plant Journal* **79**: 492–506.

Caffall KH, Mohnen D. **2009**. The structure, function, and biosynthesis of plant cell wall pectic polysaccharides. *Carbohydrate Research* **344**: 1879–1900.

Campbell P, Braam J. **1998**. Co- and/or post-translational modifications are critical for TCH4 XET activity. *Plant Journal* **15**: 553–561.

Carpita NC. **1996**. Structure and biogenesis of the cell walls of grasses. *Annual Review of Plant Physiology and Plant Molecular Biology* **47**: 445–76.

Carpita NC, Defernez M, Findlay K, Wells B, Shoue DA, Catchpole G, Wilson RH, McCann MC. **2001**. Cell wall architecture of the elongating maize coleoptile. *Plant Physiology* **127**: 551–65.

Carpita NC, Gibeaut DM. **1993**. Structural models of primary cell walls in flowering plants: consistency of molecular structure with the physical properties of the walls during growth. *The Plant Journal* **3**: 1–30.

Casler M, Jung H. **1999**. Selection and evaluation of smooth bromegrass clones with divergent lignin and etherified ferulic acid concentration. *Crop Science* **39**: 1866–1873.

Catalan P, Chalhoub B, Chochois V, Garvin DF, Hasterok R, Manzaneda AJ, Mur LAJ, Pecchioni N, Rasmussen SK, Vogel JP, *et al.* 2014. Update on the genomics and basic biology of Brachypodium: International Brachypodium Initiative (IBI). *Trends in Plant Science* **19**: 414–418.

Catalan P, Muller J, Hasterok R, Jenkins G, Mur LAJ, Langdon T, Betekhtin A, Siwinska D, Pimentel M, Lopez-Alvarez D. **2012**. Evolution and taxonomic split of the model grass *Brachypodium distachyon*. *Annals of Botany* **109**: 385–405.

Céccoli G, Ramos JC, Ortega LI, Acosta JM, Perreta MG. **2011**. Salinity induced anatomical and morphological changes in *Chloris gayana* Kunth roots. *Biocell* **35**: 9–17.

Chang X, Chandra R, Berleth T, Beatson RP. **2008**. Rapid, microscale, acetyl bromide-based method for high-throughput determination of lignin content in *Arabidopsis thaliana*. *Journal of Agricultural and Food Chemistry* **56**: 6825–6834.

Chehab EW, Eich E, Braam J. **2009**. Thigmomorphogenesis: A complex plant response to mechano-stimulation. *Journal of Experimental Botany* **60**: 43–56.

Chehab EW, Yao C, Henderson Z, Kim S, Braam J. **2012**. *Arabidopsis* touch-induced morphogenesis is jasmonate mediated and protects against pests. *Current Biology* **22**: 701–706.

Chen L, Auh C, Chen F, Cheng X, Aljoe H, Dixon RA, Wang Z. **2002**. Lignin deposition and associated changes in anatomy, enzyme activity, gene expression, and ruminal degradability in stems of tall fescue at different developmental stages. *Journal of Agricultural and Food Chemistry* **50**: 5558–5565.

Chen F, Dixon RA. **2007**. Lignin modification improves fermentable sugar yields for biofuel production. *Nature Biotechnology* **25**: 759–761.

Chen WY, Liu ZM, Deng GB, Pan ZF, Liang JJ, Zeng XQ, Tashi NM, Long H, Yu MQ. **2014**. Genetic relationship between lodging and lodging components in barley (*Hordeum vulgare*) based on unconditional and conditional quantitative trait locus analyses. *Genetics and Molecular Research* **13**: 1909–1925.

Christensen U, Alonso-Simon A, Scheller H V., Willats WGT, Harholt J. **2010**. Characterization of the primary cell walls of seedlings of *Brachypodium distachyon* - A potential model plant for temperate grasses. *Phytochemistry* **71**: 62–69.

Cipollini DF. **1997**. Wind-induced mechanical stimulation increases pest resistance in common bean. *Oecologia* **111**: 84–90.

Cipollini DF. **1999**. Costs to flowering of the production of a mechanically hardened phenotype in *Brassica napus* L. *International Journal of Plant Sciences* **160**: 735–741.

Clausen MH, Willats WGT, Knox JP. **2003**. Synthetic methyl hexagalacturonate hapten inhibitors of anti-homogalacturonan monoclonal antibodies LM7, JIM5 and JIM7. *Carbohydrate Research* **338**: 1797–1800.

Clemente H. **2001**. Trade winds reduce growth and influence gas exchange patterns in papaya seedlings. *Annals of Botany* **88**: 379–385.

Cleugh HA, Miller JM, Böhm M. **1998**. Direct mechanical effects of wind on crops. *New Phytologist* **41**: 85–112.

Close DC, Mcarthur C. **2002**. Rethinking the role of many plant phenolics -protection from photodamage not herbivores? *OIKOS* **99**: 166–172.

Cordero R. **1999**. Ecophysiology of *Cecropia schreberiana* saplings in two wind regimes in an elfin cloud forest: growth, gas exchange, architecture and stem biomechanics. *Tree Physiology* **19**: 153–163.

da Costa RMF, Lee SJ, Allison GG, Hazen SP, Winters A, Bosch M. **2014**. Genotype, development and tissue-derived variation of cell-wall properties in the lignocellulosic energy crop Miscanthus. *Annals of Botany* **114**: 1265–1277.

Crook MJ, Ennos AR. **1994**. Stem and root characteristics associated with lodging resistance in four winter wheat cultivars. *The Journal of Agricultural Science* **123**: 167–174.

Deepak S, Shailasree S, Kini RK, Muck A, Mithöfer A, Shetty SH. **2010**. Hydroxyproline-rich glycoproteins and plant defence. *Journal of Phytopathology* **158**: 585–593.

Delauney A., Verma DP. **1993**. Proline Biosynthesis and osmoregulation in plants. *The Plant Journal* **4**: 215–223.

DeMartini JD, Pattathil S, Miller JS, Li H, Hahn MG, Wyman CE. **2013**. Investigating plant cell wall components that affect biomass recalcitrance in poplar and switchgrass. *Energy and Environmental Science* **6**: 898–909.

Devi R, Munjral N, Gupta AK, Kaur N. **2007**. Cadmium induced changes in carbohydrate status and enzymes of carbohydrate metabolism, glycolysis and pentose phosphate pathway in pea. *Environmental and Experimental Botany* **61**: 167–174.

Dobra J, Motyka V, Dobrev P, Malbeck J, Prasil IT, Haisel D, Gaudinova A, Havlova M, Gubis J, Vankova R. **2010**. Comparison of hormonal responses to heat, drought and combined stress in tobacco plants with elevated proline content. *Journal of Plant Physiology* **167**: 1360–1370.

Donohoe BS, Decker SR, Tucker MP, Himmel ME, Vinzant TB. **2008**. Visualizing lignin coalescence and migration through maize cell walls following thermochemical pretreatment. *Biotechnology and Bioengineering* **101**: 913–925.

Downie B, Dirk LMA, Hadfield KA, Wilkins TA, Bennett AB, Bradford KJ. **1998**. A gel diffusion assay for quantification of pectin methylesterase activity. *Analytical Biochemistry* **264**: 149–157.

Draper J, Mur LAJ, Jenkins G, Ghosh-Biswas GC, Bablak P, Hasterok R, Routledge APM. **2001**. *Brachypodium distachyon*. A new model system for functional genomics in grasses. *Plant Physiology* **127**: 1539–1555.

Ebringerova A, Ebringerova Z, Heinze T. **2005**. Hemicellulose. *Advances in Polymer Science* **186**: 1–67.

Ellis C, Karafyllidis I, Wasternack C, Turner JG. **2002**. The Arabidopsis mutant cev1 links cell wall signaling to jasmonate and ethylene responses. *Society* **14**: 1557–1566.

Engvall E, Perlmann P. **1971**. Enzyme-linked immunosorbent assay (ELISA) quantitative assay of immunoglobulin G. *Immunochemistry* **8**: 871–874.

Erner Y, Jaffe MJ. **1982**. Thigmomorphogensis: the involvement of auxin and abscisic acid in growth retardation due to mechanical perturbation. *Plant and Cell Physiology* **23**: 935–941.

Fan C, Feng S, Huang J, Wang Y, Wu L, Li X, Wang L, Tu Y, Xia T, Li J, *et al.* 2017. AtCesA8-driven OsSUS3 expression leads to largely enhanced biomass saccharification and lodging resistance by distinctively altering lignocellulose features in rice. *Biotechnology for Biofuels* **10**: 221.

Feuillet C, Keller B. **2002**. Comparative genomics in the grass family: Molecular characterization of grass genome structure and evolution. *Annals of Botany* **89**: 3–10.

Filiz E, Koc I, Tombuloglu H. **2014**. Genome-wide identification and analysis of growth regulating factor genes in *Brachypodium distachyon*: In silico approaches. *Turkish Journal of Biology* **38**: 296–306.

Fincher GB. **2009**. Revolutionary times in our understanding of cell wall biosynthesis and remodeling in the grasses. *Plant Physiology* **149**: 27–37.

Finnell HH. **1928**. Effect of wind on plant growth. *Journal of American Society of Agronomy* **20**: 1206–1210.

Foster CE, Martin TM, Pauly M. **2010**. Comprehensive compositional analysis of plant cell walls (Lignocellulosic biomass) Part I: Lignin. *Journal of Visualized Experiments* **37**: e1745.

Fraser CM, Chapple C. **2011**. The phenylpropanoid pathway in Arabidopsis. *The Arabidopsis Book* **9**.

Frey L. **2007**. Wszędobylskie trawy. *Academia* **4**: 4–7.

Gadea J, Conejero V, Vera P. **1999**. Developmental regulation of a cytosolic ascorbate peroxidase gene from tomato plants. *Molecular and General Genetics* **262**: 212–219.

Garner LC, Björkman T. **1996**. Mechanical conditioning for controlling excessive elongation in tomato transplants: Sensitivity to dose, frequency, and timing of brushing. *Journal of the American Society for Horticultural Science* **121**: 894–900.

Garvin DF, Gu YQ, Hasterok R, Hazen SP, Jenkins G, Mockler TC, Mur LAJ, Vogel JP. **2008**. Development of genetic and genomic research resources for *Brachypodium distachyon*, a new model system for grass crop research. *Crop Science* **48**: 69–84.

Gere JM. **2004**. *Mechanics of Materials*. Belmont: Thomson Learning.

Gibeaut DM, Pauly M, Bacic A, Fincher GB. **2005**. Changes in cell wall polysaccharides in developing barley (*Hordeum vulgare*) coleoptiles. *Planta* **221**: 729–738.

Gibson LJ. **2012**. The hierarchical structure and mechanics of plant materials. *Journal of The Royal Society Interface* **9**: 2749–2766.

Goeschl JD, Rappaport L, Pratt HK. **1966**. Ethylene as a factor regulating the growth of pea epicotyls subjected to physical stress. *Plant physiology* **41**: 877–84.

Goodman AM, Ennos AR. **1996**. A comparative study of the response of the roots and shoots of sunflower and maize to mechanical stimulation. *Journal of Experimental Botany* **47**: 1499–1507.

Gorshkova TA, Mokshina N, Chernova T, Ibragimova NN, Salnikov V, Mikshina P, Tryfona T, Banasiak A, Immerzeel P, Dupree P, *et al.* 2015. Aspen tension wood fibers contain β-(1→4)-galactans and acidic arabinogalactans retained by cellulose microfibrils in gelatinous walls. *Plant Physiology* **169**: 2048–2063.

Grabber JH, Ralph J, Lapierre C, Barriere Y. **2004**. Genetic and molecular basis of grass cell-wall degradability. I. Lignin-cell wall matrix interactions. *Comptes Rendus - Biologies* **327**: 455–465.

Grace J, Russell G. **1977**. The effect of wind on grasses. *Journal of Experimental Botany* **28**: 268–278.

Gu YQ, Ma Y, Huo N, Vogel JP, You FM, Lazo GR, Nelson WM, Soderlund C, Dvorak J, Anderson OD, *et al.* 2009. A BAC-based physical map of *Brachypodium distachyon* and its comparative analysis with rice and wheat. *BMC Genomics* **10**: 469.

Guillemin F, Guillon F, Bonnin E, Devaux MF, Chevalier T, Knox JP, Liners F, Thibault JF. **2005**. Distribution of pectic epitopes in cell walls of the sugar beet root. *Planta* **222**: 355–371.

Guillon F, Larré C, Petipas F, Berger A, Moussawi J, Rogniaux H, Santoni A, Saulnier L, Jamme F, Miquel M, *et al.* 2012. A comprehensive overview of grain development in *Brachypodium distachyon* variety Bd21. *Journal of Experimental Botany* **63**: 739–755.

Gupta B. **2014**. Plant abiotic stress: 'Omics' approach. *Journal of Plant Biochemistry & Physiology* **01**: 16–18.

Gupta AK, Kaur N. **2005**. Sugar signalling and gene expression in relation to carbohydrate metabolism under abiotic stresses in plants. *Journal of Biosciences* **30**: 761–776.

Ha MA, Viëtor RJ, Jardine GD, Apperley DC, Jarvis MC. **2005**. Conformation and mobility of the arabinan and galactan side-chains of pectin. *Phytochemistry* **66**:

1817–1824.

Hamant O. **2013**. Widespread mechanosensing controls the structure behind the architecture in plants. *Current Opinion in Plant Biology* **16**: 654–660.

Hames B, Ruiz R, Scarlata C, Sluiter A, Sluiter J, Templeton D. **2008**. Preparation of samples for compositional analysis laboratory. *National Renewable Energy Laboratory* **1617**: 1–9.

Hare PD, Cress WA. **1997**. Metabolic implications of stress-induced proline accumulation in plants. *Plant Growth Regulation* **21**: 79–102.

Harris PJ, Smith BG. **2006**. Plant cell walls and cell-wall polysaccharides: Structures, properties and uses in food products. *International Journal of Food Science and Technology* **41**: 129–143.

Harris D, Stork J, DeBolt S. **2009**. Genetic modification in cellulose-synthase reduces crystallinity and improves biochemical conversion to fermentable sugar. *GCB Bioenergy* **1**: 51–61.

Hasterok R, Draper J, Jenkins G. **2004**. Laying the cytotaxonomic foundations of a new model grass, *Brachypodium distachyon* (L.) Beauv. *Chromosome Research* **12**: 397–403.

Hasterok R, Marasek A, Donnison IS, Armstead I, Thomas A, King IP, Wolny E, Idziak D, Draper J, Jenkins G. **2006**. Alignment of the genomes of *Brachypodium distachyon* and temperate cereals and grasses using bacterial artificial chromosome landing with fluorescence *in situ* hybridization. *Genetics* **173**: 349–362.

Hatfield RD, Marita JM. **2010**. Enzymatic processes involved in the incorporation of hydroxycinnamates into grass cell walls. *Phytochemistry Reviews* **9**: 35–45.

Hatfield RD, Marita JM, Frost K, Grabber J, Ralph J, Lu F, Kim H. **2009**. Grass lignin acylation: *p*-coumaroyl transferase activity and cell wall characteristics of C3 and C4 grasses. *Planta* **229**: 1253–1267.

Hatfield RD, Ralph J, Grabber JH. **1999**. Cell wall cross-linking by ferulates and diferulates in grasses. *Journal of the Science of Food and Agriculture* **79**: 403–407.

Hatfield R, Ralph J, Grabber JH. **2008**. A potential role for sinapyl *p*-coumarate as a radical transfer mechanism in grass lignin formation. *Planta* **228**: 919–928.

Hendry GA. 1993. Evolutionary origins and natural functions of fructans – a climatological, biogeographic and mechanistic appraisal. *New Phytologist* **123**: 3–14.

Henry HAL, Thomas SC. **2002**. Interactive effects of lateral shade and wind on stem allometry, biomass allocation, and mechanical stability in *Abutilon theophrasti*

(Malvaceae). *American Journal of Botany* **89**: 1609–1615.

Hepworth D, Vincent J. **1999**. The growth response of the stems of genetically modified tobacco plants (*Nicotiana tabacum* 'Samsun') to flexural stimulation. *Annals of Botany* **83**: 39–43.

Hirsinger C, Salvà I, Marbach J, Durr A, Fleck J, Jamet E. **1999**. The tobacco extensin gene Ext 1.4 is expressed in cells submitted to mechanical constraints and in cells proliferating under hormone control. *Journal of Experimental Botany* **50**: 343–355.

Hofinger M, Chapelle B, Boyer N, Gaspar T. **1979**. GC-MS identification and titration of IAA in mechanically perturbed *Bryonia dioica*. *Plant Physiology* **63**: S52.

Holladay JE, Bozell JJ, White JF, Johnson D. **2007**. *Top Value-Added Chemicals from Biomass Volume II - Results of Screening for Potential Candidates from Biorefinery Lignin*.

Hondroyianni E, Papakosta DK, Gagianas AA, Tsatsarelis KA. **2000**. Corn stalk traits related to lodging resistance in two soils of differing salinity. *Maydica* **45**: 125–133.

Hong SY, Park JH, Cho SH, Yang MS, Park CM. **2011**. Phenological growth stages of *Brachypodium distachyon*: Codification and description. *Weed Research* **51**: 612–620.

Hong SY, Seo PJ, Yang MS, Xiang F, Park CM. **2008**. Exploring valid reference genes for gene expression studies in *Brachypodium distachyon* by real-time PCR. *BMC Plant Biology* **8**: 1–11.

Hongo S, Sato K, Yokoyama R, Nishitani K. **2012**. Demethylesterification of the primary wall by PECTIN METHYLESTERASE35 provides mechanical support to the *Arabidopsis* stem. *The Plant Cell* **24**: 2624–2634.

Hunt ER, Jaffe MJ. **1980**. Thigmomorphogenesis - the interaction of wind and temperature in the field on the growth of *Phaseolus-Vulgaris* L. *Annals of Botany* **45**: 665–672.

Huo N, Gu YQ, Lazo GR, Vogel JP, Coleman-Derr D, Luo M-C, Thilmony R, Garvin DF, Anderson OD. **2006**. Construction and characterization of two BAC libraries from *Brachypodium distachyon*, a new model for grass genomics. *Genome* **49**: 1099–108.

Huo N, Lazo GR, Vogel JP, You FM, Ma Y, Hayden DM, Coleman-Derr D, Hill TA, Dvorak J, Anderson OD, *et al.* 2008. The nuclear genome of *Brachypodium distachyon*: Analysis of BAC end sequences. *Functional and Integrative Genomics* **8**: 135–147.

Iliev EA, Xu W, Polisensky DH, Oh M, Torisky RS, Clouse SD, Braam J. **2002**.

Transcriptional and posttranscriptional regulation of Arabidopsis TCH4 expression by diverse stimuli. Roles of cis regions and brassinosteroids. *Plant Physiology* **130**: 770–783.

Ishii T. **1997**. Structure and functions of feruloylated polysaccharides. *Plant Science* **127**: 111–127.

De Jaegher G, Boyer N, Gaspar T. **1985**. Thigmomorphogenesis in *Bryonia dioica*: Changes in soluble and wall peroxidases, phenylalanine ammonia-lyase activity, cellulose, lignin content and monomeric constituents. *Plant Growth Regulation* **3**: 133–148.

Jaffe MJ. **1973**. Thigmomorphogenesis: The response of plant growth and development to mechanical stimulation. *Planta* **114**: 143–157.

Jaffe MJ. **1976**. Thigmomorphogenesis: A detailed characterization of the response of beans (*Phaseolus vulgaris* L.) to mechanical stimulation. *Zeitschrift für Pflanzenphysiologie* **77**: 437–453.

Jaffe MJ. **1980**. Morphogenetic responses of plants to mechanical stimuli or stress. *American Institiute of Biological Sciences* **30**: 239–243.

Jaffe MJ, Forbes S. **1993**. Thigmomorphogenesis: the effect of mechanical perturbation on plants. *Plant Growth Regulation* **12**: 313–324.

Jaffe MJ, Leopold AC, Staples RC. **2002**. Thigmo responses in plants and fungi. *American Journal of Botany* **89**: 375–382.

Jaffe MJ, Telewski FW. **1984**. Thigmomorphogenesis: Callose and ethylene in the hardening of mechanically stressed plants. In: Phytochemical adaptations to stress. Springer, Boston, MA. 79–95.

Jellum M. **1962**. Relationships between lodging resistance and certain culm characters in oats. *Crop Science* **2**: 263–267.

Jeong Y, Ota Y. **1980**. A relationship between growth inhibition and abscisic acid content by mechanical stimulation in rice plant. *Japanese Journal od Crop Science* **49**: 615–616.

Jin X, Fourcaud T, Li B, Guo Y. **2009**. Towards modeling and analyzing stem lodging for two contrasting rice cultivars. *Plant Growth Modeling and Applications* **IEEE**: 253–260.

Johnson KA, Sistrunk ML, Polisensky DH, Braam J. **1998**. *Arabidopsis thaliana* responses to mechanical stimulation do not require ETR1 or EIN2. *Plant Physiology* **116**: 643–649.

Jones L, Ennos AR, Turner SR. **2001**. Cloning and characterization of irregular xylem4 (irx4): a severely lignin-deficient mutant of Arabidopsis. *The Plant Journal* **26**: 205–

216.

Jones L, Milne JL, Ashford D, McCann MC, McQueen-Mason SJ. **2005**. A conserved functional role of pectic polymers in stomatal guard cells from a range of plant species. *Planta* **221**: 255–264.

Jones L, Milne JL, Ashford D, McQueen-Mason SJ. **2003**. Cell wall arabinan is essential for guard cell function. *Proceedings of the National Academy of Sciences* **100**: 11783–11788.

Jones L, Seymour GB, Knox JP. **1997**. Localization of pectic galactan in tomato cell walls using a monoclonal antibody specific to (1[->]4)-[β]-D-galactan. *Plant Physiology* **113**: 1405–1412.

Jongerius AL. **2013**. Catalytic conversion of lignin for the production of aromatics.

Kaack K, Schwarz KU. **2001**. Morphological and mechanical properties of *Miscanthus* in relation to harvesting, lodging, and growth conditions. *Industrial Crops and Products* **14**: 145–154.

Kaack K, Schwarz KU, Brander PE. **2003**. Variation in morphology, anatomy and chemistry of stems of *Miscanthus* genotypes differing in mechanical properties. *Industrial Crops and Products* **17**: 131–142.

Kaplan F, Guy CL. **2004**. β-Amylase induction and the protective role of maltose during temperature shock. *Plant Physiology* **135**: 1674–1684.

Kellogg EA. **1998**. Relationships of cereal crops and other grasses. *Proceedings of the National Academy of Sciences of the United States of America* **95**: 2005–2010.

Kempa S, Krasensky J, Dal Santo S, Kopka J, Jonak C. **2008**. A central role of abscisic acid in stress-regulated carbohydrate metabolism. *PLoS ONE* **3**: e3935.

Kern KA, Ewers FW, Telewski FW, Koehler L. **2005**. Mechanical perturbation affects conductivity, mechanical properties and aboveground biomass of hybrid poplars. *Tree Physiology* **25**: 1243–1251.

Khelil A, Menu T, Ricard B. **2007**. Adaptive response to salt involving carbohydrate metabolism in leaves of a salt-sensitive tomato cultivar. *Plant Physiology and Biochemistry* **45**: 551–559.

Khodary SEA. **2004**. Effect of salicylic acid on the growth, photosynthesis and carbohydrate metabolism in salt stressed maize plants. *International Journal of Agriculture & Biology* **6**: 5–8.

Kiemle SN, Zhang X, Esker AR, Toriz G, Gatenholm P, Cosgrove DJ. **2014**. Role of (1,3)(1,4)- β -glucan in cell walls: Interaction with cellulose. *American Chemical Society* **15**: 1727–1736.

Kim J, Lim J, Lee C. **2013**. Quantitative real-time PCR approaches for microbial

community studies in wastewater treatment systems: Applications and considerations. *Biotechnology Advances* **31**: 1358–1373.

Kong E, Liu D, Guo X, Yang W, Sun J, Li X, Zhan K, Cui D, Lin J, Zhang A. **2013**. Anatomical and chemical characteristics associated with lodging resistance in wheat. *The Crop Journal* **1**: 43–49.

Kozlova L V., Ageeva M V., Ibragimova NN, Gorshkova TA. **2014**. Arrangement of mixed-linkage glucan and glucuronoarabinoxylan in the cell walls of growing maize roots. *Annals of Botany* **114**: 1135–1145.

Krasensky J, Jonak C. **2012**. Drought, salt, and temperature stress-induced metabolic rearrangements and regulatory networks. *Journal of Experimental Botany* **63**: 1593–1608.

Kumar P, Barrett DM, Delwiche MJ, Stroeve P. **2009**. Methods for pretreatment of lignocellulosic biomass for efficient hydrolysis and biofuel production. *Industrial and Engineering Chemistry* **48**: 3713–3729.

Latimer JG. **1990**. Drought or mechanical stress affects broccoli transplant growth and establishment but not yield. *HortScience* **25**: 1233–1235.

Lee D, Polisensky DH, Braam J. **2005**. Genome-wide identification of touch- and darkness-regulated Arabidopsis genes: A focus on calmodulin-like and XTH genes. *New Phytologist* **165**: 429–444.

Lee C, Teng Q, Huang W, Zhong R, Ye ZH. **2009**. Down-regulation of PoGT47C expression in poplar results in a reduced glucuronoxylan content and an increased wood digestibility by cellulase. *Plant and Cell Physiology* **50**: 1075–1089.

Le Gall H, Philippe F, Domon J-M, Gillet F, Pelloux J, Rayon C. **2015**. Cell wall metabolism in response to abiotic stress. *Plants* **4**: 112–166.

Li M. **1997**. Anatomical and morphological characteristics of maize genotypes varying in resistance to brittlesnap.

Liepman AH, Wightman R, Geshi N, Turner SR, Scheller HV. **2010**. Arabidopsis - A powerful model system for plant cell wall research. *Plant Journal* **61**: 1107–1121.

Limayem A, Ricke SC. **2012**. Lignocellulosic biomass for bioethanol production: Current perspectives, potential issues and future prospects. *Progress in Energy and Combustion Science* **38**: 449–467.

Lionetti V. **2015**. PECTOPLATE: the simultaneous phenotyping of pectin methylesterases, pectinases, and oligogalacturonides in plants during biotic stresses. *Frontiers in Plant Science* **6**: 331.

Lionetti V, Raiola A, Camardella L, Giovane A, Obel N, Pauly M, Favaron F, Cervone F, Bellincampi D. **2007**. Overexpression of pectin methylesterase inhibitors in

Arabidopsis restricts fungal infection by *Botrytis cinerea*. *Plant Physiology* **143**: 1871–1880.

Liu Y, Schieving F, Stuefer JF, Anten NPR. **2007**. The effects of mechanical stress and spectral shading on the growth and allocation of ten genotypes of a stoloniferous plant. *Annals of Botany* **99**: 121–130.

Liwanag AJM, Ebert B, Verhertbruggen Y, Rennie EA, Rautengarten C, Oikawa A, Andersen MCF, Clausen MH, Scheller H V. 2012. Pectin biosynthesis: GALS1 in *Arabidopsis thaliana* is a β-1,4-galactan β-1,4-galactosyltransferase. *The Plant Cell* **24**: 5024–5036.

Madden TD, Bally MB, Hope MJ, Cullis PR, Schieren H., Janoff AS. **1985**. Protection of large unilamellar vesicles by trehalose during dehydration: retention of vesicle contents. *Biochimica et Biophysica Acta* **817**: 67–74.

Majewska-Sawka A, Nothnagel EA. **2000**. The multiple roles of arabinogalactan proteins in plant development. *Plant Physiology* **122**: 3–9.

Malinovsky FG, Fangel JU, Willats WGT. **2014**. The role of the cell wall in plant immunity. *Frontiers in Plant Science* **5**: 178.

Marcia M de O. **2009**. Feruloylation in grasses: Current and future perspectives. *Molecular Plant* **2**: 861–872.

Marler TE. **2011**. Growth responses to wind differ among papaya roots, leaves, and stems. *HortScience* **46**: 1105–1109.

Marriott PE, Sibout R, Lapierre C, Fangel JU, Willats WGT, Hofte H, Gómez LD, McQueen-Mason SJ. **2014**. Range of cell-wall alterations enhance saccharification in *Brachypodium distachyon* mutants. *Proceedings of the National Academy of Sciences of the United States of America* **111**: 14601–14606.

Martín I, Dopico B, Muñoz FJ, Esteban R, Oomen RJFJ, Driouich A, Vincken JP, Visser R, Labrador E. **2005**. In vivo expression of a *Cicer arietinum* β-galactosidase in potato tubers leads to a reduction of the galactan side-chains in cell wall pectin. *Plant and Cell Physiology* **46**: 1613–1622.

Masuko T, Minami A, Iwasaki N, Majima T, Nishimura SI, Lee YC. **2005**. Carbohydrate analysis by a phenol-sulfuric acid method in microplate format. *Analytical Biochemistry* **339**: 69–72.

Matos DA, Whitney IP, Harrington MJ, Hazen SP. **2013**. Cell walls and the developmental anatomy of the *Brachypodium distachyon* stem internode. *PLoS ONE* **8**: e80640.

Mattinen ML, Suortti T, Gosselink R, Argyropoulos DS, Evtuguin D, Suurnäkki A, De Jong E, Tamminen T. **2008**. Polymerization of different lignins by laccase.

BioResources **3**: 549–565.

Mauch F, Kmecl A, Schaffrath U, Volrath S, Görlach J, Ward E, Ryals J, Dudler R. **1997**. Mechanosensitive expression of a lipoxygenase gene in wheat. *Plant Physiology* **114**: 1561–1566.

McArthur C, Bradshaw OS, Jordan GJ, Clissold FJ, Pile AJ. **2010**. Wind affects morphology, function, and chemistry of eucalypt tree seedlings. *International Journal of Plant Sciences* **171**: 73–80.

McCann MC, Carpita NC. **2008**. Designing the deconstruction of plant cell walls. *Current Opinion in Plant Biology* **11**: 314–320.

McCartney L, Ormerod AP, Gidley MJ, Knox JP. **2000**. Temporal and spatial regulation of pectic (1→4)-β-D-galactan in cell walls of developing pea cotyledons: Implications for mechanical properties. *Plant Journal* **22**: 105–113.

McCartney L, Steele-King CG, Jordan E, Knox JP. **2003**. Cell wall pectic (1-4)-β-D-galactan marks the acceleration of cell elongation in the *Arabidopsis* seedling root meristem. *The Plant Journal* **33**: 447–454.

McCormack E, Braam J. **2003**. Calmodulins and related potential calcium sensors of Arabidopsis. *New Phytologist* **159**: 585–598.

McCormack E, Tsai YC, Braam J. **2005**. Handling calcium signaling: Arabidopsis CaMs and CMLs. *Trends in Plant Science* **10**: 383–389.

McVicar TR, Roderick ML, Donohue RJ, Li LT, Van Niel TG, Thomas A, Grieser J, Jhajharia D, Himri Y, Mahowald NM, *et al.* 2012. Global review and synthesis of trends in observed terrestrial near-surface wind speeds: Implications for evaporation. *Journal of Hydrology* **416**–**417**: 182–205.

Mitchell CA. **1977**. Influence of mechanical stress on auxin- stimulated growth on excised pea stem sections. *Physiologia Plantarum* **41**: 412–424.

Mitchell CA, Severson CJ, Wott JA, Hamner PA. **1975**. Seismomorphogenic regulation of plant growth. *Journal of the American Society for Horticultural Science* **100**: 161–165.

Mizoguchi T, Iriet K, Hirayama T, Hayashida N. **1996**. A gene encoding a mitogen-activated protein kinase kinase kinase is induced simultaneously with genes for a mitogen-activated protein kinase and an S6 ribosomal protein kinase by touch, cold, and water stress in *Arabidopsis thaliana*. *Proceedings of the National Academy of Sciences of the United States of America* **93**: 765–769.

Mohnen D. **2008**. Pectin structure and biosynthesis. *Current Opinion in Plant Biology* **11**: 266–277.

Moore JP, Farrant JM, Driouich A. **2008**. A role for pectin-associated arabinans in

maintaining the flexibility of the plant cell wall during water deficit stress. *Plant Signaling and Behavior* **3**: 102–104.

Morsy MR, Jouve L, Hausman JF, Hoffmann L, Stewart JMD. **2007**. Alteration of oxidative and carbohydrate metabolism under abiotic stress in two rice (*Oryza sativa* L.) genotypes contrasting in chilling tolerance. *Journal of Plant Physiology* **164**: 157–167.

Mostajeran A, Rahimi-Eichi V. **2008**. Drought stress effects on anatomical characteristics of rice cultivers (*Oriza sativa* L.). *Pakistan Journal of Biological Sciences* **11**: 2173–2183.

Mur LAJ, Allainguillaume J, Catalan P, Hasterok R, Jenkins G, Lesniewska K, Thomas I, Vogel J. **2011**. Exploiting the Brachypodium tool box in cereal and grass research. *New Phytologist* **191**: 334–347.

Murren CJ, Pigliucci M. **2005**. Morphological responses to stimulated wind in the genus *Brassica* (Brassicaceae): Allopolyploids and Their Parental Species. *American Journal of Botany* **92**: 810–818.

Nakamura A, Furuta H, Maeda H, Takao T, Nagamatsu Y. **2002**. Structural studies by stepwise enzymatic degradation of the main backbone of soybean soluble polysaccharides consisting of galacturonan and rhamnogalacturonan. *Bioscience, Biotechnology, and Biochemistry* **66**: 1301–1313.

Neel PL, Harris RW. **1971**. Motion-induced inhibition of elongation and induction of dormancy in Liquidamber. *Science* **173**: 58–59.

Niklas KJ. **1992**. Plant biomechanics: An engineering approach to plant form and function. In: University of Chicago press.

Niklas KJ. **1996**. Differences between *Acer saccharum* leaves from open and wind-protected sites. *Annals of Botany* **78**: 61–66.

Niklas KJ. **1998**. Effects of vibration on mechanical properties and biomass allocation pattern of *Capsella bursa-pastoris* (Cruciferae). *Annals of Botany* **82**: 147–156.

Øbro J, Borkhardt B, Harholt J, Skjøt M, Willats WGT, Ulvskov P. **2009**. Simultaneous in vivo truncation of pectic side chains. *Transgenic Research* **18**: 961–969.

Ochoa-Villarreal M, Aispuro-Hernández, Emmanuel Vargas-Arispuro I, Martínez-Téllez MÁ. **2012**. Plant cell wall polymers: Function, structure and biological activity of their derivatives. *Polymerization* **4**: 63–86.

Onguso J., Mizutani F, Hossain A. 2006. The effect of trunk electric vibration on the growth, yield and fruit quality of peach trees (*Prunus persica* (L.) Batsch). *Scientia Horticulturae* **108**: 359–363.

Onoda Y, Anten NPR. **2011**. Challenges to understand plant responses to wind. *Plant*

Signaling & Behavior **6**: 1057–1059.

Opanowicz M, Vain P, Draper J, Parker D, Doonan JH. **2008**. *Brachypodium distachyon*: making hay with a wild grass. *Trends in Plant Science* **13**: 172–177.

Oxenboll Sorensen S, Pauly M, Bush M, Skjot M, McCann MC, Borkhardt B, Ulvskov P. **2000**. Pectin engineering: Modification of potato pectin by in vivo expression of an endo-1,4-β-D-galactanase. *Proceedings of the National Academy of Sciences* **97**: 7639–7644.

Pandey MP, Kim CS. **2011**. Lignin depolymerization and conversion: A review of thermochemical methods. *Chemical Engineering and Technology* **34**: 29–41.

Park YB, Cosgrove DJ. **2015**. Xyloglucan and its interactions with other components of the growing cell wall. *Plant and Cell Physiology* **56**: 180–194.

Pattathil S, Avci U, Baldwin D, Swennes AG, Mcgill JA, Bootten T, Albert A, Davis RH, Chennareddy C, Dong R, *et al.* 2010. A comomprehensive toolkit of plant cell wall glycan-directed monoclonal antibodies. *Plant Physiology* **153**: 514–525.

Pattathil S, Avci U, Miller J., Hahn MG. **2012**. Immunological approaches to plant cell wall and biomass characterization: Glycome profiling. In: Methods in Molecular Biology. 251–268.

Paul-Victor C, Rowe N. **2011**. Effect of mechanical perturbation on the biomechanics, primary growth and secondary tissue development of inflorescence stems of *Arabidopsis thaliana*. *Annals of Botany* **107**: 209–218.

Pauly M, Keegstra K. **2010**. Plant cell wall polymers as precursors for biofuels. *Current Opinion in Plant Biology* **13**: 305–312.

Peaucelle A, Louvet R, Johansen JN, Höfte H, Laufs P, Pelloux J, Mouille G. **2008**. *Arabidopsis* phyllotaxis is controlled by the methyl-esterification status of cell-wall pectins. *Current Biology* **18**: 1943–1948.

Pelleschi S, Rocher JP, Prioul JL. **1997**. Effect of water restriction on carbohydrate metabolism and photosynthesis in mature maize leaves. *Plant, Cell and Environment* **20**: 493–503.

Pelletier S, Van Orden J, Wolf S, Vissenberg K, Delacourt J, Ndong YA, Pelloux J, Bischoff V, Urbain A, Mouille G, *et al.* 2010. A role for pectin de-methylesterification in a developmentally regulated growth acceleration in dark-grown Arabidopsis hypocotyls. *New Phytologist* **188**: 726–739.

Pelloux J, Rustérucci C, Mellerowicz EJ. **2007**. New insights into pectin methylesterase structure and function. *Trends in Plant Science* **12**: 267–277.

Peng D, Chen X, Yin Y, Lu K, Yang W, Tang Y, Wang Z. **2014**. Lodging resistance of winter wheat (*Triticum aestivum* L.): Lignin accumulation and its related enzymes

activities due to the application of paclobutrazol or gibberellin acid. *Field Crops Research* **157**: 1–7.

Pereira A. **2016**. Plant abiotic stress challenges from the changing environment. *Frontiers in Plant Science* **7**: 2013–2015.

Perera IY, Zielinski RE. **1992**. Structure and expression of the *Arabidopsis* CaM-3 calmodulin gene. *Plant Molecular Biology* **19**: 649–664.

Pérez S, Rodríguez-Carvajal MA, Doco T. **2003**. A complex plant cell wall polysaccharide: Rhamnogalacturonan II. A structure in quest of a function. *Biochimie* **85**: 109–121.

Pigliucci M. **2002**. Touchy and bushy: Phenotypic plasticity and integration in response to wind stimulation in *Arabidopsis thaliana*. *International Journal of Plant Sciences* **163**: 399–408.

Pilling E, Höfte H. **2003**. Feedback from the wall. *Current Opinion in Plant Biology* **6**: 611–616.

Pinzon-Latorre D, Deyholos MK. **2014**. Pectinmethylesterases (PME) and Pectinmethylesterase Inhibitors (PMEI) enriched during phloem fiber development in flax (*Linum usitatissimum*). *PLoS ONE* **9**: e105386.

Plaxton WC. **1996**. The organization and regulation of plant glycolysis. *Annual Review of Plant Physiology and Plant Molecular Biology* **47**: 185–214.

Posé S, Marcus SE, Knox JP. **2018**. Differential metabolism of pectic galactan in tomato and strawberry fruit: detection of the LM26 branched galactan epitope in ripe strawberry fruit. *Physiologia Plantarum* **164**: 95–105.

Priest HD, Fox SE, Rowley ER, Murray JR, Michael TP, Mockler TC. **2014**. Analysis of global gene expression in *Brachypodium distachyon* reveals extensive network plasticity in response to abiotic stress. *PLoS ONE* **9**: e87499.

Pruyn ML, Ewers BJ, Telewski FW. **2000**. Thigmomorphogenesis: changes in the morphology and mechanical properties of two *Populus* hybrids in response to mechanical perturbation. *Tree Physiology* **20**: 535–540.

Purugganan M, Fry S, Braam J. **1997**. The Arabidopsis TCH4 xyloglucan endotransglycosylase (substrate specificity, pH optimum, and cold tolerance). *Plant physiology* **115**: 181–190.

Ralph J, Grabber JH, Hatfield RD. **1995**. Lignin-ferulate cross-links in grasses: active incorporation of ferulate polysaccharide esters into ryegrass lignins. *Carbohydrate Research* **275**: 167–178.

Ralph J, Quideau S, Grabber JH, Hatfieida RD. **1994**. Identification and synthesis of new ferulic acid dehydrodimers present in grass cell walls. *Journal of the Chemical Society, Perkin Transations* **23**: 3485–3498.

Rancour DM, Marita JM, Hatfield RD. **2012**. Cell wall composition throughout development for the model grass *Brachypodium distachyon*. *Frontiers in Plant Science* **3**: 236.

Rani Sinniah U, Wahyuni S, Syahputra BSA, Gantait S. **2012**. A potential retardant for lodging resistance in direct seeded rice (*Oryza sativa* L.). *Canadian Journal of Plant Science* **92**: 13–18.

Reiter W. **2002**. Biosynthesis and properties of the plant cell wall. *Current Opinion in Plant Biology* **5**: 536–542.

Retuerto R, Woodward FI. **1992**. Effects of windspeed on the growth and biomass allocation of white mustard *Sinapis alba* L. *Oecologia* **92**: 113–123.

Reynolds MP. **2008**. Challenges to international wheat breeding. In: International Symposium on Wheat Yield Potential.

Ridley BL, O'Neill MA, Mohnen D. **2001**. Pectins: Structure, biosynthesis, and oligogalacturonide-related signaling. *Phytochemistry* **57**: 929–967.

Rigo J. **2016**. The effect of mechanical perturbation on the cell wall composition and development of inflorescence stems of *Arabidopsis thaliana*. Doctoral dissertation, University of Ghent.

Rizhsky L, Liang H, Shuman J, Shulaev V, Davletova S, Mittler R. **2004**. When defense pathways collide. The response of Arabidopsis to a combination of drought and heat stress. *American Society of Plant Biologists* **134**: 1683–1696.

Roach MJ, Mokshina NY, Badhan A, Snegireva A V., Hobson N, Deyholos MK, Gorshkova TA. **2011**. Development of cellulosic secondary walls in flax fibers requires β-galactosidase. *Plant Physiology* **156**: 1351–1363.

Robertson DJ, Julias M, Gardunia BW, Barten T, Cook DD. **2015**. Corn stalk lodging: A forensic engineering approach provides insights into failure patterns and mechanisms. *Crop Science* **55**: 2833–2841.

Rose JKC, Braam J, Fry SC, Nishitani K. **2002**. The XTH family of enzymes involved in xyloglucan endotransglucosylation and endohydrolysis: Current perspectives and a new unifying nomenclature. *Plant and Cell Physiology* **43**: 1421–1435.

Roulin S, Buchala AJ, Fincher GB. **2002**. Induction of (1-3,1-4)-β-D-glucan hydrolases in leaves of dark-incubated barley seedlings. *Planta* **215**: 51–59.

Rybka K. **1993**. Polimery sciany komorkowej roslin dwulisciennych i traw. Nazewnictwo i klasyfikacja. *Postepy Nauk Rolniczych* **4**: 89–100.

Sahoo DK, Stork J, Debolt S, Maiti IB. **2013**. Manipulating cellulose biosynthesis by expression of mutant Arabidopsis proM24:: CESA3ixr1-2 gene in transgenic tobacco. *Plant Biotechnology Journal* **11**: 362–372.

Sarkar P, Bosneaga E, Auer M. **2009**. Plant cell walls throughout evolution: Towards a molecular understanding of their design principles. *Journal of Experimental Botany* **60**: 3615–3635.

Seifert GJ, Blaukopf C. **2010**. Irritable walls: The plant extracellular matrix and signaling. *Plant Physiology* **153**: 467–478.

Service R. **2007**. Biofuel researchers prepare to reap a new harvest. *Science* **315**: 1488–1491.

Shao HB, Chu LY, Jaleel CA, Zhao CX. **2008**. Water-deficit stress-induced anatomical changes in higher plants. *Comptes Rendus - Biologies* **331**: 215–225.

Shi Y, Draper J, Stace C. **1993**. Ribosomal DNA variation and its phylogenetic implication in the genus *Brachypodium* (Poaceae). *Plant Systematics and Evolution* **188**: 125–138.

Showalter A. **1993**. Structure and function of plant cell wall proteins. *The Plant Cell* **5**: 9–23.

Sistrunk ML, Antosiewicz DM, Purugganan MM, Braam J. **2007**. Arabidopsis TCH3 encodes a novel Ca2+ binding protein and shows environmentally induced and tissue-specific regulation. *The Plant Cell* **6**: 1553–1565.

Sluiter A, Hames B, Ruiz R, Scarlata C, Sluiter J, Templeton D, Crocker D. **2012**. Determination of structural carbohydrates and lignin in biomass. *Laboratory Analytical Procedure (LAP)*: 1–17.

Smith VC, Ennos AR. **2003**. The effects of air flow and stem flexure on the mechanical and hydraulic properties of the stems of sunflowers *Helianthus annuus* L. *Journal of Experimental Botany* **54**: 845–849.

Somerville C. **2006**. Cellulose synthesis in higher plants. *Annual Review of Cell and Developmental Biology* **22**: 53–78.

Speck O. **2003**. Field measurements of wind speed and reconfiguration in *Arundo donax* (Poaceae) with estimates of drag forces. *American Journal of Botany* **90**: 1253–1256.

Speck T, Rowe NP. **2003**. Modelling primary and secondary growth processes in plants: a summary of the methodology and new data from an early lignophyte. *Philosophical transactions of the Royal Society of London. Series B, Biological sciences* **358**: 1473–1485.

Steele NM, Sulova Z, Campbell P, Braam J, Farkas V, Fry SC. **2001**. Select and cleave the donor substrate stochastically. *Biochemical Journal* **355**: 671–679.

Stelmach BA, Muller A, Henning P, Laudert D, Andert L, Weiler EW. **1998**. Quantitation of the octadecanoid 12-oxo-phytodienoic acid, a signalling compound in plant

mechanotransduction. *Phytochemistry* **47**: 539–546.

Steucek GL, Gordon LK. **1975**. Response of wheat (*Triticum aestivum*) seedlings to mechanical stress. *Botanical Gazette* **136**: 17–19.

Studer MH, DeMartini JD, Davis MF, Sykes RW, Davison B, Keller M, Tuskan GA, Wyman CE, . 2011. Lignin content in natural *Populus* variants affects sugar release. *Proceedings of the National Academy of Sciences* **108**: 6300–6305.

Szabados L, Savouré A. **2010**. Proline: a multifunctional amino acid. *Trends in Plant Science* **15**: 89–97.

Tatsuki M, Mori H. **1999**. Rapid and transient expression of ACS isogenes by touch and wound stimuli in tomato. *Plant and Cell Physiology* **40**: 709–715.

Telewski FW, Jaffe MJ. **1986a**. Thigmomorphogenesis: field and laboratory studies of *Abies fraseri* in response to wind and mechanical perturbation. *Physiologia Plantarum* **66**: 211–218.

Telewski FW, Jaffe MJ. **1986b**. Thigmomorphogenesis: anatomical, morphological and mechanical analysis of genetically different sibs of *Pinus taeda* in response to mechanical perturbation. *Physiologia Plantarum* **66**: 219–226.

Telewski FW, Pruyn ML. **1998**. Thigmomorphogenesis: A dose response to flexing in *Ulmus americana* seedlings. *Tree Physiology* **18**: 65–68.

The International Brachypodium Initiative. **2010**. Genome sequencing and analysis of the model grass *Brachypodium distachyon*. *Nature* **463**: 763–768.

Thompson DS. **2008**. Space and time in the plant cell wall: Relationships between cell type, cell wall rheology and cell function. *Annals of Botany* **101**: 203–211.

Todaka D, Matsushima H, Morohashi Y. **2017**. Water stress enhances β-amylase activity in cucumber cotyledons. *Journal of Experimental Botany* **51**: 739–745.

Tretner C, Huth U, Hause B. **2008**. Mechanostimulation of *Medicago truncatula* leads to enhanced levels of jasmonic acid. *Journal of Experimental Botany* **59**: 2847–2856.

Tripathi SC, Sayre KD, Kaul JN, Narang RS. **2003**. Growth and morphology of spring wheat (*Triticum aestivum* L.) culms and their association with lodging: Effects of genotypes, N levels and ethephon. *Field Crops Research* **84**: 271–290.

Ulvskov P, Wium H, Bruce D, Jørgensen B, Qvist KB, Skjøt M, Hepworth D, Borkhardt B, Sørensen SO. **2005**. Biophysical consequences of remodeling the neutral side chains of rhamnogalacturonan I in tubers of transgenic potatoes. *Planta* **220**: 609–620.

Unver T, Budak H. **2009**. Conserved micrornas and their targets in model grass species *Brachypodium distachyon*. *Planta* **230**: 659–669.

Vega-Sánchez ME, Verhertbruggen Y, Christensen U, Chen X, Sharma V, Varanasi P, Jobling SA, Talbot M, White RG, Joo M, *et al.* 2012. Loss of cellulose synthase-like F6 function affects mixed-linkage glucan deposition, cell wall mechanical properties, and defense responses in vegetative tissues of rice. *Plant Physiology* **159**: 56–69.

Venning F. 1949. Stimulation by wind motion of collenchyma formation in celery petioles. *Botanical Gazette* **110**: 571–574.

Verbruggen N, Hermans C. **2008**. Proline accumulation in plants: A review. *Amino Acids* **35**: 753–759.

Verelst W, Bertolini E, De Bodt S, Vandepoele K, Demeulenaere M, Pè ME, Inzé D. **2013**. Molecular and physiological analysis of growth-limiting drought stress in brachypodium distachyon leaves. *Molecular Plant* **6**: 311–322.

Verhertbruggen Y, Marcus SE, Chen J, Knox JP. **2013**. Cell wall pectic arabinans influence the mechanical properties of *Arabidopsis thaliana* inflorescence stems and their response to mechanical stress. *Plant and Cell Physiology* **54**: 1278–1288.

Verhertbruggen Y, Marcus SE, Haeger A, Ordaz-Ortiz JJ, Knox JP. **2009a**. An extended set of monoclonal antibodies to pectic homogalacturonan. *Carbohydrate Research* **344**: 1858–1862.

Verhertbruggen Y, Marcus SE, Haeger A, Verhoef R, Schols HA, McCleary B V., McKee L, Gilbert HJ, Knox JP. **2009b**. Developmental complexity of arabinan polysaccharides and their processing in plant cell walls. *Plant Journal* **59**: 413–425.

Vogel J. **2008**. Unique aspects of the grass cell wall. *Current Opinion in Plant Biology* **11**: 301–307.

Vogel JP, Gu YQ, Twigg P, Lazo GR, Laudencia-Chingcuanco D, Hayden DM, Donze TJ, Vivian LA, Stamova B, Coleman-Derr D. **2006**. EST sequencing and phylogenetic analysis of the model grass *Brachypodium distachyon*. *Theoretical and Applied Genetics* **113**: 186–195.

Vogel JP, Tuna M, Budak H, Huo N, Gu YQ, Steinwand MA. **2009**. Development of SSR markers and analysis of diversity in Turkish populations of *Brachypodium distachyon*. *BMC Plant Biology* **9**: 88.

Volpi C, Janni M, Lionetti V, Bellincampi D, Favaron F, D'Ovidio R. **2011**. The ectopic expression of a pectin methyl esterase inhibitor increases pectin methyl esterification and limits fungal diseases in wheat. *Molecular Plant-Microbe Interactions* **24**: 1012–1019.

Walker WS. **1957**. The effect of mechanical stimulation on the collenchyma of *Apium graveolens* L. *Proceedings of the Iowa Academy of Science* **64**: 177–186.

Wang T, Salazar A, Zabotina OA, Hong M. **2014**. Structure and dynamics of *Brachypodium* primary cell wall polysaccharides from two-dimensional 13C solid-state nuclear magnetic resonance spectroscopy. *Biochemistry* **53**: 2840–2854.

Wang J, Zhu J, Huang R, Yang Y. **2012**. Investigation of cell wall composition related to stem lodging resistance in wheat (*Triticum aestivum* L.) by FTIR spectroscopy. *Plant Signaling & Behavior* **7**: 856–863.

Whirehead FH, Luti R. **1962**. Experimental studies of the effect of wind on plant growth and anatomy. I *Zea Mays*. *New Phytologist* **61**: 56–58.

Whitehead F. **1963**. Experimental studies of the effect of wind on plant growth and anatomy. IV. Growth substances and adaptative anatomical and morphological changes. *New Phytologist* **62**: 86–90.

Wilder B, Albersheim P. **1973**. The structure of plant cell walls. *Plant Physiology* **51**: 889–893.

Willats WGT, Orfila C, Limberg G, Buchholt HC, Van Alebeek GJWM, Voragen AGJ, Marcus SE, Christensen TMIE, Mikkelsen JD, Murray BS, *et al.* 2001. Modulation of the degree and pattern of methyl-esterification of pectic homogalacturonan in plant cell walls: Implications for pectin methyl esterase action, matrix properties, and cell adhesion. *Journal of Biological Chemistry* **276**: 19404–19413.

Willatts WGT, Mccartney L, Mackie W, Knox J. **2001**. Pectin: Cell biology and prospects for functional analysis. *Plant Molecular Biology* **47**: 9–27.

Willför S, Sundberg A, Pranovich A, Holmbom B. **2005**. Polysaccharides in some industrially important hardwood species. *Wood Science and Technology* **39**: 601–617.

Wilson SM, Burton RA, Doblin MS, Stone BA, Newbigin EJ, Fincher GB, Bacic A. **2006**. Temporal and spatial appearance of wall polysaccharides during cellularization of barley (*Hordeum vulgare*) endosperm. *Planta* **224**: 655–667.

Winzeler UZH, Keller MMMM, Schmid BKJE, Stamp P. **1999**. Morphological traits associated with lodging resistance of spring wheat (*Triticum aestivum* L.). *Journal of Agronomy and Crop Science* **182**: 17–24.

Wolf S, Mouille G, Pelloux J. **2009**. Homogalacturonan methyl-esterification and plant development. *Molecular Plant* **2**: 851–860.

Woods DP, Bednarek R, Bouché F, Gordon SP, Vogel JP, Garvin DF, Amasino RM. **2016**. Genetic rrchitecture of flowering-time variation in *Brachypodium distachyon*. *Plant Physiology* **173**: 269–279.

Worley B, Powers R. **2013**. Multivariate analysis in metabolomics. *Current Metabolomics* **1**: 92–107.

Xu W, Campbell P, Vargheese AK, Braam J. **1996**. The *Arabidopsis* XET-related gene family: Environmental and hormonal regulation of expression. *The Plant Journal* **9**: 879–889.

Xu W, Purugganan MM, Polisensky DH, Antosiewicz DM, Fry SC, Braam J. **1995**. *Arabidopsis* TCH4, regulated by hormones and the environment, encodes a xyloglucan endotransglycosylase. *The Plant Cell* **7**: 1555–1567.

Xue J, Bosch M, Knox JP. **2013**. Heterogeneity and glycan masking of cell wall microstructures in the stems of *Miscanthus x giganteus*, and its parents *M. sinensis* and *M. sacchariflorus*. *PLoS ONE* **8**: e82114.

Xue GP, McIntyre CL, Glassop D, Shorter R. **2008**. Use of expression analysis to dissect alterations in carbohydrate metabolism in wheat leaves during drought stress. *Plant Molecular Biology* **67**: 197–214.

Zhang Z, Qiang L, Hai-xing S, Xiang-min R, Ismail A. **2012**. Responses of different rice (*Oryza sativa* L.) genotypes to salt stress and relation to carbohydrate metabolism and chlorophyll content. *African Journal of Agricultural Reseearch* **7**: 19–27.

Zhang JE, Quan GM, Huang ZX, Luo SM, Ouyang Y. **2013a**. Evidence of duck activity induced anatomical structure change and lodging resistance of rice plant. *Agroecology and Sustainable Food Systems* **37**: 975–984.

Zhang W, Wu L, Wu X, Ding Y, Li G, Li J, Weng F, Liu Z, Tang S, Ding C, *et al.* 2016. Lodging resistance of Japonica rice (*Oryza Sativa* L.): Morphological and anatomical traits due to top-dressing nitrogen application rates. *Rice* **9**: 31.

Zhang Z, Zhang X, Wang S, Xin W, Tang J, Wang Q. **2013b**. Effect of mechanical stress on cotton growth and development. *PLoS ONE* **8**: 8–13.

Zhao B, Teng L, Zhang JE, Xiang H, Li M, Liang K. **2018**. Thigmotropic responses of *Oryza sativa* L. to external rubbing stimulation. *Archives of Biological Sciences* **70**: 129–139.

Zhu W, Van Hout R, Luznik L, Kang HS, Katz J, Meneveau C. **2006**. A comparison of PIV measurements of canopy turbulence performed in the field and in a wind tunnel model. *Experiments in Fluids* **41**: 309–318.

APPENDIX

Appendix 1. Water consumption during stress experiments.

Tables present average of water intake (mL) per plant per day and total water consumed per plant during the whole greenhouse stress experiment (14 days) looking at wind stress (WS) and mechanical stress (MS). Data presented for all four experiments for both genotypes Bd21 (A) and ABR6 (B).

A.

Experiment	Control		WS		MS	
	Average mL per day	Total mL per the whole experiment	Average mL per day	Total mL per the whole experiment	Average mL per day	Total mL per the whole experiment
1st	15.4 ± 8.4	200	27.7 ± 6.9	360	16.2 ± 8.4	210
2nd	18.5 ± 5.3	240	26.2 ± 6.2	340	19.2 ± 4.7	250
3rd	16.4 ± 4.8	230	26.4 ± 8.9	370	17.9 ± 4.1	250
4th	15 ± 5	210	27.1 ± 9.6	380	14.3 ± 4.9	200

B.

Experiment	Control		WS		MS	
	Average mL per day	Total mL per the whole experiment	Average mL per day	Total mL per the whole experiment	Average mL per day	Total mL per the whole experiment
1st	13.8 ± 9.2	180	26.9 ± 4.6	350	16.9 ± 7.2	220
2nd	18.5 ± 10.3	240	30.8 ± 7.3	400	21.5 ± 7.7	280
3rd	13.8 ± 4.7.4	180	30.8 ± 6.1	400	16.1 ± 6.2	210
4th	14.3 ± 4.9	200	25 ± 8.2	350	15.7 ± 4.9	220

Appendix 2. Flowering time

Experiment #1

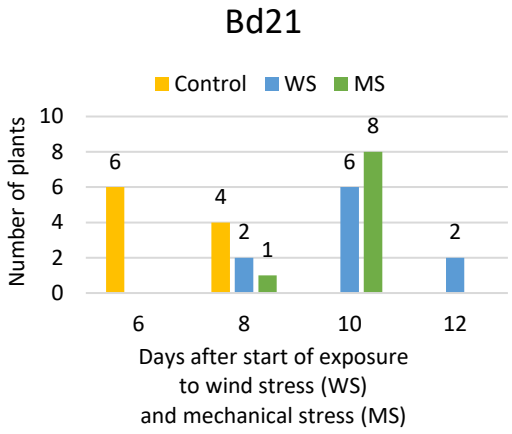

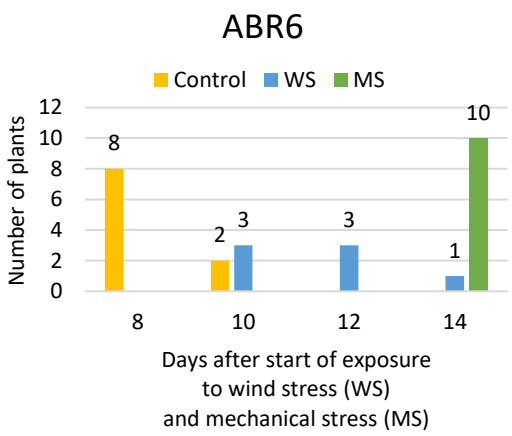

Experiment #2

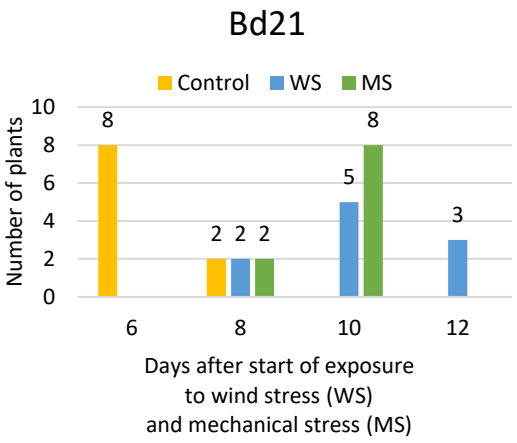

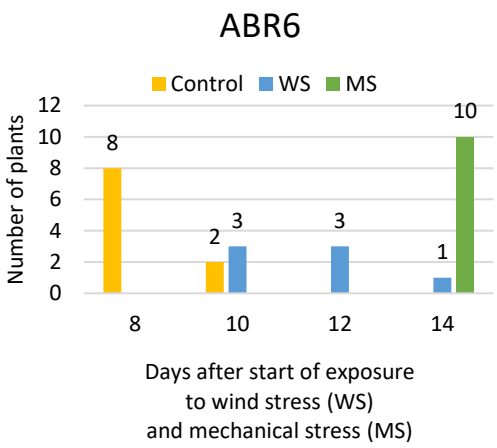

Experiment #3

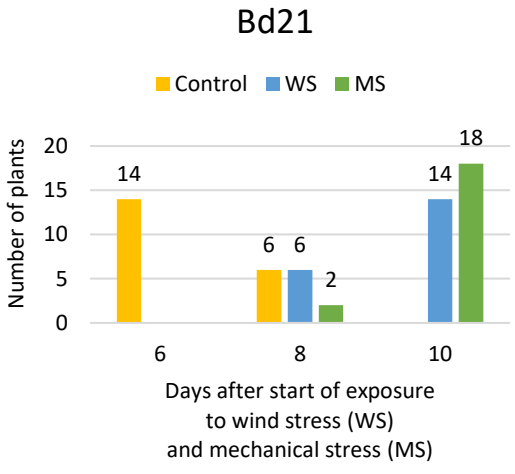

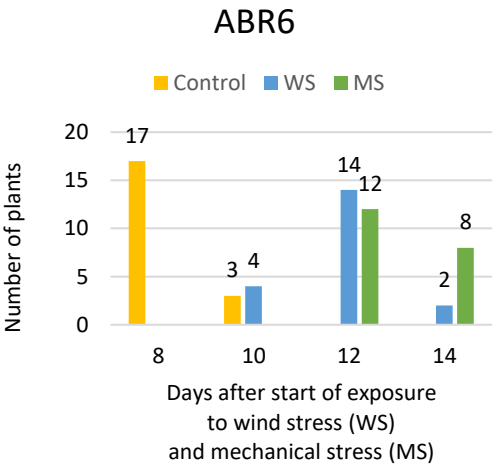

Appendix 3.

Scanning electron microscope images of whole cross-sections for control, wind stress (WS) and mechanical stress (MS) treatments for both genotypes Bd21 and ABR6.

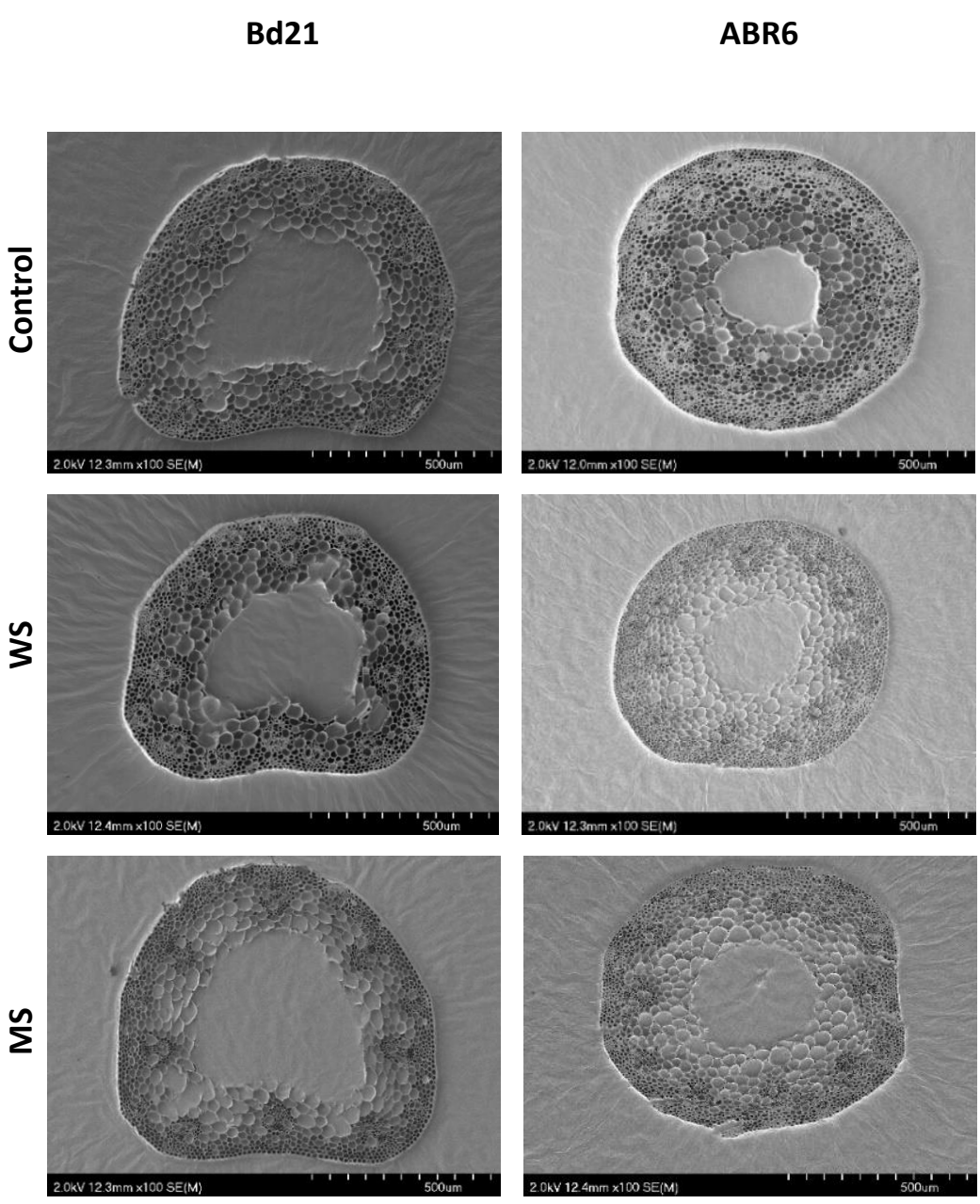

Appendix 4. Immuno-localisation

Appendix 4A.

Immuno-localisation of the LM13 cell wall epitope in ABR6 stem cross-sections after three treatments (control, wind stress [WS], and mechanical stress [MS]). Scale bar = 100 µm.

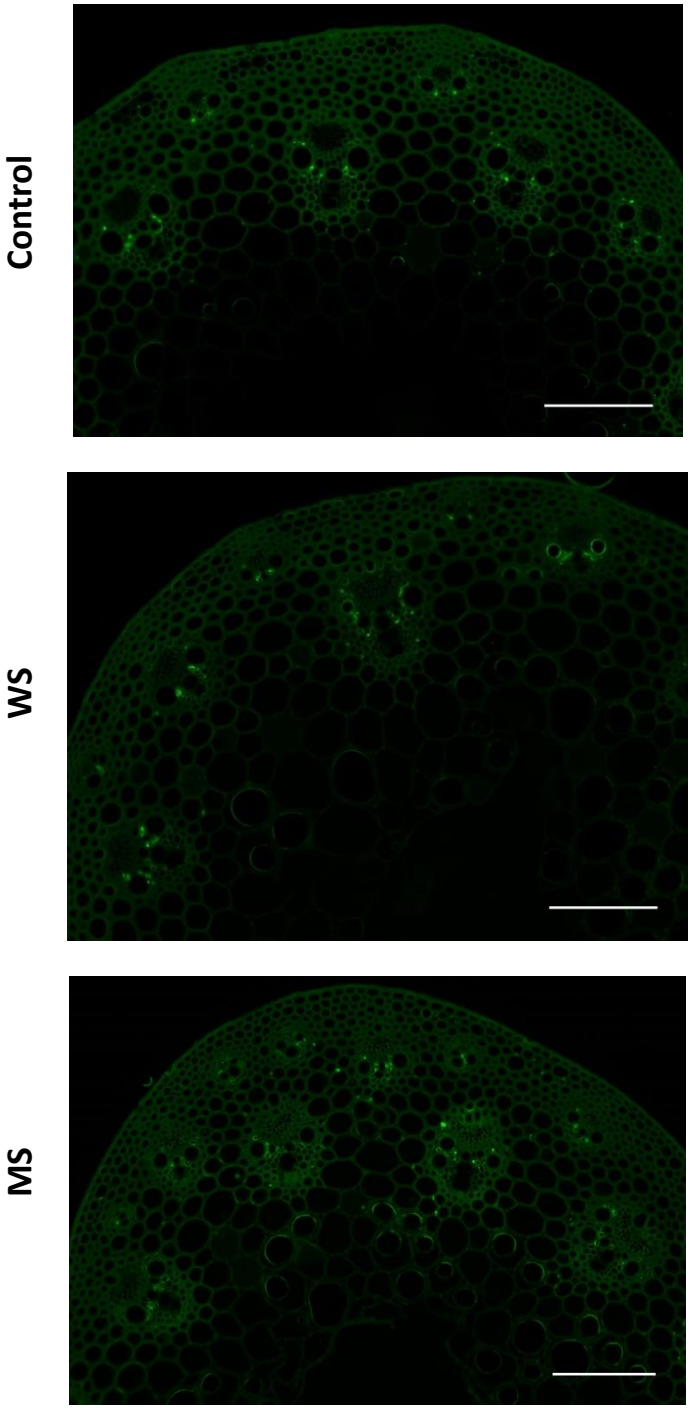

Appendix 4B.

Immuno-localisation of JIM7 epitope in ABR6 cell walls in three treatments (control, wind stress [WS], and mechanical stress [MS]). Scale bar = 100 µm.

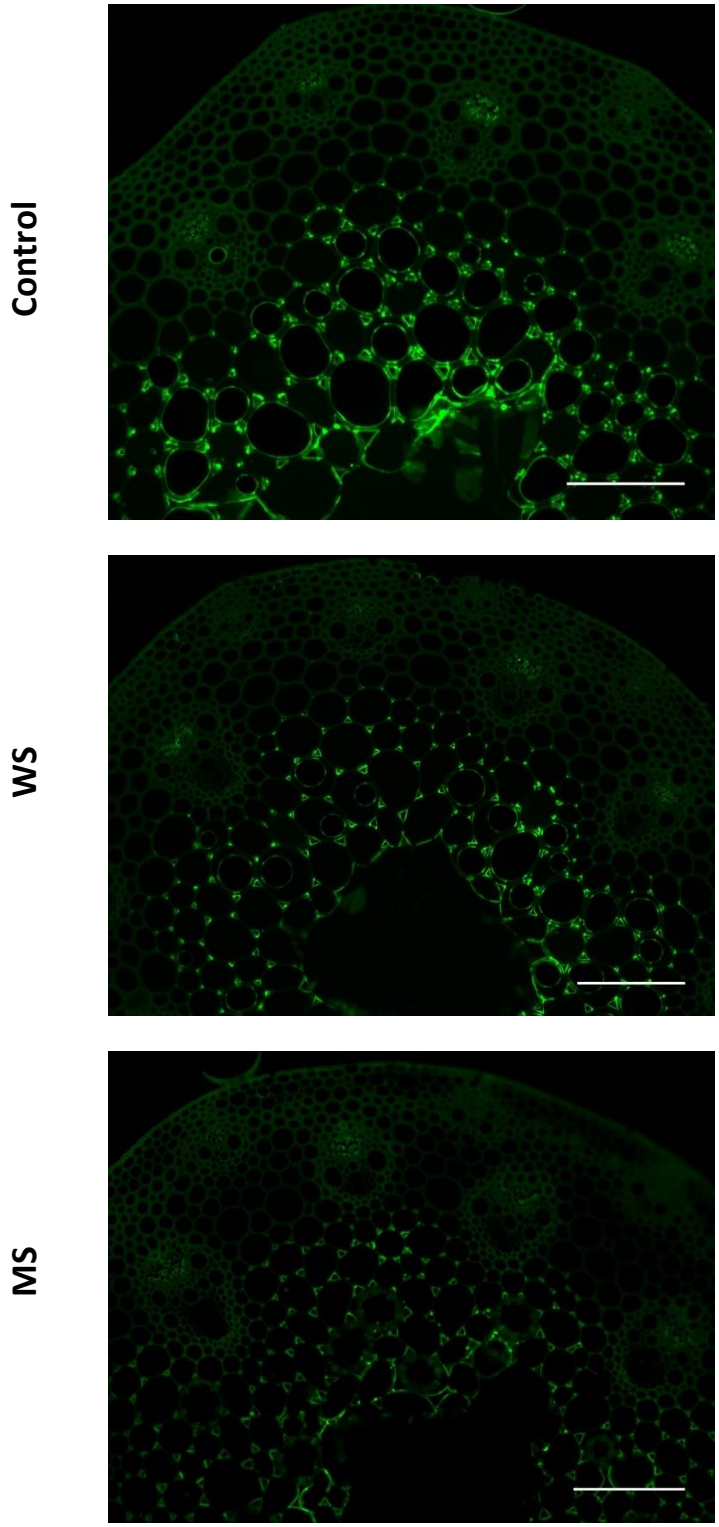

Appendix 4C.

Immuno-localisation of LM19 epitope in Bd21 cell walls in three treatments (control, wind stress [WS], and [MS]). Scale bar = 100 µm.

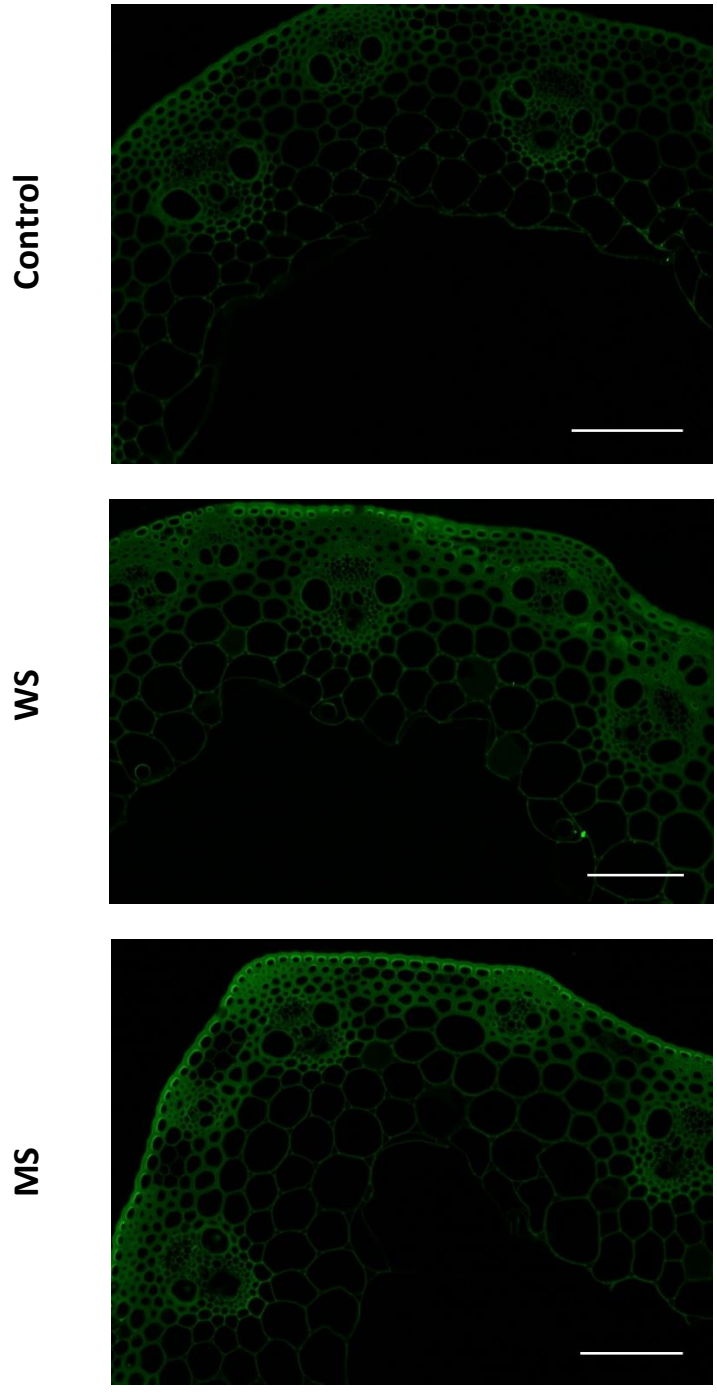

Appendix 4D.

Immuno-localisation of LM6 epitope in ABR6 and Bd21 cell walls in three treatments (control, wind stress [WS], and mechanical stress [MS]). Scale bar = 100 µm.

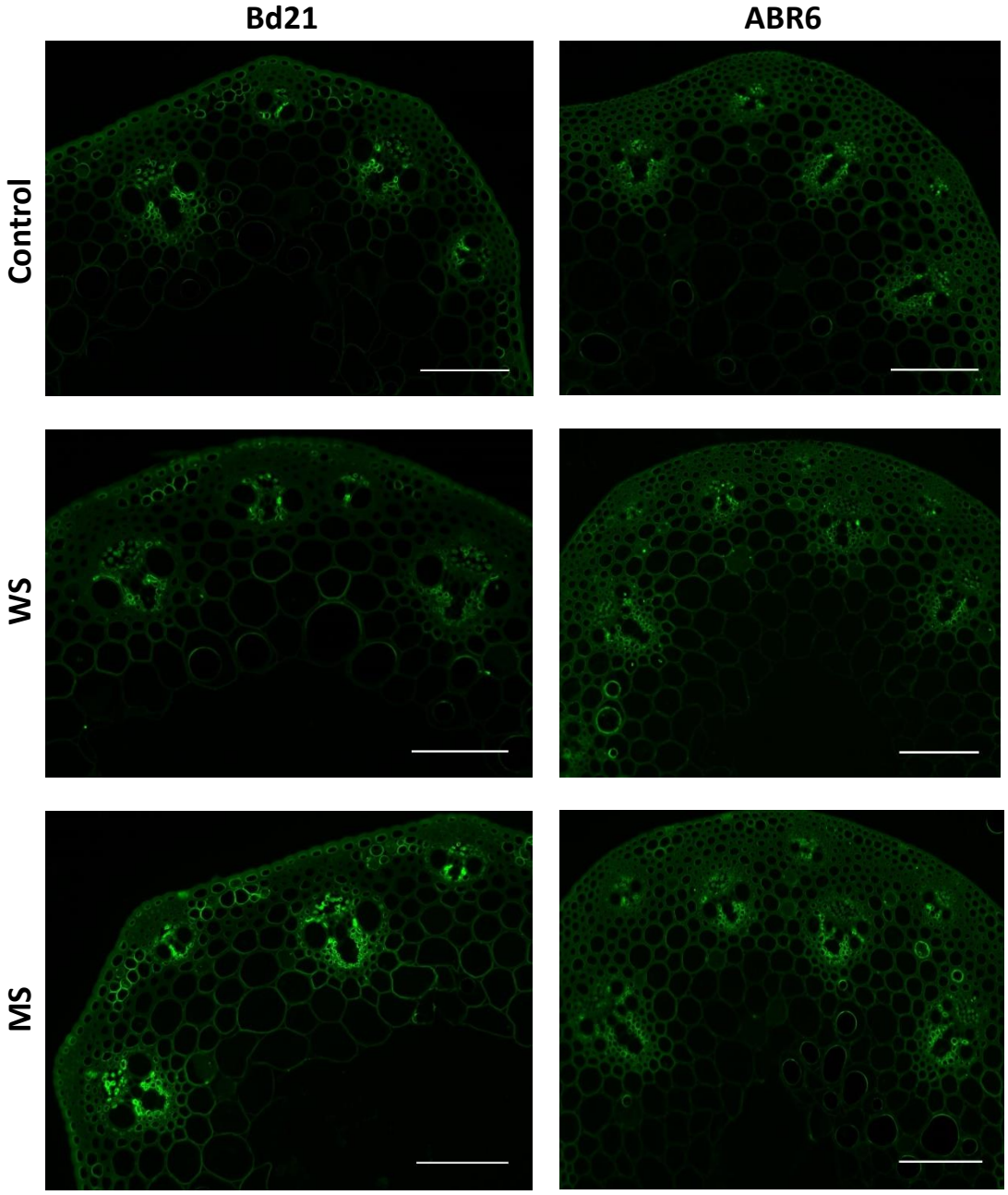

Appendix 4E.

Immuno-localisation of LM20 epitope in Bd21 and ABR6 cell walls in three treatments (control, wind stress [WS], and mechanical stress [MS]). Scale bar = 100 µm.

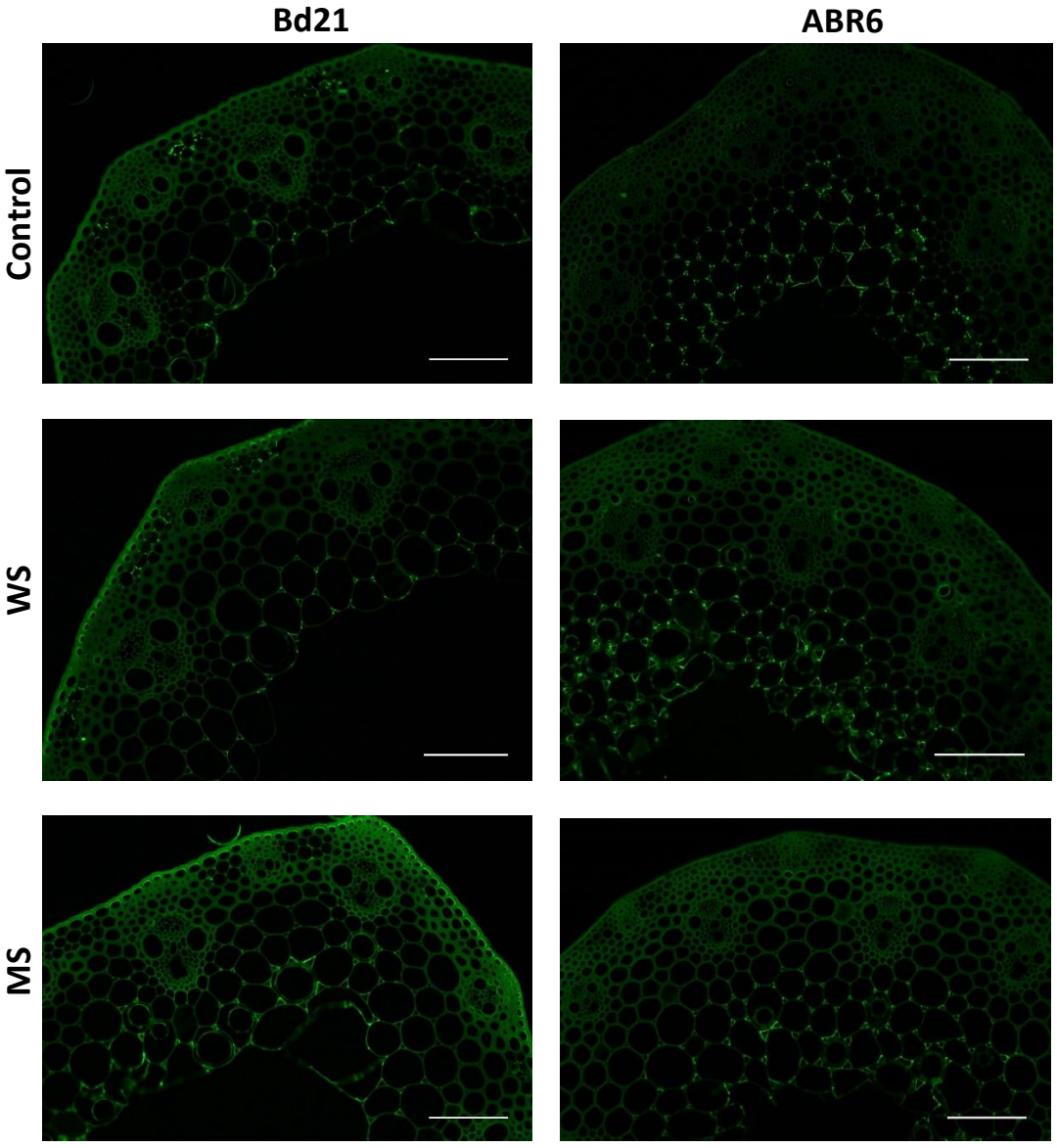

Appendix 4F.

Immuno-localisation of LM25 epitope in Bd21 and ABR6 cell walls in three treatments (control, wind stress [WS], and mechanical stress [MS]). Scale bar = 100 µm.

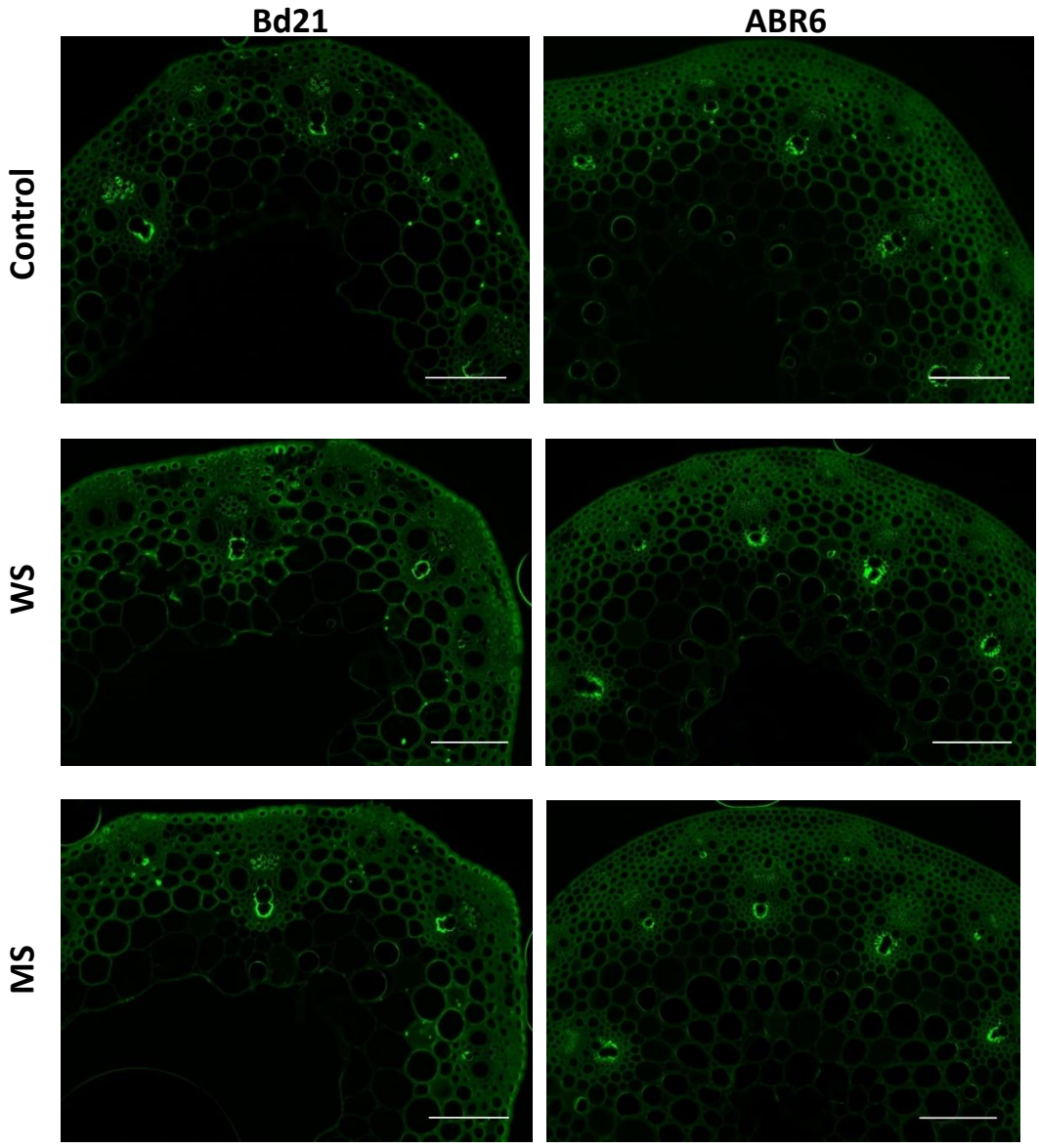

Appendix 4G.

Immuno-localisation of LM28 epitope in Bd21 and ABR6 cell walls in three treatments (control, wind stress [WS], and mechanical stress [MS]). Scale bar = 100 µm.

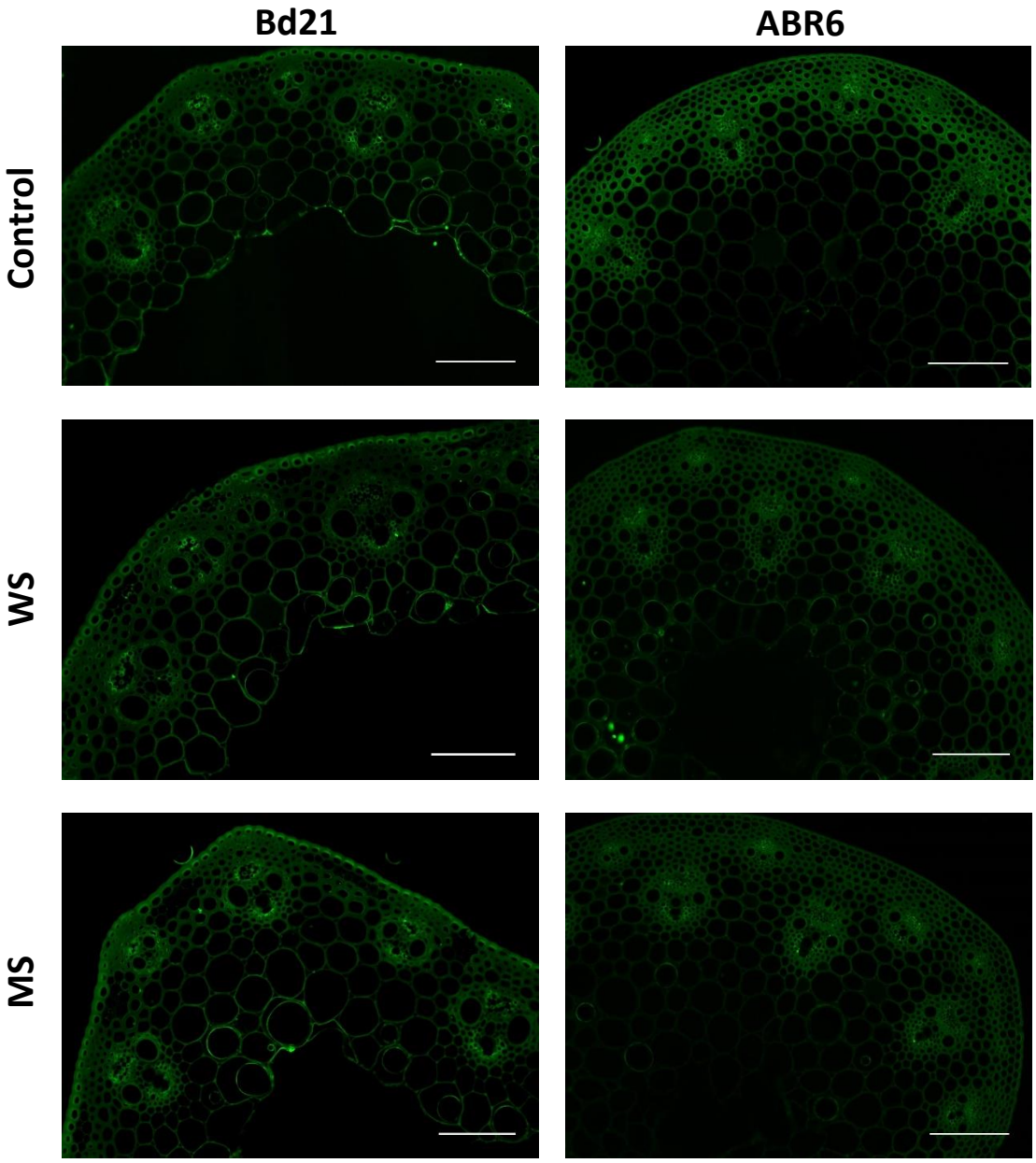

Appendix 4H.

Immuno-localisation of LM10 epitope in Bd21 and ABR6 cell walls in three treatments (control, wind stress [WS], and mechanical stress [MS]). Scale bar = 100 µm.

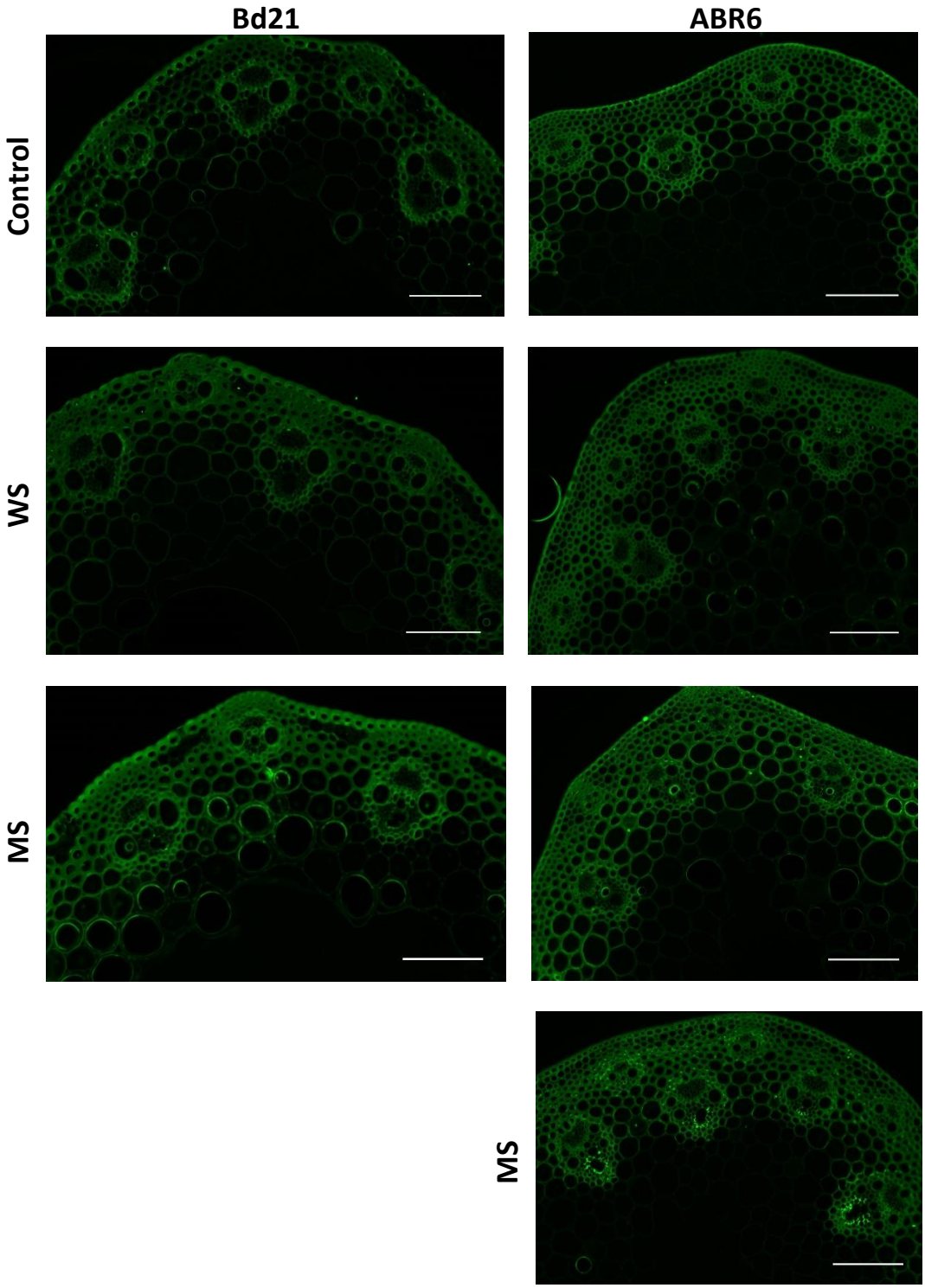

Appendix 4I.

Immuno-localisation of LM1 epitope in Bd21 and ABR6 cell walls in three treatments (control, wind stress [WS], and mechanical stress [MS]). Scale bar = 100 µm.

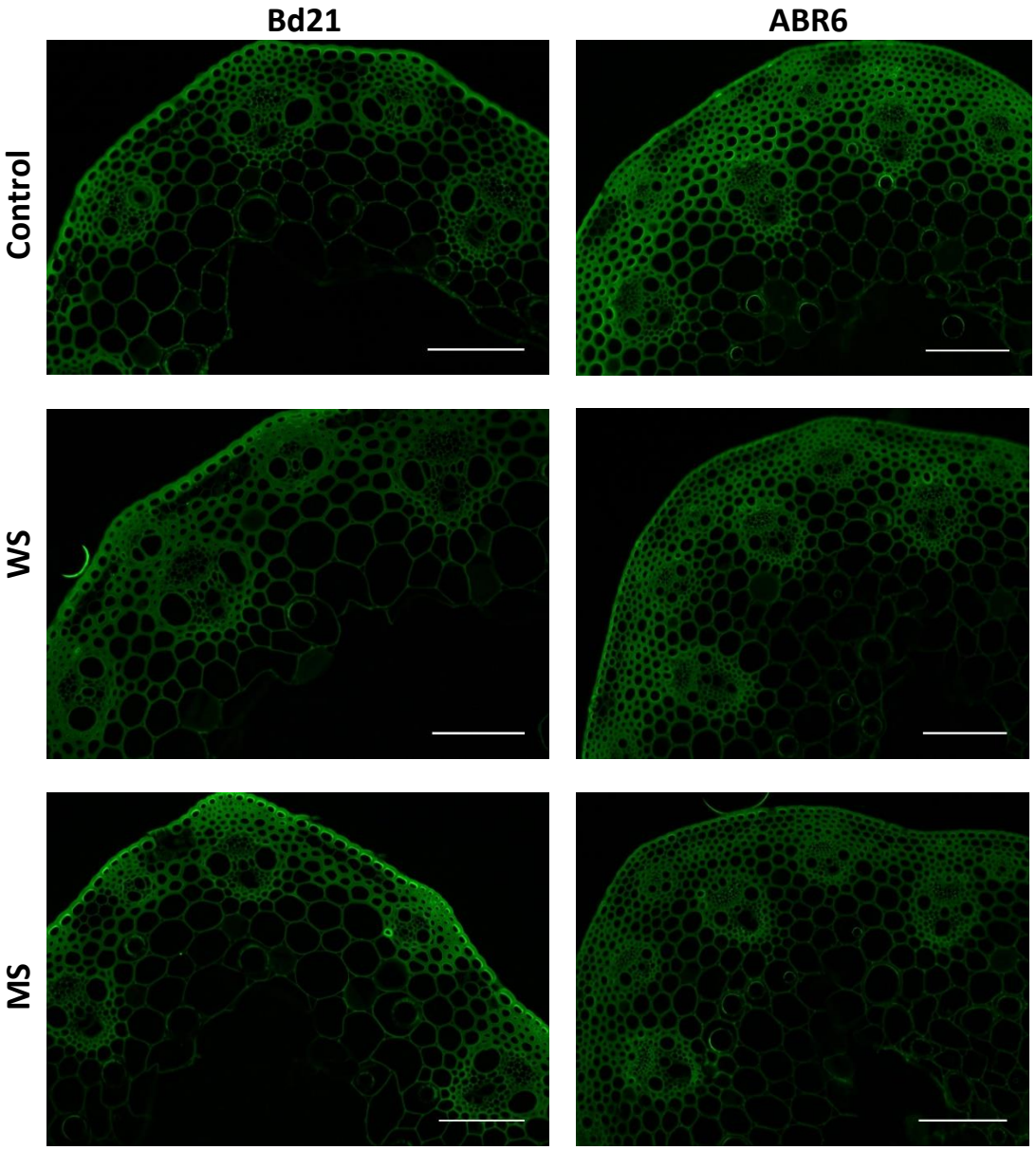

Appendix 4J.

Immuno-localisation of LM2 epitope in Bd21 and ABR6 cell walls in three treatments (control, wind stress [WS], and mechanical stress [MS]). Scale bar = 100 µm.

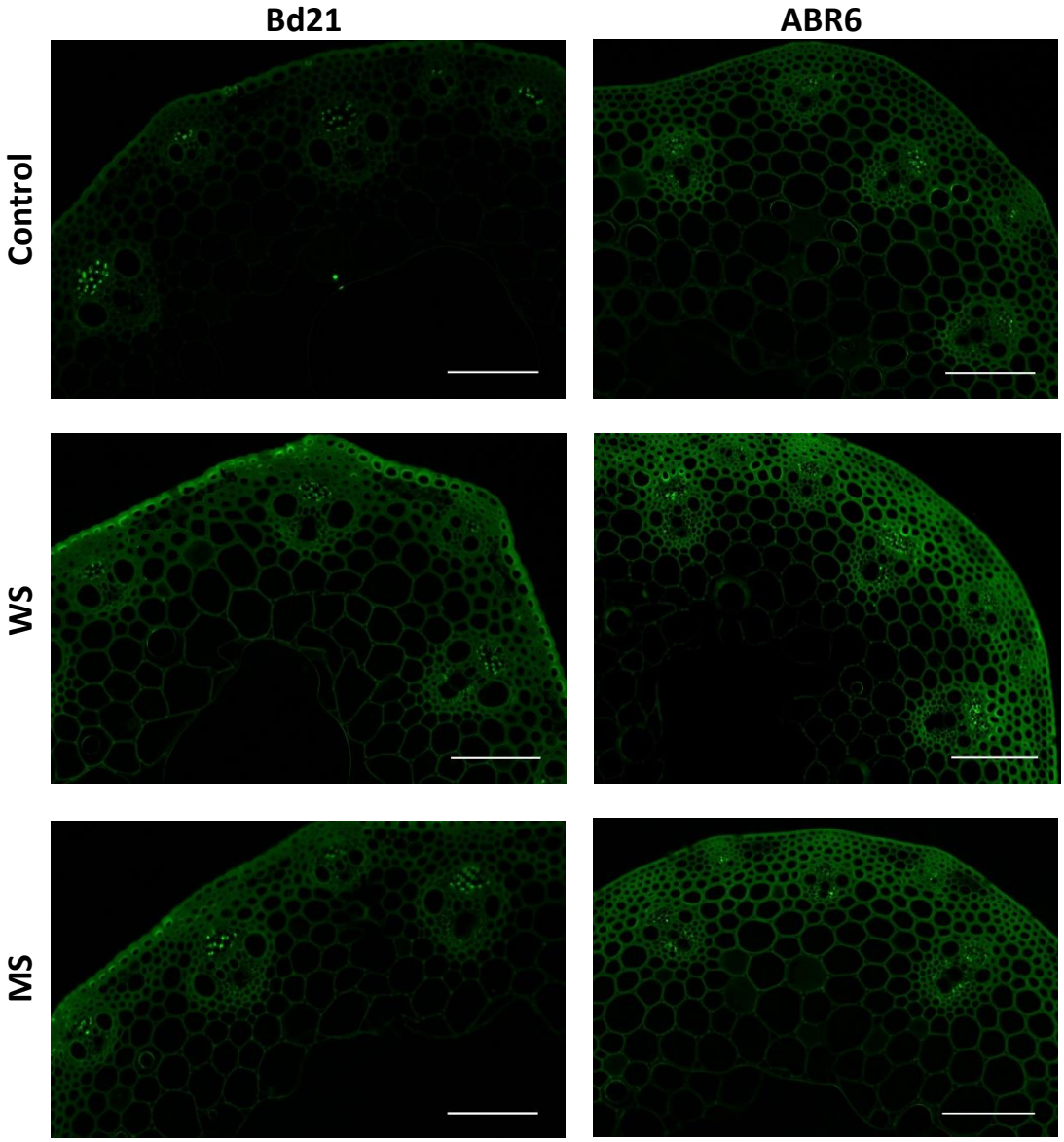

Appendix 4K.

Immuno-localisation of LM12 epitope in Bd21 and ABR6 cell walls in three treatments (control, wind stress [WS], and mechanical stress [MS]). Scale bar = 100 µm.

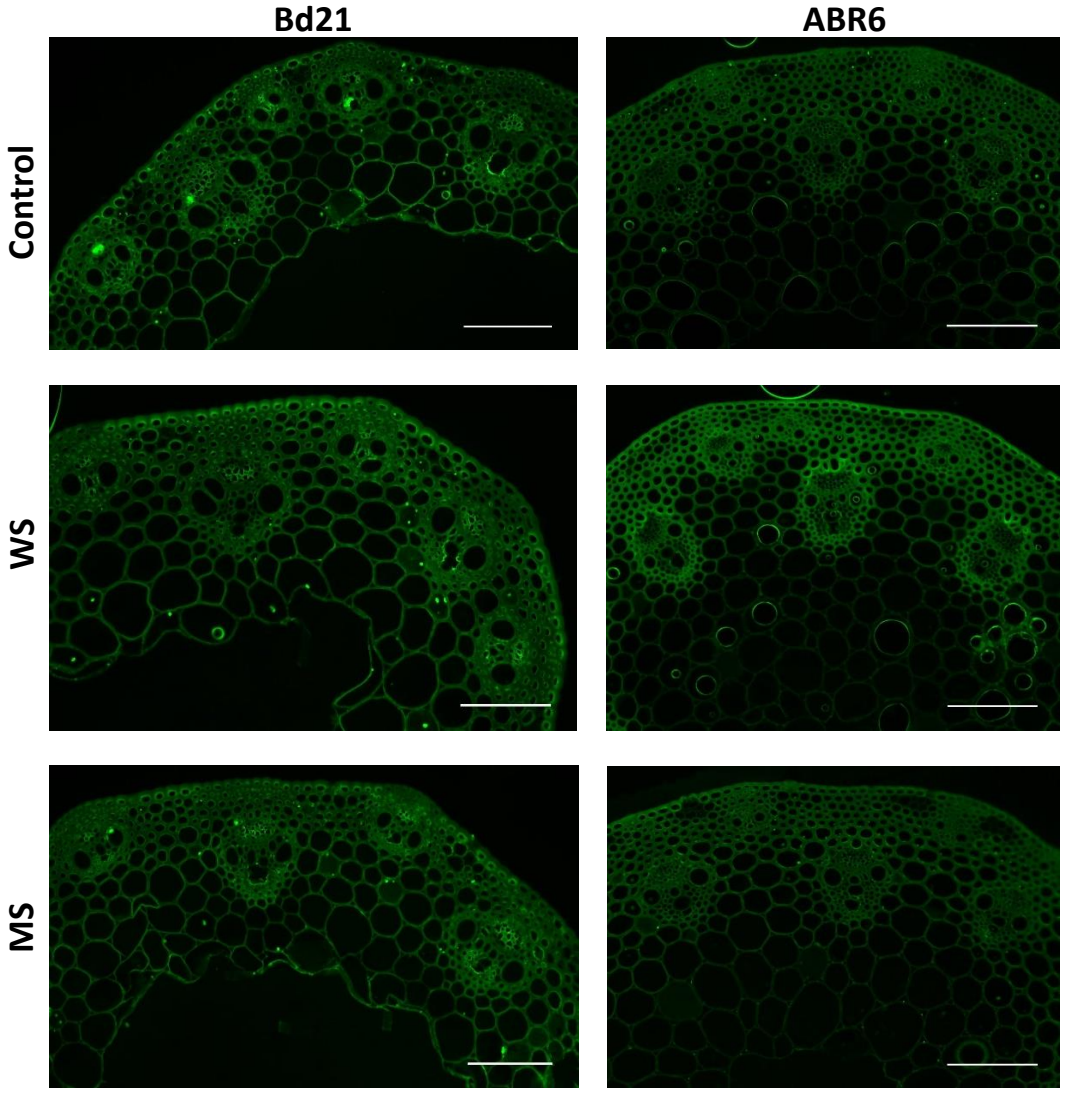

Appendix 4L.

Immuno-localisation of BG1 epitope in Bd21 and ABR6 cell walls in three treatments (control, wind stress [WS], and mechanical stress [MS]). Scale bar = 100 µm.

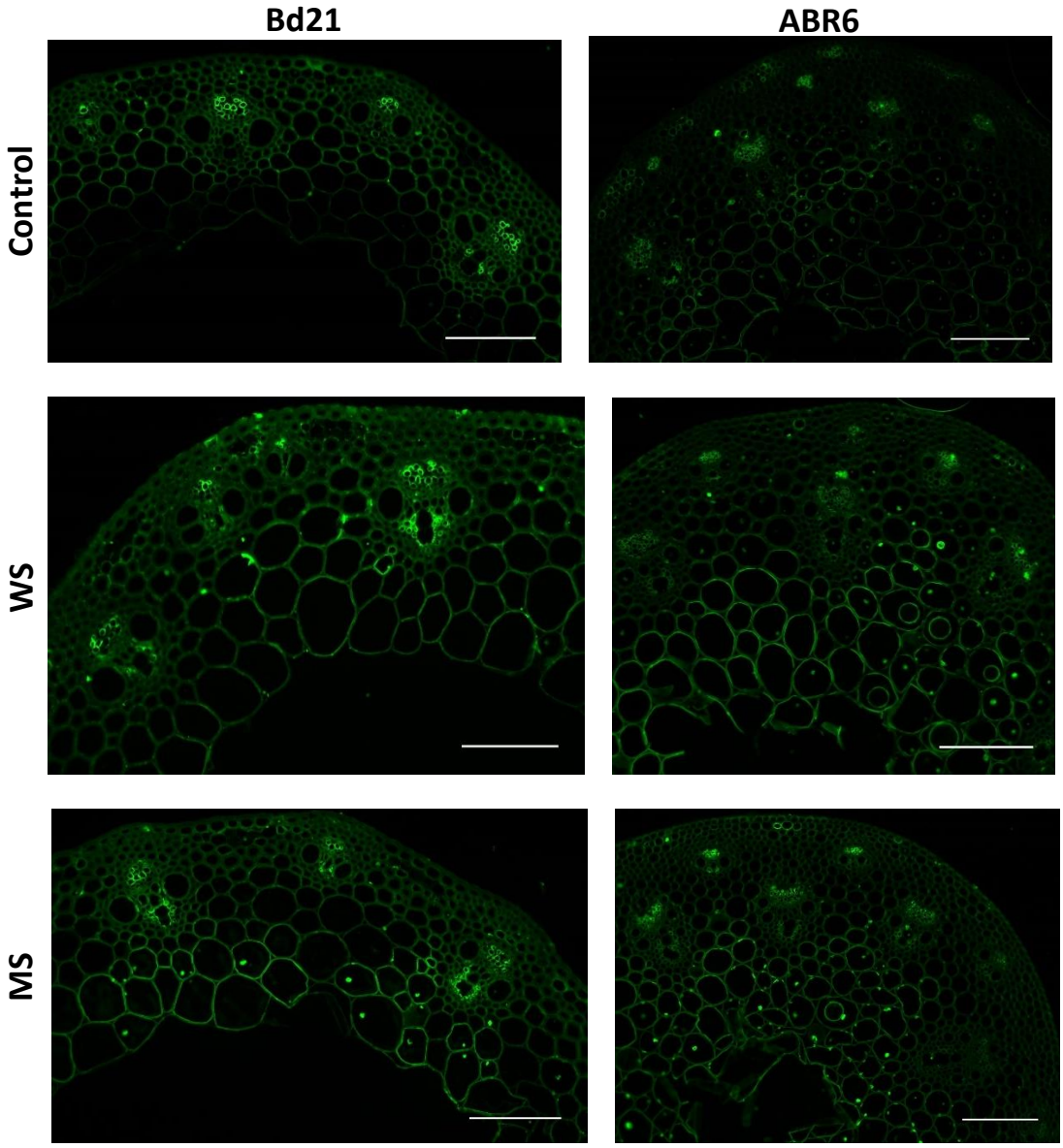

Appendix 5.

The list of all designed primer sets used for the analysis of specific *Brachypodium distachyon* genes. Blue coloured pairs of primers indicate primers that did not show expected results on electrophoresis gel and therefore were excluded from further RT-PCR analysis.

Family	Gene	Designed primer	Sequence of gene-specific primers	Amplicon size (bp)
CaM1	Bradi2g21460	AG01	F:5'-TCAACGAGGTTGACGCTGAT-3'	135
		AG02	R:5'-TCTGGTCCTTGTCGAAGACAC-3'	
		AG03	F:5'-TTTCTGAACCTGATGGCAAGGA-3'	144
		AG04	R:5'-CTTCTCCCCGAGGTTGGTCAT-3'	
CaM5	Bradi2g10010	AG05	F:5'-GGCAACGGCACCATTGATTT-3'	137
		AG06	R:5'-TCAGCAGCAGAGATGAAGCC-3'	
		AG07	F:5'-AGTTGGGAACTGTCATGCGT-3'	103
		AG08	R:5'-AAATCAATGGTGCCGTTGCC-3'	
CaM5	Bradi1g17237	AG09	F:5'-TTAAGGAGGCTTTCCGTGTG-3'	127
		AG10	R:5'-TCACGGATCATCTCATCCAC-3'	
		AG11	F:5'-GGCTGAACTCCGTCATGTCA-3'	101
		AG12	R:5'-TCTGACCGTCACCATCAACG-3'	
CDP	Bradi2g02340	AG13	F:5'-GGGTTCGAGGAGTTCAAGAAG-3'	92
		AG14	R:5'-TCTTTCTTGGGCTTGTCAGG-3'	
	Bradi2g31900	AG15	F:5'-TTGGTCGTGGGAAACTCAC-3'	114
		AG16	R:5'-AATTCCTTCCGTTCCTCTCC-3'	
CML23	Bradi2g51090	AG17	F:5'-TGGTGCAAGACCACATTCAC-3'	126
		AG18	R:5'-TGCTCATCATCAGCTTCAGG-3'	
		AG19	F:5'-CATCACTTCGCTGAGCCTGA-3'	100
		AG20	R:5'-CCCGTTGAGATCAAACCTGC-3'	
GH	Bradi1g33810	AG21	F:5'-TGTCGTTCCCAAAGTCGCAG-3'	135
		AG22	R:5'-CGTTGAAGTCGCGGAAAGAG-3'	
		AG23	F:5'-CTCAGCGACATGAGCTACCG-3'	73
		AG24	R:5'-CGTCGGTGCAGTAGTTGTAGA-3'	
GH	Bradi1g33840	AG25	F:5'-CCTTCTCGGCATCCTACCG-3'	145
		AG26	R:5'-AGGTCGAGCTCCTGGTTGTA-3'	
		AG27	F:5'-AACCTGGAGGGGAAAGGGAT-3'	142
		AG28	R:5'-GGTAGGATGCCGAGAAGGG-3'	
ExpA1	Bradi1g76260	AG37	F:5'-TGTGGGCAGAGAAGGAAGTG-3'	109
		AG38	R:5'-GTGTCGCAAGGGAAGCAG-3'	
		AG39	F:5'-CAAGTGGGTGTGGGCAGAGA-3'	132
		AG40	R:5'-CACCTCCACTCCTGCGTGTC-3'	
ExpA1	Bradi1g76270	AG41	F:5'-TAGGGTCGTCGAACTGGAAG-3'	142
		AG42	R:5'-ACTTCCTTCTCCACCCACAG-3'	
		AG43	F:5'-GGGTGGAGAAGGAAGTGCTG-3'	77
		AG44	R:5'-GATGTCGGTGATCTGGAGCC-3'	
ExpA3	Bradi1g28130	AG45	F:5'-TGGGTGTGGGCTGATAAAG-3'	137
		AG46	R:5'-GCCACTTTCATTTCCCAGTC-3'	
		AG47	F:5'-GTTCATGGGCCCGTTTGGAG-3'	103
		AG48	R:5'-TATCAGCCCACACCCACTTG-3'	
AGP	Bradi2g45510	AG49	F:5'-AGGGTCTCTCTTCTTCTGATGG-3'	
		AG50	R:5'-ACGAACATGAGCACATACGC-3'	131
		AG51	F:5'-GTGAGCTCCAGGGTCTCTCT-3'	128
		AG52	R:5'-ACATACGCGATCCCTTGGTC-3'	
CSLD2	Bradi1g50170	AG53	F:5'-GTATGGCAGCAATGGTGAAG-3'	89

		AG54	R:5'-TTTCACGGGACACATAGACC-3'	
		AG55	F:5'-CGATGCGGTGGAAGCTGTTA-3'	147
		AG56	R:5'-TCGCTAGGTGGTTTCAGCATT-3'	
b-Glu	Bradi3g03520	AG57	F:5'-TGGGTCGACAAGAATGTCTC-3'	79
		AG58	R:5'-GGAAAGGCTCATTACCAACC-3'	
		AG59	F:5'-AACTACCTCAACGACGGCTG-3'	110
		AG60	R:5'-TTTCGGAGGGCAGGAAAAGT-3'	
WAK	Bradi5g24311	AG61	F:5'-CGGTGGTTGCAAGACTCACA-3'	146
		AG62	R:5'-TGGAGCATTCTGGCTCACTC-3'	
PME	Bradi2g11850	AG29	F:5'-GTATGTCATGATGGTCGGTGAC-3'	134
		AG30	R:5'-TCATGTTCACCGCCACGAAC-3'	
		AG31	F:5'-GGCTGGACCACCTTCAACTC-3'	149
		AG32	R:5'-CACTGGTAGAACGTCGACAGG-3'	
PME	Bradi2g27930	AG33	F:5'-ACGGTGGTCATGGAGTCCTA-3'	96
		AG34	R:5'-GGCGTAGTAGAGCGTGTCAA-3'	
		AG35	F:5'-AACGCTGCCTTTACAACGGT-3'	84
		AG36	R:5'-GCCCAGGTAGGACTCCATGA-3'	
PME	Bradi2g11860	AG67	F:5'-CGTGTTCATGGAGTCGCAGA-3'	93
		AG68	R:5'-CCGTAGTAGAGCGTGTCGAG-3'	
		AG69	F:5'-GGGCAGAGCAACACCTACAC-3'	133
		AG70	R:5'-CCAGGTACGTCCTGAAGCTC-3'	
		AG113	F:5'-ACGTGGAAGTGGGGAAGAAC-3'	174
		AG114	R:5'-CCGAGTTCTCGATGGTCAGG-3'	
		AG115	F:5'-CTTCACCGTGGGATCGTTCA-3'	115
		AG116	R:5'-TCGCTTGTGACCCTTCAGTC-3'	
PME	Bradi2g56820	AG71	F:5'-TATGGCGAGTACGACAGTGC-3'	119
		AG72	R:5'-TGTATGAAGCTAGCGACGCC-3'	
		AG73	F:5'-GACCTAACGATCGCGAACAC-3'	147
		AG74	R:5'-GGTGTAGAATTGCCGCATGG-3'	
		AG117	F:5'-CGCTAGCTTCATACAGGGGG-3'	171
		AG118	R:5'-AGTGTTTGCCCAACCTCACA-3'	
PME	Bradi5g17850	AG75	F:5'-ATGACGGCGTTCTTTGGGAT-3'	141
		AG76	R:5'-GAGCCAGTGGAATCCGTTGA-3'	
		AG77	F:5'-AGCCGTACATCACGTTCGAG-3'	129
		AG78	R:5'-ATAGAACGGTTACGGAGGCG-3'	
		AG119	F:5'-TCAACGGATTCCACTGGCTC-3'	106
		AG120	R:5'-TGCCTGTGCTGTACGAATGA-3'	
		AG121	F:5'-TCATTCGTACAGCACAGGCA-3'	140
		AG122	R:5'-GTGGAACTTGTGACCACCCT-3'	
PMEI	Bradi3g30770	AG79	F:5'-GGAGAAGGTTCGAGGTGGAC-3'	83
		AG80	R:5'-CTTGAACCCTTCCACGCACA-3'	
		AG123	F:5'-ATGATGATGACCAGACGCCG-3'	177
		AG124	R:5'-ATAGATGGGGCCGGGGATTA-3'	
		AG125	F:5'-CTGCTGCTTGTCGTCTCGTA-3'	167
		AG126	R:5'-TACGGGGACAGTGTCGAGTC-3'	
PMEI	Bradi5g27675	AG81	F:5'-CTTTTGGAGGCACGGGAGTC-3'	80
		AG82	R:5'-ACGAACGCCTCGTCGTAATA-3'	
		AG83	F:5'-TCCTGCTGCTCTCCGTATCT-3'	113
		AG84	R:5'-AAGGGCACGCACTAATACCG-3'	
		AG127	F:5'-AGCTAGCTAATGGCGACTGC-3'	131
		AG128	R:5'-CGAAACGTGGTGTGATGCTG-3'	
		AG129	F:5'-CTCTTCAGGAGGAAGCGAGTG-3'	143
		AG130	R:5'-CTTGAGCAGTCGCCATTAGC-3'	
PMEI	Bradi3g45080	LF66	F:5'-GTGGACTACCACTTCTGCGT-3'	132
		LF67	R:5'-CTTGATGTCGTACACCCCGT-3'	

		LF68	F:5'-GGTGTACGACATCAAGCGCA-3'	150
		LF69	R:5'-CTGATCCCGTCGTACGCCTC-3'	
LOX	Bradi1g11680	AG63	F:5'-ACAATGATCCCAGCCTCAAG-3'	76
		AG64	R:5'-TCGGAGGTATTGGGGTAGAG-3'	
		AG65	F:5'-TCGAGCAGTACGTGAACGAG-3'	91
		AG66	R:5'-TCCTTCCACCATGACTGTAGC-3'	
LOX1/LOX5	Bradi1g09270	AG85	F:5'-GCAAAAGCGTTGGAGGCATT-3'	123
		AG86	R:5'-GTATGGAAACTTGGCTGGGC-3'	
		AG87	F:5'-CTTCGTCATCGCCACAAGCC-3'	142
		AG88	R:5'-GGTCATCTCGATGATCCCGC-3'	
LOX1/LOX5	Bradi1g11670	AG89	F:5'-AATATCGCCCGTCGGAATCA-3'	143
		AG90	R:5'-CGCTCAGGAAAAAGGGACCA-3'	
		AG91	F:5'-TCAACTTGCCCTTTCCACATG-3'	100
		AG92	R:5'-GCAAACCGGATTAACTCCTGC-3'	
LOX2	Bradi3g07000	AG97	F:5'-ATCCATCTGAAGCAGCCTCT-3'	116
		AG98	R:5'-CGAGCTCCTCGTCTGATCTTC-3'	
LOX2	Bradi3g07010	AG99	F:5'-GAGCGGCCAGCAAATCAGA-3'	135
		AG100	R:5'-GTAGCCGTCACCGTCAGAG-3'	
LOX2	Bradi3g39980	AG101	F:5'-GATCCGTTGATCCCGCTAGT-3'	148
		AG102	R:5'-ACCTCATCTTGTTACCCCTCA-3'	
LOX3	Bradi5g11590	AG107	F:5'-GTGTTCAAGCTGCTCAAGCC-3'	80
		AG108	R:5'-TCGCCGTTGATGAGGATCTG-3'	
		AG109	F:5'-GATCCAGGAGAACAGCGAGG-3'	150
		AG110	R:5'-GGGAACTCCTGAAGACGCTC-3'	
LOX3	Bradi1g72690	AG93	F:5'-ATCTAAGAAGGCGGGGGAGT-3'	96
		AG94	R:5'-AGATGAGTTTGCAGATAGGCG-3'	
		AG95	F:5'-TGATCTCGGCTAAGAATCTGACT-3'	143
		AG96	R:5'-ACTCCCCCGCCTTCTTAGAT-3'	
LOX5	Bradi3g59942	AG111	F:5'-CGGCTCAATGAAAACGCCAT-3'	81
		AG112	R:5'-GACACACATGCCGATGATGC-3'	
LOX5	Bradi3g59710	AG103	F:5'-CTGGACTTCTACATCCCGCC-3'	145
		AG104	R:5'-GCTCCATGGACCTGAAGTCG-3'	
		AG105	F:5'-AACGACCTGTACAGCAAGCC-3'	133
		AG106	R:5'-GGAACTTGACGGGGTTCTCC-3'	

Appendix 6.

Appendix 6A. Real-time PCR analysis report on determining gene-specific primer amplification efficiency of Bradi2g21460.

Tm Calling, Abs Quant/2nd Derivative Max & standard curve for **Bradi2g21460 (AG01/AG02) –** CAM1

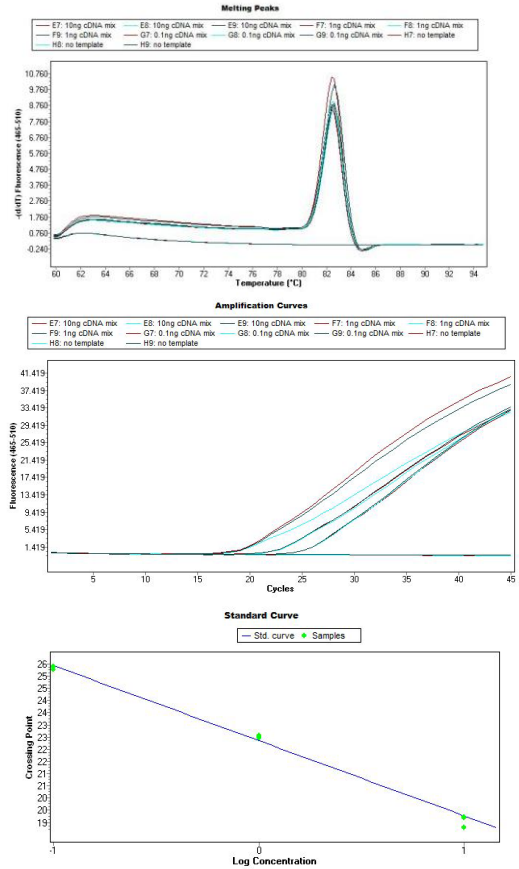

Tm Calling, Abs Quant/2nd Derivative Max & standard curve for **Bradi2g21460 (AG03/AG04) –** CAM1

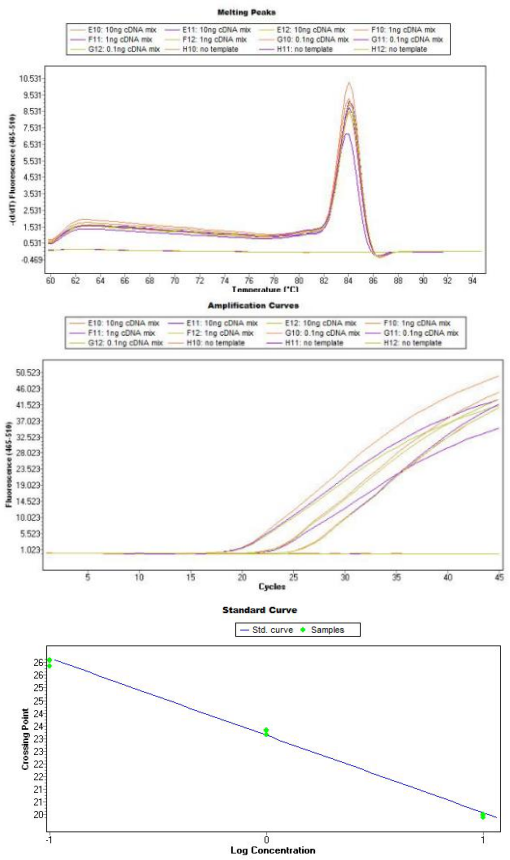

Appendix 6B. Real-time PCR analysis report on determining gene-specific primer amplification efficiency of Bradi2g10010.

Tm Calling, Abs Quant/2nd Derivative Max & standard curve for **Bradi2g10010 (AG05/AG06) –** CAM5

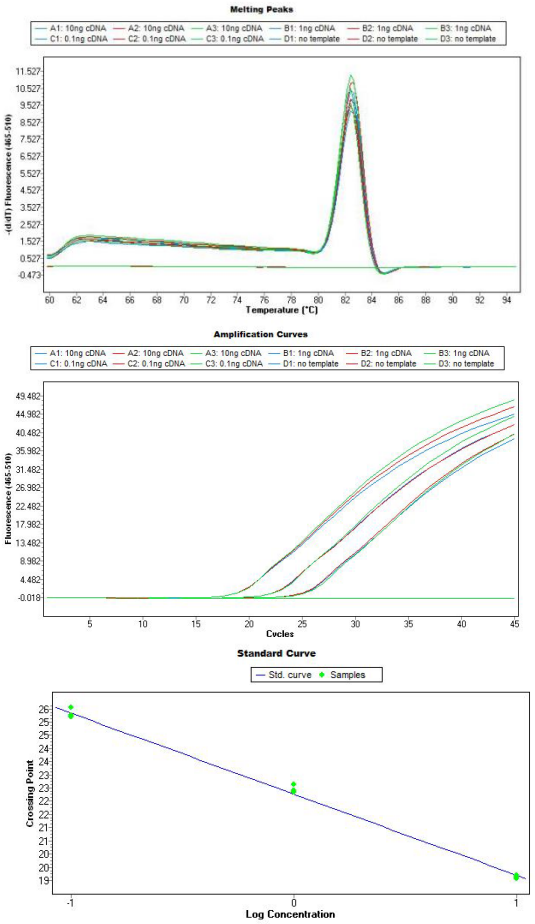

Tm Calling, Abs Quant/2nd Derivative Max & standard curve for **Bradi2g10010 (AG07/AG08) –** CAM5

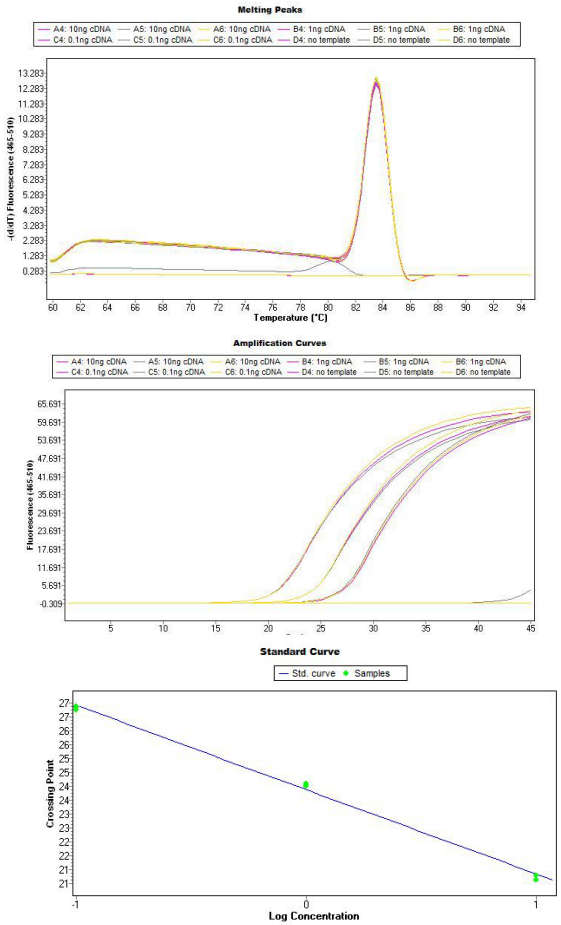

Appendix 6C. Real-time PCR analysis report on determining gene-specific primer amplification efficiency of Bradi1g17237.

Tm Calling, Abs Quant/2nd Derivative Max & standard curve for **Bradi1g17237 (AG09/AG10) –** CAM5

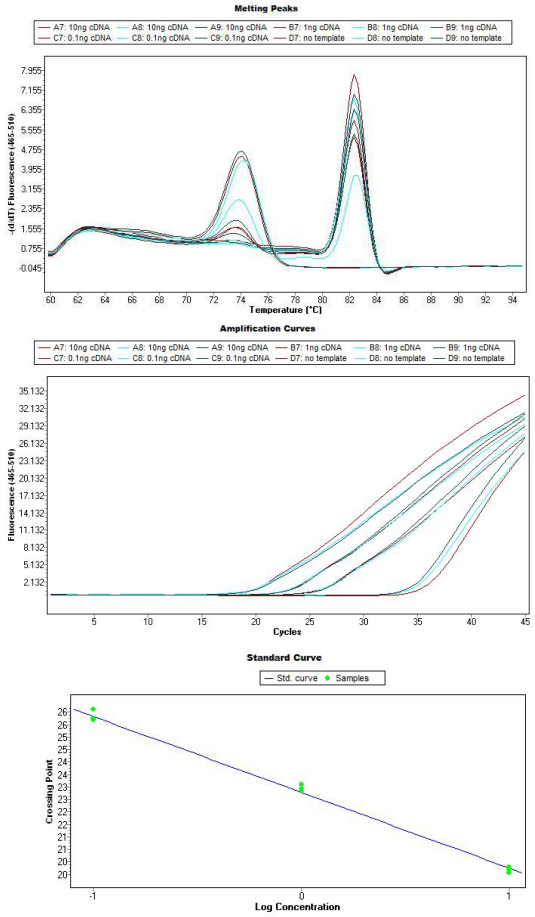

Tm Calling, Abs Quant/2nd Derivative Max & standard curve for **Bradi1g17237 (AG11/AG12) –** CAM5

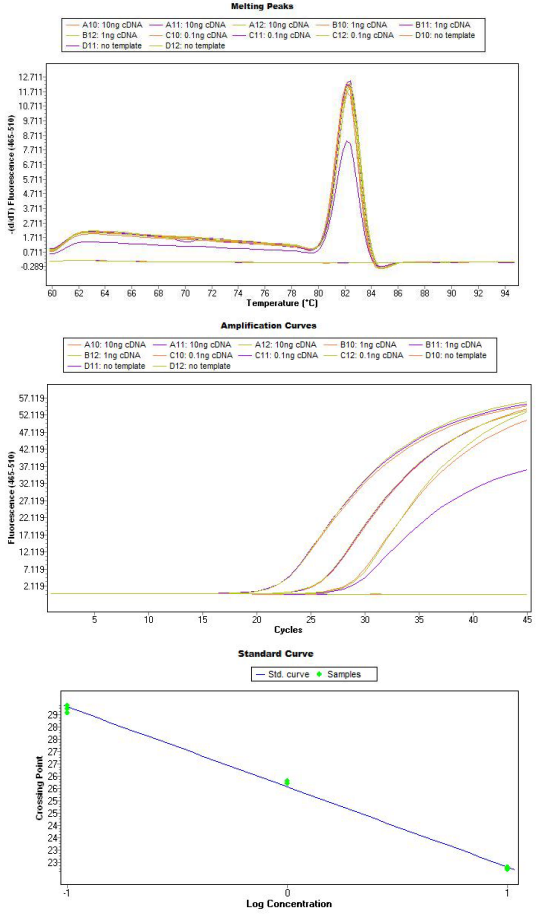

Appendix 6D. Real-time PCR analysis report on determining gene-specific primer amplification efficiency of Bradi2g10010.

Tm Calling, Abs Quant/2nd Derivative Max & standard curve for **Bradi1g33810 (AG21/AG22) –** GH

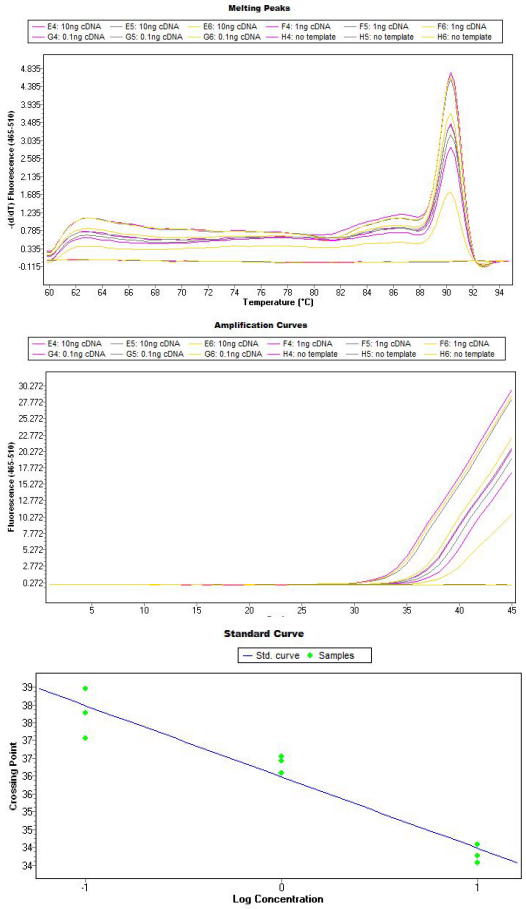

Tm Calling, Abs Quant/2nd Derivative Max & standard curve for **Bradi1g33810 (AG23/AG24) –** GH

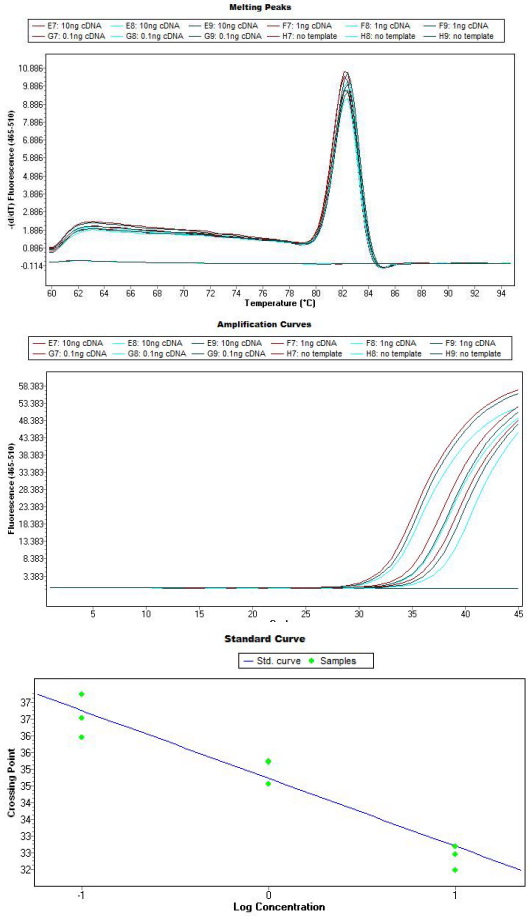

Appendix 6E. Real-time PCR analysis report on determining gene-specific primer amplification efficiency of Bradi1g33840 and Bradi2g51090

Tm Calling, Abs Quant/2nd Derivative Max & standard curve for **Bradi1g33840 (AG27/AG28) –** GH

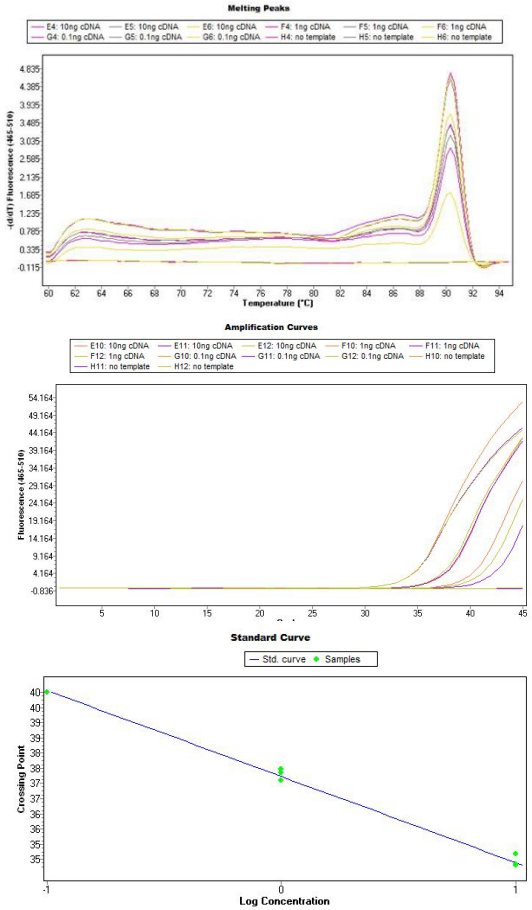

Tm Calling, Abs Quant/2nd Derivative Max & standard curve for **Bradi2g51090 (AG19/AG20) –** CLM23

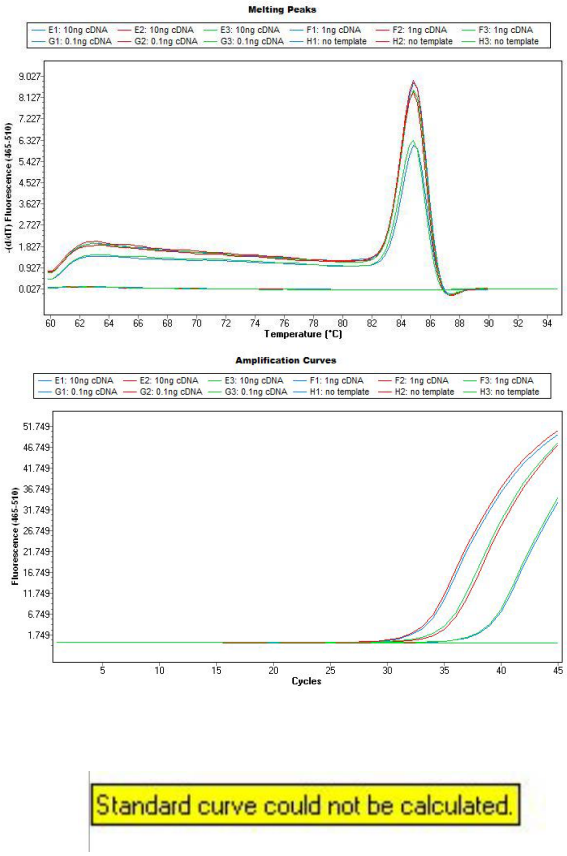

Appendix 6F. Real-time PCR analysis report on determining gene-specific primer amplification efficiency of Bradi1g76260.

Tm Calling, Abs Quant/2nd Derivative Max & standard curve for **Bradi1g76260 (AG37/AG38) –** ExpA1

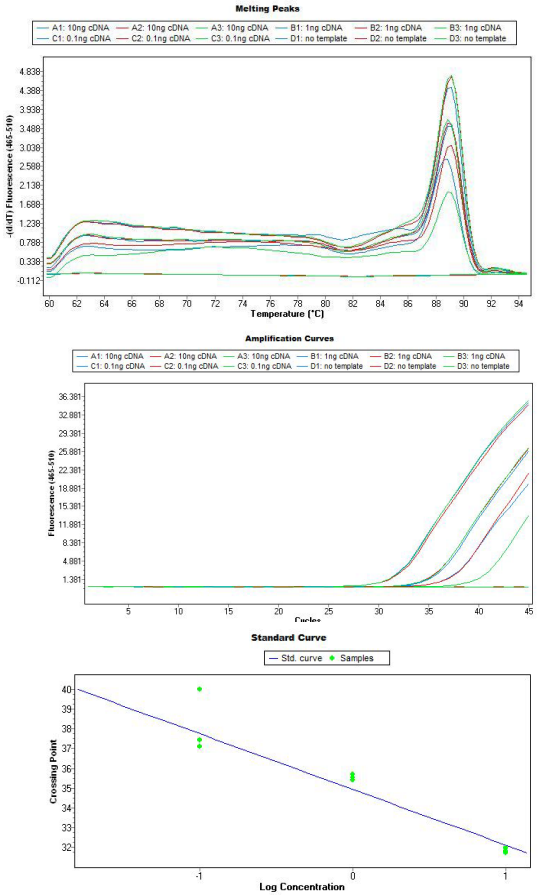

Tm Calling, Abs Quant/2nd Derivative Max & standard curve for **Bradi1g76260 (AG39/AG40) –** ExpA1

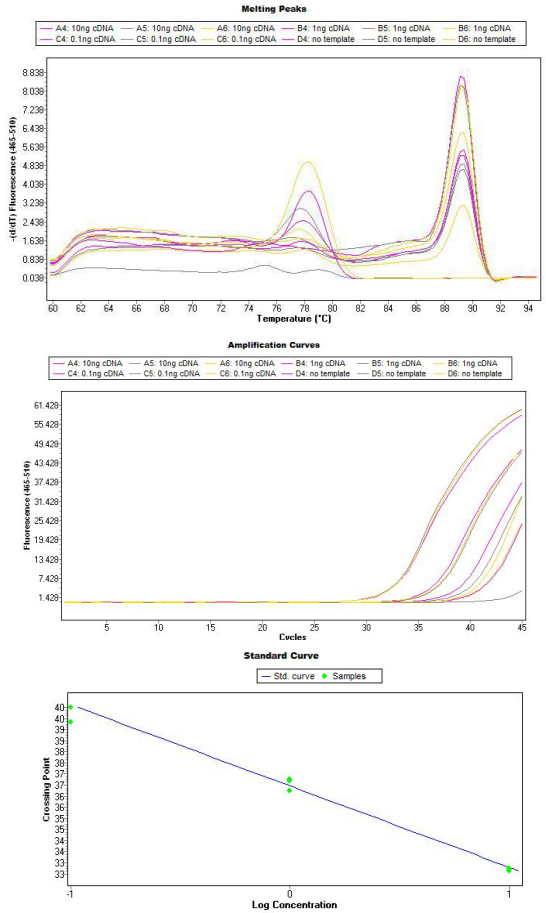

Appendix 6G. Real-time PCR analysis report on determining gene-specific primer amplification efficiency of Bradi1g76270.

Tm Calling, Abs Quant/2nd Derivative Max & standard curve for **Bradi1g76270 (AG41/AG42) –** ExpA1

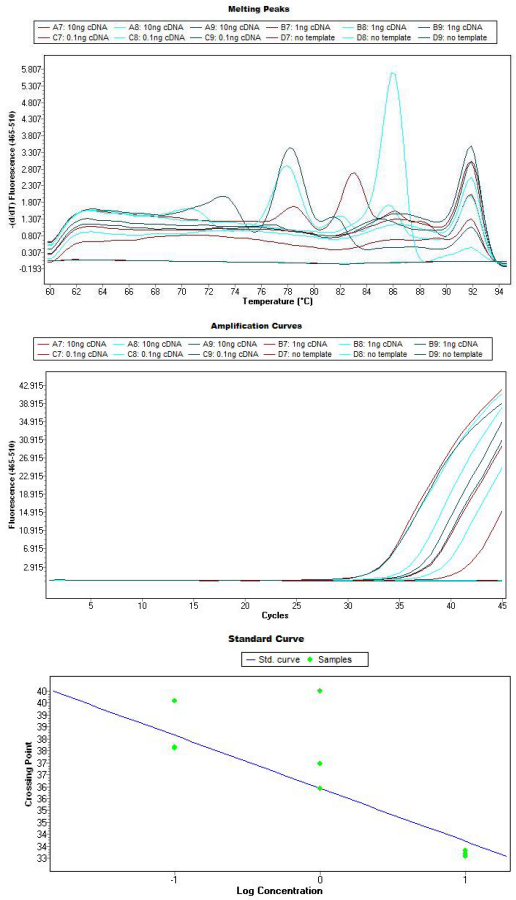

Tm Calling, Abs Quant/2nd Derivative Max & standard curve for **Bradi1g76270 (AG43/AG44) –** ExpA1

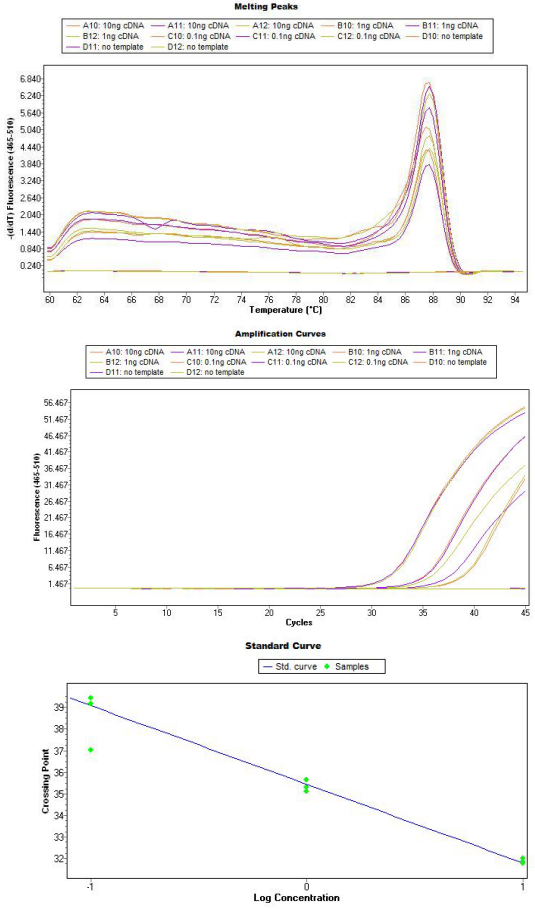

Appendix 6H. Real-time PCR analysis report on determining gene-specific primer amplification efficiency of Bradi1g28130 and Bradi1g50170.

Tm Calling, Abs Quant/2nd Derivative Max & standard curve for **Bradi1g28130 (AG45/AG46) –** ExpA3

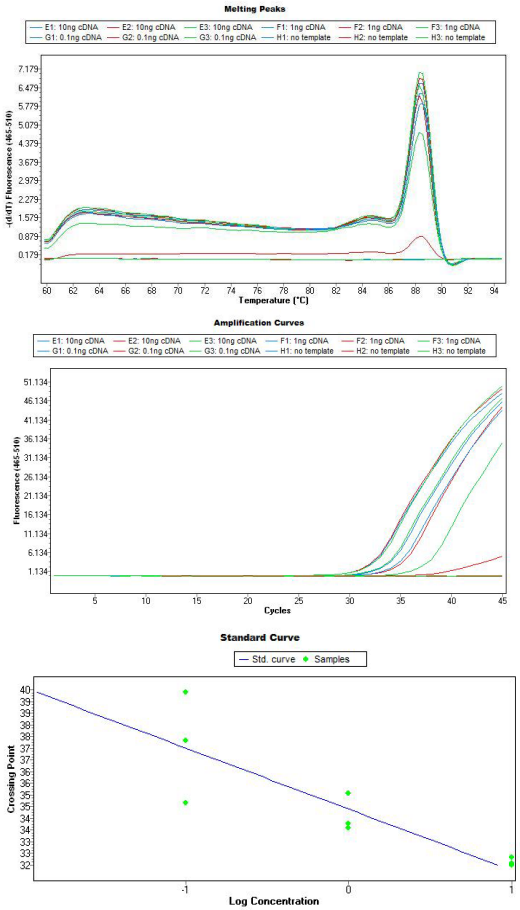

Tm Calling, Abs Quant/2nd Derivative Max & standard curve for **Bradi1g50170 (AG53/AG54**) **–** CSLD2

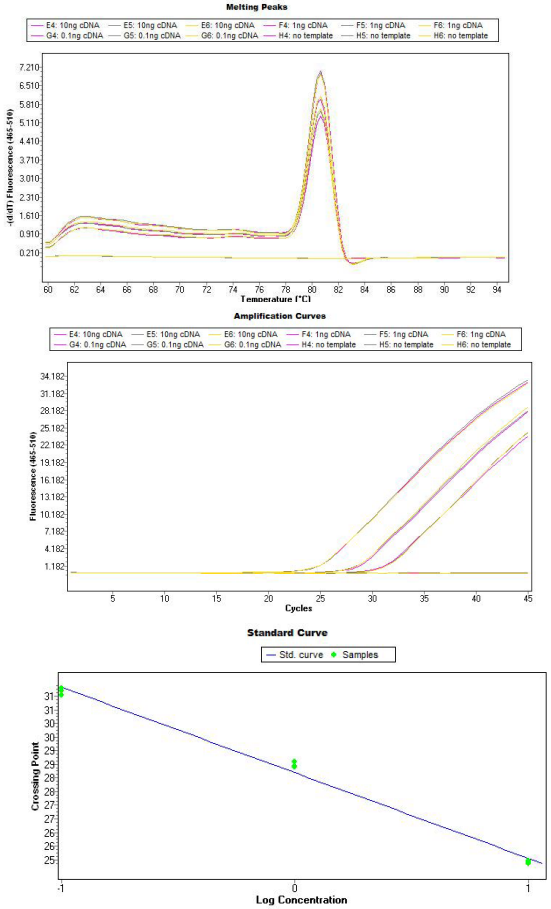

Appendix 6I. Real-time PCR analysis report on determining gene-specific primer amplification efficiency of Bradi3g03520 and Bradi5g2431.

Tm Calling, Abs Quant/2nd Derivative Max & standard curve for **Bradi3g03520 (AG59/AG60) –** b-Glu

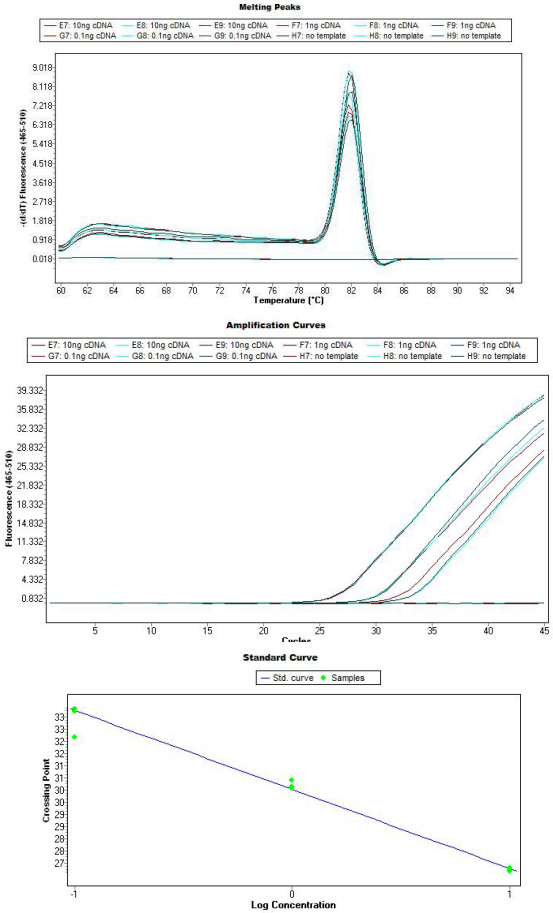

Tm Calling, Abs Quant/2nd Derivative Max & standard curve for **Bradi5g24311 (AG61/AG62) –** WAK

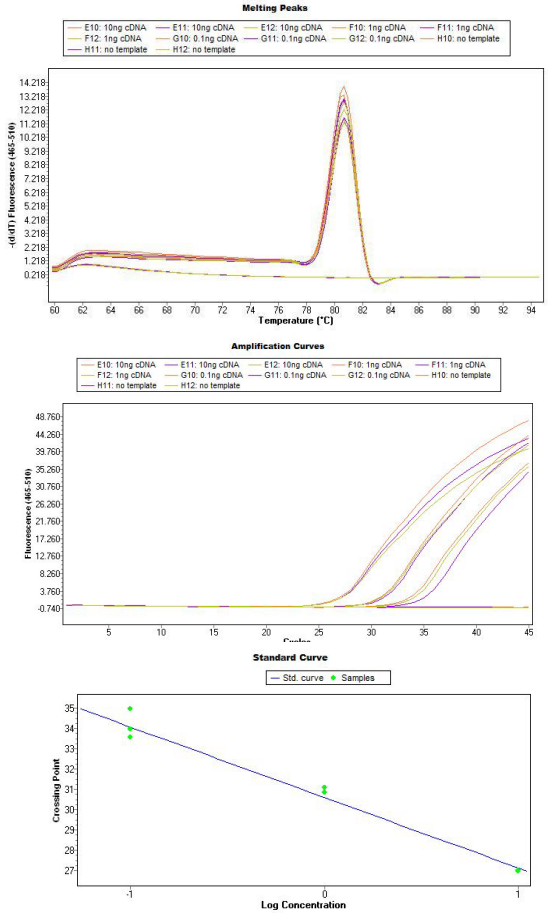

Appendix 6J. Real-time PCR analysis report on determining gene-specific primer amplification efficiency of Bradi1g17850.

Tm Calling, Abs Quant/2nd Derivative Max & standard curve for **Bradi1g17850 (AG75/AG76) –** PME

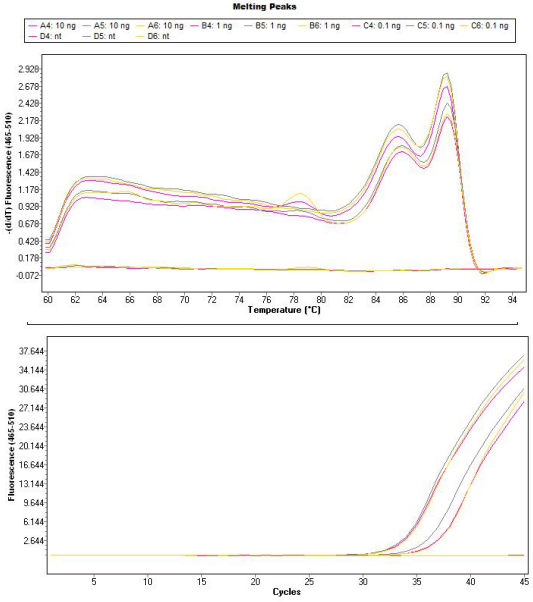

Standard curve could not be calculated.

Tm Calling, Abs Quant/2nd Derivative Max & standard curve for **Bradi1g17850 (AG119/AG120) –** PME

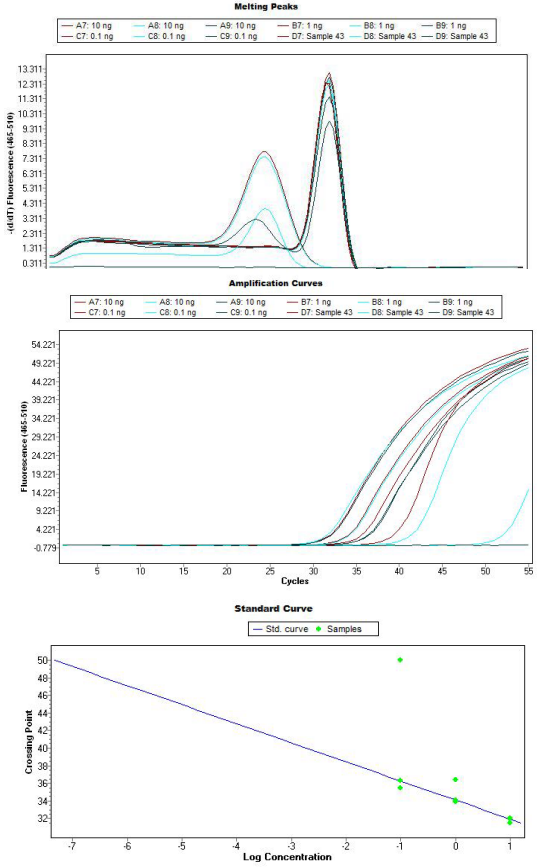

Tm Calling, Abs Quant/2nd Derivative Max & standard curve for **Bradi1g178500 (AG121/AG122) –** PME

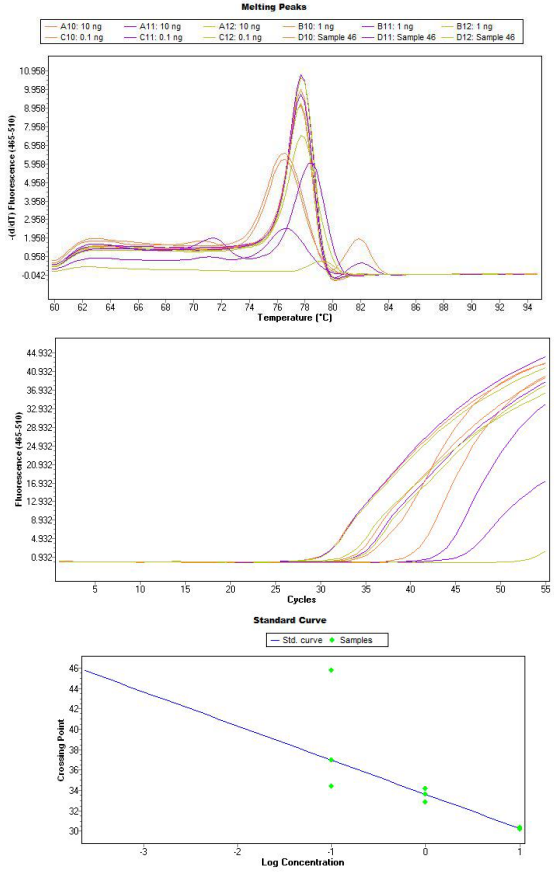

Appendix 6K. Real-time PCR analysis report on determining gene-specific primer amplification efficiency of Bradi2g5682.

Tm Calling, Abs Quant/2nd Derivative Max & standard curve for **Bradi2g56820 (AG71/AG72) –** PME

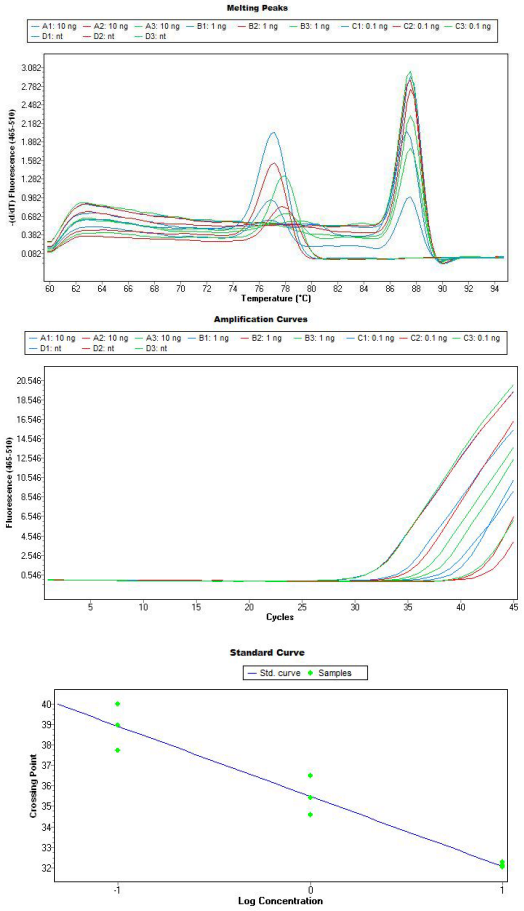

Tm Calling, Abs Quant/2nd Derivative Max & standard curve for **Bradi2g56820 (AG117/AG118**) **–** PME

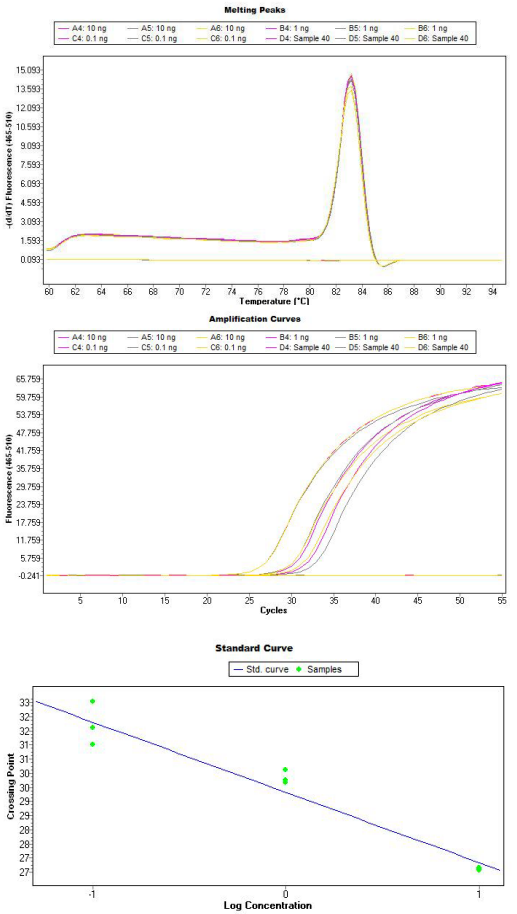

Appendix 6L. Real-time PCR analysis report on determining gene-specific primer amplification efficiency of Bradi2g11860 and Bradi5g27675.

Tm Calling, Abs Quant/2nd Derivative Max & standard curve for **Bradi2g11860 (AG115/AG116) –** PME

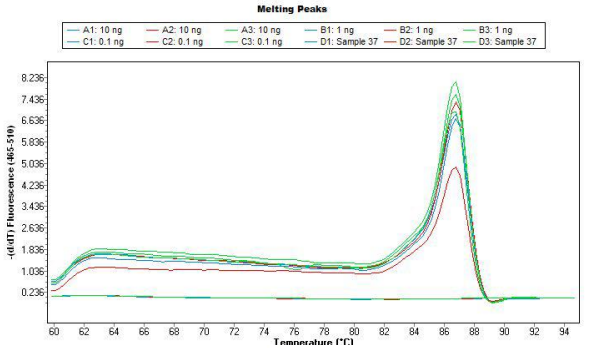

Standard curve could not be calculated.

Tm Calling, Abs Quant/2nd Derivative Max & standard curve for **Bradi5g27675 (AG129/AG130**) **–** PMEI

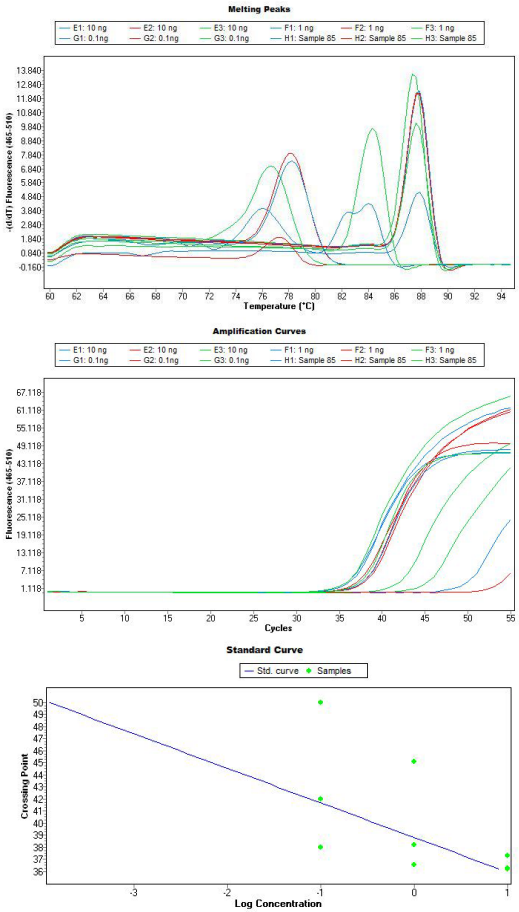

Appendix 6M. Real-time PCR analysis report on determining gene-specific primer amplification efficiency of Bradi1g11680.

Tm Calling, Abs Quant/2nd Derivative Max & standard curve for **Bradi1g11680 (AG63/AG64) –** LOX

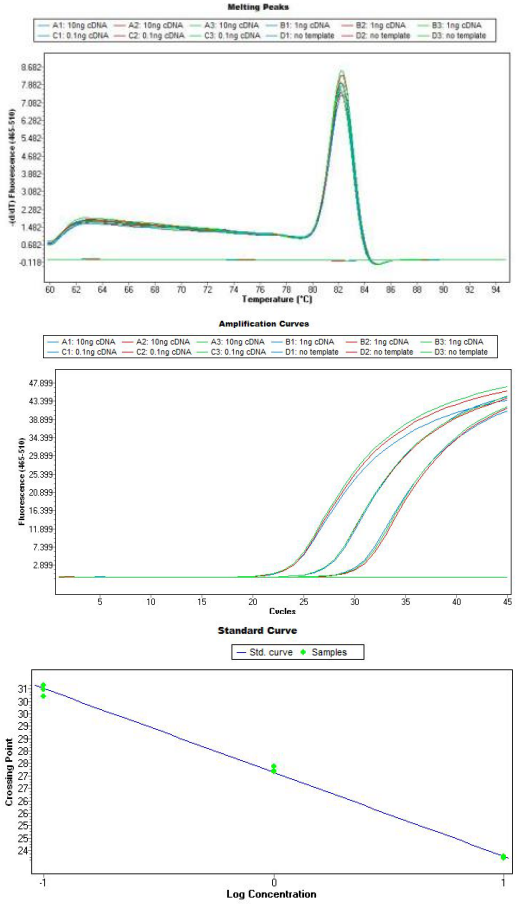

Tm Calling, Abs Quant/2nd Derivative Max & standard curve for **Bradi1g11680 (AG65/AG66) –** LOX

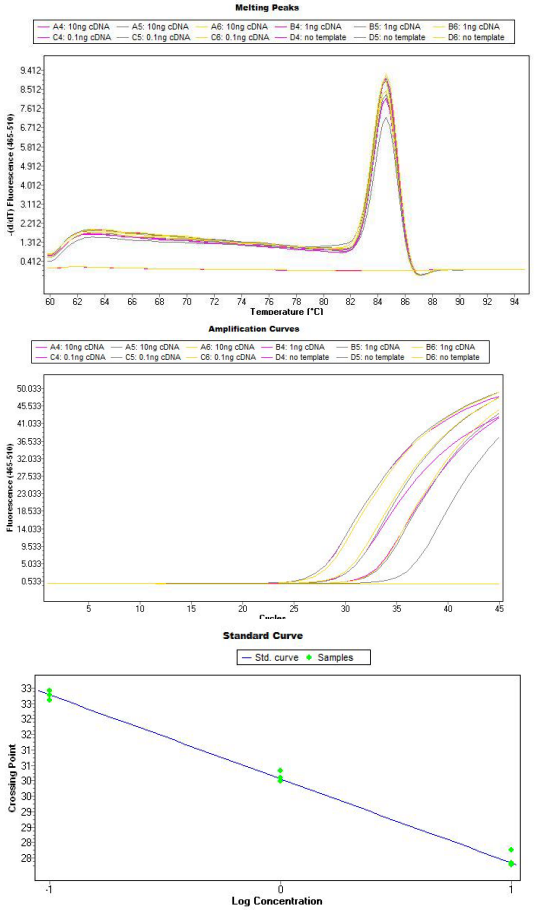

Appendix 6N. Real-time PCR analysis report on determining gene-specific primer amplification efficiency of Bradi1g09270.

Tm Calling, Abs Quant/2nd Derivative Max & standard curve for **Bradi1g09270 (AG85/AG86) –** LOX1/LOX5

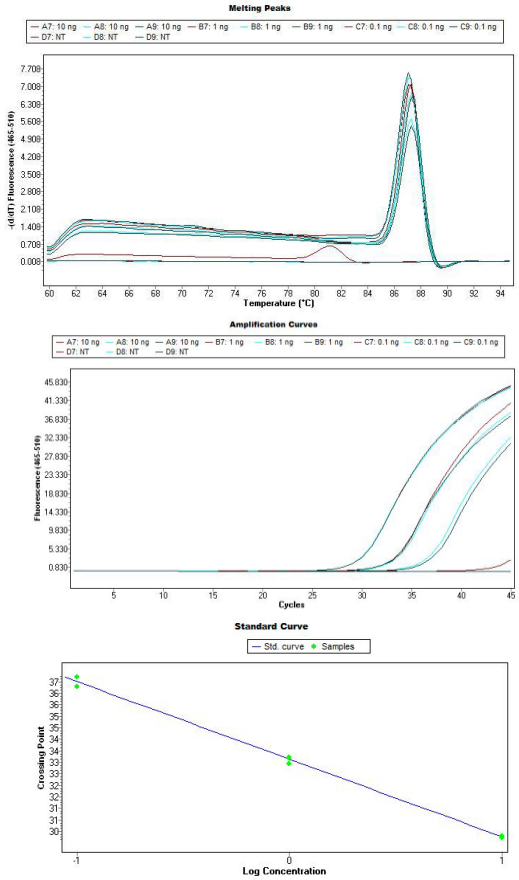

Tm Calling, Abs Quant/2nd Derivative Max & standard curve for **Bradi1g09270 (AG87/AG88) –** LOX1/LOX5

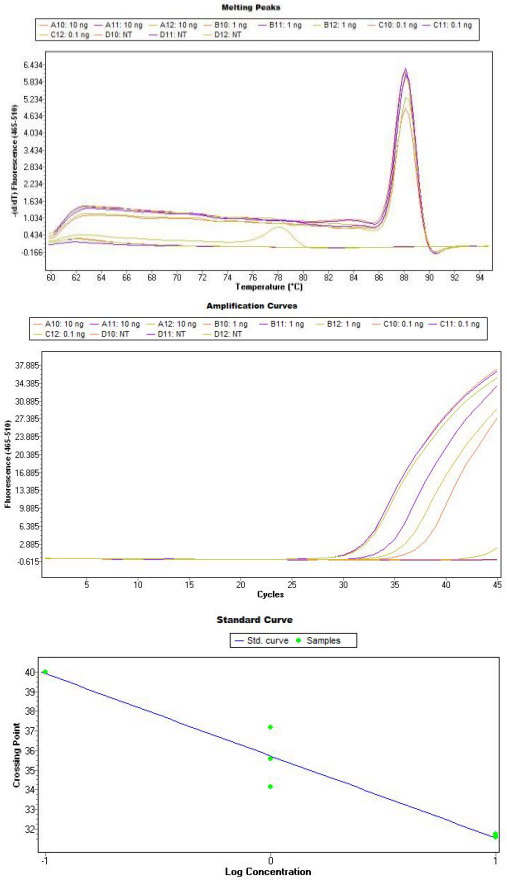

Appendix 6O. Real-time PCR analysis report on determining gene-specific primer amplification efficiency of Bradi1g11670.

Tm Calling, Abs Quant/2nd Derivative Max & standard curve for **Bradi1g11670 (AG89/AG90) –** LOX1/LOX5

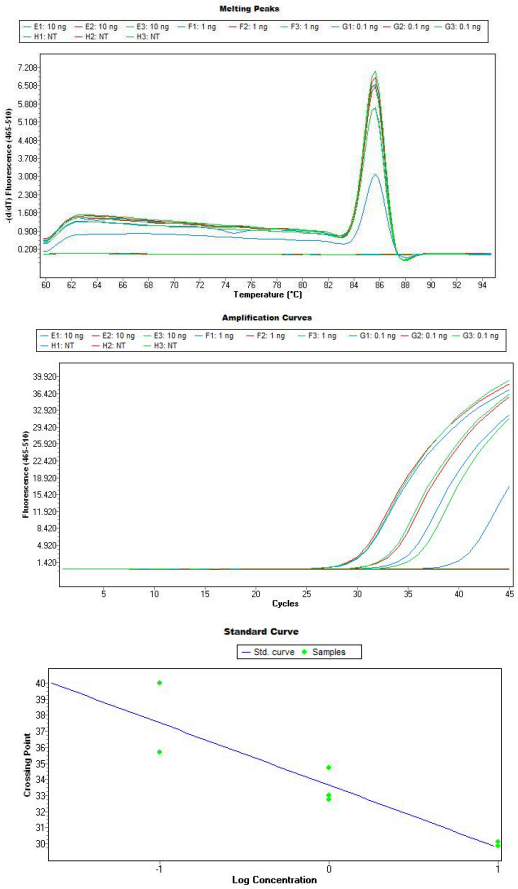

Tm Calling, Abs Quant/2nd Derivative Max & standard curve for **Bradi1g11670 (AG91/AG92) –** LOX1/LOX5

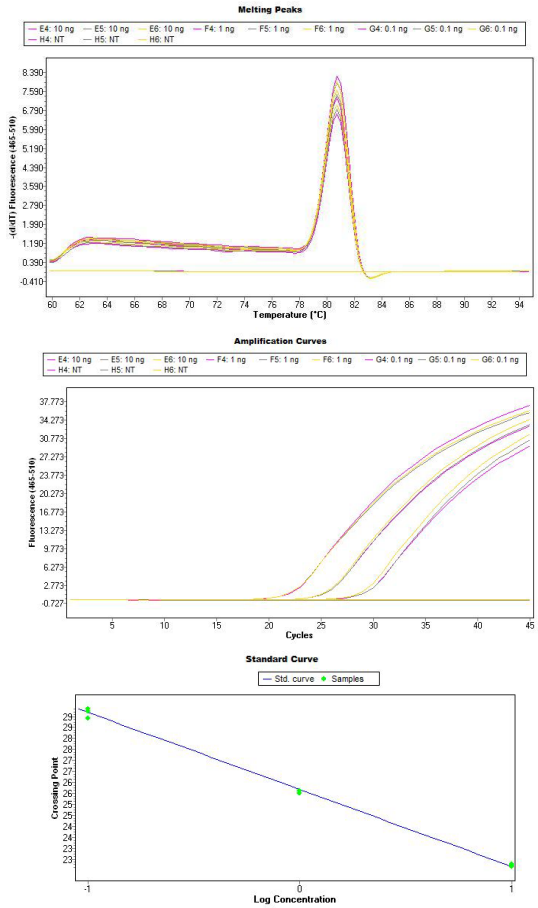

Appendix 6P. Real-time PCR analysis report on determining gene-specific primer amplification efficiency of Bradi1g72690.

Tm Calling, Abs Quant/2nd Derivative Max & standard curve for **Bradi1g72690 (AG93/AG94) –** LOX3

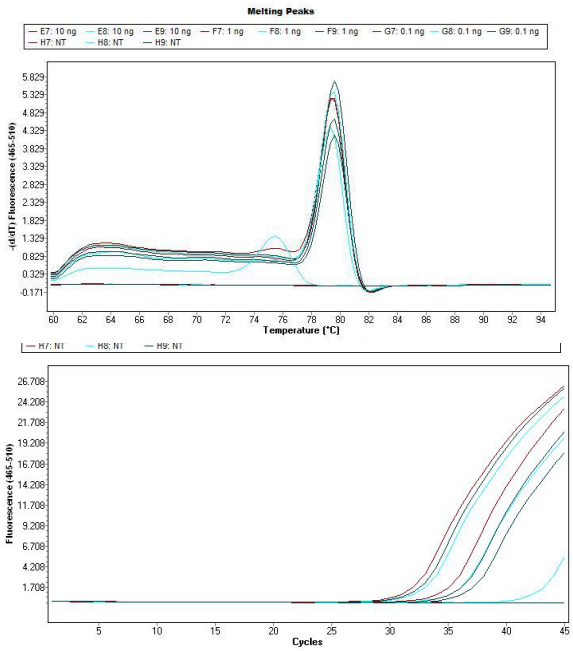

Standard curve could not be calculated.

Tm Calling, Abs Quant/2nd Derivative Max & standard curve for **Bradi1g72690 (AG95/AG96) –** LOX3

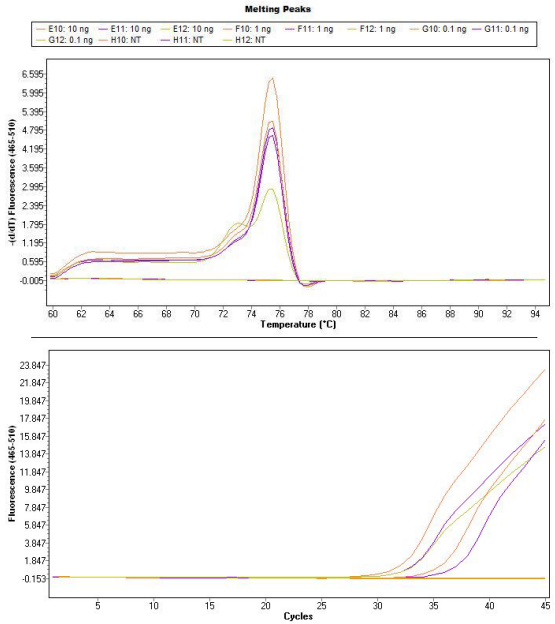

Standard curve could not be calculated.

Appendix 6R. Real-time PCR analysis report on determining gene-specific primer amplification efficiency of Bradi5g11590.

Tm Calling, Abs Quant/2nd Derivative Max & standard curve for **Bradi5g11590 (AG107/AG108) –** LOX3

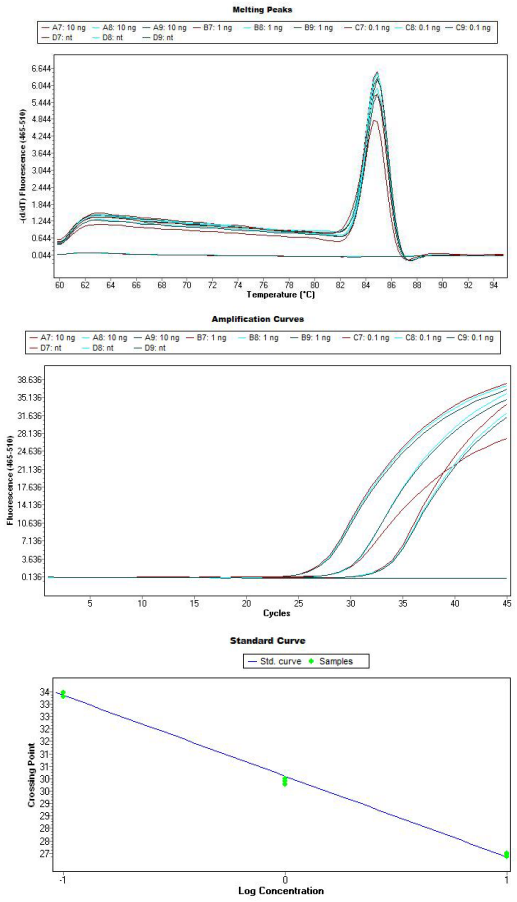

Tm Calling, Abs Quant/2nd Derivative Max & standard curve for **Bradi5g11590 (AG109/AG110) –** LOX3

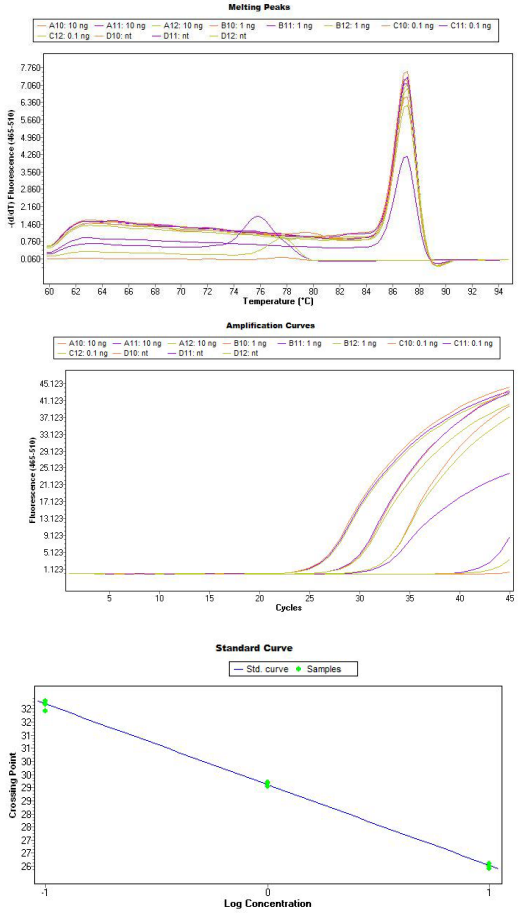

Appendix 6S. Real-time PCR analysis report on determining gene-specific primer amplification efficiency of Bradi3g39980, Bradi3g59710 and Bradi3g59942.

Tm Calling, Abs Quant/2nd Derivative Max & standard curve for **Bradi3g39980 (AG101/AG102) –** LOX2

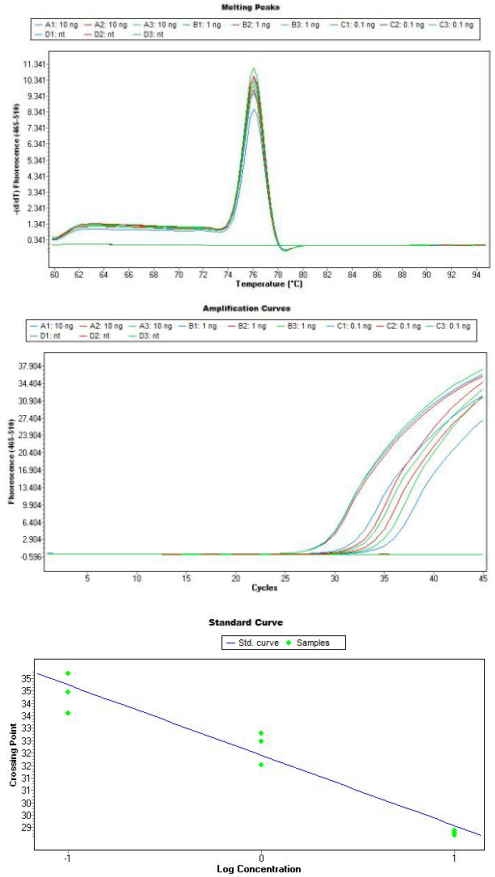

Tm Calling, Abs Quant/2nd Derivative Max & standard curve for **Bradi3g59710 (AG105/AG106) –** LOX5

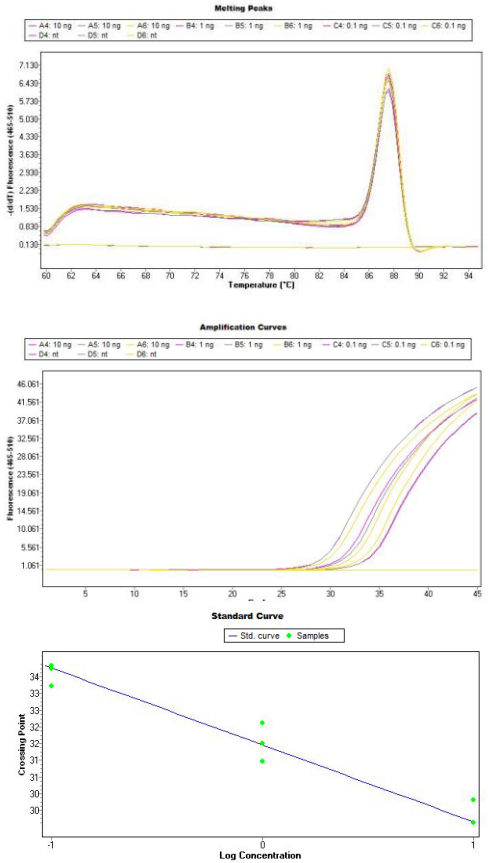

Tm Calling, Abs Quant/2nd Derivative Max & standard curve for **Bradi3g59942 (AG111/AG112) –** LOX5

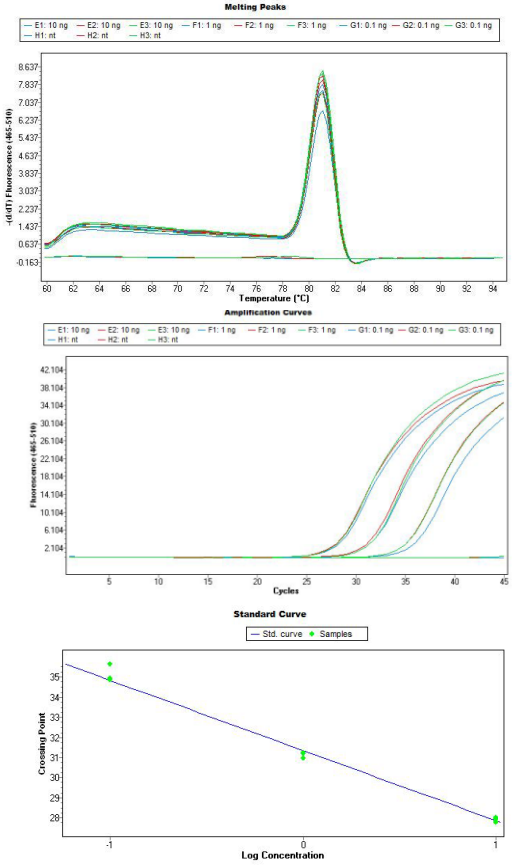

Appendix 6T. Real-time PCR analysis report on determining gene-specific primer amplification efficiency of Bradi5g14640 and Bradi4g00660.

Tm Calling, Abs Quant/2nd Derivative Max & standard curve for **Bradi5g14640 (LF72/LF73) –** Reference gene

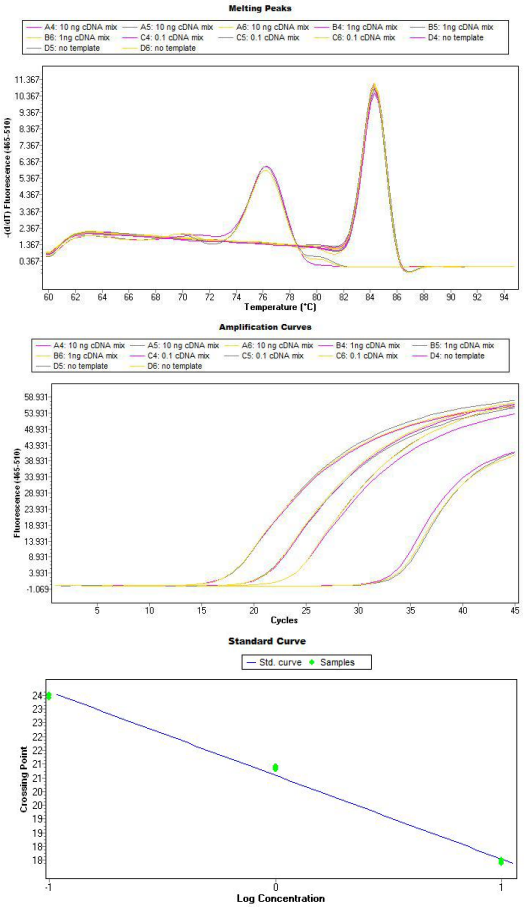

Tm Calling, Abs Quant/2nd Derivative Max & standard curve for **Bradi4g00660 (LF74/LF76) –** Reference gene

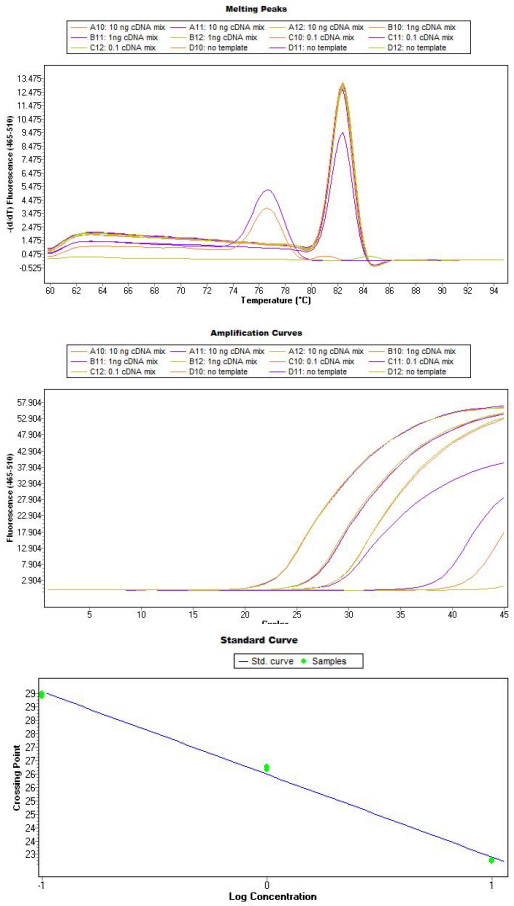

Appendix 7. Expression levels of PME/PMEI genes

Pectin methylesterase genes and pectin methylesterase inhibitor genes showing expression in early inflorescence and/or emerging inflorescence and/or leaves. Expression levels were analysed with the use of EnsemblPlants database and EMBL-EBI Expression Atlas. Expression values are given in TPM units (Transcripts Per Kilobase Million).

Gene	Family	Early inflorescence	Emerging inflorescence	Leaf
Bradi5g17850	PME	223	134	0
Bradi3g30770	PMEI	2	20	151
Bradi2g11860	PME	15	85	13
Bradi5g27675	PMEI	33	55	0
Bradi2g56820	PME	38	40	13
Bradi3g45080	PMEI	20	3	3
Bradi3g13275	PMEI	12	19	0.6
Bradi2g49500	PME	11	18	0
Bradi2g19420	PME	15	17	0
Bradi3g37340	PME	16	17	0
Bradi1g15230	PMEI	16	15	0.7
Bradi1g34920	PMEI	12	16	0
Bradi3g52060	PMEI	14	2	0
Bradi3g24750	PME	12	12	10
Bradi1g17940	PME	12	8	0
Bradi2g09090	PME	4	4	0
Bradi2g08950	PMEI	0	4	2
Bradi5g10700	PME	3	2	1
Bradi2g52140	PME	1	3	1
Bradi4g38250	PMEI	0	0	2
Bradi2g00930	PMEI	0.6	0.9	0
Bradi2g27930	PME	0	0	0.9

Appendix 8. 9-lipoxygenase and 9-hydroperoxide lyase pathway

Appendix 8A. 9-lipoxygenase and 9-hydroperoxide lyase pathway – scheme

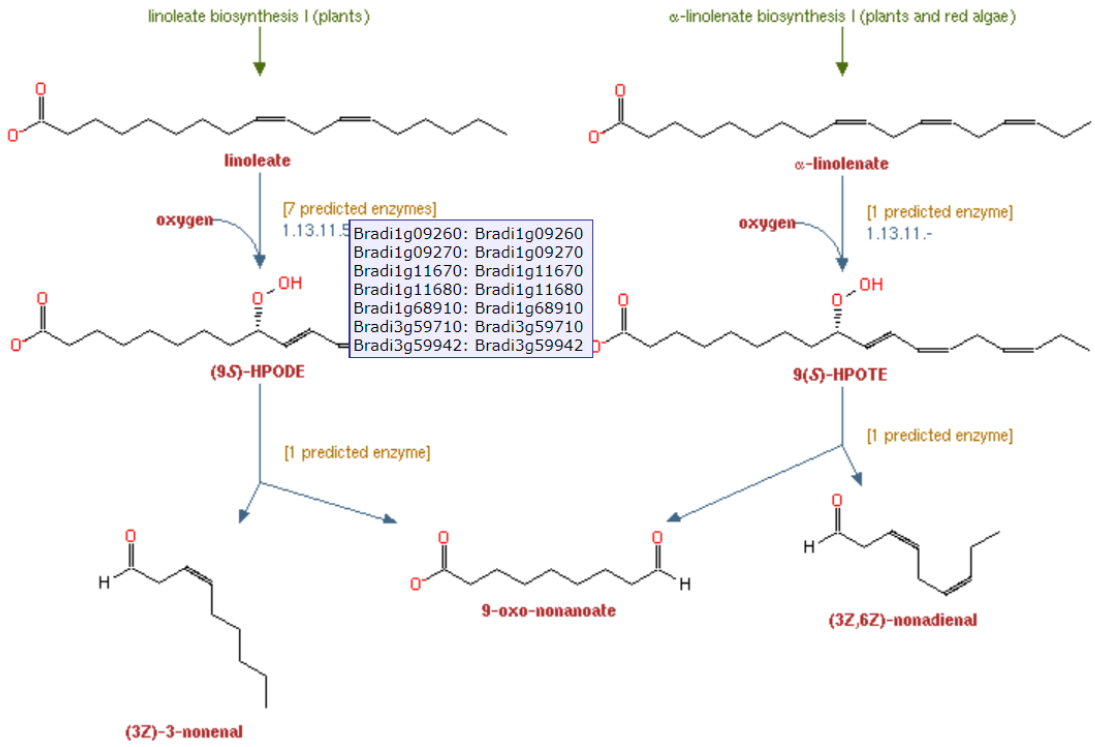

Appendix 8B. 9-lipoxygenase and 9-hydroperoxide lyase pathway – genes.

List of genes belonging to 9-lipoxygenase and 9-hydroperoxide lyase pathway with expression levels in early inflorescence and/or emerging inflorescence and/or leaves. Expression levels are given in TPM units (Transcripts Per Kilobase Million).

Gene	Family	Early inflorescence	Emerging inflorescence	Leaf
Bradi3g59942	LOX	2	5	4
Bradi1g09270	LOX	2	2	0
Bradi1g11680	LOX	366	333	38
Bradi3g59710	LOX	6	6	15
Bradi1g09260	LOX	0	0	0
Bradi3g08160	Cytochrome P450	121	42	7
Bradi1g68910	Proline-rich family protein	27	14	16

Appendix 9. Lipoxygenase genes with expression levels.

List of Lipoxygenase genes with expression levels above zero in early inflorescence and/or emerging inflorescence and/or leaves. Expression levels are given in TPM units (Transcripts Per Kilobase Million). * Indicates genes, which belong to 9-lipoxygenase and 9-hydroperoxide lyase pathways.

Gene	Family	Early inflorescence	Emerging inflorescence	Leaf
Bradi1g11680*	LOX	366	333	38
Bradi3g07000	LOX	84	346	457
Bradi3g07010	LOX	89	441	38
Bradi1g11670	LOX	102	93	68
Bradi1g72690	LOX	24	29	12
Bradi5g11590	LOX	5	5	23
Bradi3g59710*	LOX	6	6	15
Bradi3g59942*	LOX	2	5	4
Bradi1g09270*	LOX	2	2	0
Bradi3g39980	LOX	0	0	1

Appendix 10.

Appendix 10A. Top 20 metabolites showing the biggest differences between treatments in Bd21 detected by mass spectrometry in negative ionisation mode.

m/z	Adduct	*P* value	Tentative ID	Pathway
392.06276	[M+FA-H]1-	2.59E-18	Deoxyguanylic acid	Purine metabolism
393.06624	[M+Cl]1-	3.16E-18	Pantetheine 4'-phosphate	Pantothenate and CoA biosynthesis
311.16888	[3M-H]1-	7.07E-18	2,3-Diaminopropanoate	-
339.20014	[M+Na-2H]1-	1.30E-17	Ent-7-α-hydroxykaurenoate	GA12 biosynthesis
567.16082	[2M+Hac-H]1-	2.75E-17	L-Arginine phosphate	Arginine and Proline metabolism
325.18443	[2M+Hac-H]1-	2.86E-17	1,1-Diethyl-2-hydroxy-2-nitrosohydrazine	-
566.15775	[3M-H]1-	3.37E-17	N-Acetyl-L-glutamate	Arginine biosynthesis
496.11002	[M+K-2H]1-	1.62E-16	5-methyl-THF	Folate transformations
297.15302	[M-H]1-	1.96E-16	Ostruthin	-
326.18792	[M+Hac-H]1-	2.96E-16	Adenosine	Salvage pathways of purine nucleosides
456.17216	[M-H]1-	3.05E-16	5,10-methylene-THF	Folate transformations
346.26015	[M-H]1-	4.36E-16	Anandamide	Anandamide degradation
420.09356	[M+TFA-H]1-	8.79E-16	Glutathione	Cysteine and methionine metabolism
312.17232	[M+Na-2H]1-	2.22E-15	12-OPDA	Alpha-Linolenic acid metabolism
696.41264	[M+K-2H]1-	2.74E-15	Phytate	Lipid-independent phytate biosynthesis
283.26427	[M-H]1-	4.13E-15	Octadecanoic acid	Fatty acid biosynthesis
588.1365	[M+FA-H]1-	8.22E-15	CMP-3-deoxy-D-manno-octulosonate	CMP-KDO biosynthesis II
347.94937	[M+Br]1-	1.20E-14	N-acetylglutamyl-phosphate	Arginine biosynthesis II
329.06674	[M-H]1-	1.33E-14	3,7-Di-O-methylquercetin	Flavone and flavonol biosynthesis
284.26772	[M-H]1-	1.48E-14	(R,S)-Coclaurine	-

A heat map with top 20 metabolites showing the biggest differences between treatments in Bd21 detected by mass spectrometry in negative ionisation mode.

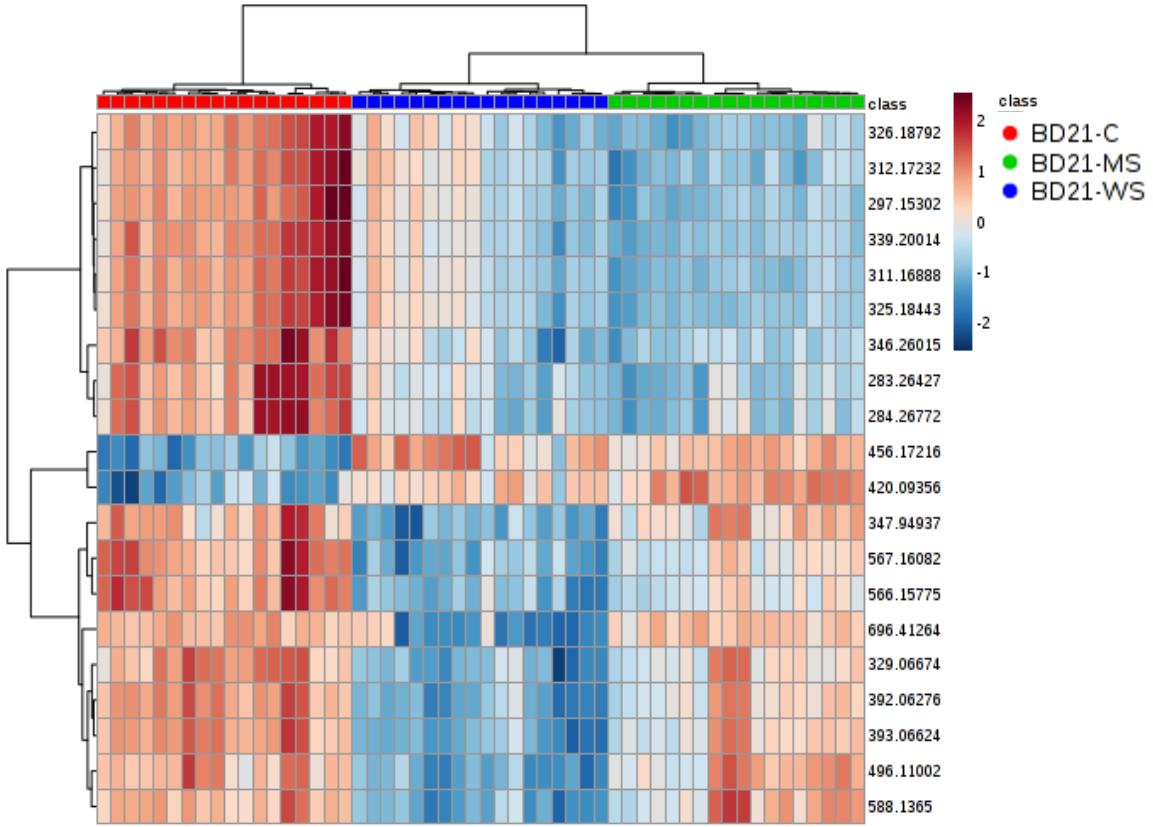

Appendix 10B. Top 20 metabolites showing the biggest differences between treatments in Bd21 detected by mass spectrometry in positive ionisation mode.

m/z	Adduct	*P* value	Tentative ID	Pathway
594.10863	[2M+NH4]1+	1.26E-20	2-Dehydro-3-deoxy-D-arabino-heptonate 7-phosphate	Phenylalanine, tyrosine and tryptophan biosynthesis
543.13179	[M+K]1+	2.15E-19	Raffinose	Galactose Metabolism
593.10538	[M+H-FA]1+	4.16E-19	Luteolin 7-O-[beta-D-glucuronosyl-(1->2)-beta-D-glucuronide]	Flavone and flavonol biosynthesis
544.13545	[M+2ACN+H]1+	5.52E-19	CDP-N-methylethanolamine	-
339.04727	[M+Na]1+	1.15E-17	3-O-Methylquercetin	Flavone and flavonol biosynthesis
116.0709	[M+H]1+	1.99E-17	L-Proline	Arginine and Proline Metabolism
565.11055	[2M+H]1+	2.64E-17	Pseudobaptigenin	Isoflavonoid biosynthesis
644.0834	[M+K]1+	3.54E-17	Guanosine diphosphate mannose	Amino sugar and nucleotide sugar metabolism
473.08411	[2M+Na]1+	6.81E-17	4-amino-4-deoxychorismate	Tetrahydrofolate biosynthesis
483.10501	[2M+Na]1+	1.84E-16	Bis-noryangonin	Resveratrol biosynthesis
369.03675	[2M+H]1+	1.91E-16	L-3,4-Dihydroxybutan-2-one 4-phosphate	Riboflavin metabolism
496.14226	[M+K]1+	2.29E-16	5,10-methylene-THF	Glycine biosynthesis
117.56326	[M+2H]2+	8.79E-16	N(omega)-Nitro-L-arginine methyl ester	-
563.09471	[2M+Na]1+	1.16E-15	Apigenin	Flavonoid biosynthesis
451.33334	[M+K]1+	1.46E-15	4α-methylfecosterol	Sterol biosynthesis
566.11383	[M+NH4]1+	2.87E-15	dTDP-α-L-rhamnose	dTDP-L-rhamnose biosynthesis I
745.03524	[2M+K]1+	3.77E-15	2,5-diamino-6-(ribosylamino)-4-(3H)-pyrimidinone 5'-phosphate	Flavin biosynthesis
526.82666	[M+2Na-H]1+	3.85E-15	Deoxythymidine triphosphate	Pyrimidine metabolism
156.98957	[M+H]1+	6.38E-15	2-Phosphoglycolate	Glyoxylate and dicarboxylate metabolism
154.02646	[M1+.]1+	2.82E-14	2,3-Dihydroxybenzoate	Benzoate degradation

A heat map with top 20 metabolites showing the biggest differences between treatments in Bd21 detected by mass spectrometry in positive ionisation mode.

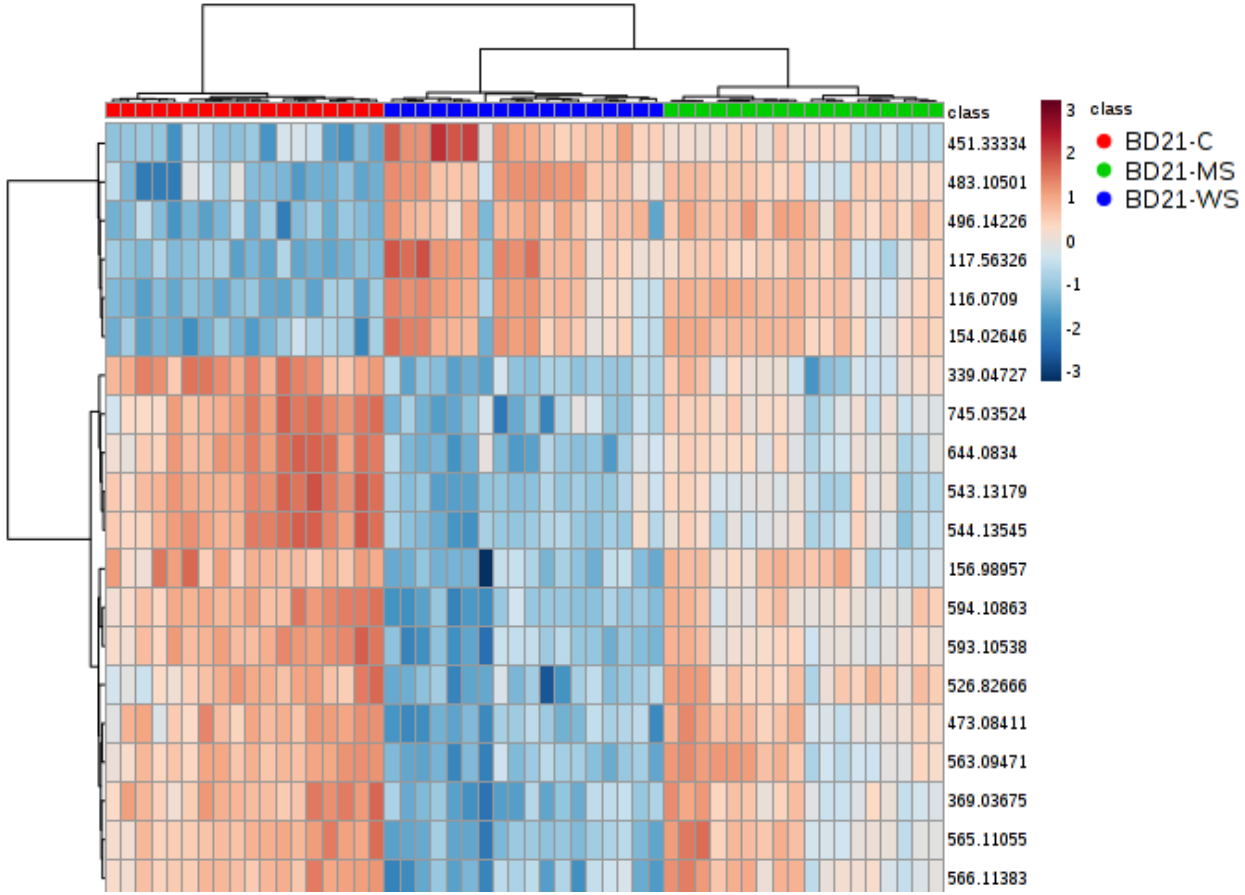

Appendix 10C. Top 20 metabolites showing the biggest differences between treatments in ABR6 detected by mass spectrometry in negative ionisation mode.

m/z	Adduct	*P* value	Tentative ID	Pathway
380.6005	[M-H]1-	3.22E-24	Sphinganine 1-phosphate	Sphingolipid Metabolism
1051.288	[2M-H]1-	1.03E-15	Inumakilactone A glycoside	-
443.1346	[2M-H]1-	1.21E-14	Cystathionine	Methionine Biosynthesis II
480.7728	[M-2H]2-	4.25E-14	3-Oxododecanoyl-CoA	Fatty acid Metabolism
507.1338	[2M-H]1-	7.06E-14	L-Arginine phosphate	Arginine and Proline Metabolism
413.1241	[M+Cl]1-	1.07E-13	Reduced riboflavin	Riboflavin Metabolism
134.9145	[M+K-2H]1-	1.22E-13	Sulfate	Purine Metabolism
481.1087	[M+Cl]1-	1.54E-13	Tetrahydrofolate	Glycine, Serine and Threonine Metabolism
426.8399	[M+K-2H]1-	1.60E-13	5-Phospho-alpha-D-ribose 1-diphosphate	Pentose Phosphate Pathway
125.9705	[M+K-2H]1-	3.51E-13	Oxamate	Purine Metabolism
464.7864	[M-H]1-	5.30E-13	Uridine 5'-triphosphate	Pyrimidine Metabolism
420.0936	[M+K-2H]1-	1.05E-12	Dihydrozeatin-9-N-glucoside	Cytokinins-O-glucoside biosynthesis
439.3261	[M+Cl]1-	1.97E-12	(22α)-hydroxy-cholestanol	-
411.1066	[M+Cl]1-	2.79E-12	Riboflavin	Riboflavin Metabolism
473.363	[M+Na-2H]1-	3.99E-12	Phylloquinol	Ubiquinone and other Terpenoid-quinone Biosynthesis
444.1379	[M-H]1-	5.61E-12	Tetrahydrofolate	Methionine, Purine, and Pyrimidine Biosynthesis
583.2183	[M+Na-2H]1-	5.82E-12	Protoporphyrin	Porphyrin and chlorophyll Metabolism
308.7956	[M-H]1-	1.80E-11	D-Ribose 1,5-bisphosphate	Pentose Phosphate Pathway
292.9051	[M+Cl]1-	1.99E-11	(Phosphate)n	Oxidative Phosphorylation
419.0983	[2M-H]1-	3.68E-11	5-hydroxy-ferulic-acid	Phenylpropanoid Biosynthesis

A heat map with top 20 metabolites showing the biggest differences between treatments (control [C], mechanical stress [MS] and wind stress [WS]) in ABR6 detected by mass spectrometry in negative ionisation mode.

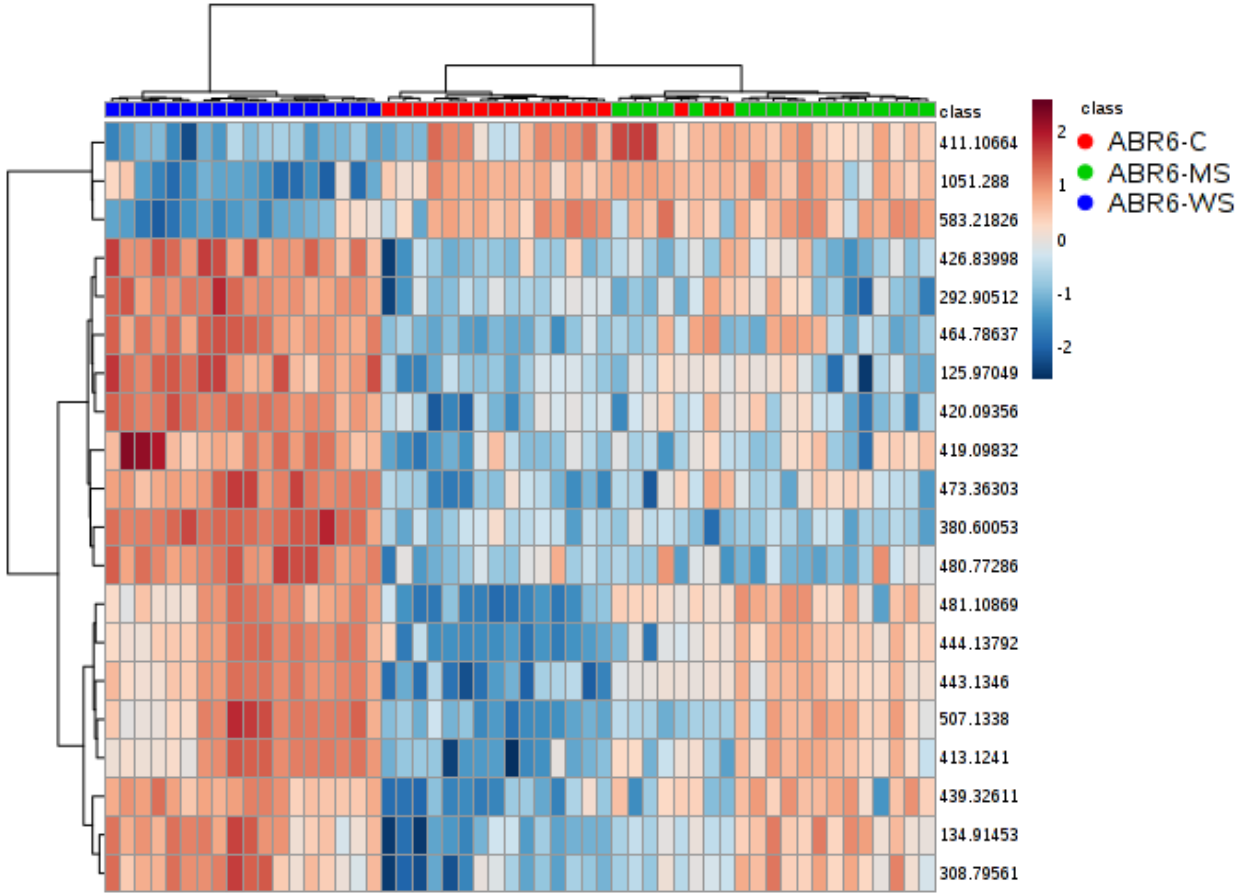

Appendix 10D. Top 20 metabolites showing the biggest differences between treatments in ABR6 detected by mass spectrometry in positive ionisation mode.

m/z	Adduct	P value	Tentative ID	Pathway
121.0649	[M+H]1+	1.52E-17	Phenylacetaldehyde	Phenylalanine Metabolism
483.105	[2M+Na]1+	8.21E-17	bis-noryangonin	Resveratrol Biosynthesis
761.1839	[2M+Na]1+	2.25E-13	6-Hydroxyprotopine	Isoquinoline Alkaloid Biosynthesis
138.0913	[M+NH4]1+	7.63E-13	Phenylacetaldehyde	Phenylalanine Metabolism
1091.2583	[2M+Na]1+	8.63E-13	UDP-4''-ketopentose	Amino Sugar and Nucleotide Sugar Metabolism
567.1167	[M+H]1+	1.53E-12	UDP-galactose	Glycolipid Biosynthesis
579.1262	[2M+K]1+	1.80E-12	D-Lombricine	Glycine, Serine and Threonine Metabolism
484.1082	[M+H+NH4]2+	3.10E-12	3-Isopropenylpimelyl-CoA	Limonene and Pinene Degradation
559.1575	[2M+Na]1+	3.84E-12	2,3-Dihydroxycarbamazepine	Drug Metabolism - Cytochrome P450
591.1925	[M+NH4]1+	4.82E-12	Biotinyl-5'-AMP	Biotin Metabolism
535.1210	[2M+K]1+	1.48E-11	5-Hydroxyindoleacetylglycine	Tryptophan Metabolism
139.0946	[M+2H]2+	1.48E-11	Saccharopine	Lysine Degradation II
386.7207	[M+H+NH4]2+	1.80E-11	18:2-16:0-MGDG	Glycolipid Biosynthesis
453.0944	[M+H+NH4]2+	1.94E-11	Salicyloyl-CoA	Salicylate Biosynthesis
307.0576	[M1+.]1+	2.47E-11	Deoxycytidylic acid	Pyrimidine Metabolism
566.1138	[M+H+NH4]2+	2.80E-11	Gentiodelphin	Gentiodelphin Biosynthesis
497.1099	[2M+K]1+	2.81E-11	5-phospho-β-D-ribosyl-amine	Purine Nucleotides de novo Biosynthesis I
467.1311	[2M+Na]1+	3.22E-11	L-Cystathionine	Glycine, serine and threonine metabolism
743.1734	[2M+K]1+	4.21E-11	Benzylpenicilloic acid	-
416.1030	[M+Na]1+	5.39E-11	Amsacrine	-

A heat map with top 20 metabolites showing the biggest differences between treatments (control [C], mechanical stress [MS] and wind stress [WS])in ABR6 detected by mass spectrometry in positive ionisation mode.

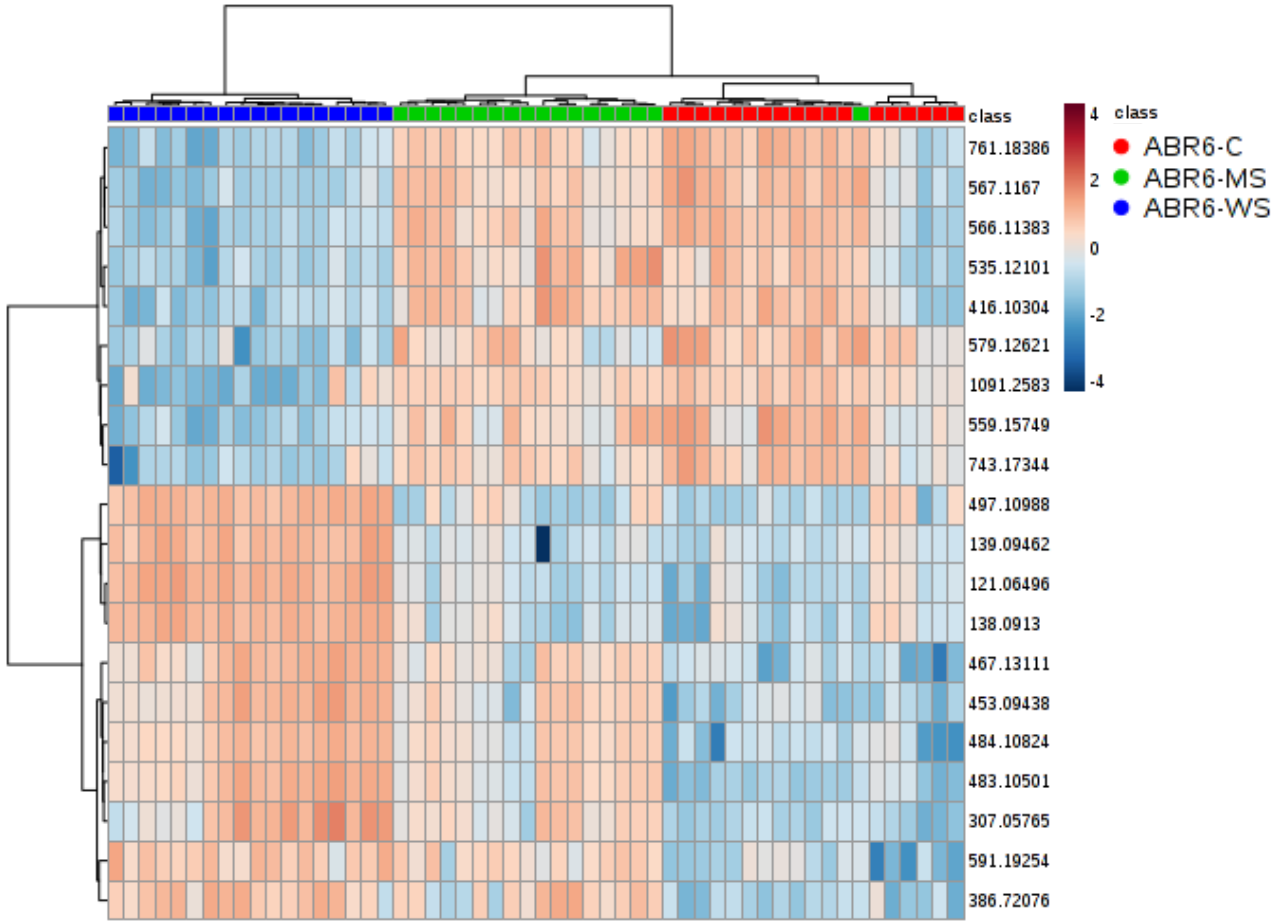

Appendix 11. Enrichment overview of top 50 pathways detected by mass spectrometry in positive and negative ionisation mode.

Appendix 11A. Bd21

Negative ionisation mode

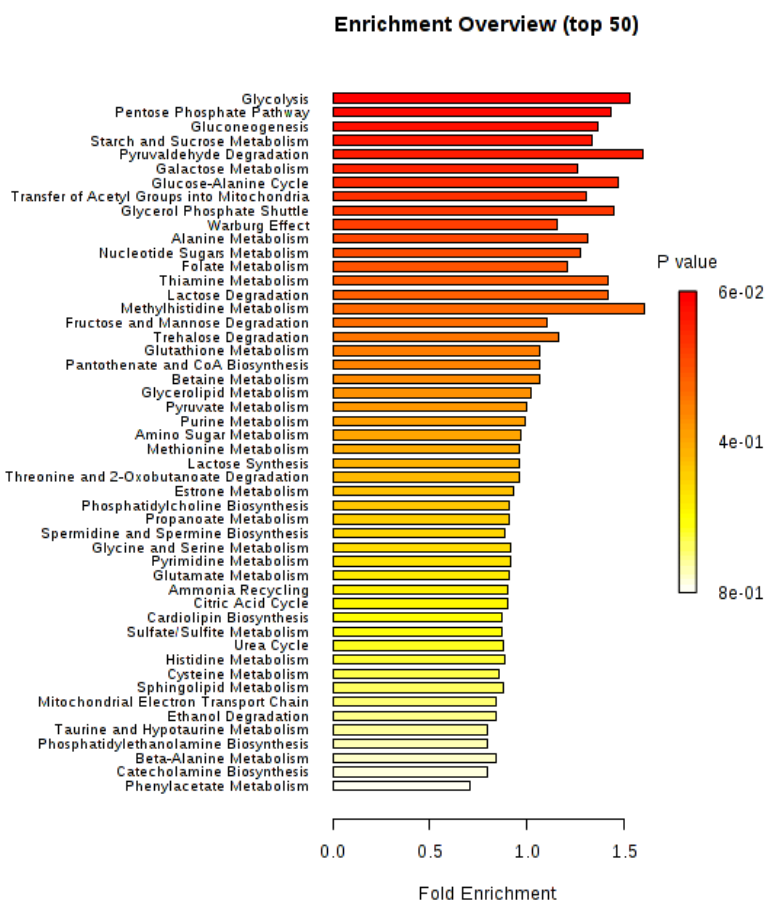

Positive ionisation mode

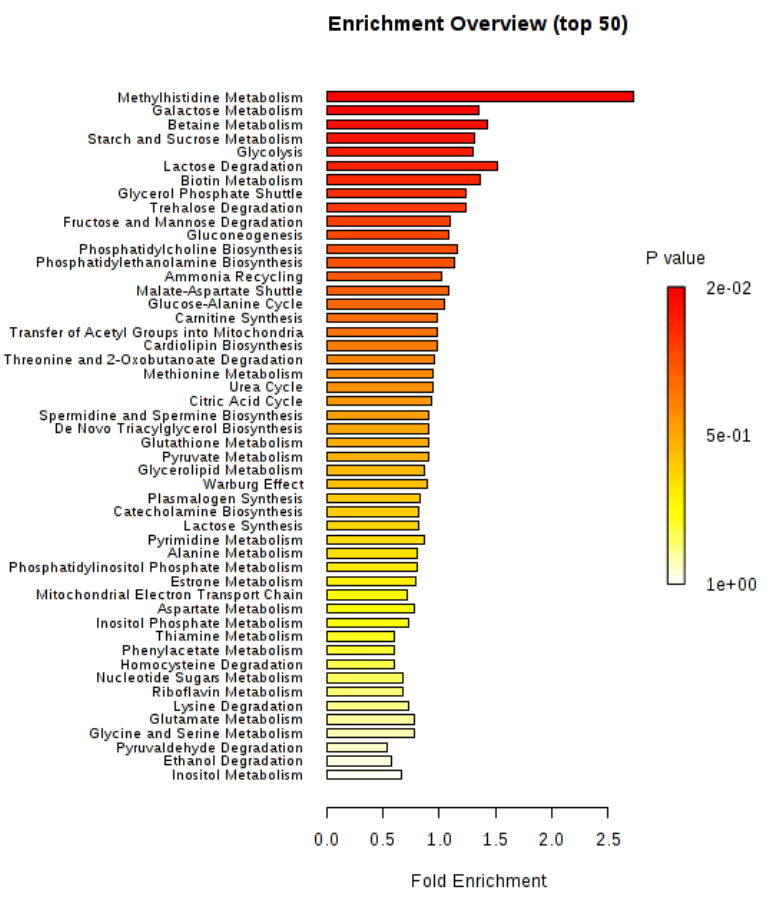

Appendix 11B. ABR6.

Negative ionisation mode

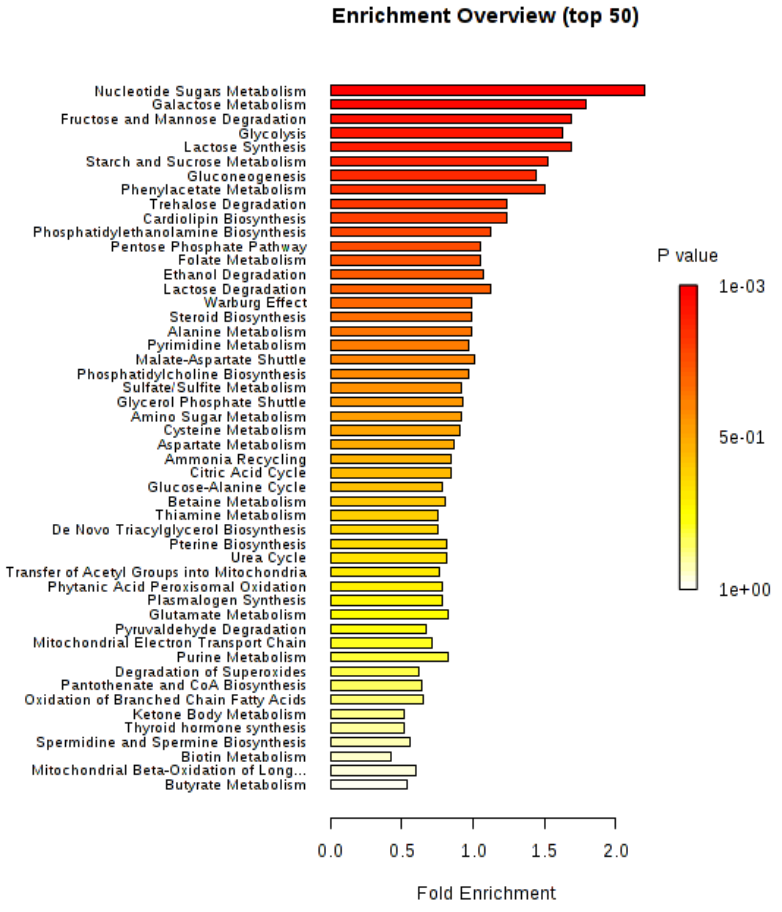

Positive ionisation mode

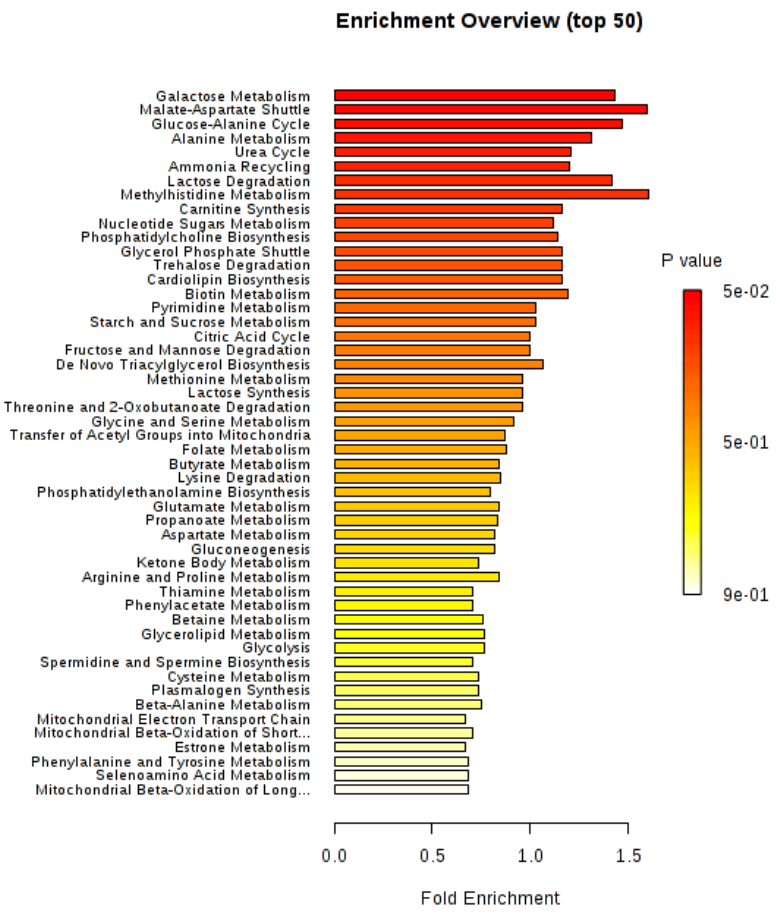

Appendix 12.

Normalised concentrations of most significant metabolites assigned to enriched pathways for Bd21 detected by mass spectrometry in negative and positive ionisation modes.

Appendix 12A. Negative ionisation.

Glycolysis Pathway

Normalised concentrations of most significant metabolites in the Glycolysis Pathway: A. NADH, B. 3-Phosphoglyceric acid, C. ADP, D. $C_3H_7O_6P$ (Including D-Glyceraldehyde 3-phosphate and Dihydroxyacetone phosphate), E. Phosphoenolpyruvic acid, F. $C_6H_{12}O_6$ (Including D-Glucose, Alfa-D-Glucose and Beta-D-glucose), G. Pyruvic acid, H. $C_3H_8O_{10}P_2$ (Including Glyceric acid 1,3-biphosphate and 2,3-Diphosphoglyceric acid). Red – control, green – mechanical stress, blue – wind stress.

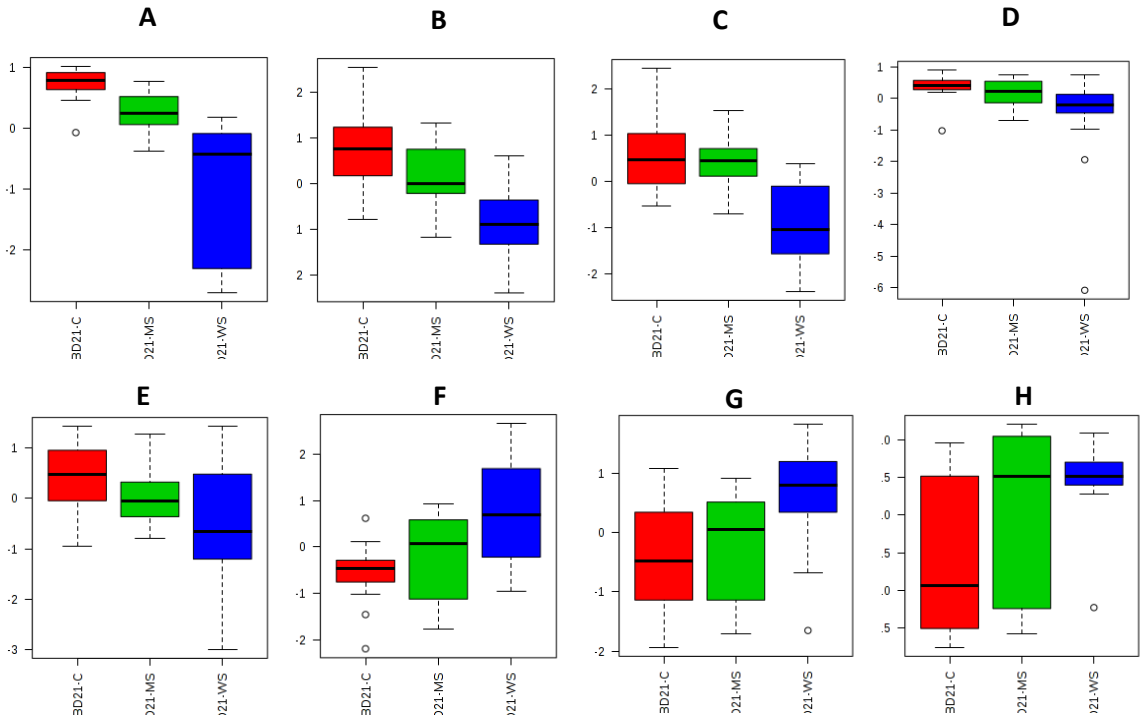

Pentose Phosphate Pathway

Normalised concentrations of most significant metabolites in the Pentose Phosphate Pathway: A. ADP, B. NADPH, C. 6-Phosphogluconic acid, D. $C_3H_7O_6P$ (Including D-Glyceraldehyde 3-phosphate and Dihydroxyacetone phosphate), E. $C_5H_{11}O_8P$ (Including D-Ribulose 5-phosphate, Xylulose 5-phosphate, Ribose 1-phosphate and D-Ribose 5-phosphate), F. D-Ribose, G. Gluconolactone, H. Carbon dioxide, I. Adenosine monophosphate. Red – control, green – mechanical stress, blue – wind stress

.

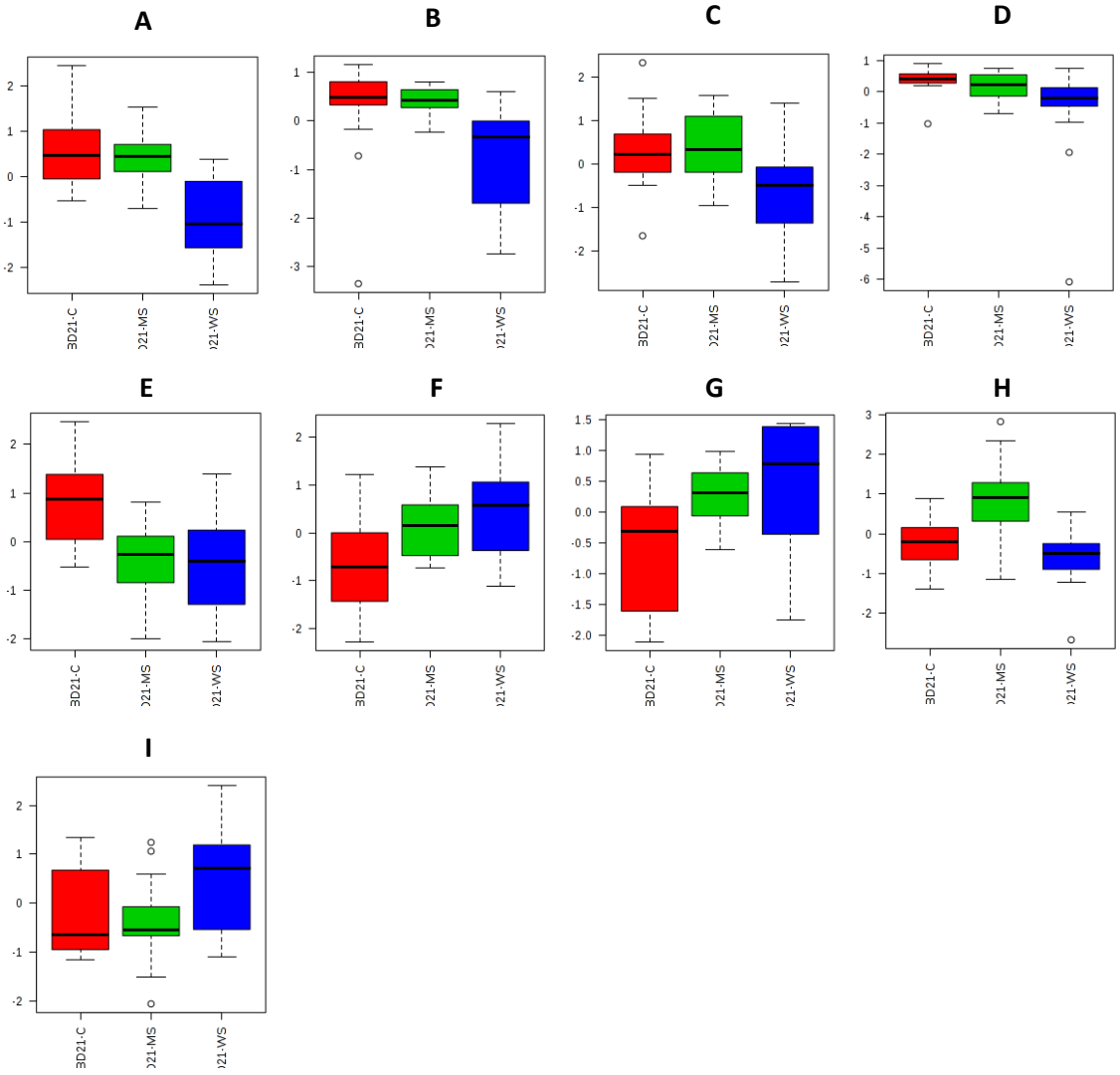

Gluconeogenesis Pathway

Normalised concentrations of most significant metabolites in the Gluconeogenesis Pathway. A. NADPH, B. 3-Phosphoglyceric acid, C. ADP, D. Phosphoenolpyruvic acid, E. $C_3H_7O_6P$ (Including D-Glyceraldehyde 3-phosphate and Dihydroxyacetone phosphate), F. Hydrogen carbonate, G. $C_6H_{12}O_6$ (Including D-Glucose, Beta-D-Glucose, Alpha-D-Glucose), H. Pyruvic acid, I. L-Lactic acid, J. $C_3H_8O_{10}P_2$ (Including Glyceric acid 1,3-biphosphate and 2,3-Diphosphoglyceric acid), K. Carbon dioxide. Red – control, green – mechanical stress, blue – wind stress.

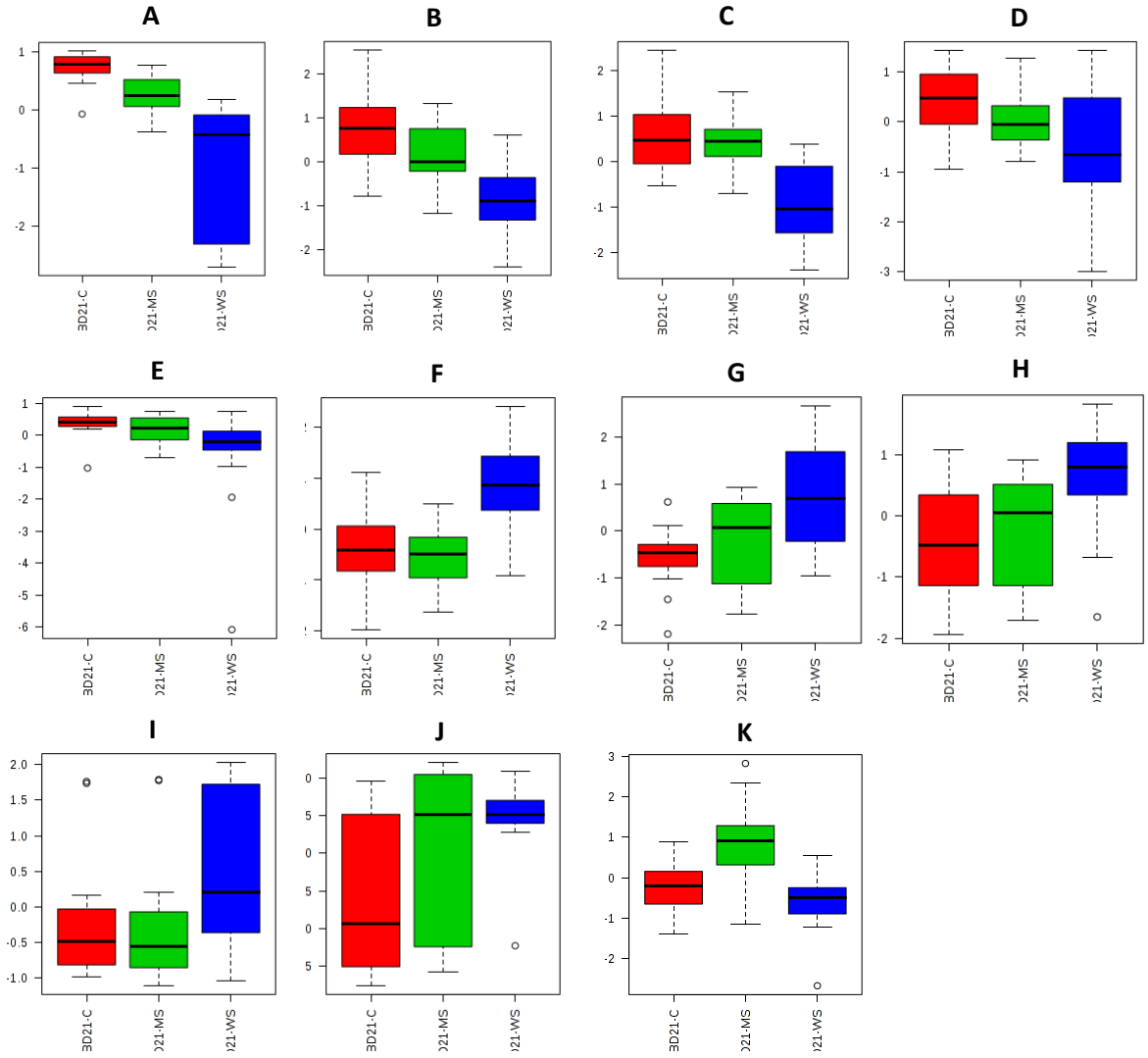

Appendix 12B. Positive ionisation mode.

Methylhistidine Metabolism

Normalised concentrations of most significant metabolites in the Methylhistidine Metabolism: A. 3-Methylhistidine, B. L-Histidine, C. S-Adenosylhomocysteine, D. S-Adenosylmethionine. Red – control, green – mechanical stress, blue – wind stress.

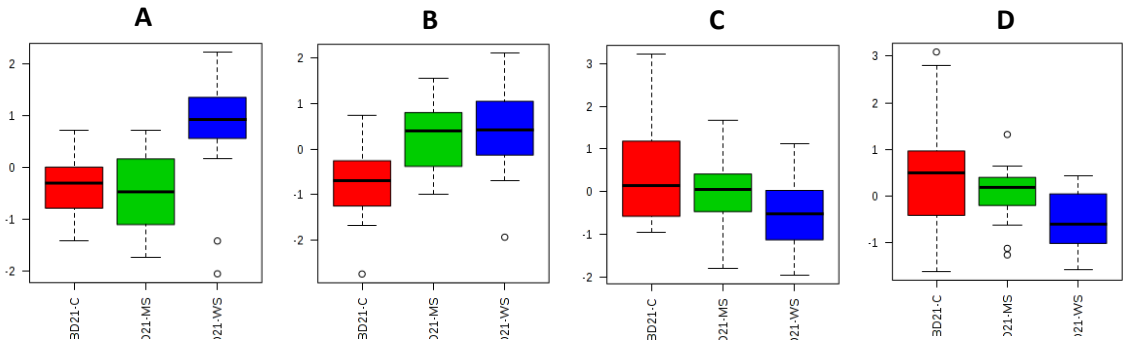

Galactose Metabolism

Normalised concentrations of most significant metabolites in the Galactose Metabolism: A. NADH, B. Raffinose, C. NAD, D. Maltotriose, E. Phosphate, F. S-Adenosylhomocysteine, G. S-Adenosylmethionine, H. Stachyose, I. Glycerol, J. Uridine 5'-diphosphate, K. 3-Methylhistidine, L. Adenosine triphosphate, M. $C_6H_{14}O_6$ (Including Sorbitol and Galactitol), N. L-Histidine, O. $C_6H_{12}O_6$ (Including D-Glucose, D-Galactose, D-Mannose, myo-Inositol, D-Fructose and Alpha-D-Glucose), P. $C_{12}H_{22}O_{11}$ (Including Alpha-Lactose and Sucrose). Red – control, green – mechancial stress, blue – wind stress.

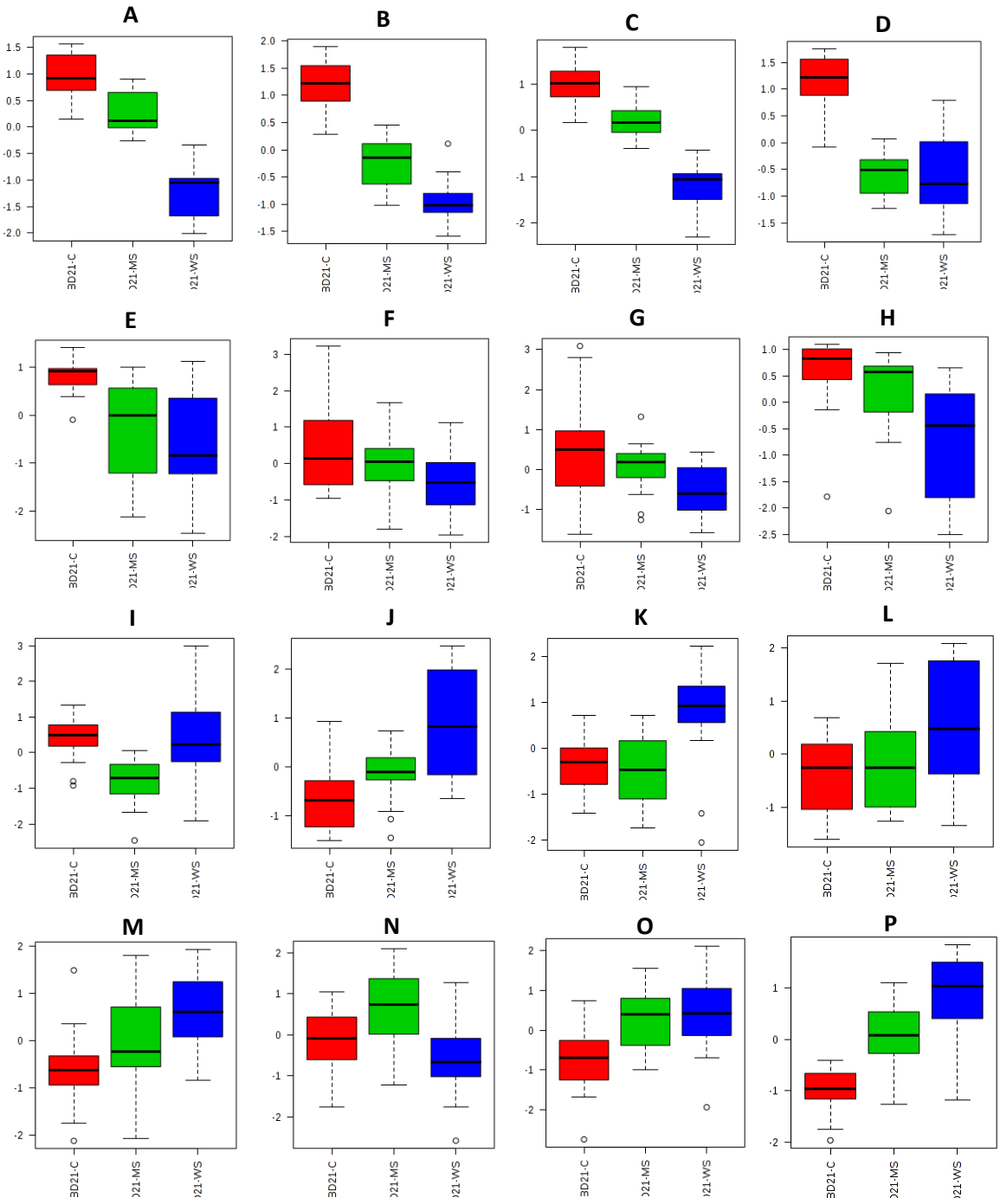

Appendix 13.

Normalised concentrations of most significant metabolites assigned to enriched pathways for ABR6 for negative and positive ionisation modes.

Appendix 13A. Negative ionisation mode.

Nucleotide Sugars Metabolism

Normalised concentrations of most significant metabolites in the Nucleotide Sugars Metabolism: A. NADH, B. UDP-D-Xylose, C. Pyrophosphate, D. Uridine diphosphate glucuronic acid, E. $C_{15}H_{24}N_2O_{17}P_2$ (Including Uridine diphosphate glucose and Uridine diphosphate galactose), F. Zinc II ion, G. $C_6H_{13}O_9P$ (Including Galactose 1-phosphate, Glucose 6-phosphate and Glucose 1-phosphate), H. $C_6H_{12}O_6$ (Including D-Galactose and Alpha-D-Glucose), I. Uridine triphosphate. Red – control, green – mechanical stress, blue – wind stress.

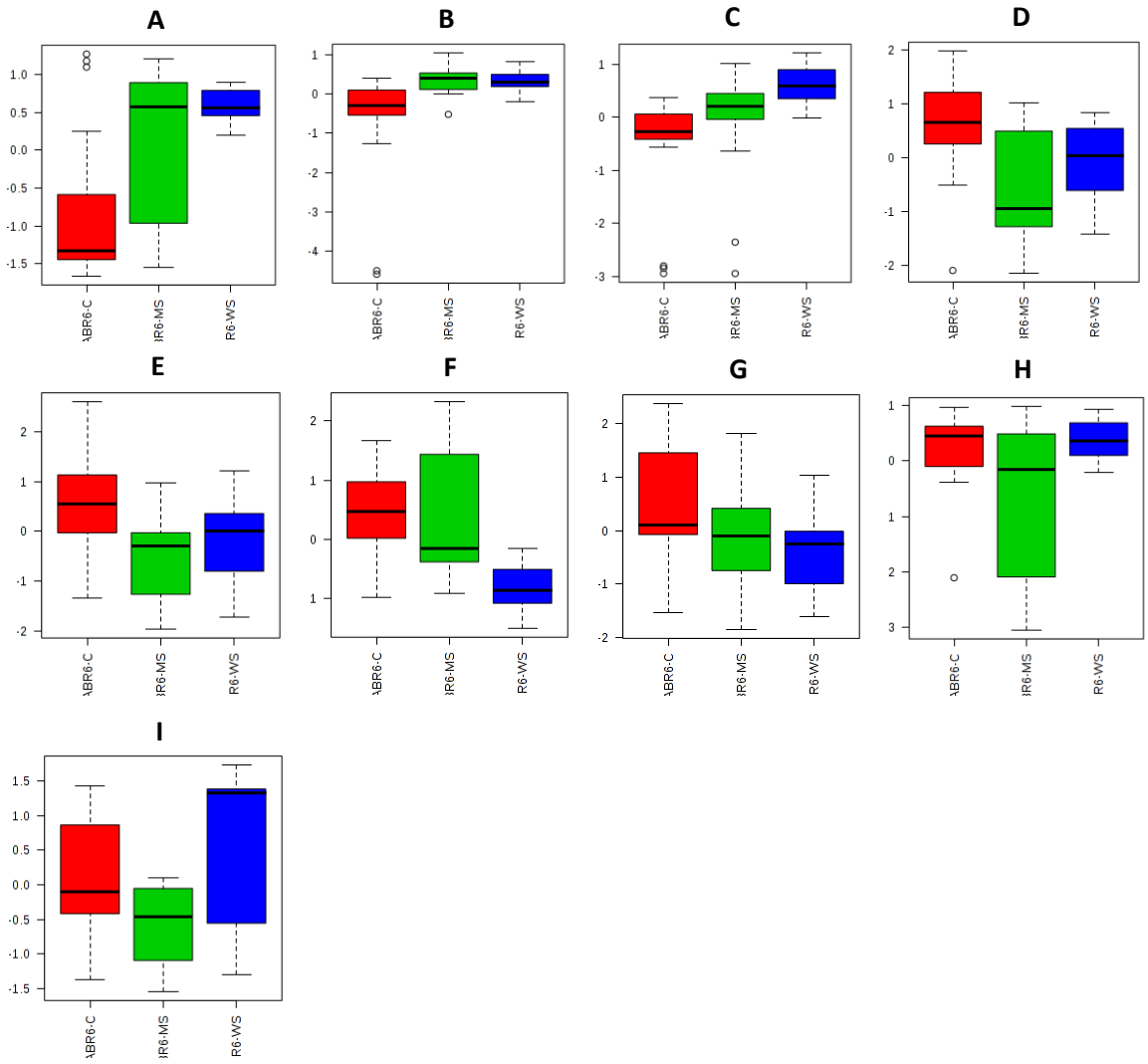

Galactose Metabolism

Normalised concentrations of most significant metabolites in the Galactose Metabolism: A. NADH, B. $C_{12}H_{22}O_{11}$ (Including Alpha-Lactose and Sucrose), C. Maltotriose, D. Pyrophosphate, E. $C_{15}H_{24}N_2O_{17}P_2$ (Including Uridine diphosphate glucose and Uridine diphosphate galactose), F. Zinc II ion, G. $C_6H_{13}O_9P$ (Including Galactose 1-phosphate, Glucose 6-phosphate and Glucose 1-phosphate), H. Uridine triphosphate, I. $C_6H_{12}O_6$ (Including D-Glucose, D-Galactose, D-Mannose, myo-Inositol, D-Fructose and Alpha-D-Glucose), J. Raffinose, K. Stachyose. Red – control, green – mechanical stress, blue – wind stress.

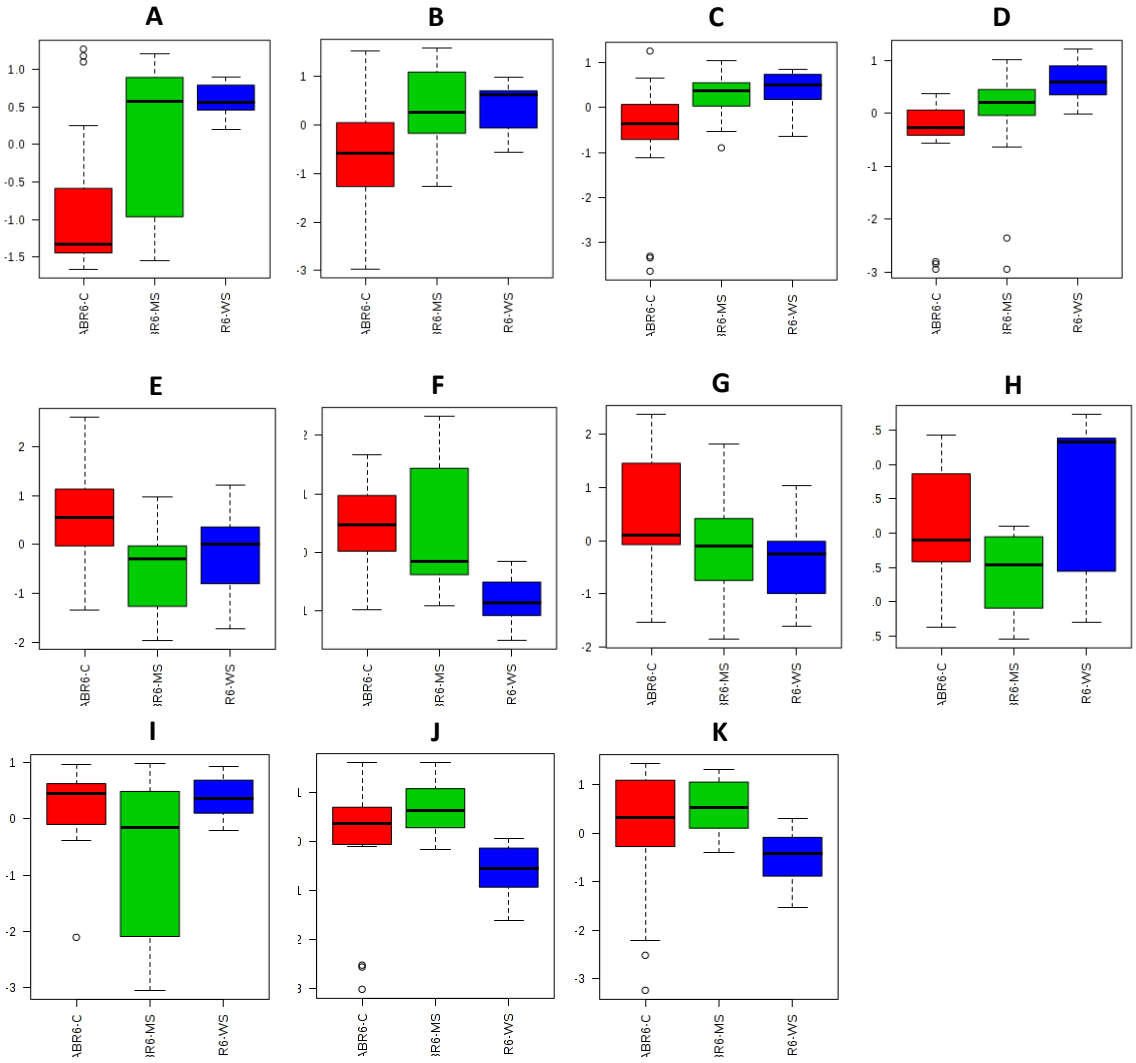

Fructose and Mannose Degradation

Normalised concentrations of most significant metabolites in the Fructose and Mannose Degradation: A. NADH, B. Guanosine triphosphate, C. Pyrophosphate, D. G. GDP-L-fucose, E. $C_3H_7O_6P$ (Including D-Glyceraldehyde 3-phosphate and Dihydroxyacetone phosphate), F. $C_6H_{14}O_{12}P_2$ (Including D-Fructose 2,6-bisphosphate and Fructose 1,6-bisphosphate), G. $C_6H_{13}O_9P$ (Including Fructose 1-phosphate, Mannose 6-phosphate, D-Mannose 1-phosphate and Fructose 6-phosphate), H. Zinc II ion, I. $C_6H_{12}O_6$ (Including D-Mannose, D-Fructose and Alpha-D-Glucose). Red – control, green – mechanical stress, blue – wind stress.

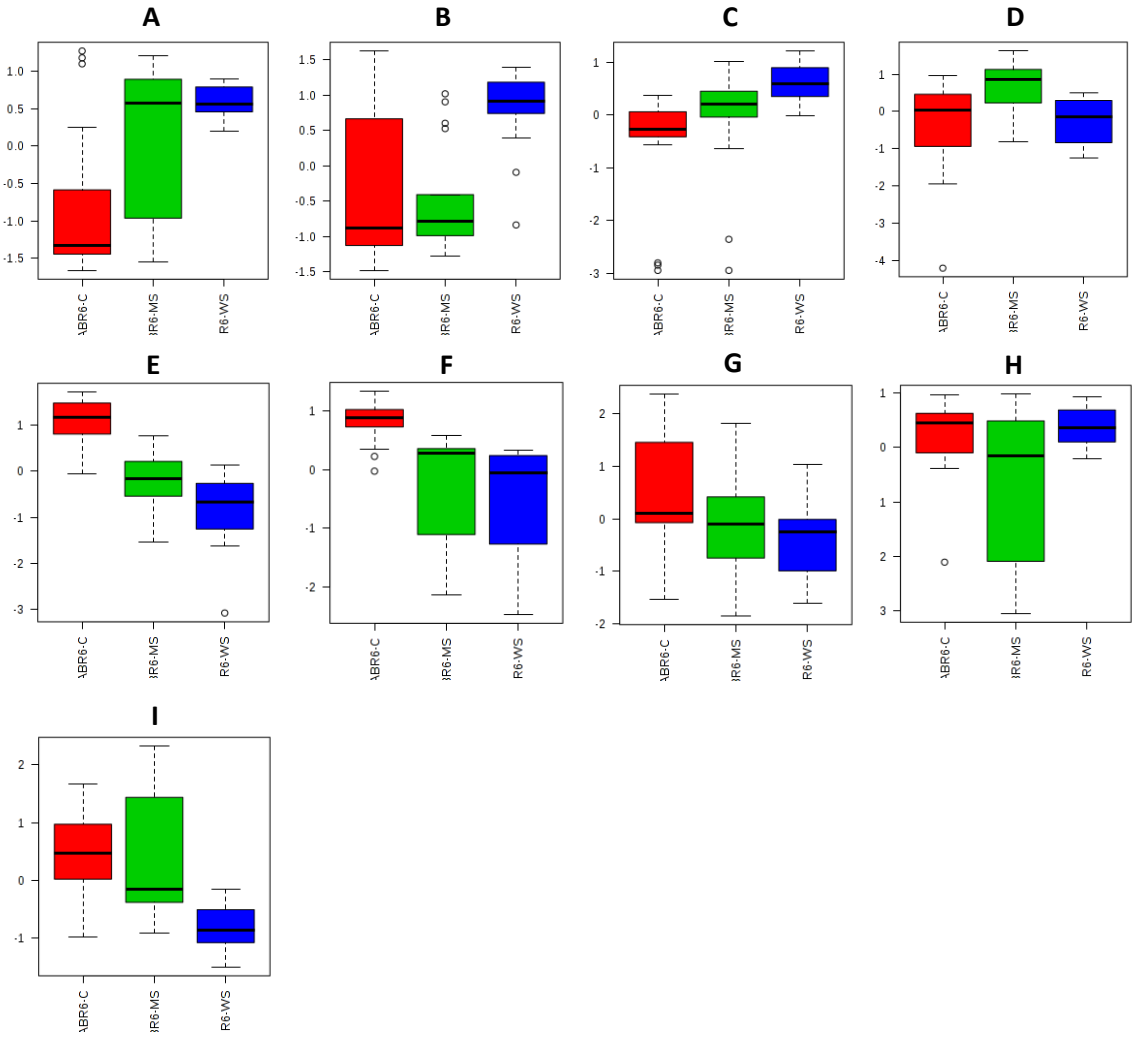

Glycolysis Pathway

Normalised concentrations of most significant metabolites in the Glycolysis Pathway: A. NADH, B. $C_3H_7O_6P$ (Including D-Glyceraldehyde 3-phosphate and Dihydroxyacetone phosphate), C. $C_6H_{14}O_{12}P_2$ (Including Fructose 1,6-bisphosphate), D. $C_6H_{13}O_9P$ (Including Fructose 6-phosphate, Glucose 6-phosphate, Glucose 1-phosphate and Beta-D-Glucose 6-phosphate), E. $C_6H_{12}O_6$ (Including D-Glucose, Beta-D-Glucose and Alpha-D-Glucose), F. 3-Phosphoglyceric acid. Red – control, green – mechanical stress, blue – wind stress.

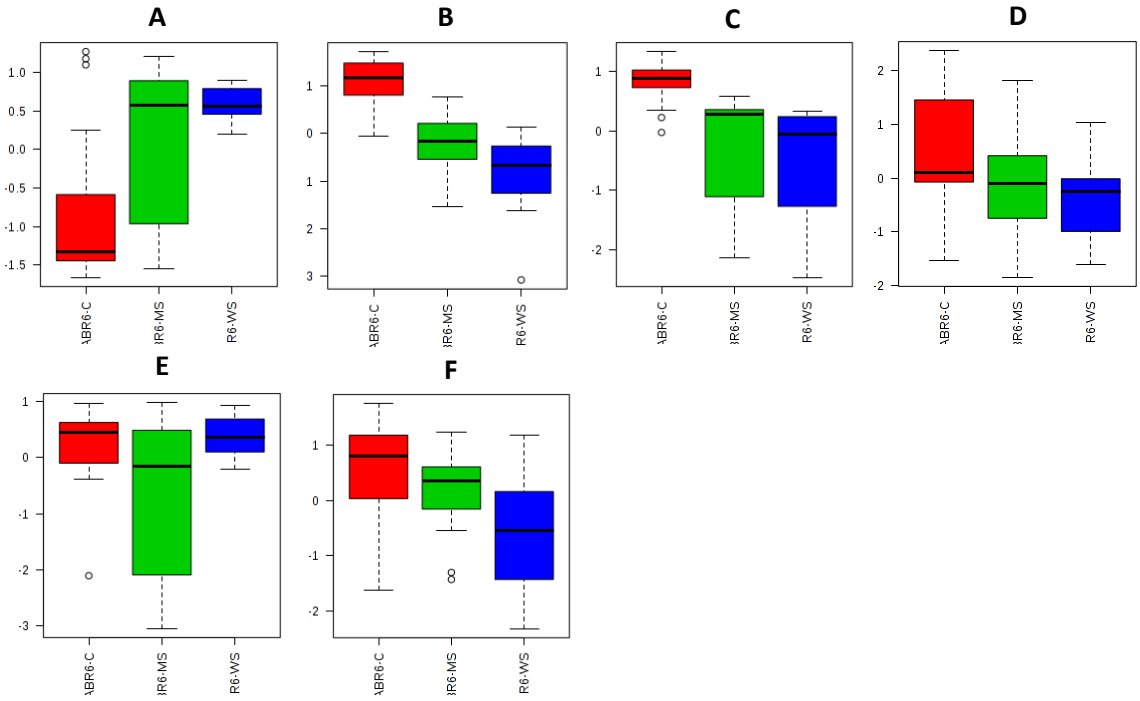

Sucrose Metabolism

Normalised concentrations of most significant metabolites in the Starch and Sucrose Metabolism: A. NADH, B. $C_{12}H_{22}O_{11}$ (Including D-Maltose and Sucrose), C. Pyrophosphate, D. $C_6H_{14}O_{12}P_2$ (Including: Alpha-D-Glucose 1,6-bisphosphate), E. 3-Phosphoglyceric acid, F. $C_{15}H_{24}N_2O_{17}P_2$ (Including Uridine diphosphate glucose), G. Uridine diphosphate glucuronic acid, H. $C_6H_{13}O_9P$ (Including Glucose 6-phosphate and Glucose 1-phosphate), I. Glycogen, J. Uridine triphosphate, K. $C_6H_{12}O_6$ (Including Alpha-D-Glucose and D-Fructose). Red – control, green – mechanical stress, blue – wind stress.

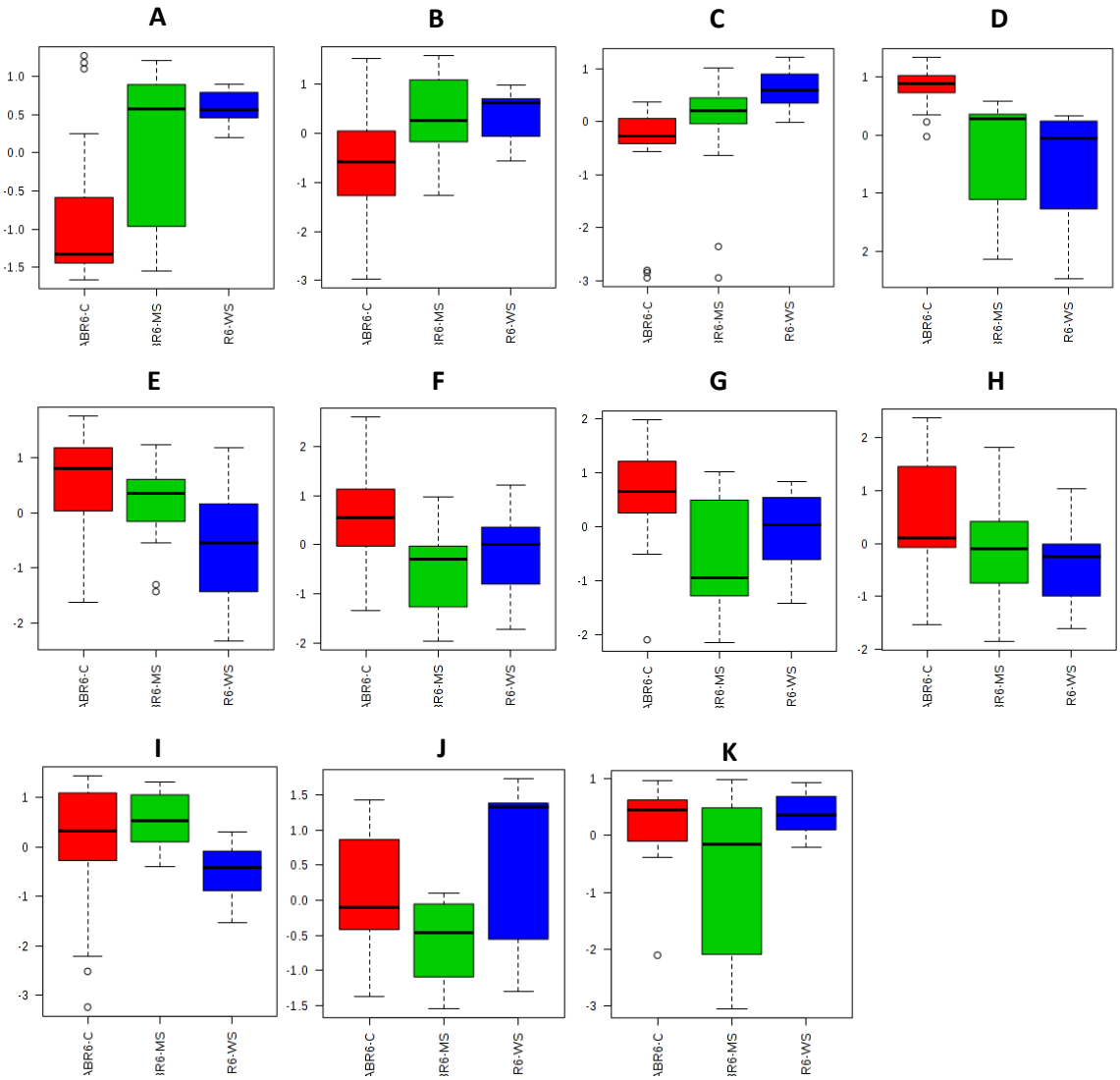

Gluconeogenesis Pathway

Normalised concentrations of most significant metabolites in the Gluconeogenesis Pathway: A. NADH, B. Guanosine triphosphate, C. Oxalacetic acid, D. Oxoglutaric acid, E. $C_3H_7O_6P$ (Including D-Glyceraldehyde 3-phosphate and Dihydroxyacetone phosphate), F. $C_6H_{14}O_{12}P_2$ (Including Fructose 1,6-bisphosphate), G. $C_6H_{13}O_9P$ (Including Beta-D-Glucose 6-phosphate, Glucose 1-phosphate, Fructose 6-phosphate and Glucose 6-phosphate), H. 3-Phosphoglyceric acid, I. $FC_6H_{12}O_6$ (Including Alpha-D-Glucose, D-Glucose and Beta-D-Glucose). Red – control, green – mechanical stress, blue – wind stress.

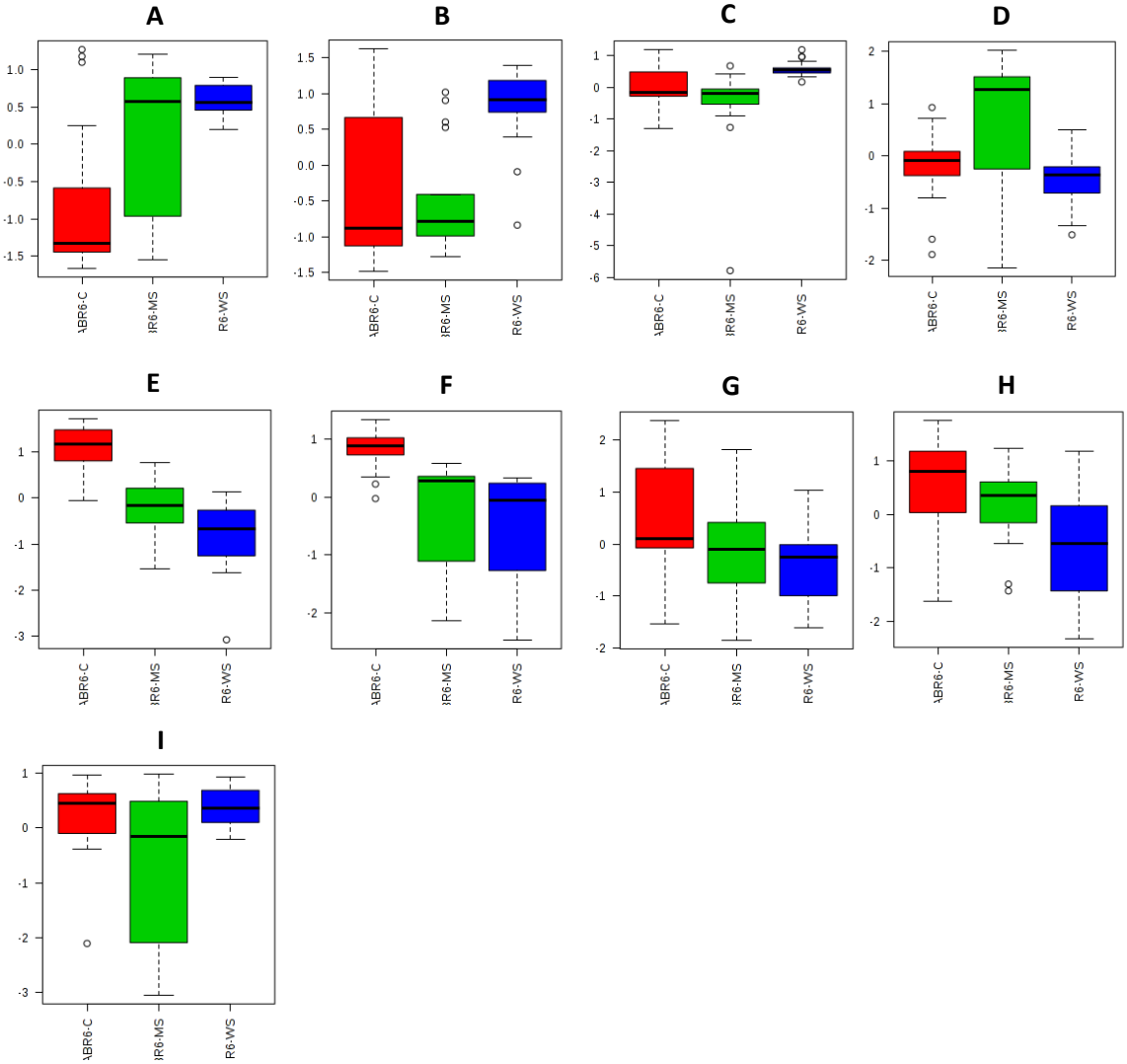

Appendix 13B. Positive ionisation mode.

Galactose Metabolism

Normalised concentrations of most significant metabolites in the Galactose Metabolism: A. $C_{15}H_{24}N_2O_{17}P_2$ (Including: Uridine diphosphate glucose and Uridine diphosphate galactose), B. NAD, C. NADH, D. Stachyose, E. Sucrose, F. $C_{18}H_{32}O_{16}$ (Including Raffinose and Maltotriose), G. ADP, H. Glycerol, I. $C_6H_{12}O_6$ (Including D-Glucose, D-Fructose, D-Galactose, D-Mannose, Alpha-Lactose, myo-Inositol and Alpha-D-Glucose). Red – control, green – mechanical stress, blue – wind stress.